



The University of
Nottingham

UNITED KINGDOM • CHINA • MALAYSIA

Manufacture and Characterisation of Bioresorbable Fibre Reinforced Composite Rods and Screws for Bone Fracture Fixation Applications

By

Reda Felfel

(BSc., MSc.)

**Thesis submitted to the University of Nottingham for the degree of
Doctor of Philosophy**

January 2013

I dedicate this work to my parents, wife and beloved children.

ABSTRACT

Bioresorbable implants are an attractive alternative to metallic bone fixation devices and offer potential to eliminate some of the clinical challenges with the latter. This work explores the manufacturing of fully bioresorbable fibre-reinforced composite rods and screws for such applications. Poly lactic acid (PLA) and phosphate glass fibres (PGF) were combined to provide mechanical reinforcement and biocompatibility characteristics. Aligned and randomly reinforced PLA/PGF composites were prepared by compression moulding prior to thermomechanical deformation into rod and screw forms. *In vitro* degradation and mechanical properties retention were investigated in phosphate buffered saline (PBS) at 37°C. The composite rods and screws exceeded published data for bioresorbable implants in their virgin state and were towards the upper range of cortical bone properties. The properties reduced rapidly in an aqueous medium and this was attributed to matrix plasticisation and fibre/matrix disbonding. The degraded samples maintained strength and stiffness close to the lower limits of the cortical bone. Water uptake and mass loss for composites exceeded equivalent values for PLA alone due to water wicking at the fibre/matrix interface. Ion release tests correlated linearly with mass loss profiles confirming that the dominant degradation mechanism was fibre dissolution. The PLA/PGF composites also exhibited good biocompatibility to human osteosarcoma and human mesenchymal stem cells.

LIST OF PUBLICATIONS:

Journal articles:

1. R. M. Felfel, I. Ahmed, A. Parsons, G. Walker, and C. Rudd, *Flexural, Shear and Compressive Properties of Bioresorbable PLA-PBG Fibre Reinforced Composite Intramedullary Rods*, *World Journal of Engineering*, (Supplement 3): 323 – 324 (2010)
2. A. J. Parsons, I. Ahmed, N. Han, R. M. Felfel, C. D. Rudd, *Mimicking Bone Structure and Function with Structural Composite Materials*, *Journal of Bionic Engineering*; 7(Supplement 1): S1-S10 (2010)
3. R. M. Felfel, I. Ahmed, A. J. Parsons, G. S. Walker, and C. D. Rudd, *In vitro degradation, flexural, compressive and shear properties of fully bioresorbable composite rods*, *Journal of the Mechanical Behavior of Biomedical Materials*, 4(7): 1462 – 1472 (2011)
4. R. M. Felfel, I. Ahmed, A. J. Parsons, P. Haque, G. S. Walker and C. D. Rudd, *Investigation of crystallinity, molecular weight change and mechanical properties of bioresorbable composites as bone fracture fixation plates*, *J Biomater Appl*, 26(7): 765 – 789 (2012)
5. R. M. Felfel, I. Ahmed, A. J. Parsons, L. T. Harper, and C. D. Rudd, *Initial Mechanical Properties of Phosphate-Glass Fibre-Reinforced Rods for use as Resorbable Intramedullary Nails*, *Journal of Material science*, 47: 4884 – 4894 (2012)
6. L. T. Harper, I. Ahmed, R. M. Felfel, C. Qian, *Finite Element Modelling of the Flexural Performance of Resorbable Phosphate Glass Fibre Reinforced PLA Composite Bone Plates*, *Journal of the Mechanical Behavior of Biomedical Materials*, 15(0): 13-23 (2012).
7. R. M. Felfel, I. Ahmed, A. J. Parsons, and C. D. Rudd, *Bioresorbable Screws Reinforced with Phosphate Glass Fibre: Manufacturing and Mechanical Property Characterisation*, *Journal of the Mechanical Behavior of Biomedical Materials*, 17: 76-88 (2013)
8. R. M. Felfel, I. Ahmed, A. J. Parsons, and C. D. Rudd, *Bioresorbable Composite Screws Manufactured via a Forging Process: Pull-out, Shear, Flexural and Degradation Characteristics*, *Journal of the Mechanical Behavior of Biomedical Materials*, 18:108-122 (2013).
9. R. M. Felfel, I. Ahmed, A. J. Parsons, G. Palmer, V. Sottile, and C. D. Rudd, *Cytocompatibility, Degradation, Mechanical Property Retention and Ion Release Profiles for Phosphate Glass Fibre Reinforced Composite Rods*, *Materials Science and Engineering C (in press)*

Patents:

Implant, Ref. No. JA59879P.GBA, Filed on 4th May 2012.

Conferences:

1. UKSB 9th Annual Conference, *Comparison between bioresorbable random mat and unidirectional fibre reinforced composites: Mechanical and Degradation properties*, 1-2 July 2010, University of Glasgow, UK (Oral Presentation)
2. Biomaterials for Aging Populations 1st UK-CHINA Summer School, *Bioresorbable Composites for Bone Repair*, 19th – 25th July 2010, Sichuan University Chengdu, Sichuan Province, China (Poster)
3. E S A O Winter School, *Advancing Roles: Biomaterials in Artificial Organs and Regenerative Medicine Passive to Active to Bioreactive, Bioresorbable Fibre Reinforced Composites as Bone Fixation Devices*, January 26th - 29th, 2011, Austria (Poster)
4. 9th World Biomaterials Congress (WBC), *In vitro Degradation and Mechanical Properties of Fully Resorbable PLA/PBG Composite Rods*, 1st - 5th June, 2012, Chengdu, China (Poster)
5. UKSB 11th Annual Conference, *Bioresorbable PLA/PBG Composite Rods: Degradation and Mechanical Retention*, 27th - 28th June 2012, University of Nottingham, UK (Poster)

ACKNOWLEDGEMENTS

I would like to thank my principal supervisors, Professor Chris Rudd and Dr Ifty Ahmed, for their endless support, help and guidance. I will always be grateful for their kindness and patience and for encouraging me throughout my study. I would also like to thank Dr Andy Parsons, Professor Gavin walker, Dr Colin Scotchford and Dr Lee Harper for their help, support, guidance and valuable comments.

Huge thanks also go to all my friends and colleagues in the Polymer Composites research and Bioengineering groups. Great and special thanks are given to Papia, Sami, Sharifah, Hannah, Zakir, Madhi, Xiaoling, Nusrat, Jin and Matthew for their help, friendship support and knowledgeable discussions. I am also really thankful to Ann Marshall for her kind help throughout my study period.

I would also like to acknowledge all the technicians for their support throughout this period. Thanks are offered to Roger Smith, Geoff Tomlinson, Keith Dinsdale, Tom Buss and Nigel Neate for their guidance and assistance in the experimental part of my work.

Most importantly, I would like thank my wife, without her love, help, patience and support; it would have been extremely difficult for me to finish this work. Lots of love also goes to my beloved children, Mazen and Moaz. I will always be hugely indebted to my parents. They brought me up and together we endured tough times and days and words cannot express my deep gratitude for them. Great thanks also go to my brothers (Abd Aziz, Ibrahim, Shaban) and my sisters (Raeifah and Amani) and to all my friends back home (Abd Elaty, Mostafa, Ibrahim, Ramzy, Hesham, Farid, Mokhtar, Henawy, Saber and Menshaw).

Finally, I would like to acknowledge the Egyptian government for offering me the opportunity to study and gain experience abroad and for their financial and social support during my studies.

ABBREVIATIONS

PLA	Poly lactic acid
PBG	Phosphate based glass
FRC	Fibre-reinforced composite
PGF	Phosphate glass fibres
P40	PGF with composition of 40P ₂ O ₅ -24MgO-16CaO-16 Na ₂ O-4Fe ₂ O ₃ in mol%
P50	PGF with composition of 50P ₂ O ₅ -40CaO-5Na ₂ O-5Fe ₂ O ₃ in mol%
RM	Chopped random fibres mat
UD	Unidirectional continuous fibres mat
UD/RM	A mixture of UD and RM fibre mats
V _f %	Fibre volume fraction
wt%	Weight fraction
ASTM	American Society for Testing and Materials
SR	Self-reinforced/self-reinforcement
ISO	International Standards Organization
BS	British Standards
SFTT	Single Fibre Tensile Test
XRD	X-Ray Diffraction
GPC	Gel Permeation Chromatography
SEM	Scanning Electron Microscope
DSC	Differential Scanning Calorimetry
HOS	Human osteosarcoma cell lines
IM	Intramedullary
ppm	Parts per million
MSCs	Human mesenchymal stem cells

TABLE OF CONTENTS

ABSTRACT	III
LIST OF PUBLICATIONS:	IV
ACKNOWLEDGEMENTS	VI
ABBREVIATIONS.....	VII
TABLE OF CONTENTS.....	VIII
LIST OF FIGURES:.....	XIV
LIST OF TABLES:.....	XXI
CHAPTER 1. INTRODUCTION AND BACKGROUND	1
1.1 BONE	1
1.1.1 Structure of the bone	1
1.1.2 Mechanical properties of bone	2
1.1.3 Bone fractures.....	3
1.2 BONE FRACTURE FIXATION.....	4
1.2.1 External bone fixation.....	4
1.2.2 Internal bone fixation	5
1.2.2.1 Wire fixation.....	5
1.2.2.2 Intramedullary nail (IM)	5
1.2.2.3 Bone plate.....	6
1.2.2.4 Bone screws.....	7
1.2.3 Bone healing.....	8
1.3 AIMS AND OBJECTIVES	9
1.4 THESIS LAYOUT.....	10
1.5 REFERENCES.....	11
CHAPTER 2. LITERATURE REVIEW	13
2.1 INTRODUCTION	13
2.2 IMPLANT MATERIALS	13
2.2.1 Metallic implant materials.....	14
2.2.2 Polymeric implant materials	16

2.2.2.1 Degradation of bioresorbable polymers	17
2.2.2.2 Poly Lactic Acid (PLA)	20
2.2.3 Composite implants	22
2.2.3.1 Particulate biocomposites	23
2.2.3.2 Self-reinforced biocomposites	28
2.2.3.3 Inorganic fibre-reinforced biocomposites.....	30
2.2.4 Phosphate based glass (PBG)	31
2.2.4.1 Introduction	31
2.2.4.2 Structure	32
2.2.4.3 Dissolution.....	35
2.2.4.4 Biocompatibility.....	38
2.2.4.5 Phosphate glass fibres (PGF)	39
2.3 REFERENCES.....	42
CHAPTER 3. PHYSICAL, MECHANICAL, DEGRADATION AND CYTOCOMPATIBILITY PROPERTIES OF BIORESORBABLE FIBRE REINFORCED COMPOSITES	58
3.1 SUMMARY	58
3.2 INTRODUCTION	59
3.3 MATERIALS AND METHODOLOGY	62
3.3.1 Phosphate Glass and Fibre Production	62
3.3.2 Preparation of non-woven random and continuous unidirectional fibre mats	64
3.3.3 Composite production.....	66
3.3.4 Single Fibre Tensile Test (SFTT).....	68
3.3.5 Differential Scanning Calorimetry (DSC)	68
3.3.6 X-Ray Diffraction (XRD)	68
3.3.7 Pycnometry	69
3.3.8 Degradation Studies	69
3.3.9 Mechanical properties	70

3.3.10 Gel Permeation Chromatography (GPC)	70
3.3.11 Scanning Electron Microscopy (SEM)	70
3.3.12 Preliminary Cytocompatibility Studies (Cell Viability and Live Dead Staining).....	70
3.3.13 Statistical analysis	71
3.4 RESULTS	71
3.4.1 Tensile properties.....	71
3.4.2 Crystallinity and density.....	73
3.4.3 X- Ray Diffraction (XRD)	75
3.4.4 Degradation study.....	76
3.4.5 Flexural properties	79
3.4.6 Molecular weight change with the time.....	82
3.4.7 SEM Analysis	83
3.4.8 Cytocompatibility Studies	84
3.5 DISCUSSION	85
3.5.1 Polymer and Composite Degradation Studies.....	87
3.5.2 Mechanical properties	89
3.6 CONCLUSIONS	91
3.7 REFERENCES.....	92
CHAPTER 4. BIORESORBABLE PHOSPHATE GLASS FIBRE-REINFORCED COMPOSITE RODS: PREPARATION AND MECHANICAL TESTING	97
4.1 SUMMARY	97
4.2 INTRODUCTION	97
4.3 MATERIALS AND METHODS.....	100
4.3.1 Composites production	100
4.3.2 Composite Rod Production.....	100
4.3.3 Mechanical tests.....	104
4.3.3.1 Flexural test	104

4.3.3.2 Double shear test.....	104
4.3.3.3 Compression test.....	105
4.3.3.4 Extracted fibre length measurement.....	107
4.3.3.5 Fibre orientation.....	107
4.3.3.6 Scanning Electron Microscopy (SEM).....	108
4.3.3.7 Rule of Mixtures.....	108
4.4 RESULTS	109
4.4.1 Flexural properties	109
4.4.2 Shear Properties.....	109
4.4.3 Compressive properties.....	110
4.4.4 SEM analysis	111
4.4.5 Fibre length and orientation analysis.....	112
4.5 DISCUSSION	115
4.6 CONCLUSIONS	121
4.7 REFERENCES	121
CHAPTER 5. DEGRADATION, MECHANICAL PROPERTY RETENTION, ION RELEASE AND CYTOCOMPATIBILITY ASSESSMENT OF PLA/PGF COMPOSITE RODS	127
5.1 SUMMARY	127
5.2 INTRODUCTION	128
5.3 MATERIALS AND METHODS.....	131
5.3.1 Composite Rod Production.....	131
5.3.2 Degradation study.....	131
5.3.3 Gel Permeation Chromatography (GPC)	132
5.3.4 Mechanical tests.....	132
5.3.5 Cumulative Ion Release Study.....	132
5.3.5.1 Cation Release.....	132
5.3.5.2 Anion Release	133
5.3.6 Biological assessment	133

5.3.6.1	<i>Cell culture</i>	134
5.3.6.2	<i>Quantification of cell metabolism and differentiation</i>	134
5.3.7	Scanning Electron Microscopy (SEM)	135
5.4	RESULTS	135
5.4.1	Degradation study	135
5.4.2	Mechanical properties	139
5.4.3	Ion release	144
5.4.4	Cytocompatibility testing	148
5.5	DISCUSSION	153
5.6	CONCLUSIONS	164
5.7	REFERENCES	165
CHAPTER 6.	PREPARATION AND CHARACTERISATION OF BIORESORBABLE SCREWS BASED ON PLA AND PBG FIBRES	171
6.1	SUMMARY	171
6.2	INTRODUCTION	172
6.3	MATERIALS AND METHODOLOGY	174
6.3.1	Composite Production	174
6.3.2	Method of screw manufacture	174
6.3.3	Mechanical tests for screws	176
6.3.3.1	<i>Flexural testing</i>	176
6.3.3.2	<i>Pull-out test</i>	177
6.3.3.3	<i>Double shear test</i>	177
6.3.3.4	<i>Torsional testing</i>	178
6.3.3.5	<i>Degradation study</i>	180
6.3.3.6	<i>Scanning Electron Microscopy (SEM)</i>	180
6.4	RESULTS	181
6.4.1	Initial Mechanical properties	181
6.4.2	Degradation Properties.....	187

6.4.3 Mechanical Retention.....190

6.5 DISCUSSION195

 6.5.1.1 Screw thread calculations.....197

6.6 CONCLUSIONS208

6.7 REFERENCES209

CHAPTER 7. OVERALL THESIS SUMMARY AND FUTURE WORK.....215

7.1 SUMMARY215

7.2 TO CONCLUDE.....220

7.3 FUTURE WORK.....221

 7.3.1 Fibre-matrix interface221

 7.3.2 Characterisation methodology221

 7.3.3 Implant materials222

 7.3.4 Implant design223

7.4 REFERENCES223

LIST OF FIGURES:

Figure 1-1: <i>The structure of flat bones in the human body, cancellous bone sandwiched in-between sheets of cortical bone [4].</i>	2
Figure 1-2: <i>Types of bone fractures [4].</i>	3
Figure 1-3: <i>Model for fixation of long bone fractures by external fixation system [14].</i>	4
Figure 1-4: <i>Intramedullary nail with interlocking screws at proximal and distal ends [18].</i>	6
Figure 1-5: <i>Different shapes of commercial metallic bone plates [23].</i>	6
Figure 1-6: <i>Different types of commercial metallic cancellous and cortical screws [25].</i>	7
Figure 1-7: <i>Types of thread in bone screws [17].</i>	8
Figure 2-1: <i>Sequence of reduction in molecular weight, mechanical strength and mass for bioresorbable polymers with the time during degradation process [23].</i>	18
Figure 2-2: <i>Mechanisms of bioresorbable polymers degradation; (a) surface erosion, (b) bulk degradation and (c) bulk degradation and autocatalysis [31].</i>	19
Figure 2-3: <i>Chemical structure for PLA, L-lactide and D-lactide isomers [56].</i>	21
Figure 2-4: <i>Schematic diagram for degradation of PLA as an example for bioresorbable polymers [29, 59].</i>	21
Figure 2-5: <i>Biomedical applications for various biocomposites [16].</i>	23
Figure 2-6: <i>Schematic diagram for self-reinforced composites; m and f represent matrix and reinforcing fibres derived from the same polymer [94].</i>	28
Figure 2-7: <i>Schematic diagram of parameters which control the mechanical properties of fibre reinforced composites [139].</i>	31
Figure 2-8: <i>chemical structure of the tetrahedral phosphate anion.</i>	33
Figure 2-9: <i>Effect of addition of monovalent cation (M^+) on the Q structure of the P_2O_5 [8].</i>	33
Figure 2-10: <i>The Q structure for $P_2O_5 - CaO - Na_2O - MgO$ glass [163].</i>	35
Figure 3-1: <i>Melt-spinning rig for pulling phosphate based glass fibres.</i>	63
Figure 3-2: <i>The change in fibre diameter against speed of rotation.</i>	64
Figure 3-3: <i>Laboratory setup for preparing phosphate glass fibre random mats.</i>	65
Figure 3-4: <i>Images for the prepared (a) random mat (RM) and (b) unidirectional mat (UD).</i>	65

Figure 3-5: Schematic diagram for film stacking process.	66
Figure 3-6: Photographs of the moulds used in this study (a) circular shim for random mat composites (RM) and (b) square shim for unidirectional composites (UD).....	67
Figure 3-7: Photographs of the prepared (a) RM and (b) UD composites.	67
Figure 3-8: Weibull parameters obtained for phosphate glass fibres (a) P40 and (b) P50 [11].	72
Figure 3-9: SEM micrograph of as-prepared phosphate based glass fibres.	73
Figure 3-10: DSC traces for PLA alone, P40 RM and P40 UD composites before degradation.	74
Figure 3-11: The percentage change of PLA crystallinity (measured using DSC) with time during degradation in PBS at 37°C.	74
Figure 3-12: The density change of PLA, RM, and UD composites with time during degradation in PBS at 37°C. The arrows indicate the axes for density values for PLA and composites.	75
Figure 3-13: XRD patterns of PLA before and after degradation in PBS at 37°C.	76
Figure 3-14: Water uptake percentage and mass loss change of PLA, RM, and UD composites over immersion time in PBS at 37°C. (Closed symbols are for water uptake and opened symbols are for mass loss).	77
Figure 3-15: The percentage change in wet mass of PLA, RM, and UD composites during immersion in PBS at 37°C. (The inset graph shows data for the first 32 h).	78
Figure 3-16: pH value change for PBS during the degradation process in PBS at 37°C for PLA alone, RM, and UD composites.	78
Figure 3-17: Flexural strength vs time for PLA, RM, and UD composites. (Samples measured wet after immersion in PBS at 37°C.	79
Figure 3-18: The flexural modulus against degradation time for PLA, RM, and UD composites. (Samples measured wet after immersion in PBS at 37°C).	80
Figure 3-19: Stress–strain curves for P40 UD and P40 RM composites before (0d) and after 95 (95d) days of degradation in PBS at 37°C.	81
Figure 3-20: Flexural properties for composites with high fibre volume fraction. Two different fibre architecture (RM and UD) and composition (P40 and P50) were used in this study.	82
Figure 3-21: The change in weight average molecular weight of PLA, RM, and UD composites, over time.	83

Figure 3-22: SEM micrographs of a fractured surface of (a) PLA before degradation, (b) PLA after 95days of degradation in PBS at 37°C, (c) P40 RM composite before degradation, (d) P40 RM composite after 95days of degradation in PBS at 37°C, (e) P40 UD composite before degradation, (d) P40 UD composite after 95days of degradation in PBS at 37°C. A scale bar for PLA and P40 RM represent 100 μm and is 50 μm for P40 UD specimens.....	84
Figure 3-23: Cytocompatibilty assessment of Pure PLA, P40 RM and P40 UD composites. Cell viability was conducted over 1day and 4 days. Magnification of images is 20X.	85
Figure 4-1: Photograph of the mould used in this study for forging PLA and composite bars into rods.	101
Figure 4-2: DSC trace for PLA plate over temperature range from 40°C to 200°C....	102
Figure 4-3: Change in temperature of PLA plate against elapsed time in oven at 210°C.	102
Figure 4-4: Images for the manufactured PLA, P40 RM, P50 UD and P40 UD composite rods.	103
Figure 4-5: Double shear test tool used for shear tests.	105
Figure 4-6: Applied force versus deflection during the double shear test for rods.	105
Figure 4-7: Applied compressive force against deflection.	106
Figure 4-8: Flexural properties for PLA, P50 RM, P50 UD and P40 UD composite rods. The test was conducted for dry samples in triplicate at room temperature (~ 20°C). Sample dimensions were 80 mm length and 4 mm diameter. Young's moduli for P50 and P40 fibres were ~ 52 GPa and ~ 62GPa respectively.....	109
Figure 4-9: Shear properties for PLA, P50 RM, P50 UD and P40 UD composite rods. The test was conducted for dry samples in triplicate at room temperature (~ 20°C). Sample dimensions were 30 mm length and 4 mm diameter.....	110
Figure 4-10: Compressive properties for PLA, P50 RM, P50 UD and P40 UD composite rods. The test was conducted for dry samples in triplicate at room temperature (~ 20°C). Sample dimensions were 10 mm height and 4 mm diameter.....	111
Figure 4-11: SEM micrographs of freeze fractured surfaces for (a) P50 RM rod, (b) P50 UD rod and (c) P40 UD rod. Scale bars for all micrographs represent 50 μm	111
Figure 4-12: Photographs for the extracted fibres after burn off from (a) UD composite rod, (b) RM composite bar and (c) RM composite rod.	112

- Figure 4-13:** Weight average length distribution of the extracted fibres from the P50 RM composite bar (30 mm (length) x 4.5 mm (width) x 3.5 mm (thickness)) and rod (30 mm (length) x 4 mm (diameter))..... 113
- Figure 4-14:** Number average length distribution of the extracted fibres from the P50RM composite bar (30 mm (length) x 4.5 mm (width) x 3.5 mm (thickness)) and rod (30 mm (length) x 4 mm (diameter)). 113
- Figure 4-15:** Optical binary images (5X) of polished cross-sections for (a) P50 RM bar and (b) P50 RM rod obtained via optical microscope. 114
- Figure 4-16:** Orientation angle distribution for P50 RM composite bar and rod..... 115
- Figure 4-17:** Schematic representation of the change in fibre orientation during rods manufacture (a) P50 RM plate and (b) P50 RM rod. Fibre reorientation (i.e, more fibres near to parallel with the extension axis) can be seen within the forged rods..... 117
- Figure 4-18:** SEM micrographs of a freeze fractured surface for (a) PLA plate and (b) PLA forged rod. PLA rod showed chain orientation..... 118
- Figure 4-19:** Schematic diagram for possible shapes of fibre cross-sections at the polished surface (grey plane)[54]. 119
- Figure 5-1:** The percentage change in wet mass of PLA, P50 RM, P50 UD and P40 UD composite rods immersed in PBS at 37°C. 136
- Figure 5-2:** pH change for PBS during immersion in PBS at 37°C for PLA alone, P50 RM, P50 UD and P40 UD composite rods. 136
- Figure 5-3:** The percentage change in mass loss with time for PLA alone, P50 RM, P50 UD and P40 UD composite rods during degradation in PBS at 37°C. 137
- Figure 5-4:** The percentage change in water uptake with time for PLA alone, P50 RM, P50 UD and P40 UD composite rods during degradation in PBS at 37°C. 138
- Figure 5-5:** Molecular weight retention for PLA, P50 RM, P50 UD and P40 UD composite rods over time during degradation in PBS at 37°C, ascertained using GPC. 138
- Figure 5-6:** Flexural strength versus time for PLA, P50 RM, P50 UD and P40 UD rods. Samples measured wet after immersion in PBS at 37°C. Sample dimensions were 80 mm length and 4 mm diameter. 140
- Figure 5-7:** Flexural modulus over time for PLA, P50 RM, P50 UD and P40 UD rods. Samples measured wet after immersion in PBS at 37°C. 140

- Figure 5-8:** Shear strength change against time for PLA, P50 RM, P50 UD and P40 UD rods. Samples were measured wet after immersion in PBS at 37°C. Sample dimensions were 30 mm length and 4 mm diameter. 141
- Figure 5-9:** The shear stiffness against degradation time for PLA, P50 RM, P50 UD and P40 UD rods. Samples measured wet after immersion in PBS at 37°C. 142
- Figure 5-10:** Compressive strength change against time for PLA, P50 RM, P50 UD and P40 UD rods. Samples measured wet after immersion in PBS at 37°C. Sample dimensions were 10 mm height and 4 mm diameter..... 143
- Figure 5-11:** Compressive stiffness change against time for PLA, P50 RM, P50 UD and P40 UD rods. Samples measured wet after immersion in PBS at 37°C. .. 143
- Figure 5-12:** Cumulative cations ion release versus time for PLA, P50 RM, P50 UD and P40 UD composite discs: (a) Sodium (Na^+), (b) Calcium (Ca^{2+}) and (c) Magnesium (Mg^{2+}). 145
- Figure 5-13:** Cumulative anions ion release versus time for PLA, P50 RM, P50 UD and P40 UD composite discs: (a) Orthophosphate (P O_4^{3-}), (b) Cyclic Trimetaphosphate ($\text{P}_3 \text{ O}_9^{3-}$), (c) Pyrophosphate ($\text{P}_2 \text{ O}_7^{4-}$) and (d) Tripolyphosphate ($\text{P}_3 \text{ O}_{10}^{5-}$). 147
- Figure 5-14:** Cytocompatibility assessment for PLA, P40 RM, P40 UD and P40 UD/RM composite. MSC cell attachment and growth of live cells (green) were visualised under a GFP-stereomicroscope over 2-day, 5-day and 20-day time points..... 149
- Figure 5-15:** Comparison of MSC proliferation and differentiation response on different composites after 20 day. (a) Alamar blue assay showing the metabolic activity observed for MSC cultured on the different composites. (b) MSC differentiation analysed by alkaline phosphatase activity and (c) Alizarin red staining showing the osteogenic response for composites. No statistical significant difference ($P > 0.05$) in cell proliferation and differentiation was seen between PLA and composites and *** is extremely significant ($P < 0.0001$). 151
- Figure 5-16:** Optical images for Alizarin red staining of cell-seeded PLA, P40 RM, P40 UD and P40 UD/RM composites..... 152
- Figure 5-17:** SEM micrographs of a freeze fractured surface for P50 RM, P50 UD and P40 UD composite rods (a), (b) and (c) before degradation, (d), (e) and (f) after 2 weeks of degradation in PBS at 37°C, (g), (h) and (i) after 4 weeks of degradation in PBS at 37°C, and (j), (k) and (l) after 9 weeks of degradation in PBS at 37°C. Scale bars for all micrographs represent 50 μm 154

Figure 5-18: Representative failure modes observed for P50 UD, P50 RM and P40 UD composite rods after compression test; (a) before degradation and (b) after 7 days of degradation in PBS at 37°C.	155
Figure 5-19: Change in molar normalised cation release at different time points against mass loss for composite rods (a) P50 RM and (b) P40 UD composite rods. Molar normalisation was calculated via dividing of amount of released cations by the molar concentration of the cation with the glass composition (0.16, 0.16 and 0.24 for Na, Ca and Mg respectively).	158
Figure 5-20: Change in anion release at different time points against mass loss for composite rods (a) P50 RM and (b) P40 UD composite rods.	159
Figure 5-21: Molar normalised rate of cations released (Na^+ , Ca^{2+} and Mg^{2+}) versus Dietzel's field strength. Molar normalisation was calculated via dividing of rate of released cations by the molar concentration of the cation with the glass composition (0.16, 0.16 and 0.24 for Na, Ca and Mg respectively).	161
Figure 6-1: (a) Photograph of the mould used for manufacturing screws and (b) Dimensions (mm) of the produced screws.	175
Figure 6-2: (a) Optical and (b) X-ray photographs for PLA, P40 UD and P40 UD/RM screws used in this chapter.	176
Figure 6-3: Mechanical testing setup for (a) Screw pull-out, (b) headless screw pull-out and push-out, (c) screw push-out and (d) torsional test.	179
Figure 6-4: Example of applied force against deflection plot during different mechanical tests for screws. The stiffness was determined as the maximum gradient of the linear portion of the force-deflection curve.	180
Figure 6-5: Flexural load to failure and stiffness for PLA, P40 UD and P40 UD/RM screws.	181
Figure 6-6: Axial pull-out strength and stiffness for PLA, P40 UD and P40 UD/RM screws.	182
Figure 6-7: Axial pull-out strength and stiffness for PLA, P40 UD and P40 UD/RM headless screws.	183
Figure 6-8: Push-out load to failure and stiffness for PLA, P40 UD and P40 UD/RM screws.	183
Figure 6-9: Push-out load to failure and stiffness for PLA, P40 UD and P40 UD/RM headless screws.	184
Figure 6-10: Shear load to failure and stiffness for PLA, P40 UD and P40 UD/RM screws.	185

Figure 6-11: <i>Maximum torque, breaking angle and torsional stiffness for PLA, P40 UD and P40 UD/RM screws.....</i>	185
Figure 6-12: <i>The percentage change in wet mass of PLA, P40 UD/RM and P40 UD composite screws immersed in PBS at 37°C.....</i>	187
Figure 6-13: <i>pH change during immersion in PBS at 37°C for PLA alone, P40 UD/RM and P40 UD composite screws.</i>	188
Figure 6-14: <i>The percentage loss of mass with time for PLA alone, P40 UD/RM and P40 UD composite screws during degradation in PBS at 37°C.</i>	189
Figure 6-15: <i>The percentage change in water uptake with time for PLA alone, P40 UD/RM and P40 UD composite screws during degradation in PBS at 37°C.</i>	189
Figure 6-16: <i>Flexural load to failure against time for PLA, P40 UD/RM and P40 UD screws. Samples measured wet, after immersion in PBS at 37°C.</i>	190
Figure 6-17: <i>Change in flexural stiffness against time for PLA, P40 UD/RM and P40 UD screws. Samples measured wet, after immersion in PBS at 37°C.</i>	191
Figure 6-18: <i>Axial pull-out strength over time for PLA, P40 UD/RM and P40 UD screws. Samples measured wet, after immersion in PBS at 37°C.</i>	192
Figure 6-19: <i>Pull-out stiffness over time for PLA, P40 UD/RM and P40 UD screws. Samples measured wet, after immersion in PBS at 37°C.</i>	192
Figure 6-20: <i>Shear load to failure versus time for PLA, P40UD/RM and P40 UD screws. Samples measured wet, after immersion in PBS at 37°C.</i>	193
Figure 6-21: <i>Shear stiffness versus time for PLA, P40UD/RM and P40 UD screws. Samples measured wet, after immersion in PBS at 37°C.</i>	194
Figure 6-22: <i>SEM micrographs of a fractured surface after flexural test for (a) P40 UD screw before degradation, (b) P40 UD screw after 6 weeks of degradation in PBS at 37°C, (c) P40 UD/RM screw before degradation and (d) P40 UD/RM screw after 6 weeks of degradation in PBS at 37°C. Scale bars for all micrographs represent 50 µm.</i>	195
Figure 6-23: <i>Failure modes associated with the pull-out test for the screws (a) tensile fracture at the core, (b) stripping of the external thread and (c) stripping of the internal thread [27].</i>	198
Figure 7-1: <i>Photographs of the rod and screw prepared via forging process.</i>	217

LIST OF TABLES:

Table 1-1: <i>Mechanical properties of human cortical and cancellous bone [2, 3, 7-9].....</i>	2
Table 2-1: <i>Mechanical properties for metallic biomaterials for orthopaedic applications [16, 18, 19].....</i>	15
Table 2-2: <i>Degradation rate, physical and mechanical properties of common bioresorbable polymers for orthopaedics applications [17, 25, 27, 38-51]...</i>	20
Table 2-3: <i>Mechanical properties for some of particulate, self-reinforced and fibre reinforced composites.....</i>	26
Table 3-1: <i>Fibre volume fractions, mass fractions and sample codes for the composites.....</i>	67
Table 1-1: <i>Sample codes for the specimens investigated in this chapter, with associated fibre volume and mass fractions.....</i>	103
Table 1-2: <i>Rule of mixtures input data.....</i>	108
Table 1-3: <i>Comparison between the experimental and theoretical flexural modulus for PLA/PBG fibre reinforced composites.....</i>	120
Table 5-1: <i>Sample codes for the specimens investigated in this chapter, with associated fibre volume and mass fractions.....</i>	131
Table 6-1: <i>Fibre volume, mass fractions and sample codes for the specimens investigated in this chapter.....</i>	176
Table 6-2: <i>Modes of failure for PLA, P40 UD/RM and P40 UD screws from the different mechanical tests conducted.....</i>	186
Table 6-3: <i>Mechanical properties (Pull-out and Torque) for some commercial metallic and bioresorbable screws.....</i>	202

CHAPTER 1.

INTRODUCTION AND BACKGROUND

1.1 BONE

The main functions of bones within the body are to provide structural support for soft tissue, protect internal organs from injury and assist in movement by providing balance [1].

1.1.1 Structure of the bone

Bone is a natural composite material comprised of approximately 70% inorganic minerals, 22% collagen and 8% water by weight [2, 3]. The mineral phase contains calcium phosphate, calcium carbonate and small amounts of sodium, magnesium, and fluoride. Hydroxyapatite (HA) $[\text{Ca}_{10}(\text{PO}_4)_6(\text{OH})_2]$ crystals and amorphous calcium phosphate are the main constituents for the mineral component of bone. The mineral phase provides bone with mechanical strength and rigidity, whilst the flexibility of the bone is attributed to collagen fibres. Moreover, bone contains cells like osteoblasts and osteoclasts. Osteoblasts are responsible for bone formation, whilst osteoclasts are responsible for bone resorption [2, 3].

Bone can be classified into cortical (compact) and cancellous (spongy) bone (see **Figure 1-1**). Cortical bone is much stronger and denser than cancellous bone. Cancellous bone is a highly porous structure (the porosity is 75 -95 % of bone volume) and density for compact and spongy bone is 1.8 g. cm^{-3} and 0.2 g. cm^{-3} respectively [2]. The cortical bone represents about 80 % of the skeletal mass whereas about 20 % refers to cancellous bone [1].

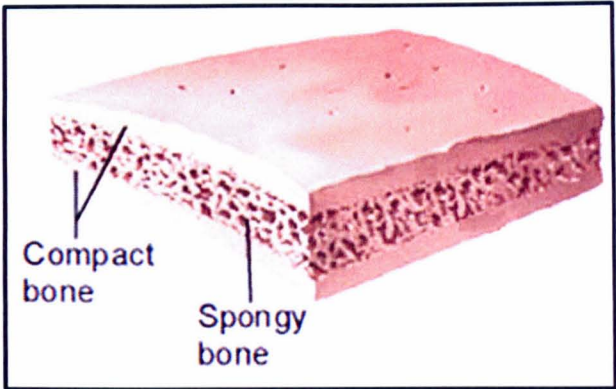


Figure 1-1: The structure of flat bones in the human body, cancellous bone sandwiched in-between sheets of cortical bone [4].

1.1.2 Mechanical properties of bone

The mechanical properties for cortical and cancellous bone are reported in **Table 1-1** below. The large range of values is down to the properties varying between bone location, testing conditions, age, sex and health [5, 6].

Table 1-1: Mechanical properties of human cortical and cancellous bone [2, 3, 7-9].

Properties	Cortical bone		Cancellous bone	
	Modulus (GPa)	Strength (MPa)	Modulus (GPa)	Strength (MPa)
Tensile	7 - 28	90 - 190	0.4	7 - 20
Compression	14 - 34	130 - 295	0.01 – 1.5	1.5 - 38
Bending	5 - 23	35 - 280	0.05 – 0.34	1 - 9
Shear	3.1 – 3.7	50 - 75		

1.1.3 Bone fractures

Bone fractures usually occur as a result of exposure to high impact during accidents (falling from a high place, sports injuries and road traffic accidents). Long bone fractures can be classified into eight categories as follows;

1. Open or compound; broken bone protrudes through the skin,
2. Closed or simple; the skin is intact at the bone fracture site,
3. Incomplete; partial breakage within the bone such as a crack,
4. Complete; bone splits into two fragments,
5. Comminuted; bone is broken into more than two fragments,
6. Transverse; bone is fractured at the right angle with respect to bone axis,
7. Spiral; helical fractures result from twisting of the bone,
8. Oblique; these fractures occur at 45° (diagonal) to the axis of the bone (see **Figure 1-2** for diagrammatic examples).

This classification is based on; severity of the injury (1 and 2 above); shape of the fracture (3 to 5 above) and direction of the fracture (6 to 8 above) [4, 10, 11].

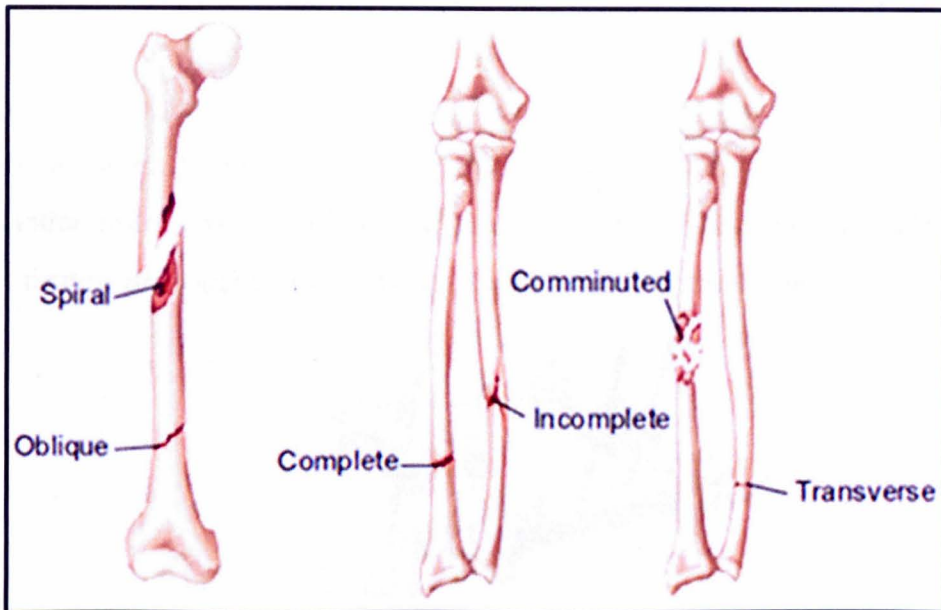


Figure 1-2: *Types of bone fractures* [4].

1.2 BONE FRACTURE FIXATION

Sufficient stability for bone fractures must be provided by fixation devices in order to reduce the interfragmentary mobility under external forces. Reducing movement of the fragments is essential for bone healing. Thus, fixation methods are assessed according to their capability to control the motion of the broken bone segments [10]. Bone fractures can be treated by using external or internal fixation devices or both in order to keep the fractured fragments at their positions during the healing period [12].

1.2.1 External bone fixation

Splinting (plaster cast) is the traditional and non-operative method of external bone fixation to align broken bone fragments. This method is suitable for closed and simple fractures. Bone shortening, joint stiffness, malunion and weakness of the muscles are common complications following the splinting method [13]. External and internal fixation devices are alternatives to reduce limitations and drawbacks associated with splinting. External fixators are commonly made of steel, titanium or carbon fibre composites [14]. The external fixator inserts away from the injury to temporarily stabilise the fragments and is composed of screws or wires connected to external bars (see **Figure 1-3** below). Deep infection associated with these screws and wires is the main complication of external fixation devices. Possibilities of fracture at pin tract, difficulty of set up, insertion of pins and screws into soft tissue and motion restriction are further disadvantages for this method of fixation [15, 16]. These fixators are usually removed after the bone fracture has healed.

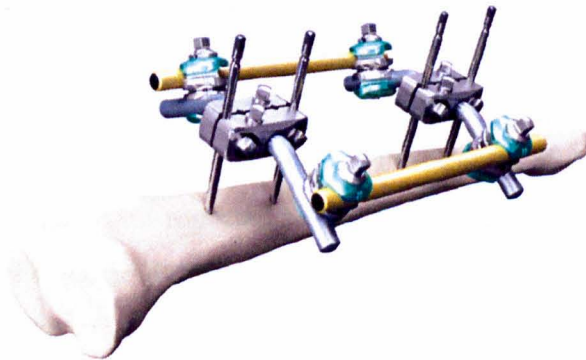


Figure 1-3: Model for fixation of long bone fractures by external fixation system [14].

1.2.2 Internal bone fixation

Internal fixation devices are implanted inside the body (i.e. close to the bone fracture) to stabilise bone fragments and promote healing [10]. There are four kinds of internal fixators; wires, intramedullary rods or nails, plates and screws.

1.2.2.1 Wire fixation

Wires are the simplest internal fixation devices used to hold broken bone fragments together. Wires either as multifilament or monofilament are used for simple fractures such as wrist fractures. Wires can also be used as supplement fixators for long bone oblique or spiral fractures (Cerclage wiring technique). Fatigue and corrosion of the metallic wires (Kirschner wires) are the most common complications associated with this type of fixation [15, 17].

1.2.2.2 Intramedullary nail (IM)

An intramedullary nail is a tube or rod that is inserted into the medullary cavity of a long bone (see **Figure 1-4**) such as a femur in order to support and align the bone fragments by acting as an internal splint [18]. The diameter of the nails is commonly 0.5 mm greater than that for the intramedullary canal to ensure tight fixation [10]. The nails can be locked at the ends by using interlocking screws that pass through cortical bone and holes machined into the nails providing compression, bending and torsional stability and obviate shortening of the healing bone [18]. Commercial nails have been made out of 316L stainless steel or titanium traditionally and are available as longitudinal slotted and non-slotted tubes [13, 19]. Eveleigh [13] described intramedullary nails as load sharing devices as they are able initially to support the majority of load and then share it with the healing bone. Furthermore, intramedullary nails have advantages of early mobilisation, joint movement and guarantee bone union [20, 21]. Disturbance of the normal biological environment during nail insertion has been reported to initially affect the bone healing process [13]. The stability of fracture fixation depends essentially on the fitting of the nail into the intramedullary canal and the mechanical properties of the nail and screws [10]. Delay and non-union for fractured bone have been reported which were associated with loosening of the nail [22].



Figure 1-4: Intramedullary nail with interlocking screws at proximal and distal ends [18].

1.2.2.3 Bone plate

Various shapes and sizes of bone plates are commercially available in order to accommodate bone fractures at different sites within the body (see *Figure 1-5*). Plates are provided with holes for locking screws [15]. The mechanical properties of the plates should be high to endure the bending forces created by the muscles particularly in femoral and tibial fractures. Adequate tightening of the plates to the bone via screws is also essential for secure fixation. Over-tightening the screws may cause failure for the fixation due to screw deformation or fracture of the bone fragment [17].

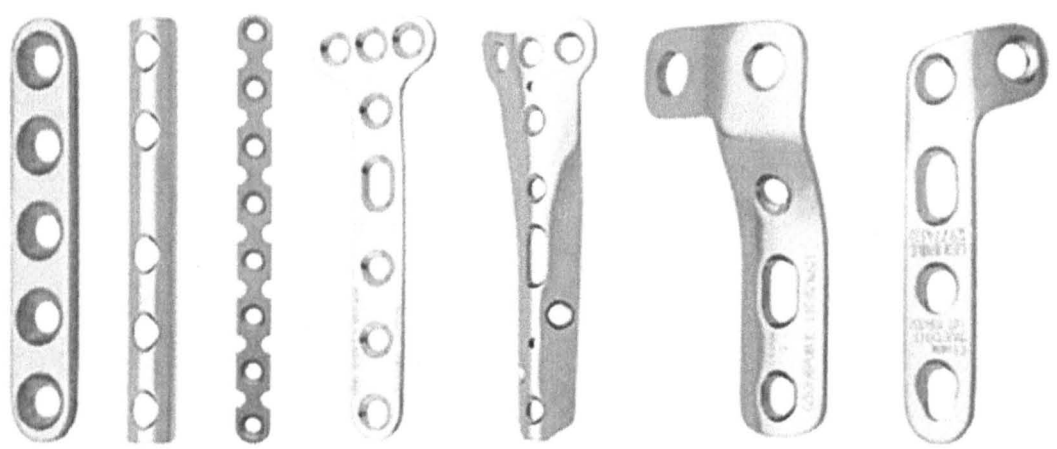


Figure 1-5: Different shapes of commercial metallic bone plates [23].

1.2.2.4 Bone screws

Screws are very efficient internal fixation devices; they can be used solely or in combination with plates and/or intramedullary nails [16]. Screw fixation alone is rarely used for fractures particularly in long bones to avoid potential fixation failure [15].

Screws are classified into cancellous and cortical according to the requirements of the bone that needs fixation. Cancellous and cortical screws are available commercially as fully or partially threaded with different dimension depending on the application (see **Figure 1-6**). Cancellous screws are designed to fix to the metaphysis and epiphysis of long bones where cancellous bone is abundant, utilising a larger surface area to spread the load in a considerably weaker bone structure [24]. Thread depth and pitch for cancellous screws are greater than those for cortical screws. Screws can be classified into self-tapping and non self-tapping. The non self-tapping screws require pre-tapping the bone prior to insertion. There are two different designs for the screw threads; buttress thread and V-shaped thread (see **Figure 1-7**). It was found that either of the screws type or the thread design had a significant effect on the pull-out strength (holding power). Pull-out strength plays a crucial role in the selection of screws, which depends also on the size of the screws and the intrinsic mechanical properties of the screw material [15, 17].



Figure 1-6: *Different types of commercial metallic cancellous and cortical screws [25].*

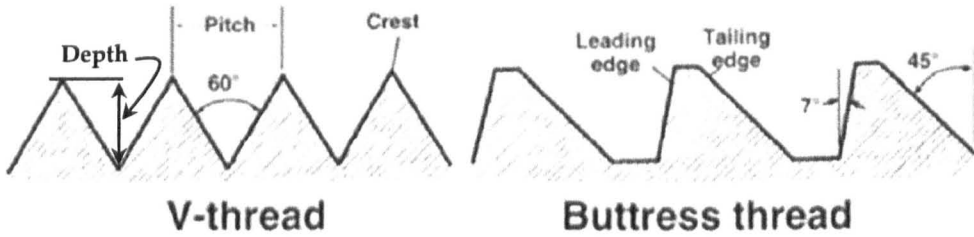


Figure 1-7: *Types of thread in bone screws [17].*

The important parameters for screw design are minor diameter, major diameter, thread depth and pitch. Pitch is the distance between two successive crests and minor and major diameters are the smallest (core) and the outer diameter for the screw thread. Thread depth represents half of the difference between the outer and core diameters of the screw. These design parameters greatly influence the performance of the screws such as holding power [6, 26]. Increase in outer thread diameter, depth and length of the engaged portion of screw thread in the bone would increase the volume of bone captured by the screw thread and this would lead to an increase in the holding power of the screw. Conversely, the holding power would decrease by decreasing the inner thread diameter and pitch [6, 26, 27].

1.2.3 Bone healing

The fracture repair process for the bone follows the sequence of inflammation, formation of callus (healing) and finally bone remodelling [28]. Inflammation occurs immediately after the fracture and lasts for approximately 3 days, followed by a reparative response for about two weeks. Afterwards, the callus (provisional bone) is formed and once the amount of callus is enough to bridge the fracture ends, the bone remodelling process ensues [15].

The healing process can be classified into primary and secondary healing depending on fixation stability. Rigid fixation hinders interfragmentary motion and leads to healing without callus formation (primary healing). In contrast, when less rigid fixation is used, secondary healing is achieved by callus formation as a result of interfragmentary movement [15]. The majority of bone fractures heal by the secondary bone healing route. Although, fracture healing processes can be accelerated via electrical, electromagnetic, ultrasound and mechanical stimulation [17]. It was also found that minerals such as calcium, phosphorus and magnesium

control the rate of bone healing [1]. The complete healing period depends on the age, health and type of bone [11] and healing for cancellous bone is faster than for cortical bone (4-6 weeks for cancellous and 12 – 24 weeks for cortical bone) [29].

1.3 AIMS AND OBJECTIVES

The main aim of the work conducted was to manufacture totally bioresorbable internal bone fixation devices such as intramedullary rods and screws. An ideal implant should provide optimum properties in order to maintain secure fixation of the bone fractures, which include;

- 1) the ability to resorb over time to avoid implant removal surgery,
- 2) bioactivity to improve the interface with the surrounding tissue,
- 3) high initial mechanical properties to sustain stress applied during the insertion procedure (i.e. match the mechanical properties of cortical bone),
- 4) gradual/controlled mechanical property loss with degradation time allowing stress transfer to the healing bone in order to strengthen newly remodelled bone and consequently hinder bone atrophy due to stress shielding,
- 5) capable of maintaining the required proportion of mechanical properties (i.e. greater than the inferior limit of cortical bone properties) till the end of the healing period (around 8 to 12 weeks [30]) to keep the fixation secure.
- 6) biocompatibility of degradation products,
- 7) appropriate degradation rate to eliminate inflammation associated with acidic breakdown products as a result of fast degradation.

The objectives to be achieved in order to produce bioresorbable implants with most of the requirements mentioned above can be outlined as;

- 1) Selection of appropriate materials for this purpose based on the literature review,
- 2) Composite preparation and characterisation to examine their suitability for the applications proposed,
- 3) Preparation of fibre reinforced composite rods,
- 4) Investigation of initial mechanical properties, mechanical retention and degradation profile for the rods produced,

- 5) Fabrication of screws based on fibre reinforced composites and investigation of initial mechanical properties, degradation behaviour and mechanical retention throughout *in vitro* degradation.

This work explores the manufacturing of fully bioresorbable fibre-reinforced composite rods and screws using a novel method (thermomechanical deformation or forging) for such applications. To the knowledge of the author, no data has been previously presented within the literature for bioresorbable inorganic fibre-reinforced composite rods or screws.

1.4 THESIS LAYOUT

Bone structure and mechanical properties have been presented to highlight target properties for the implants devised. Types of bone fractures and different fixation techniques have been covered in Chapter 1. Following this introduction and background, Chapter 2 will present a literature review on the different types of implant materials used to manufacture implants for biomedical applications such as metals, ceramics, polymers and composites.

Chapter 3 presents the fabrication and characterisation of phosphate glass fibre reinforced polylactic acid composite (PLA/PGF). Degradation profiles and mechanical property retention over time (95 days) will be reported for the composites degraded in phosphate buffered saline (PBS) at 37°C. Cytocompatibility of the composites was also examined by cell viability and attachment using human osteosarcoma cell lines.

Chapter 4 illustrates the preparation method used for PLA/PGF composite rods via forging of the composite plates at ~ 90°C. Initial mechanical properties (flexural, shear and compressive) were measured for the rods. Optical microscopy was used to characterise fibre length and orientation distribution.

In vitro degradation, mechanical retention and biocompatibility properties for the composite rods manufactured are covered in chapter 5. Furthermore, quantitative analysis was conducted for the ions released during degradation of the composite rods.

Chapter 6 describes the manufacture procedure for PLA/PGF composite screws via a forging technique. Several mechanical tests were conducted for the screws such as

pull-out, push-out, flexural, double shear and torsion. Basic theoretical calculations for screw threads were used to predict the pull-out strength and explain the failure mode of the screws. *In vitro* degradation and retention of mechanical properties were also conducted for the screws throughout 42 days in PBS at 37°C.

Finally, Chapter 7 presents a synergistic summary bringing together the main conclusions and highlights recommendations for future work.

1.5 REFERENCES

1. Tortora, G.J., *Introduction to the human body*, 1988, New York: Harper & Row.
2. Athanasiou, K.A., C.F. Zhu, D.R. Lancot, C.M. Agrawal, and X. Wang, *Fundamentals of Biomechanics in Tissue Engineering of Bone*. *Tissue Engineering*, 2000. 6(4): p. 361-381.
3. Nather, A., *Bone grafts and bone substitutes: basic science and clinical applications* 2005: World Scientific.
4. Tate, P., *Seeley's Principles of Anatomy & Physiology Connect Plus Access Card*. second ed 2012: McGraw-Hill Science Engineering, ch.6, p.129.
5. Evans, F.G., *Factors affecting the mechanical properties of bone*. *Bull N Y Acad Med*, 1973. 49(9): p. 751-64.
6. An, Y. and R. Draughn, *Mechanical Testing of Bone and the Bone-Implant Interface* 1999: CRC.
7. Ramakrishna, S., J. Mayer, E. Wintermantel, and K.W. Leong, *Biomedical applications of polymer-composite materials: a review*. *Composites Science and Technology*, 2001. 61(9): p. 1189-1224.
8. Rho, J.-Y., L. Kuhn-Spearing, and P. Zioupos, *Mechanical properties and the hierarchical structure of bone*. *Medical Engineering & Physics*, 1998. 20(2): p. 92-102.
9. Reilly, D.T. and A.H. Burstein, *Review article. The mechanical properties of cortical bone*. *J Bone Joint Surg Am*, 1974. 56(5): p. 1001-22.
10. Mow, V.C. and R. Huiskes, *Basic orthopaedic biomechanics & mechano-biology*. Third ed 2005: Lippincott Williams & Wilkins.
11. Kampa, R.J., J. Pang, and R. Gleeson, *Broken bones and fractures - an audit of patients' perceptions*. *Ann R Coll Surg Engl*, 2006. 88(7): p. 663-6.
12. Wintermantel, E., *An introduction to biocomposites* 2004, London: Imperial college press.
13. Eveleigh, R.J., *A review of biomechanical studies of intramedullary nails*. *Medical Engineering & Physics*, 1995. 17(5): p. 323-331.
14. Mauffrey, C., D. Seligson, C. Roberts, and J. Statton, *External Fixation in Orthopedic Traumatology*: Springer.

15. Wnek, G.E. and G.L. Bowlin, *Encyclopedia of Biomaterials and Biomedical Engineering, Second Edition (Four-Volume Set)*2008: Informa Healthcare.
16. Rüedi, T.P. and W.M. Murphy, *AO principles of fracture management*2000, Stuttgart; New York; Davos Platz, [Switzerland]: Thieme ; AO Pub.
17. Park, J.B. and R.S. Lakes, *Biomaterials : an introduction*2007, New York: Springer.
18. Bong, M.R., F.J. Kummer, K.J. Koval, and K.A. Egol, *Intramedullary nailing of the lower extremity: biomechanics and biology*. *J Am Acad Orthop Surg*, 2007. 15(2): p. 97-106.
19. Lewis, D., C. Lutton, L. Wilson, R. Crawford, and B. Goss, *Low cost polymer intramedullary nails for fracture fixation: a biomechanical study in a porcine femur model*. *Archives of Orthopaedic and Trauma Surgery*, 2009. 129(6): p. 817-822.
20. Toms, A.D., R.L. Morgan-Jones, and R. Spencer-Jones, *Intramedullary femoral nailing: removing the nail improves subjective outcome*. *Injury*, 2002. 33(3): p. 247-249.
21. Weinstein, A.M., A.J. Clemow, W. Starkebaum, M. Milicic, J.J. Klawitter, and H.B. Skinner, *Retrieval and analysis of intramedullary rods*. *J Bone Joint Surg Am*, 1981. 63(9): p. 1443-8.
22. Thakur, A.J., *The elements of fracture fixation*1997: Churchill Livingstone.
23. <http://www.medin.eu/upload/catalogs/catalog-of-traumatology-plates.pdf>.
24. Lawson, K.J. and J. Brems, *Effect of insertion torque on bone screw pullout strength*. *Orthopedics*, 2001. 24(5): p. 451-4.
25. https://productlit.synthes.com/prod_support/Product%20Support%20Materials/Technique%20Guides/VET/SUTGCRIF7322B.pdf.
26. Chapman, J.R., R.M. Harrington, K.M. Lee, P.A. Anderson, A.F. Tencer, and D. Kowalski, *Factors Affecting the Pullout Strength of Cancellous Bone Screws*. *Journal of Biomechanical Engineering*, 1996. 118(3): p. 391-398.
27. Asnis, S.E., J.J. Ernberg, M.P.G. Bostrom, T.M. Wright, R.M. Harrington, A. Tencer, and M. Peterson, *Cancellous Bone Screw Thread Design and Holding Power*. *Journal of Orthopaedic Trauma*, 1996. 10(7): p. 462-469.
28. McKibbin, B., *The biology of fracture healing in long bones*. *J Bone Joint Surg Br*, 1978. 60-B(2): p. 150-62.
29. Törmälä, P., J. Vasenius, S. Vainionpää, J. Laiho, T. Pohjonen, and P. Rokkanen, *Ultra-high-strength absorbable self-reinforced polyglycolide (SR-PGA) composite rods for internal fixation of bone fractures: In vitro and in vivo study*. *Journal of Biomedical Materials Research*, 1991. 25(1): p. 1-22.
30. Furukawa, T., Y. Matsusue, T. Yasunaga, Y. Shikinami, M. Okuno, and T. Nakamura, *Biodegradation behavior of ultra-high-strength hydroxyapatite/poly (-lactide) composite rods for internal fixation of bone fractures*. *Biomaterials*, 2000. 21(9): p. 889-898.

CHAPTER 2.

LITERATURE REVIEW

2.1 INTRODUCTION

The majority of deaths around the world related to those under the age of 40 are mainly due to trauma and especially accidental injuries. In 1998, approximately 5.8 million deaths in the worldwide population were due to road traffic injuries. The probability of disability after trauma is high in comparison to other diseases consequences [1].

The orthopaedic market has improved markedly since 1993 from around \$5 billion to \$35 billion revenue generation at the end of 2008. Furthermore, it was expected that by 2020 approximately 167 million of the global population will suffer from different orthopaedic problems e.g. fractures, back pain, osteoarthritis and arthritis. Fractures will represent ~ 78 % of these cases [2].

Biomaterials technologies have been developed during the last few decades, which reflect enhancement in quality of life [3]. However, biodegradable devices in the USA were around \$300 billion in 1995 and orthopaedic implants represented only 5% and the rest was for sutures. The orthopaedic market is improving by around 6 % a year and this is due to the advantages of biodegradable polymers over metals (which will be discussed later in this chapter) [4]. Recently, almost every orthopaedic manufacturer has started producing bioabsorbable implants beside the traditional metallic devices [5].

2.2 IMPLANT MATERIALS

Synthetic materials intended for use in contact with biological systems to replace living systems or functions of the body are called biomaterials [6]. Thus, biocompatibility is a key parameter in the selection of materials for biomedical applications. According to Williams dictionary [6], biocompatibility is defined as “the ability of a material to perform with an appropriate host response in a specific

application''. Hench *et al.* [7] divided biomaterials into three generations. The first generation was developed in the 1960s and 1970s to match the physical properties of the tissue replaced. Biologically inert is the common feature of 1st generation biomaterials. Bioactive and bioresorbable materials were classified as 2nd generation. They suggested that 3rd generation of biomaterials would be bioactive, bioresorbable and biofunctional (i.e. their degradation products would be able to stimulate tissue regeneration) [8]. Abou Neel *et al.* [9] considered phosphate based glasses as a third generation biomaterial.

There are some key features that should be present in implant materials; (i) biocompatible with the surrounding living tissues, (ii) nontoxic and non carcinogenic, (iii) appropriate mechanical properties (i.e. matches cortical bone properties), (iv) high resistance to fatigue and (v) ease of processability [10].

2.2.1 Metallic implant materials

Metals have been utilised for biomedical applications such as bone fracture fixation devices (plates, nails, wires and screws) due to their excellent mechanical properties (see Table 2-1). Stainless steel, cobalt-chromium-molybdenum alloys (Vitallium), titanium and its alloys are the most common metals used as orthopaedic devices [11-13]. Although metallic devices offer good stability for fractures, several problems were raised after their application [14]. Complications associated with metals as implants include [11];

- removal (i.e. second surgery) after healing of the fracture,
- corrosion and toxicity of the corrosion products,
- vast mismatch in elastic moduli between metals and bone, causing stress shielding (see Table 2-1),
- lack of bioactivity,
- high density; which results in elevated stresses on the surrounding tissues,
- difficulty of examination with magnetic resonance imaging (MRI).

The stiffness mismatch between bone and metals allows metallic implants to carry the majority of load, whilst applied load on the healing bone is minor [16]. Wolff’s law stated that the structure of bones was controlled by the applied stresses [6]. Therefore, weak bone (bone atrophy) could be formed after fracture healing particularly in vicinity of the implant [14]. Furthermore, re-fracture of the healed bone would probably occur during/after implant removal [17]. In order to overcome these complications, polymers were presented as a possible alternative.

Recently, biodegradable metals such as magnesium alloys have attracted a great attention for biomedical applications such as coronary stent. Biodegradable metallic stents have been assessed *in vitro*, *in vivo* and clinically and showed good results. However, more investigations for the interaction between cells and degradation products should be considered. Biodegradable magnesium based alloys have several advantages over traditional metallic biomaterials (e.g. stainless steel and titanium); fast corrosion rate in the physiological environment, light weight, lower mechanical properties (220 MPa for Tensile strength and 44 GPa for Young’s modulus) [18, 19]. Moreover, their mechanical and physical properties are close to those for natural bone and removal surgery is not required after bone healing. However, fast degradation rate of magnesium alloys in human body fluid is the main limitation for their use as bone fixation devices [20].

Table 2-1: *Mechanical properties for metallic biomaterials for orthopaedic applications in comparison to cortical bone [16, 21, 22].*

Material	Tensile modulus (GPa)	Tensile strength (MPa)
Stainless steel	190 - 210	465 - 950
Vitallium alloys	210 - 230	600 - 1785
Titanium and titanium alloys	105 - 116	785 - 1021
Cortical bone	7 - 28	90 - 190

2.2.2 Polymeric implant materials

Polymeric materials are useful for various applications due to their advantages such as low cost, wide range of mechanical and physical properties and ease of fabrication into films, textiles, rods, fibres and gels [3, 12]. Polymers can be divided into two categories based on their durability in biological environments; biostable and biodegradable [6]. Polymers such as polyethylene (PE), poly (methyl methacrylate) (PMMA) and polyetheretherketone (PEEK) are examples of biostable and biocompatible polymers which have been used in various medical applications such as hip replacements and dental implants [16]. Ultrahigh molecular weight polyethylene (UHMWPE) has also been used extensively for hip and knee joints [12].

Biodegradable polymers are able to breakdown gradually over time in a physiological environment into biocompatible degradation products [23]. Biodegradable polymers such as poly(ϵ -caprolactone) (PCL), poly(glycolic acid) (PGA), poly(lactic acid) (PLA) and poly(lactic-co-glycolic acid) (PLGA) have been paid a great deal of attention for biomedical purposes especially for bone fixation devices. These polymers are available in different forms (e.g. sutures, plates, rods, pins and screws) as internal fixators for bone fracture. There are several advantages of biodegradable polymers over their metal counterparts for fixation [24, 25];

- they are biodegradable and as such removal surgery is not required,
- more economical than metallic devices,
- can be reformed more easily in surgery,
- degradation over time allows the applied stress to gradually transfer to healing bone (i.e. obviating stress shielding and the bone atrophy effect),
- degradation products are biocompatible and can be excreted easily through the natural pathways (i.e. bioresorption process) [26].

Juutilainen *et al.* [25] compared the cost of repairing ankle fractures using bioresorbable and metallic implants. They found that the use of bioresorbable devices saved 13 % - 22 % of the cost for metallic implants. They ascribed this reduction in expenses to reduced periods of stay in hospitals, reduced cost of care and dispensing with removal surgery.

The ideal polymer for biomedical application should have appropriate mechanical properties and degradation time to the required application. It should also be easy to sterilise and have good shelf life [17].

2.2.2.1 Degradation of bioresorbable polymers

Polymers degrade by random chain and chain-end scission to produce short chain oligomers and monomers [27]. Polymers can undergo four types of degradation namely; thermal, mechanical, hydrolytic, enzymatic and radiation. Polymers degrade thermally during manufacturing and processing due to holding at higher temperature (i.e. above the melting temperature) for longer periods. Polymeric materials might be also degraded as a result of applied stress on the implant during application such as bone plates and screws. Sterilisation of implants is essential before implantation and gamma radiation is one of the most common sterilisation techniques used [28].

Hydrolytic degradation refers to water hydrolysis or enzymatic hydrolysis in the biological environment [28]. The hydrolytic degradation profile for biodegradable polymers is generally divided into two stages. Stage I starts directly after implantation when water molecules cleave the long chains into several short chain oligomers (hydrolysis process). Consequently, the molecular weight for the polymer decreases, which results in loss of mechanical strength. Finally, mass loss would be observed (stage II) as presented in **Figure 2-1**. Therefore, biomechanical function of the implant could vanish before a significant decrease in their mass was detected [23, 29].

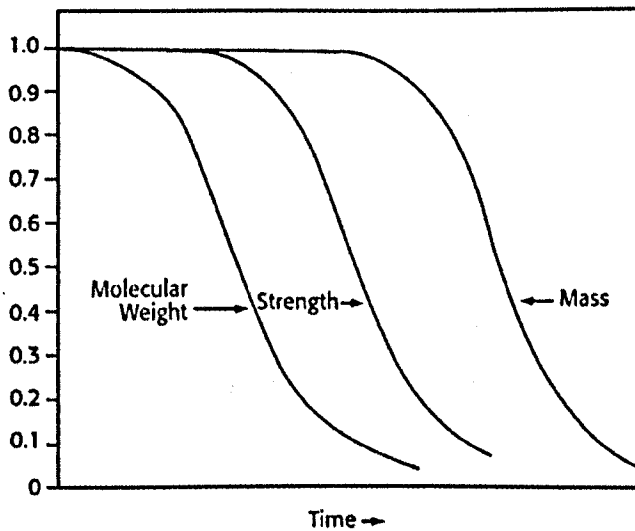


Figure 2-1: Sequence of reduction in molecular weight, mechanical strength and mass for bioresorbable polymers with the time during degradation process [23].

Hydrolytic degradation of poly(α -hydroxy)acids such as PLA is classified into surface or bulk erosion based on the diffusion rate of water into the polymer and the degradation rate of the polymer backbone via chain scission. Surface erosion (heterogeneous) occurs when the rate of chain scission is faster than the rate of water diffusion into the polymer. Gradual reduction in the thickness of material and stability of molecular weight for the interior polymer over time are indicative of surface degradation (see Figure 2-2a) [30].

On the other hand, the polymer will undergo bulk erosion if the diffusion rate of water into the polymer is faster than the rate of chain scission. Random chain scission throughout the whole material would happen creating a decrease in molecular weight (bulk erosion). Bulk erosion (homogenous) would continue gradually if the degradation by-products (oligomers) were able to leach into the surrounding medium (see Figure 2-2b). Otherwise, internal autocatalysis would be initiated by acidic media due to accumulation of carboxyl and hydroxyl end groups that result from cleavage of the ester bonds. Consequently, the interior erosion rate would be faster than surface erosion. This variation in degradation rate results in a bimodal molecular weight distribution (high at the surface and low inside the implant). Finally, a hollow structure would be produced after release of oligomers or monomers (see Figure 2-2c) [28, 31, 32]. Rapid leaching of degradation products (monomers or oligomers) at the latter stages of degradation has been associated with late inflammation with use of PLLA and PGA from *in vivo* studies [33-36].

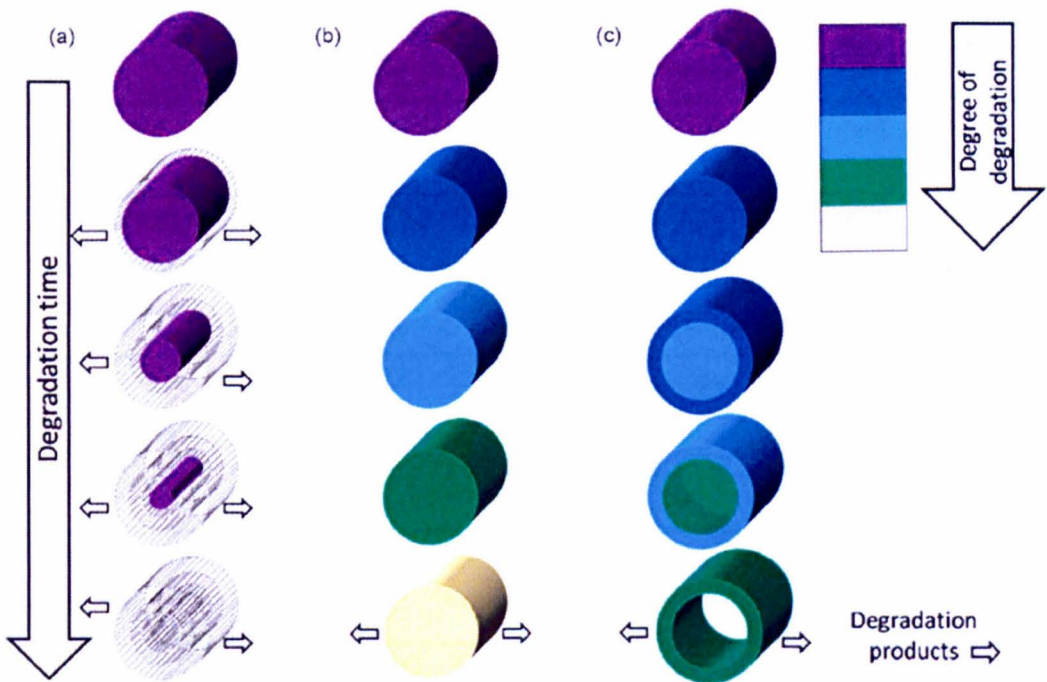


Figure 2-2: Mechanisms of bioresorbable polymers degradation; (a) surface erosion, (b) bulk degradation and (c) bulk degradation and autocatalysis [31].

The degradation rate of the polymeric implant depends on several factors such as crystallinity, mass, surface area, size, geometry, chemical composition, molecular weight, chain orientation, porosity, additives, site of implantation and applied stress. The degradation rate would decrease by increasing the molecular weight, crystallinity, mass and chain orientation within the device. Conversely, increase of porosity, stresses and exposed surface area would lead to an increase in degradation rates [17, 37-39]. MacDonald *et al.* [40] found that rate of mass loss decreased by approximately 90 % in comparison with amorphous PLA as the crystallinity increased to ~ 50 %. Tsuji *et al.* [41] investigated the effect of chain orientation on the degradation rate of PLLA fibres. They found that the rate of mass loss decreased by 75 % as compared to the undrawn specimen after drawing to draw ratio of ~ 1.4.

There are various sterilisation techniques for implants which include; autoclave, dry heat, ethylene oxide (EtO), electron beam and gamma radiation. Although there are issues with gamma radiation and ethylene oxide, such as high toxicity for EtO and the degradation effect of radiation, they are commonly used for sterilising polymeric devices [17, 42].

Table 2-2: Degradation rate, physical and mechanical properties of common bioresorbable polymers for orthopaedics applications [17, 29, 31, 42-55].

Property	PCL	PGA	PLLA	PDLLA	PLGA	POE
Glass transition temperature T_g (°C)	-60 - -65	35-45	55 - 65	50 - 60	40 - 50	70 - 98
Melting temperature T_m (°C)	58 - 65	220 - 233	170 - 200	am.	am.	am.
Elastic modulus (GPa) *	0.2 – 0.4	6 - 7	3 - 6	1 – 3.5	1 - 3	1 – 1.6
Flexural strength (MPa)	16 -29	195 - 375	109 - 145	95 - 130	~ 65	~ 65
Tensile strength (MPa)	20 - 35	60 - 80	50 - 80	20 - 60	40 - 55	~ 34
Degradation time (month) **	24 - 48	6 - 12	24 - 72	12 - 16	1 -12	-

*PCL: poly(ϵ -caprolactone), PGA: poly(glycolide), PDLLA: poly(DL-lactide), PLGA: poly(L-lactide-co-glycolide), PLLA: poly(L-lactide), POE: Poly(Ortho Ester) and am. refers to amorphous * Tensile or flexural modulus and ** represents the required time for complete resorption.*

2.2.2.2 Poly Lactic Acid (PLA)

PLA is the most common bioresorbable polymer for internal bone fixation implants due to appropriate degradation rates, good mechanical properties and availability in different chemical forms. The starting monomer (dilactide) can be extracted from natural sources e.g. starch and sugar and then polymerised via polycondensation, chain extension or ring-opening polymerisation to produce PLA polymer [56]. There are two isomers for PLA monomer; levo- (L-)lactide and dextro- (D-)lactide (see Figure 2-3) [24]. Therefore, it is possible to prepare PLLA (100 % Lactide) and PDLLA as a copolymer with different L- to D- lactide ratios. Resorption time, molecular weight, physical and mechanical properties for PDLLA depend on the L/D ratio [57, 58]. PLLA has high percentage of crystallinity, while crystallinity for

PDLLA depends on the amount of D-lactide. The crystallinity of PDLLA is high when D- concentration is less than 2 % and decreases as the D- content increases [56]. Degree of crystallinity has a significant effect on the degradation for polymers as mentioned early. Therefore, the degradation rate for PLLA is much slower than that for PDLLA [29].

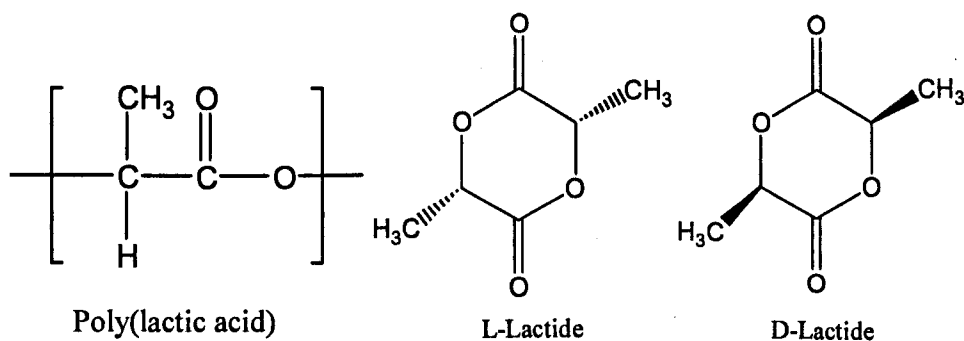


Figure 2-3: Chemical structure for PLA, L-lactide and D-lactide isomers [56].

PLA breaks down by hydrolysis into lactic acid which converts to carbon dioxide and water through the tricarboxylic acid cycle (TCA) (see Figure 2-4) [29, 59].

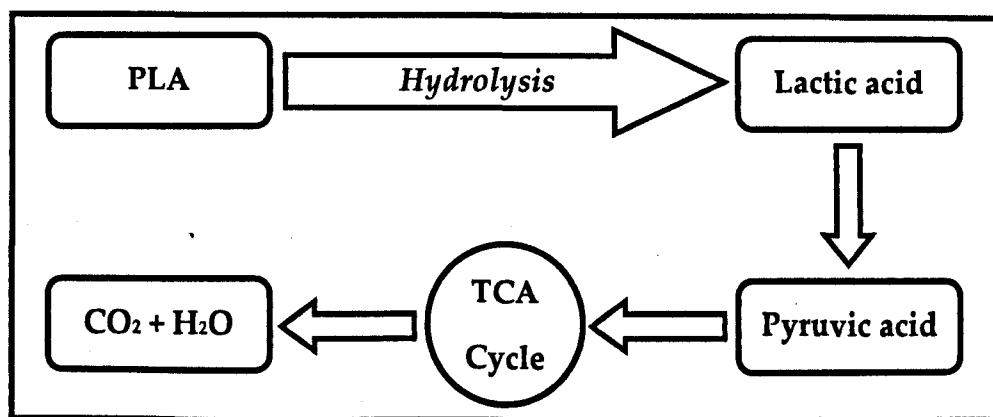


Figure 2-4: Schematic diagram for degradation of PLA as an example for bioresorbable polymers [29, 59].

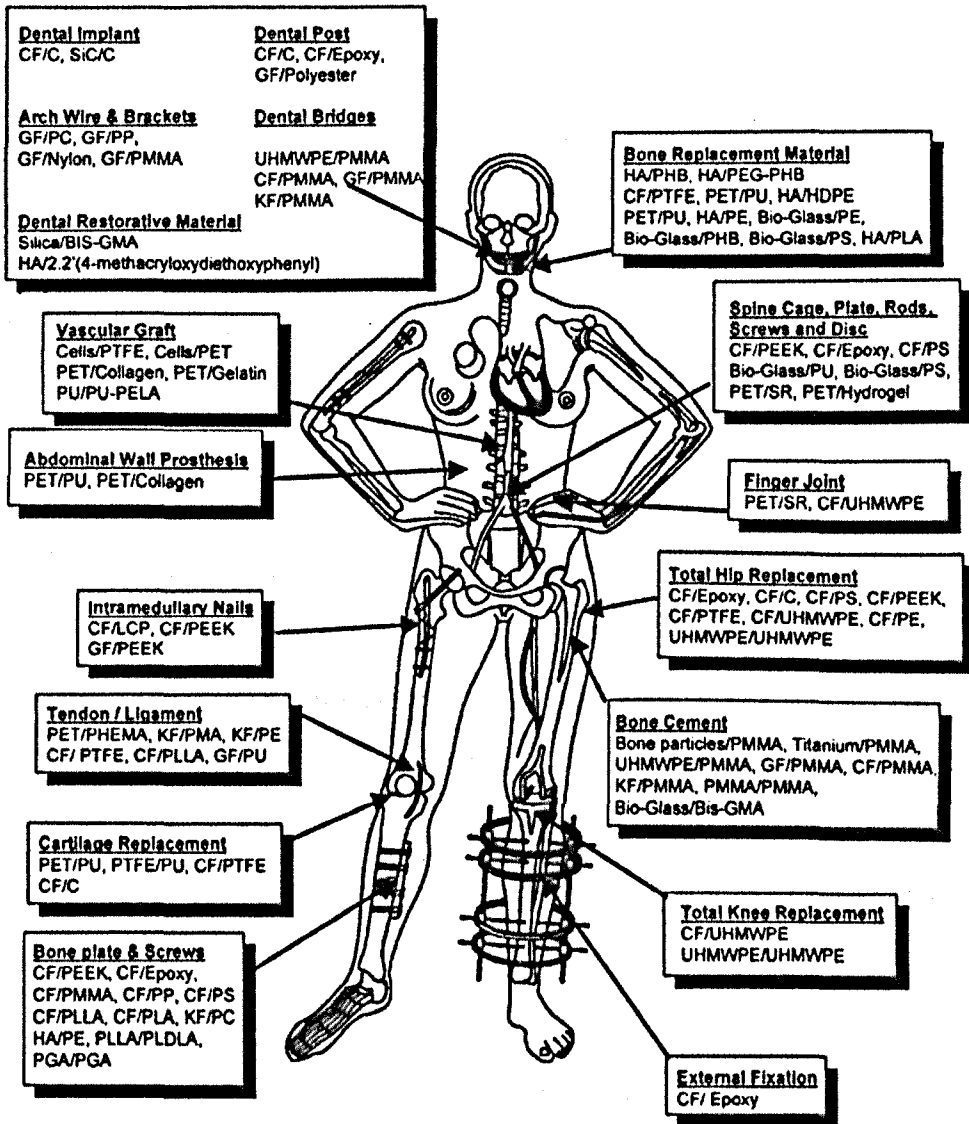
Mechanical properties are the principal limitation for widespread use of bioresorbable polymers. However, the mechanical characteristics for plain bioresorbable polymers are known to be sufficient for non-load bearing applications such as the cranial (skull) bones and maxillofacial fractures where high mechanical properties are not required as the applied stresses are not high [14]. Fractures at load bearing sites (e.g. femur and tibia) require sufficiently strong fixation devices

to avoid implant failure until the fractured bone has completely recovered. Therefore, reinforcement of these polymers is essential in order to produce composite implants with mechanical properties comparable to cortical bone. In order to produce totally bioresorbable implants, reinforcement should be made out of biocompatible and bioresorbable material. Totally bioresorbable composite devices could also eliminate potential inflammatory responses associated with use of some plain resorbable polymers. This inflammation was ascribed to the acidic degradation product of polymers such as lactic acid for PLA [33, 34, 60]. This acidity could be buffered via the degradation by-products of the reinforcements. Moreover, the amount of polymer (matrix) within the composite decreases at the expense of the reinforcement (i.e. the amount of releasing acidic product would also decrease).

2.2.3 Composite implants

A composite is a combination of two or more materials in order to achieve desired biological, mechanical, physical and/or chemical properties. Composites are comprised generally of a stiff and strong dispersed phase (reinforcement) and continuous phase (matrix). Properties of the composites depend on properties of the constituents as well as the geometry, size, distribution and volume fraction of the reinforcement phase. Furthermore, the bonding strength (adhesion) between the phases plays a crucial role in their properties. Increase in reinforcement (particles or fibres)/matrix bonding allows for effective load transfer leading to higher strength for the composite [61].

Biocomposites are composite materials that can be implanted inside the body to replace the function of living tissue [6]. They may be grouped into fully, partial and non bioresorbable composites based on the ability of the constituents to degrade and resorb within the body [16]. The matrix and reinforcement have to be bioresorbable for a fully bioresorbable composite (e.g. PCL/PGF, PLA/PGF [46, 62]), whilst both are biostable for non bioresorbable composites (e.g. ultra high molecular weight polyethylene/hydroxyapatite (UHMWPE/HA) [63]). For partial bioresorbable composites, one of the composite components (usually the reinforcement) is biostable (e.g. PLA/bioglass, PLA/carbon fibre [64-66]). **Figure 2-5** shows various types of biocomposites that have been investigated for different biomedical applications [67].



CF: carbon fibers, C: carbon, GF: glass fibers, KF: kevlar fibers, PMMA: Polymethylmethacrylate, PS: polysulfone, PP: Polypropylene, UHMWPE: ultra-high-molecular weight polyethylene, PLDLA: poly(L-DL-lactide), PLLA: poly (L-lactic acid), PGA: polglycolic acid, PC: polycarbonate, PEEK: polyetheretherketone; HA: hydroxyapatite, PMA: polymethylacrylate, BIS-GMA: bis-phenol A glycidyl methacrylate, PU: polyurethane, PTFE: polytetrafluoroethylene, PET: polyethyleneterephthalate, PEA: polyethylacrylate, SR: silicone rubber, PELA: Block co-polymer of lactic acid and polyethylene glycol, LCP: liquid crystalline polymer, PHB: polyhydroxybutyrate, PEG: polyethyleneglycol, PHEMA: poly(20hydroxyethyl methacrylate)

Figure 2-5: Biomedical applications for various biocomposites [16].

Composites can also be classified into particulate and fibre reinforced according to the geometry of the reinforcement phase.

2.2.3.1 Particulate biocomposites

Particulate composites consist of particles of one material embedded and dispersed in another material. The reinforcing particles are generally derived from stiff and

hard material such as ceramics, glasses and metals [61, 68]. Ease of manufacture (injection moulding) is the principal advantage of using particulate composites as implant materials. Their mechanical properties depend mainly on the particle-matrix interface, particle size and weight fraction. Fu *et al.* [61] reported that the mechanical stiffness for polymers could be enhanced by incorporation of stiff particles, whilst their strength mainly depends on the adhesion strength between the polymer and fillers which allow effective stress transfer from the matrix to the particles hence increase the strength. Moreover, the strength of particulate composites could decrease by incorporation of particles as a result of poor interface [68]. Size of the fillers has a clear effect on mechanical properties of the composites; smaller particles provide greater strength for polymer composites. Use of nanoparticle filler would result a significant increase in rigidity, strength and stiffness for the polymers [61, 69] which was attributed to the increase in the interfacial surface area for nanoparticles [70].

Bioceramics such as calcium phosphate and HA are common fillers used for particulate biocomposites [61, 71-73]. Bioceramics/bioglasses can be classified into bioinert, bioactive and bioresorbable according to their bioactivity. A bioinert material is stable in the physiological environment such as zirconia and alumina. A material able to promote particular biological activity such as bone remodelling is known as a bioactive material and Bioglass® and sintered hydroxyapatite (s-HA) are examples of this material [69, 74-77]. Finally, bioresorbable ceramics such as amorphous (uncalcined and unsintered) hydroxyapatite (u-HA) and Tricalcium phosphate (TCP) are able to degrade and be absorbed completely or eliminated by the body [6, 49, 78]. The degradation rate for crystalline HA is the slowest in comparison to other calcium phosphates. The dissolution rates for the calcium phosphates follow the order of amorphous HA >> TCP >> crystalline HA [45].

Bioactive glasses and ceramics (e.g. 45S5 Bioglass and HA), promote formation of a biologically active hydroxycarbonate apatite (HCA) layer on their surfaces when

implanted in the body. HCA deposit has equivalent structural and chemical composition to the mineral phase of the natural bone. Therefore, it can provide interfacial bond between the implant and the bone. It was also found that calcium phosphates (TCP) have also an excellent ability to form a bond with bone (excellent bioactivity) due to their similarity to the mineral constituent of the bone [79]. The main ingredients of the most bioactive glasses are SiO_2 , Na_2O , CaO and P_2O_5 . However, these glasses are not generally bioresorbable. Ions like Ca, P, Na and Si can be released from the glass surfaces which could stimulate cellular responses [45]. Osteoconduction is the process of bone growing and remodelling on a surface such as bioactive glasses, whilst osteoinduction represents stimulation process for bone formation [6, 80]. It was reported that calcium phosphates are an osteoconductive material but they do not have osteoinductive ability [45].

Examples for the particulate composites are reported in Table 2-3. HA is the most common filler for bone fixation applications [49, 81-84]. It was reported that released particles (from matrix or reinforcement phases) after deterioration of the implant could stimulate inflammation in the surrounding tissues [49]. The effect of these particles will depend on their size and shape and not on biocompatibility or chemical composition. Irregular and small particles (less than 20 μm) have greater influence than spherical and larger particles (50 – 350 μm) [85]. Tissue inflammation was reportedly associated with particles not only made of bioinert materials (high density of polyethylene) but also to biocompatible materials (sintered HA) [49, 85]. Conversely, no signs of inflammation were seen for PLLA rods reinforced with calcined and uncalcined HA (c-HA and u-HA) implanted into the medullary canal of rabbits for 4 years [86, 87]. This referred to dissolution of c-HA and u-HA over time in physiological medium which was confirmed via SEM analysis at the end of the study. Therefore, inflammation effects could be reduced or eliminated via use of fully resorbable fillers.

Table 2-3: Mechanical properties for some of particulate, self-reinforced and fibre reinforced composites manufactured by melt impregnation.

Composite	Sample geometry	Flexural Modulus (GPa)	Flexural Strength (MPa)	Shear strength (MPa)	Ref.
Cortical bone	NA	5 - 23	35 - 280	50 - 75	[16, 22]
<i>Particulate composites</i>					
PCL-PBG	Plate	~ 1.8	~ 17		[47]
Chitosan - HA	Rod	~ 3.4	~ 86		[81]
PLLA-u-HA	Rod, plates	7 - 12	250 - 270	127 - 144	[49, 82, 84, 86, 88]
PLLA-c-HA	Rod	7.8 – 10	130 - 280		[82, 86, 88, 89]
PLLA- β -CMP	Rod	~ 4.4	~ 126		[90]
PLLA- β -TCP	Plate	4.2 – 4.6	80 - 92		[91]
PLLA-CaP	Rod	~ 3.7	~ 95		[92]
PLLA/PCL/HA **	Plate	2.3 - 6	50 - 120		[83]
PLLA/BG	Plate	~ 3.3	~ 234	~ 128	[93]
<i>Self-reinforced composites</i>					
Sintered SR-PGA	Rod	~ 10	~ 350	~ 180	[94-96]
Extruded SR-PDLLA ^o	Rod	3.6 - 8.8	125 - 237	90 - 157	[97-100]
Sintered SR-PLA	Rod		~ 270	~ 94	[101]
Drawn (λ 12) SR-PLLA	Plate	~ 10	~ 300	~ 210	[102]
Drawn SR-PLGA	Rod	~ 7		~ 88	[103]

Drawn SR-PGA	Rod	~ 13	~ 270		[95]
<i>Self-reinforced / particulate composites</i>					
SR-PDLLA- β -TCP	Rods	~ 3.3	88 - 130	36 - 81	[100, 104]
SR-PDLLA-BG	Rods	1.8 – 3.2	58 - 140	39 - 90	[97, 98, 105, 106]
<i>Fibre reinforced composites</i>					
PCL-PGF	Plate	1.5 - 2.5	30 - 50		[46, 107]
PLA-PGF* (UD)	Plate	~ 16	~ 115		[108]
		~ 15	~ 170		[109]
		~ 28	~ 350		[110]
		9 - 24	110 - 320		[111-113]
PLA-PGF* (RM)	Plate	~ 4.5	~ 80		[62]
		~ 6	~ 95		[109]
		5 – 11.5	80 - 130		[111-113]
PLA-HAf	Plate	~ 8	~ 60		[114]
PCL-Bioglass °	Plate	9 - 16	130 - 200		[66]
PDLLA/BG hybride □	Plate	2.8 - 23	72 - 275		[115]
POE/CSMP* (RM)	Plate	3.2 – 9.5	75 - 115		[48, 53]

*CMP Calcium metaphosphate, CaP Calcium phosphate, BG bioactive glass, ° L- content within copolymer was varied from 70 to 96 %, PBG Phosphate based glass, UD and RM Unidirectional and random mat composite, λ the draw ratio, * Fibre volume fraction was variable, HAf hydroxyapatite fibres (40-150 μm in length and 2-10 μm in diameter), ** composites with different content of PLLA, PCL and HA, ° composites with different coupling agents. □ hybride composite contains BG and PDLLA fibre with different orientation and arrangement. CSMP is Calcium sodium metaphosphate, * the fibre volume fraction varied from 10 to 50 %.*

2.2.3.2 Self-reinforced biocomposites

Self-reinforcement is an alternative method to improve the mechanical properties of polymers. The principal of self-reinforcement is generation of orientated chains within the same polymer (matrix). These aligned chains could be strong and stiff to act as reinforcement as seen in **Figure 2-6**. The adhesion between the reinforcement and the matrix is strong and thus no need for adhesion promoters such as coupling agents [116]. There are different methods for production of self-reinforced composites such as fibre sintering, mechanical deformation (drawing process) and die extrusion [37, 94, 102, 117]. Processing temperatures should be above glass transition temperature (T_g) and lower than the melt temperature (T_m) for the polymer. Cold drawing (at room temperature) might be applied for polymers with T_g lower than room temperature. During the mechanical deformation process, fraction of crystalline spherulites could convert into aligned chains (reinforcement phase) [94, 118].

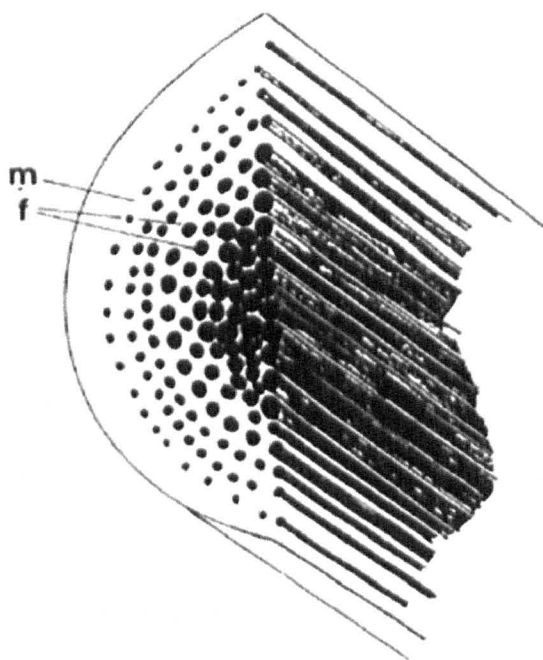


Figure 2-6: Schematic diagram for self-reinforced composites; *m* and *f* represent matrix and reinforcing fibres derived from the same polymer [94].

Fibre sintering is also known as hot compaction [119]. In this process, the fibres or mixture of fibres and powder derived from the same polymer are sintered into mould cavities and the temperature should be controlled to melt the fibres partially. High pressure should also be applied to produce highly compacted materials. Thus, a portion of the fibres remaining act as reinforcement and the melted fibres represent the matrix. Self-reinforced composites could also be prepared by rapid solidification of the molten polymer flowing through extrusion die [117]. Self-reinforced techniques have been conducted for various bioresorbable polymers and copolymers such as PLLA, PDLLA, PGA and PLGA [94]. The mechanical properties for some of the self-reinforced composites for biomedical application are reported in **Table 2-3**.

Light weight, ease of manufacturing, low cost, high initial mechanical strength and ductile failure mode are advantages for self-reinforced composites over other composites. The mechanical properties for self-reinforced composites depend on the molecular weight of the polymer and the fraction of aligned chains [37, 120].

The main drawbacks of self-reinforced polymers are; inflammation due to polymer degradation products and a limited ability to bond with bone or initiate new bone formation [4]. Several attempts were conducted to combine the advantages of self-reinforcement to particulate composites by adding bioactive fillers into self-reinforced composites (see **Table 2-3**). The target was to improve bioactivity, mechanical properties and to buffer acidic degradation products of the polymers. It was found that the initial mechanical properties decreased by addition of particles due to formation of pores and weak adhesion between the polymer and the filler [97, 98, 100, 105, 121].

Self-reinforcement provides good mechanical strength in comparison with pure polymers. However, self-reinforced composites have shown limited stiffness in comparison with glass fibre-reinforced composites. The optimum reported flexural modulus for self-reinforced composites (SR-PGA) was approximately 13 GPa [95],

whilst values of up to 28 GPa have been recorded for bioresorbable fibre-reinforced composites (see Table 2-3) [110-113].

2.2.3.3 *Inorganic fibre-reinforced biocomposites*

Fibre reinforced composites (FRC) could potentially provide a wide range of mechanical and biological properties that could match the properties and structure of natural bone [122, 123]. For instance, the anisotropic nature of the bone (longitudinal mechanical properties for bone are greater than the transverse direction) can be achieved by continuous unidirectional fibre reinforced composites [122]. Fibre reinforced composites are divided according to fibre length into chopped strand and continuous fibre reinforced composites. The orientation of fibres could be aligned or random which has a significant influence on the properties of the composites [124, 125]. Properties of fibre reinforced composites are controlled by fibre volume fraction, type, length, distribution and strength of fibre/matrix interface [122, 123]. Various types of fibres have been utilised in the orthopaedic field such as carbon [43, 64, 65, 126-129], bioglass [66, 69, 74, 130-133] and phosphate glass fibres [46, 62, 108-110, 112, 134-136].

Aspect ratio (length to diameter ratio) of the fillers has a significant influence on the modulus/stiffness of a particulate composite [137, 138]. Mechanical properties of composites increase as the aspect ratio of the particles increases. Therefore, it was expected that the reinforcing efficiency of fibres was significantly greater than particles. The parameters which affect the mechanical behaviour of FRCs are summarised below in Figure 2-7.

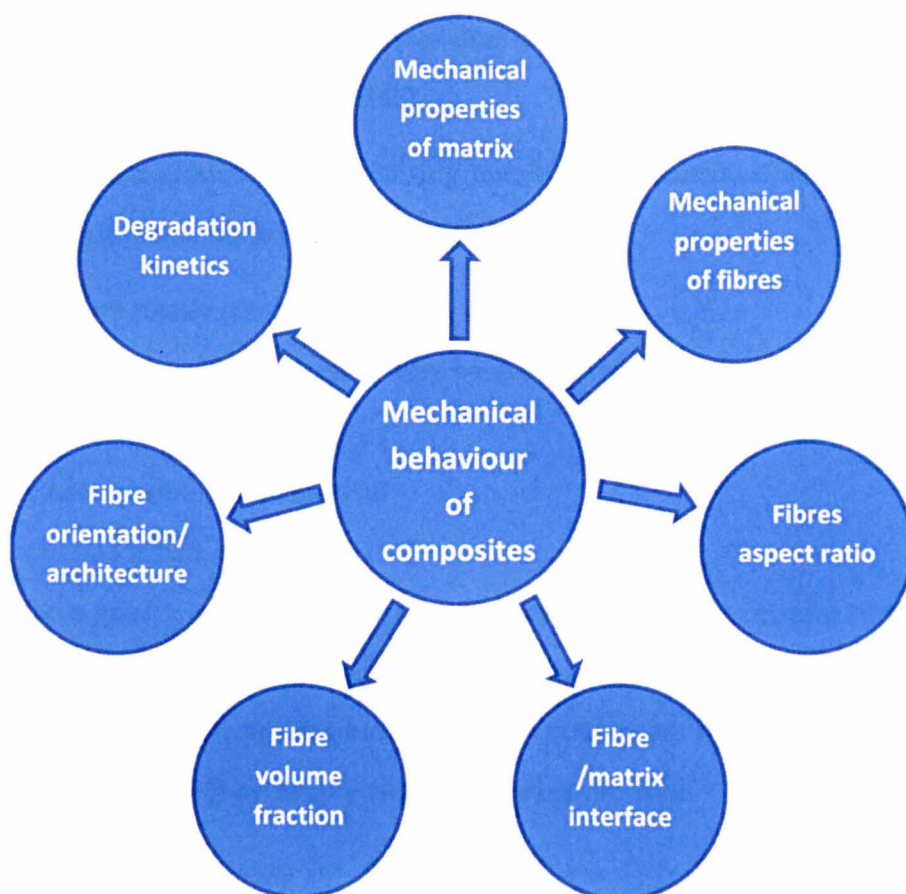


Figure 2-7: Schematic diagram of parameters which control the mechanical properties of fibre reinforced composites [139].

In order to manufacture totally bioresorbable composites, bioresorbable fibres are required. Phosphate glass fibres due to their unique properties could be used as reinforcement.

2.2.4 Phosphate based glass (PBG)

2.2.4.1 Introduction

Phosphate glasses were developed around 100 years ago [140]. They have high refractive indices, low optical dispersion and high UV transparency. Optical applications were limited significantly due their poor chemical durability [140]. During the middle of the last century, phosphate glasses with modified compositions were introduced to industrial applications such as water treatment, pigments manufacturing and solid state lasers. Iron phosphate glasses were

investigated as hosts for nuclear waste due to their low processing temperatures and high chemical durability [141-145].

Phosphate based glasses are a promising material for biomedical applications due to their unique characteristics [143, 146, 147]:

- they are totally soluble in aqueous environment,
- their chemical composition can be similar to the mineral phase of bone (calcium phosphate),
- biocompatible and bioactive,
- can be formed into fibres [148],
- have good mechanical properties in fibre form (approximately 74 GPa and 400 MPa for tensile modulus and of tensile strength [109, 149]),
- controllable and predictable dissolution rates (from hours, days, months to years [150, 151]) by simply altering their composition.

Based on these advantages for phosphate glasses, they have various potential medical applications. For example fluoride phosphate glasses can be used in oral applications to initiate remineralisation of early carious teeth by releasing fluoride. They have been utilised to provide cobalt, zinc and copper supplements in veterinary applications. Silver and copper phosphate glasses have shown potent antibacterial effects [152]. Furthermore, phosphate glass microtubes have also been applied for neural repair purposes. Importantly, they have been applied for hard tissue applications such as bone fracture in the form of reinforcement for bioresorbable polymers (to manufacture totally bioresorbable composites) [8, 9, 153].

2.2.4.2 Structure

There are three common glass former oxides (SiO_2 , B_2O_3 and P_2O_5). Phosphorus pentoxide (P_2O_5) is the former for phosphate glasses and the basic structural unit is a tetrahedral phosphate anion (PO_4^{3-}) (see Figure 2-8) [142, 154]. Tetrahedra are classified based on Q^i terminology into Q^3 , Q^2 , Q^1 and Q^0 where i represents the number of bridging oxygen per tetrahedron (i.e. number of P-O-P links of a PO_4

tetrahedron) (see **Figure 2-9**) [8, 155]. Vitreous P_2O_5 consists of a three dimensional network (Q^3) [8, 156] and use of pure vitreous P_2O_5 glasses is extremely limited due to their hygroscopic nature (i.e. able to absorb and retain the moisture) [8, 142]. Addition of modifiers (MO/M_2O) results in depolymerisation of the phosphate network by creation of terminal oxygens at the expense of bridging oxygens. It was also reported that existence of water within the glass composition also had a depolymerisation effect by forming $P-OH$ [9, 142]. Different oxides such as sodium oxide (Na_2O), calcium oxide (CaO), magnesium oxide (MgO), iron oxide (Fe_2O_3) and titanium oxide (TiO_2) have been used as modifiers to suit varying end applications [157]. **Figure 2-9** shows the transformation from one species to another via addition of monovalent cations (M^+).

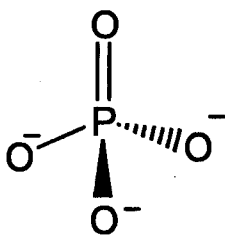


Figure 2-8: chemical structure of the tetrahedral phosphate anion.

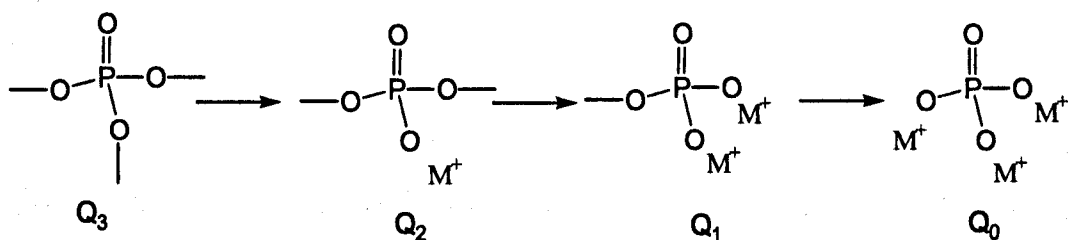


Figure 2-9: Effect of addition of monovalent cation (M^+) on the Q structure of the P_2O_5 [8].

Phosphate glasses can be classified into binary, ternary, quaternary and complex glass systems based on the number of oxides within the composition. CaO and Na_2O are the most common modifiers in the preparation of binary phosphate glasses. Binary glasses ($x M_{2/v}O - (1-x) P_2O_5$) can be divided into three groups based on the composition, where v is the valance of the metal cation [8, 9, 142, 154, 158]:

- a) Ultraphosphates ($0 \leq x < 0.5$):

Structure is based on Q^3 and Q^2 species,

b) Metaphosphates ($x = 0.5$):

Structure consists of infinity long chains of Q^2 ,

c) Polyphosphates ($x > 0.5$):

Structure of polyphosphate glasses can be divided into four subgroups according to x ratio:

i. ($0.5 < x < 0.67$):

Structure contains mixture of Q^2 and Q^1 species,

ii. Pyrophosphates ($x = 0.67$):

Structure dominated by phosphate dimers (two Q^1 species sharing a bridging oxygen atom),

iii. ($0.67 < x < 0.75$):

Structure contains a mixture of Q^1 and Q^0 species,

iv. Orthophosphate ($x = 0.75$):

Structure consists of isolated Q^0 units.

The $P_2O_5 - CaO - Na_2O$ glass system has been the most commonly investigated system for structural, thermal, dissolution and cytocompatibility properties [146, 159-161]. Ahmed *et al.* [146] found that these glasses contained a mixture of Q^1 and Q^2 structures and the amount of Q^2 for compositions with fixed P_2O_5 at 45 mole % was lower than 50 and 55 mole %. For 45 mole % system, Q^1 species were identified as dimers. Conversely, the fraction of Q^1 structure within 50 and 55 mole % compositions was very little (less than 4%) and was suggested to be chain terminators.

Bunker *et al.* [150] stated that phosphate glasses ($50 P_2O_5 - (50 - x) Na_2O - (x) CaO$; $x = 10$ and 20 mole %) are composed of long polymeric anion chains connected to one another by modifier cations via ionic bonds. Therefore, monovalent cations (Na^+) disrupt the network by breaking the bridging oxygen bonds to form terminal oxygen bonds (depolymerisation effect), whereas the divalent cations (Ca^{2+}) could

cross-link between chains. During the depolymerisation process, the Q species converted into shorter species (i.e. Q³ into Q² and Q² into Q¹) [162].

Structure of quaternary phosphate glasses (P₂O₅ – CaO – Na₂O – MgO) were investigated using ³¹P MAS-NMR spectroscopy by Walter *et al.* [163]. Good agreement was seen with the theoretical [142] and experimental Q structure (see Figure 2-10). Similar findings were demonstrated by Brauer *et al.* [164].

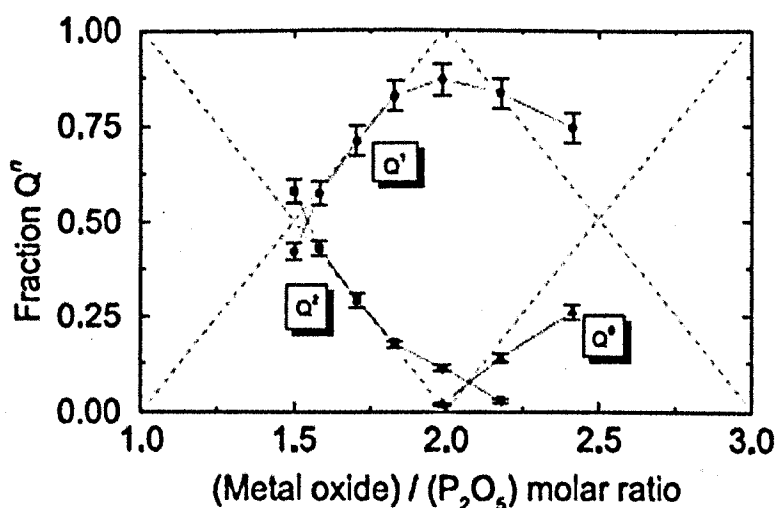


Figure 2-10: The Q structure for P₂O₅ – CaO – Na₂O – MgO glass [163].

2.2.4.3 Dissolution

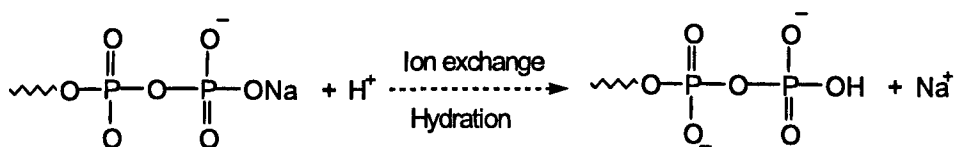
Although, the poor chemical durability of phosphate glasses in aqueous environments restricted their industrial applications. It was the main motivation for their use in medical applications such as temporary bone fracture fixation devices [8, 150, 165]. Dissolution rate or resorption time of the implant could be adjusted according to the requirements of end applications. Degradation rate of PBG does not only depend on the chemical composition but also on the pH of the degradation medium, degradation temperature, thermal history and ratio of surface area to volume [166]. Based on their structure, polyphosphate glasses are more durable than metaphosphate due to a decrease in the fraction of highly hydrolysable Q² species [9]. It was found that the degradation rate for phosphate glasses in stimulated body fluid (SBF) was lower than that in deionised water. This was

attributed to the fact that SBF is a buffering solution, whilst pH for the water would decrease due to degradation of the glasses causing acceleration of the process with ions leaching into the media [150, 167-169].

The degradation process of phosphate glass is divided into two steps [166, 170, 171]:

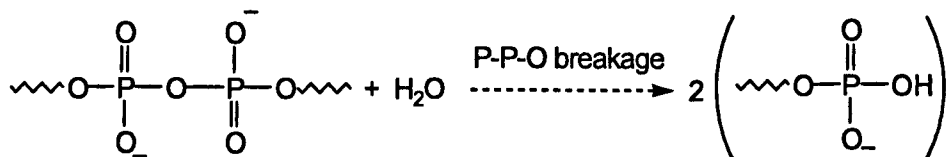
(i) Hydration reaction:

During this stage, the outer layer of the glass (i.e. at the interface with the surrounding medium) would be hydrated due to ion exchange reaction. The glass exchanges the cations (Na^+) with hydrogen ion (H^+) from the water.



(ii) Network breakage:

The hydrated layers would be attacked by the water (hydrolysis) resulting in cleavage of the P-O-P bonds and breakdown of the network structure. Consequently, phosphate chains with different lengths would be released into the medium.



Bunker *et al.* [150] proposed that the ion exchange (Na-H) is the dominant reaction of the dissolution process, whilst Gao *et al.* [166] considered the ion exchange as an initiator for the dominant reaction which was network breakage.

The dissolution rate (DR) can be determined by the following equation [144];

$$\text{DR} = \frac{\Delta W}{A_s \cdot t} \quad \text{Equation 2-1}$$

where ΔW , A_s and t are the mass loss, surface area and degradation time respectively.

Chemical durability of phosphate glasses is dependent on the size, Dietzel field strength (F) (simplified as Coulomb's force between ions in the oxides) and charge of modifying ions. $F = \frac{Z}{a^2}$ (\AA^{-2}); Z is the cation valence and a is the distance between cation and anion [172]. Therefore, addition of metallic ions with small ionic radius and high electrical charges would form strong P-O-M bonds (which have high resistance to hydration) at the expense of P-O-P bonds. Consequently, dissolution rate for $\text{P}_2\text{O}_5 - \text{CaO} - \text{Na}_2\text{O}$ system would decrease by addition of metallic oxides such as Al_2O_3 , ZnO_2 , Fe_2O_3 , and TiO_2 [141, 167, 172-179]. It was also found that mass loss for the ternary phosphate glasses decreased from 3 % to 0.25 % via incorporation of 5 mole % TiO_2 [176]. Brauer *et al.* [164, 179] reported similar effect for addition of TiO_2 to $\text{P}_2\text{O}_5 - \text{CaO} - \text{Na}_2\text{O} - \text{MgO}$ glasses. The lower solubility was ascribed to the cross-linking of phosphate chains by Ti^{4+} ion. In contrast, they found that solubility increased by incorporation of SiO_2 which was suggested to be due to disruption of the phosphate network, since SiO_2 is a competing glass former [47, 107, 168, 180].

Parsons *et al.* [181] and Shih *et al.* [182, 183] demonstrated the effect for the addition of Fe_2O_3 , CaO , MgO and CuO oxides on physical and degradation properties of $\text{P}_2\text{O}_5 - \text{Na}_2\text{O}$ binary phosphate glasses. Glass transition temperature and density were reported to increase whilst a significant decrease was seen in degradation rate by increasing the amount of oxides. Similar findings were presented for $\text{P}_2\text{O}_5 - \text{CaO} - \text{Na}_2\text{O}$ ternary glasses [146, 160, 162]. Trivalent ions such as iron (Fe^{3+}) and (Ti^{3+}) showed greater influence on the solubility of phosphate glasses than divalent or monovalent ions [184-186]. This was suggested to be due to strengthening of the phosphate network via cross-linking effect of di- and tri-valent ions [150]. Parsons *et al.* [184] found that the dissolution rate for sodium iron phosphate glasses decreased from $2 \times 10^{-1} \text{ g cm}^{-2} \text{ h}^{-1}$ to $1 \times 10^{-6} \text{ g cm}^{-2} \text{ h}^{-1}$ as the iron content increased from 1 to 20 mole %.

Ahmad *et al.* [187] studied the degradation and cytocompatibility of a series of phosphate glasses of compositions $40 \text{ P}_2\text{O}_5 - 25 \text{ CaO} - (35 - x) \text{ Na}_2\text{O} - x \text{ MgO}$ (in mole %) where x varied from 0 to 30 mole %. Rate of mass loss decreased from 0.116

to 0.0023 (%/h) as the MgO content increased as expected due to replacing a monovalent cation (Na^+) by divalent cation (Mg^{2+}). The influence of replacing of CaO by MgO on dissolution behaviour for $\text{P}_2\text{O}_5 - \text{CaO} - \text{Na}_2\text{O}$ was also manifested by Franks *et al.* [188]. Since Mg^{2+} and Ca^{2+} ions have the same valence; a significant change in glass solubility was not expected. They suggested that the solubility might be increased as a result of replacing a large ion (Ca^{2+}) by a small ion (Mg^{2+}). However, they found that the dissolution rate decreased by adding MgO and no explanation was given. Ahmed *et al.* [187] suggested that this due to a change in structure by adding MgO from less stable metaphosphate (MgP_2O_6) to the pyrophosphate ($\text{Mg}_2\text{P}_2\text{O}_7$) which is much more stable, while only the $\text{Ca}_3(\text{PO}_4)_2$ phase was seen in all the compositions.

2.2.4.4 Biocompatibility

Biocompatibility of the implant materials is essential to avoid adverse or inflammatory reactions after implantation. PLA is a known biocompatible polymer approved by US food and drug administration (FDA) [189, 190] however, late inflammatory responses have been observed for PLLA from *in vivo* studies, which were attributed to rapid release of degradation products (i.e. monomers or oligomers) at ultimate stages of degradation [33, 36]. Addition of HA, TCP, CaP or PBG to the PLA might improve the biocompatibility by ion release during degradation and/or buffering the acidic degradation products of PLA [174, 191-193]. Incorporation of phosphate glass fibres (PGF) into the matrix (PLA) has been shown to improve both biological response as well as the material mechanical properties [109, 111, 112, 194, 195].

Since the mineral phase of bone is composed mainly of calcium (Ca) and phosphorus (P), they should have an essential role in the bone remodelling process [174]. Therefore, it was expected that PBGs would have great potential for hard tissue applications such as bone repair. PBG showed capability of stimulating the new bone formation via release of ions (mainly Ca, Mg and P) during their degradation. The rate of ion release should be controllable to avoid the cytotoxicity effect [161]. Hoppe *et al.* [174] reported that a concentration of Ca^{2+} up to 320 ppm in

culture media was suitable for osteoblast proliferation, differentiation and extracellular matrix mineralisation and concentrations above 400 ppm would become cytotoxic.

Biological response of P_2O_5 – CaO – Na_2O ternary glasses to human osteoblast cells were investigated elsewhere [196]. It was reported that cell proliferation was adversely affected by glasses containing high amounts of Na_2O . Cell proliferation enhanced by increasing the amount of CaO at the expense of Na_2O (less soluble glass). These findings were supported by Bitar *et al.* [197] and Navarro *et al.* [176] in their studies on human osteoblast and fibroblast cells interaction with P_2O_5 – CaO – Na_2O ternary glasses. Therefore, it can be stated that the dissolution rate of the glass had a direct influence (inversely) on their biological performances [169, 174, 176, 179].

Biocompatibility was assessed for 50 P_2O_5 – 30 CaO – $(20 - x)Na_2O - x TiO_2$ (x varied from 0 to 15 mole %) glasses using cell viability and cell proliferation tests with human osteosarcoma cells by Abou Neel *et al.* [177, 178, 198]. The cell proliferation viability and attachment for glasses containing 3 mole % or higher of TiO_2 was greater than the titanium free composition. Glasses containing titanium maintained cell viability greater than 99 % over the period of the study (7days). Enhancement of biocompatibility for the glasses by inclusion of titanium oxides was associated with decrease in solubility of the glasses.

Leonardi *et al.* [168] examined the response of human bone marrow cells to complex compositions of phosphate glass (45% P_2O_5 - 3% SiO_2 - 26% CaO - 7% MgO - 15% Na_2O - 4% K_2O). The glass showed good cell adhesion as well as cell differentiation. HA layer was formed on the glass surface after soaking in SBF which was indicative of glass bioactivity.

2.2.4.5 Phosphate glass fibres (PGF)

Glass fibres can be drawn from molten glass via melt spinning technique. The existence of strong bonds within molten glass is required to produce continuous thread. These bonds should withstand the applied tensile stresses during the pulling process at high temperatures [159, 199]. Continuity of the fibres depends

also on composition and structure of the glasses. Heat treatment (annealing) of the prepared fibres is essential in order to release internal stresses which are created by the rapid cooling of the pulled fibres [162, 200]. The internal stresses were ascribed to broken bonds and stretched bonds greater than the original length at equilibrium state. Annealing of glass fibres around the glass transition temperature would stabilise their structure by reforming broken bonds and allowing some bonds to reach a more stable state. The mechanical strength of the fibres might slightly decrease by annealing. Although, dissolution rate would decrease making the fibres more appropriate as reinforcement for bioresorbable implants [148, 200, 201].

Cozien-Cazuc *et al.* [201, 202] investigated the effect of annealing on dissolution and mechanical retention of quaternary phosphate glass fibres (40 P₂O₅-20 Na₂O-16 CaO-24 MgO – in mol %). However, the initial tensile strength for the annealed fibres decreased due to formation of flaws at the fibre surface as a result of annealing in a humid environment. The fibres failed during the tensile test by fracture which originated from surface flaws [203]. Interestingly, they found that the annealed fibres recovered the as-prepared (non-annealed) fibres strength after 3 days of degradation in distilled water at 37°C. The increase in tensile strength for the annealed fibres was ascribed to peeling off of the outer tensile layer with its inherent flaws. Removal of the outer layer of the fibres was seen by using scanning electron microscopy (SEM). Conversely, non-annealed fibres lost ~ 25 % of their initial value due to hydrolysis and pitting corrosion at the surface. Approximately 50 % decrease in dissolution rate for the fibres was seen after annealing.

Thermal, mechanical, structure and dissolution properties for glass fibres differ greatly from those for bulk glass. This difference is due to the preparation method, drawing parameters (temperature, speed, viscosity) and fibre diameter [159]. Ahmed *et al.* [159] compared degradation properties for P₂O₅ – CaO – Na₂O ternary phosphate glass fibres with bulk glass results. They found that the degradation rate for fibres significantly increased in comparison to the bulk glasses due to the huge increase in surface area. Furthermore, the degradation rate for fibres decreased with increasing fibre diameter due to surface area effect also [92, 148, 159].

Dissolution and biocompatibility were examined for iron phosphate glass fibre ($\text{P}_2\text{O}_5 - \text{CaO} - \text{Na}_2\text{O} - \text{Fe}_2\text{O}_3$) [92, 185]. A reduction in solubility of the fibres was seen by increasing the amount of CaO and Fe_2O_3 from 1 to 5 mole %. Biocompatibility was performed by using an immortal muscle precursor cell (MPC) line and the fibres showed good cell attachment and differentiation. Furthermore, biocompatibility was improved via the addition of 5 mol % Fe_2O_3 , due to enhancement in chemical durability of the glass [185]. Parsons *et al.* [184] also showed that osteoblasts responded well to phosphate glasses containing as much as 20 mol% iron oxide.

It was reported that the strength of phosphate glass fibres decreased by 15 % to 34 % of the freshly pulled fibres after exposure to air (around 10 days). This reduction was attributed to be due to degradation as a result of moisture [141, 204]. Navarro *et al.* [167] found that Young's modulus for $\text{P}_2\text{O}_5 - \text{CaO} - \text{Na}_2\text{O}$ increased by incorporation of TiO_2 and remained almost constant during degradation in SBF for 112 day.

Mechanical testing for calcium-iron phosphate glass fibres of approximately 20 μm were evaluated by Lin *et al.* [204]. Tensile strength and modulus were reported to increase by ~ 80 and 40 % of the initial values (~ 600 MPa and ~ 43 GPa) respectively as the amount of iron increased from 3.6 to 16.9 mole %. Increase in the mechanical properties was attributed to the formation of cross linked chains due to existence of iron ions.

More recently work has been conducted using PGF as reinforcement for bioresorbable polymers to produce totally bioresorbable composites [62, 108, 109]. Composite plates based on PLA and PGF were produced with different fibre content and lay-up geometries. Flexural properties for unidirectional composites with fibre volume fraction (V_f) ~ 30% and ~ 55% were 115 MPa and 170 MPa for strength and 16 GPa and 15 GPa for modulus respectively [108, 109]. Furthermore, PLA reinforced with random PGF mats (V_f ~14 %) showed properties of 90 MPa and 5 GPa for bending strength and modulus respectively [62].

PLA and phosphate glass fibres (PGF) were selected as constituents for the bioresorbable fibre-reinforced composites based on their mechanical,

biodegradability and biocompatibility properties. PGA has superior mechanical properties (~ 6 GPa for Young's modulus and flexural strength up to 375 MPa) among bioresorbable polymers (see Table 2-2). However, the degradation rate for PGA is faster than PLA and PCL. Thus, PGA has been used extensively for short term medical applications such as sutures [17, 45]. Mechanical properties of PCL are inferior (~ 0.4 GPa and 30 MPa for flexural modulus and strength) in comparison to PLA. Therefore, PLA was chosen as matrix to obtain a balance between mechanical properties and degradation time (see Table 2-2). Phosphate glass fibre with composition of 40 P₂O₅-24 MgO-16 CaO-16 Na₂O- 4 Fe₂O₃ in mol% (denoted as P40) was designated for this study based on previous work within the group [109, 111, 149, 187, 195, 201, 202, 205]. This was attributed to its relatively low degradation rate, excellent biocompatibility and high Young's modulus in fibre form [109, 149, 187]. However, less durable fibres (50P₂O₅-40CaO-5Na₂O-5Fe₂O₃ (denoted as P50)) were also used due to the ease of fibre production in an attempt to normalise and standardise the preparation procedure for the composite rods. Fibre volume fractions for the composites were selected to be in the range of 15 – 35 % in order to produce composite with mechanical properties similar to that of the cortical bone (5 – 23 GPa for Young's modulus and 35 – 280 MPa for flexural strength, see Table 1-1) based on the Rule of Mixtures.

In conclusion, fibre-reinforced composites based on PLA reinforced with PGF were used as implant materials to manufacture composite rods and screws. Fibre reinforced composites based on bioresorbable polymers and phosphate glass fibres and their mechanical properties were summarised in Table 2-3. Degradation, mechanical and biocompatibility properties of these composite will be covered in details throughout the forthcoming chapters.

2.3 REFERENCES

1. Mauffrey, C., D. Seligson, C. Roberts, and J. Statton, *External Fixation in Orthopedic Traumatology: Springer*.
2. Engelhardt, S.A., *Orthopaedics and the Future: Growth in Challenging and Uncertain Times. U.S. Orthopaedic Product News, 2009. May/June.*

3. Mahapatro, A., A.S. Kulshrestha, M. American Chemical Society, S. American Chemical Society. Division of Polymeric Materials, and Engineering. *Polymers for biomedical applications*. Washington, DC: American Chemical Society : Distributed by Oxford University Press.
4. Wnek, G.E. and G.L. Bowlin, *Encyclopedia of Biomaterials and Biomedical Engineering, Second Edition (Four-Volume Set)*2008: Informa Healthcare.
5. Ambrose, C.G. and T.O. Clanton, *Bioabsorbable Implants: Review of Clinical Experience in Orthopedic Surgery*. *Annals of Biomedical Engineering*, 2004. 32(1): p. 171-177.
6. Williams, D.F., *The Williams dictionary of biomaterials*1999, Liverpool: Liverpool University Press.
7. Hench, L.L. and J.M. Polak, *Third-Generation Biomedical Materials*. *Science*, 2002. 295(5557): p. 1014-1017.
8. Knowles, J.C., *Phosphate based glasses for biomedical applications*. *Journal of Materials Chemistry*, 2003. 13(10): p. 2395-2401.
9. Abou Neel, E.A., D.M. Pickup, S.P. Valappil, R.J. Newport, and J.C. Knowles, *Bioactive functional materials: a perspective on phosphate-based glasses*. *Journal of Materials Chemistry*, 2009. 19(6): p. 690-701.
10. Sawhney, G.S., *Fundamentals of biomedical engineering*2007, New Delhi: New Age International.
11. Teoh, S.H., *Engineering materials for biomedical applications*2004, Singapore; Hackensack, NJ: World Scientific Pub.
12. Park, J.B. and R.S. Lakes, *Biomaterials : an introduction*2007, New York: Springer.
13. Niinomi, M., *Metallic biomaterials*. *Journal of Artificial Organs*, 2008. 11(3): p. 105-110.
14. George A. Graves and B.K. Jr., *Bioabsorbable Glass Fibres of Bioresorbable Polymers for Bone Fixation Devices and Artificial Ligments in Untied States Patent*1986, University of Dayton.
15. https://www.stanford.edu/group/bmr/cgibin/mediawiki/index.php/MRI_near_metallic_implants.
16. Ramakrishna, S., J. Mayer, E. Wintermantel, and K.W. Leong, *Biomedical applications of polymer-composite materials: a review*. *Composites Science and Technology*, 2001. 61(9): p. 1189-1224.
17. Middleton, J.C. and A.J. Tipton, *Synthetic biodegradable polymers as orthopedic devices*. *Biomaterials*, 2000. 21(23): p. 2335-2346.
18. Gu, X.-N. and Y.-F. Zheng, *A review on magnesium alloys as biodegradable materials*. *Frontiers of Materials Science in China*, 2010. 4(2): p. 111-115.
19. Hendra Hermawan, Dadan Ramdan and Joy R. P. Djuansjah (2011). *Metals for Biomedical Applications, Biomedical Engineering - From Theory to Applications*, Reza Fazel-Rezai (Ed.), ISBN: 978-953-307-637-9, InTech.

20. Xue, D., Y. Yun, Z. Tan, Z. Dong, and M.J. Schulz, *In Vivo and In Vitro Degradation Behavior of Magnesium Alloys as Biomaterials*. *Journal of Materials Science & Technology*, 2012. 28(3): p. 261-267.
21. Navarro, M., A. Michiardi, O. Castano, and J.A. Planell, *Biomaterials in orthopaedics*. *Journal of The Royal Society Interface*, 2008. 5(27): p. 1137-1158.
22. Jonathan, B. and G.W. Hastings, *Handbook of biomaterial properties*1998: Chapman & Hall.
23. Pietrzak, W.S., D.R. Sarver, and M.L. Verstynen, *Bioabsorbable Polymer Science for the Practicing Surgeon*. *Journal of Craniofacial Surgery*, 1997. 8(2): p. 87-91.
24. Gupta, B., N. Revagade, and J. Hilborn, *Poly(lactic acid) fiber: An overview*. *Progress in Polymer Science*, 2007. 32(4): p. 455-482.
25. Juutilainen, T., H. Päätiälä, M. Ruuskanen, and P. Rokkanen, *Comparison of costs in ankle fractures treated with absorbable or metallic fixation devices*. *Archives of Orthopaedic and Trauma Surgery*, 1997. 116(4): p. 204-208.
26. Onuma, Y. and P.W. Serruys, *Bioresorbable Scaffold*. *Circulation*, 2011. 123(7): p. 779-797.
27. Shih, C., *Chain-end scission in acid catalyzed hydrolysis of poly (d,l-lactide) in solution*. *Journal of Controlled Release*, 1995. 34(1): p. 9-15.
28. Göpferich, A., *Mechanisms of polymer degradation and erosion*. *Biomaterials*, 1996. 17(2): p. 103-114.
29. Maurus, P.B. and C.C. Kaeding, *Bioabsorbable implant material review*. *Operative Techniques in Sports Medicine*, 2004. 12(3): p. 158-160.
30. Burkersroda, F.v., L. Schedl, and A. Göpferich, *Why degradable polymers undergo surface erosion or bulk erosion*. *Biomaterials*, 2002. 23(21): p. 4221-4231.
31. Woodruff, M.A. and D.W. Hutmacher, *The return of a forgotten polymer - Polycaprolactone in the 21st century*. *Progress in Polymer Science*, 2010. 35(10): p. 1217-1256.
32. Smith, R., *Biodegradable polymers for industrial applications*2005: Woodhead.
33. Bergsma, J.E., W.C. de Bruijn, F.R. Rozema, R.R.M. Bos, and G. Boering, *Late degradation tissue response to poly(L-lactide) bone plates and screws*. *Biomaterials*, 1995. 16(1): p. 25-31.
34. Weiler, A., R.F.G. Hoffmann, A.C. Stahelin, H.-J. Helling, and N.P. Sudkamp, *Biodegradable implants in sports medicine: The biological base*. *Arthroscopy: The Journal of Arthroscopic & Related Surgery*, 2000. 16(3): p. 305-321.
35. Spitalny, A.D., *Bioabsorbable Implants*. *Clinics in podiatric medicine and surgery*, 2006. 23(4): p. 673-694.
36. Gomes, M.E. and R.L. Reis, *Biodegradable polymers and composites in biomedical applications: from catgut to tissue engineering. Part 1 Available systems and their properties*. *International Materials Reviews*, 2004. 49(5): p. 261-273.

37. Törmälä, P., T. Pohjonen, and P. Rokkanen, Ultrahigh-strength self-reinforced polylactide composites and their surgical applications. *Macromolecular Symposia*, 1997. 123(1): p. 123-131.
38. Gogolewski, S., Resorbable polymers for internal fixation. *Clinical Materials*, 1992. 10(1-2): p. 13-20.
39. Voutilainen NH, Hess MW, Toivonen TS, Krogerus LA, Partio EK, and P. HV., A long-term clinical study on dislocated ankle fractures fixed with self-reinforced polylevolactide (SR-PLLA) implants. *J Long Term Eff Med Implants*, 2002. 12(1): p. 35-52.
40. MacDonald, R.T., S.P. McCarthy, and R.A. Gross, Enzymatic Degradability of Poly(lactide): Effects of Chain Stereochemistry and Material Crystallinity. *Macromolecules*, 1996. 29(23): p. 7356-7361.
41. Tsuji, H., Y. Kidokoro, and M. Mochizuki, Enzymatic degradation of poly(L-lactic acid) fibers: Effects of small drawing. *Journal of Applied Polymer Science*, 2007. 103(3): p. 2064-2071.
42. Gogolewski, S., Bioresorbable polymers in trauma and bone surgery. *Injury*, 2000. 31 Suppl 4: p. 28-32.
43. Daniels, A.U., M.K.O. Chang, K.P. Andriano, and J. Heller, Mechanical properties of biodegradable polymers and composites proposed for internal fixation of bone. *Journal of Applied Biomaterials*, 1990. 1(1): p. 57-78.
44. Van de Velde, K. and P. Kiekens, Biopolymers: overview of several properties and consequences on their applications. *Polymer Testing*, 2002. 21: p. 433-442.
45. Rezwan, K., Q.Z. Chen, J.J. Blaker, and A.R. Boccaccini, Biodegradable and bioactive porous polymer/inorganic composite scaffolds for bone tissue engineering. *Biomaterials*, 2006. 27(18): p. 3413-3431.
46. Ahmed, I., A.J. Parsons, G. Palmer, J.C. Knowles, G.S. Walker, and C.D. Rudd, Weight loss, ion release and initial mechanical properties of a binary calcium phosphate glass fibre/PCL composite. *Acta Biomaterialia*, 2008. 4(5): p. 1307-1314.
47. Mohammadi, S.M., I. Ahmed, B. Marelli, C. Rudd, M.N. Bureau, and S.N. Nazhat, Modulation of polycaprolactone composite properties through incorporation of mixed phosphate glass formulations. *Acta Biomaterialia*, 2010. 6(8): p. 3157-3168.
48. Andriano, K.P., A.U. Daniels, and J. Heller, Biocompatibility and mechanical properties of a totally absorbable composite material for orthopaedic fixation devices. *Journal of Applied Biomaterials*, 1992. 3(3): p. 197-206.
49. Shikunami, Y. and M. Okuno, Bioresorbable devices made of forged composites of hydroxyapatite (HA) particles and poly-L-lactide (PLLA): Part I. Basic characteristics. *Biomaterials*, 1999. 20(9): p. 859-877.
50. Jamshidian, M., E.A. Tehrany, M. Imran, M. Jacquot, and S. Desobry, Poly-Lactic Acid: Production, Applications, Nanocomposites, and Release Studies. *Comprehensive Reviews in Food Science and Food Safety*. 9(5): p. 552-571.

51. Andriano, K.P., A.U. Daniels, W.P. Smutz, R. Wyatt, W. B. , and J. Heller, Preliminary biocompatibility screening of several biodegradable phosphate fiber reinforced polymers. *Journal of Applied Biomaterials*, 1993. 4(1): p. 1-12.
52. Daniels, A.U., P.A. Kirk, W.P. Smutz, K.O.C. Melissa, and H. Jorge, Evaluation of absorbable poly(ortho esters) for use in surgical implants. *Journal of Applied Biomaterials*, 1994. 5(1): p. 51-64.
53. Wise, D.L., *Encyclopedic handbook of biomaterials and bioengineering: Materials*, volume 11995: Marcel Dekker.
54. Sabir, M., X. Xu, and L. Li, A review on biodegradable polymeric materials for bone tissue engineering applications. *Journal of Materials Science*, 2009. 44(21): p. 5713-5724.
55. Eshraghi, S. and S. Das, Mechanical and microstructural properties of polycaprolactone scaffolds with one-dimensional, two-dimensional, and three-dimensional orthogonally oriented porous architectures produced by selective laser sintering. *Acta Biomaterialia*, 2010. 6(7): p. 2467-2476.
56. Avinc, O. and A. Khoddami, Overview of Poly(lactic acid) (PLA) Fibre. *Fibre Chemistry*, 2009. 41(6): p. 391-401.
57. Athanasiou, K.A., C.M. Agrawal, F.A. Barber, and S.S. Burkhart, Orthopaedic applications for PLA-PGA biodegradable polymers. *Arthroscopy: The Journal of Arthroscopic & Related Surgery*, 1998. 14(7): p. 726-737.
58. Waris, E., N. Ashammakhi, O. Kaarela, T. Raatikainen, and J. Vasenius, Use of Bioabsorbable Osteofixation Devices in the Hand. *Journal of Hand Surgery (British and European Volume)*, 2004. 29(6): p. 590-598.
59. An, Y.H., S.K. Woolf, and R.J. Friedman, Pre-clinical in vivo evaluation of orthopaedic bioabsorbable devices. *Biomaterials*, 2000. 21(24): p. 2635-2652.
60. Bühler, M., P.-E. Bourban, and J.-A.E. Månson, Cellular composites based on continuous fibres and bioresorbable polymers. *Composites Part A: Applied Science and Manufacturing*, 2008. 39(12): p. 1779-1786.
61. Fu, S., X. Feng, B. Lauke, and Y.-W. Mai, Effects of particle size, particle/matrix interface adhesion and particle loading on mechanical properties of particulate-polymer composites. *Composites Part B: Engineering*, 2008. 39(6): p. 933-961.
62. Ahmed, I., P.S. Cronin, E.A. Abou Neel, A.J. Parsons, J.C. Knowles, and C.D. Rudd, Retention of mechanical properties and cytocompatibility of a phosphate-based glass fiber/polylactic acid composite. *Journal of Biomedical Materials Research Part B: Applied Biomaterials*, 2009. 89B(1): p. 18-27.
63. Bonfield, W., Hydroxyapatite-Reinforced Polyethylene as an Analogous Material for Bone Replacement. *Annals of the New York Academy of Sciences*, 1988. 523(1): p. 173-177.
64. Wan, Y.Z., Y.L. Wang, X.H. Xu, and Q.Y. Li, In vitro degradation behavior of carbon fiber-reinforced PLA composites and influence of interfacial adhesion strength. *Journal of Applied Polymer Science*, 2001. 82(1): p. 150-158.

65. Zimmerman Mark, C., H. Alexander, J.R. Parsons, and P.K. Bajpai, *The Design and Analysis of Laminated Degradable Composite Bone Plates for Fracture Fixation, in High-Tech Fibrous Materials*1991, American Chemical Society. p. 132-148.
66. Jiang, G., M.E. Evans, I.A. Jones, C.D. Rudd, C.A. Scotchford, and G.S. Walker, *Preparation of poly([epsilon]-caprolactone)/continuous bioglass fibre composite using monomer transfer moulding for bone implant. Biomaterials*, 2005. 26(15): p. 2281-2288.
67. Salernitano, E. and C. Migliaresi, *Composite materials for biomedical applications: a review. J Appl Biomater Biomech*, 2003. 1(1): p. 3-18.
68. Bigg, D.M., *Mechanical properties of particulate filled polymers. Polymer Composites*, 1987. 8(2): p. 115-122.
69. Boccaccini, A.R., M. Erol, W.J. Stark, D. Mohn, Z. Hong, and J.F. Mano, *Polymer/bioactive glass nanocomposites for biomedical applications: A review. Composites Science and Technology*, 2010. 70(13): p. 1764-1776.
70. Misra, S.K., D. Mohn, T.J. Brunner, W.J. Stark, S.E. Philip, I. Roy, V. Salih, J.C. Knowles, and A.R. Boccaccini, *Comparison of nanoscale and microscale bioactive glass on the properties of P(3HB)/Bioglass® composites. Biomaterials*, 2008. 29(12): p. 1750-1761.
71. Lu, J., M. Descamps, J. Dejou, G. Koubi, P. Hardouin, J. Lemaitre, and J.P. Proust, *The biodegradation mechanism of calcium phosphate biomaterials in bone. J Biomed Mater Res*, 2002. 63(4): p. 408-12.
72. Dorozhkin, S.V., *Bioceramics of calcium orthophosphates. Biomaterials*, 2010. 31(7): p. 1465-1485.
73. Hench, L.L., *Bioceramics: From Concept to Clinic. Journal of the American Ceramic Society*, 1991. 74(7): p. 1487-1510.
74. Boccaccini, A.R. and V. Maquet, *Bioresorbable and bioactive polymer/Bioglass® composites with tailored pore structure for tissue engineering applications. Composites Science and Technology*, 2003. 63(16): p. 2417-2429.
75. Misra, S.K., T. Ansari, D. Mohn, S.P. Valappil, T.J. Brunner, W.J. Stark, I. Roy, J.C. Knowles, P.D. Sibbons, E.V. Jones, A.R. Boccaccini, and V. Salih, *Effect of nanoparticulate bioactive glass particles on bioactivity and cytocompatibility of poly(3-hydroxybutyrate) composites. J R Soc Interface*, 2010. 7(44): p. 453-65.
76. Misra, S.K., T. Ansari, D. Mohn, S.P. Valappil, T.J. Brunner, W.J. Stark, I. Roy, J.C. Knowles, P.D. Sibbons, E.V. Jones, A.R. Boccaccini, and V. Salih, *Effect of nanoparticulate bioactive glass particles on bioactivity and cytocompatibility of poly(3-hydroxybutyrate) composites. Journal of The Royal Society Interface*, 2010. 7(44): p. 453-465.
77. Misra, S.K., S.N. Nazhat, S.P. Valappil, M. Moshrefi-Torbati, R.J.K. Wood, I. Roy, and A.R. Boccaccini, *Fabrication and Characterization of Biodegradable Poly(3-hydroxybutyrate) Composite Containing Bioglass. Biomacromolecules*, 2007. 8(7): p. 2112-2119.

78. Ohtsuki, C., M. Kamitakahara, and T. Miyazaki, *Bioactive ceramic-based materials with designed reactivity for bone tissue regeneration*. *Journal of The Royal Society Interface*, 2009. 6(Suppl 3): p. S349-S360.
79. Manjubala, I., M. Sivakumar, R.V. Sureshkumar, and T.P. Sastry, *Bioactivity and osseointegration study of calcium phosphate ceramic of different chemical composition*. *Journal of Biomedical Materials Research*, 2002. 63(2): p. 200-208.
80. Albrektsson, T.A. and C.J. Johansson, *Osteoinduction, osteoconduction and osseointegration*. *European Spine Journal*, 2001. 10(0): p. S96-S101.
81. Hu, Q., B. Li, M. Wang, and J. Shen, *Preparation and characterization of biodegradable chitosan/hydroxyapatite nanocomposite rods via in situ hybridization: a potential material as internal fixation of bone fracture*. *Biomaterials*, 2004. 25(5): p. 779-785.
82. Furukawa, T., Y. Matsusue, T. Yasunaga, Y. Shikinami, M. Okuno, and T. Nakamura, *Biodegradation behavior of ultra-high-strength hydroxyapatite/poly (l-lactide) composite rods for internal fixation of bone fractures*. *Biomaterials*, 2000. 21(9): p. 889-898.
83. Charles, L., M. Shaw, J. Olson, and M. Wei, *Fabrication and mechanical properties of PLLA/PCL/HA composites via a biomimetic, dip coating, and hot compression procedure*. *Journal of Materials Science: Materials in Medicine*, 2010. 21(6): p. 1845-1854.
84. Ashammakhi, N., A.M. Gonzalez, P. Törmälä, and I.T. Jackson, *New resorbable bone fixation*. *Biomaterials in craniomaxillofacial surgery: present and future*. *European Journal of Plastic Surgery*, 2004. 26(8): p. 383-390.
85. Sun, J.-S., H.-C. Liu, W. Hong-Shong Chang, J. Li, F.-H. Lin, and H.-C. Tai, *Influence of hydroxyapatite particle size on bone cell activities: An in vitro study*. *Journal of Biomedical Materials Research*, 1998. 39(3): p. 390-397.
86. Hasegawa, S., S. Ishii, J. Tamura, T. Furukawa, M. Neo, Y. Matsusue, Y. Shikinami, M. Okuno, and T. Nakamura, *A 5-7 year in vivo study of high-strength hydroxyapatite/poly(l-lactide) composite rods for the internal fixation of bone fractures*. *Biomaterials*, 2006. 27(8): p. 1327-1332.
87. Ishii, S., J. Tamura, T. Furukawa, T. Nakamura, Y. Matsusue, Y. Shikinami, and M. Okuno, *Long-term study of high-strength hydroxyapatite/poly(L-lactide) composite rods for the internal fixation of bone fractures: a 2-4-year follow-up study in rabbits*. *J Biomed Mater Res B Appl Biomater*, 2003. 66(2): p. 539-47.
88. Paul, J.P., *Strength requirements for internal and external prostheses*. *Journal of Biomechanics*, 1999. 32(4): p. 381-393.
89. Russias, J., E. Saiz, R.K. Nalla, K. Gryn, R.O. Ritchie, and A.P. Tomsia, *Fabrication and mechanical properties of PLA/HA composites: A study of in vitro degradation*. *Materials Science and Engineering: C*, 2006. 26(8): p. 1289-1295.
90. Hiermer, T., K.G. Schmitt-Thomas, and Z.G. Yang, *Mechanical properties and failure behaviour of cylindrical CFRP-implant-rods under torsion load*. *Composites Part A: Applied Science and Manufacturing*, 1998. 29(11): p. 1453-1461.

91. Kobayashi, S. and K. Sakamoto, Effect of hydrolysis on mechanical properties of tricalcium phosphate/poly-L-lactide composites. *Journal of Materials Science: Materials in Medicine*, 2009. 20(1): p. 379-386.
92. Abou Neel, E.A., I. Ahmed, J.J. Blaker, A. Bismarck, A.R. Boccaccini, M.P. Lewis, S.N. Nazhat, and J.C. Knowles, Effect of iron on the surface, degradation and ion release properties of phosphate-based glass fibres. *Acta Biomaterialia*, 2005. 1(5): p. 553-563.
93. Zhou, Z., Q. Yi, X. Liu, L. Liu, and Q. Liu, In vitro degradation behaviors of Poly-l-lactide/bioactive glass composite materials in phosphate-buffered solution. *Polymer Bulletin*, 2009.
94. Törmälä, P., J. Vasenius, S. Vainionpää, J. Laiho, T. Pohjonen, and P. Rokkanen, Ultra-high-strength absorbable self-reinforced polyglycolide (SR-PGA) composite rods for internal fixation of bone fractures: In vitro and in vivo study. *Journal of Biomedical Materials Research*, 1991. 25(1): p. 1-22.
95. Vasenius, J., S. Vainionpää, K. Vihtonen, M. Mero, J. Mikkola, P. Rokkanen, and P. Törmälä, Biodegradable self-reinforced polyglycolide (SR-PGA) composite rods coated with slowly biodegradable polymers for fracture fixation: strength and strength retention in vitro and in vivo. *Clinical Materials*, 1989. 4(4): p. 307-317.
96. Vainionpää, S., J. Kilpikari, J. Laiho, P. Helevirta, P. Rokkanen, and P. Tormala, Strength and strength retention in vitro, of absorbable, self-reinforced polyglycolide (PGA) rods for fracture fixation. *Biomaterials*, 1987. 8(1): p. 46-8.
97. Niemelä, T., H. Niiranen, M. Kellomäki, and P. Törmälä, Self-reinforced composites of bioabsorbable polymer and bioactive glass with different bioactive glass contents. Part I: Initial mechanical properties and bioactivity. *Acta Biomaterialia*, 2005. 1(2): p. 235-242.
98. Niiranen, H., T. Pyhältö, P. Rokkanen, M. Kellomäki, and P. Törmälä, In vitro and in vivo behavior of self-reinforced bioabsorbable polymer and self-reinforced bioabsorbable polymer/bioactive glass composites. *Journal of Biomedical Materials Research Part A*, 2004. 69A(4): p. 699-708.
99. Hu, Y.S., P.Z. Zhang, D. Song, Y.M. Wang, and D.R. Bai, Preparation and Properties of Self-reinforced L- and D,L-lactide Copolymer Rods. *Chinese Chemical Letters* 2000. 11(11): p. 1023-1026.
100. Niemela, T., Effect of β -tricalcium phosphate addition on the in vitro degradation of self-reinforced poly-L,D-lactide. *Polymer Degradation and Stability*, 2005. 89(3): p. 492-500.
101. Majola, A., S. Vainionpää, P. Rokkanen, H.M. Mikkola, and P. Törmälä, Absorbable self-reinforced polylactide (SR-PLA) composite rods for fracture fixation: strength and strength retention in the bone and subcutaneous tissue of rabbits. *Journal of Materials Science: Materials in Medicine*, 1992. 3(1): p. 43-47.
102. Törmälä, P., T. Pohjonen, and P. Rokkanen, Bioabsorbable polymers: materials technology and surgical applications. *Proceedings of the Institution of Mechanical Engineers - H*, 1998. 212(2): p. 101 - 111.

103. Pietrzak, W.S., D.S. Caminear, and S.V. Perns, Mechanical characteristics of an absorbable copolymer internal fixation pin. *The Journal of Foot and Ankle Surgery*, 2002. 41(6): p. 379-388.
104. Niemelä, T., M. Kellomäki, and P. Törmälä, In Vitro Degradation of Osteoconductive Poly-L/DL-Lactide / β -TCP Composites. *Key Engineering Materials*, 2004. 254-256: p. 509 -512.
105. Niemelä, T., H. Niiranen, and M. Kellomäki, Self-reinforced composites of bioabsorbable polymer and bioactive glass with different bioactive glass contents. Part II: In vitro degradation. *Acta Biomaterialia*, 2008. 4(1): p. 156-164.
106. Tuomo, P., L. Matti, P. Hannu, R. Pentti, N. Henna, and T. Pertti, Fixation of distal femoral osteotomies with self-reinforced poly(L/DL)lactide 70 : 30/bioactive glass composite rods. An experimental study on rats. *Journal of Materials Science: Materials in Medicine*, 2004. 15(3): p. 275-281.
107. Mohammadi, M.S., I. Ahmed, N. Muja, S. Almeida, C.D. Rudd, M.N. Bureau, and S.N. Nazhat, Effect of Si and Fe doping on calcium phosphate glass fibre reinforced polycaprolactone bone analogous composites. *Acta Biomater*, 2012. 8(4): p. 1616-1626.
108. Brauer, D., C. Rüssel, S. Vogt, J. Weisser, and M. Schnabelrauch, Degradable phosphate glass fiber reinforced polymer matrices: mechanical properties and cell response. *Journal of Materials Science: Materials in Medicine*, 2008. 19(1): p. 121-127.
109. Parsons, A.J., I. Ahmed, P. Haque, B. Fitzpatrick, M.I.K. Niazi, G.S. Walker, and C.D. Rudd, Phosphate Glass Fibre Composites for Bone Repair. *Journal of Bionic Engineering*, 2009. 6(4): p. 318-323.
110. Lin, S., S. Krebs, A. Nazre, and R. King, Totally Bioabsorbable composites, in 39th International SAMPE Symposium1994. p. 1981 - 1985.
111. Parsons, A.J., I. Ahmed, N. Han, R. Felfel, and C.D. Rudd, Mimicking Bone Structure and Function with Structural Composite Materials. *Journal of Bionic Engineering*, 2010. 7(Supplement 1): p. S1-S10.
112. Ahmed, I., I. Jones, A. Parsons, J. Bernard, J. Farmer, C. Scotchford, G. Walker, and C. Rudd, Composites for bone repair: phosphate glass fibre reinforced PLA with varying fibre architecture. *Journal of Materials Science: Materials in Medicine*, 2011. 22: p. 1825 - 1834.
113. Han, N., I. Ahmed, A.J. Parsons, L. Harper, C.A. Scotchford, B.E. Scammell, and C.D. Rudd, Influence of screw holes and gamma sterilization on properties of phosphate glass fiber-reinforced composite bone plates. *J Biomater Appl*, 2011.
114. Kasuga, T., Y. Ota, M. Nogami, and Y. Abe, Preparation and mechanical properties of polylactic acid composites containing hydroxyapatite fibers. *Biomaterials*, 2001. 22(1): p. 19-23.
115. Huttunen, M., P. Tormala, P. Godinho, and M. Kellomäki, Fiber-reinforced bioactive and bioabsorbable hybrid composites. *Biomedical Materials*, 2008. 3(3): p. 034106.

116. Ashammakhi, N. and P. Rokkanen, Absorbable polyglycolide devices in trauma and bone surgery. *Biomaterials*, 1997. 18(1): p. 3-9.
117. Kmetty, Á.k., T.s. BÃ¡rÃ¡ny, and J.z. Karger-Kocsis, Self-reinforced polymeric materials: A review. *Progress in Polymer Science*, 2010. 35(10): p. 1288-1310.
118. Wang, H.P., S.P. Chum, A. Hiltner, and E. Baer, Deformation of elastomeric polyolefin spherulites. *Journal of Polymer Science Part B: Polymer Physics*, 2009. 47(13): p. 1313-1330.
119. Ward, I.M. and P.J. Hine, Novel composites by hot compaction of fibers. *Polymer Engineering & Science*, 1997. 37(11): p. 1809-1814.
120. Ashammakhi, N., H. Peltoniemi, E. Waris, R. Suuronen, W. Serlo, M. Kellomäki, P. Tormala, and T. Waris, Developments in craniomaxillofacial surgery: use of self-reinforced bioabsorbable osteofixation devices. *Plast Reconstr Surg*, 2001. 108(1): p. 167-80.
121. Niemela, T., D.B. Aydogan, M. Hannula, J. Hyttinen, and M. Kellomäki, Determination of bioceramic filler distribution and porosity of self-reinforced bioabsorbable composites using micro-computed tomography. *Composites Part A: Applied Science and Manufacturing*, 2011. 42(5): p. 534-542.
122. Kharazi, A.Z., M.H. Fathi, and F. Bahmany, Design of a textile composite bone plate using 3D-finite element method. *Materials & Design*, 2010. 31(3): p. 1468-1474.
123. Evans, S.L. and P.J. Gregson, Composite technology in load-bearing orthopaedic implants. *Biomaterials*, 1998. 19(15): p. 1329-1342.
124. Hull, D. and T.W. Clyne, *An Introduction to Composite Materials Cambridge Solid State Science Series* 1981, Cambridge.
125. Smith, P.A. and J.A. Yeomans, Benefits of Fiber and Particulate Reinforcement, in *MATERIAL SCIENCE AND ENGINEERING*, R.D. Rawlings, Editor 2009. p. 133 - 154.
126. Saidpour, S., Assessment of Carbon Fibre Composite Fracture Fixation Plate Using Finite Element Analysis. *Annals of Biomedical Engineering*, 2006. 34(7): p. 1157-1163.
127. Wan, Y.Z., Y.L. Wang, Q.Y. Li, and X.H. Dong, Influence of surface treatment of carbon fibers on interfacial adhesion strength and mechanical properties of PLA-based composites. *Journal of Applied Polymer Science*, 2001. 80(3): p. 367-376.
128. Wenfeng, X. The Mechanical Properties of Carbon Fiber/Poly(lactide)/Chitosan Composites. in *Bioinformatics and Biomedical Engineering (iCBBE)*, 2010 4th International Conference on.
129. Liao, X.-l., W.-f. Xu, Y.-l. Wang, B. Jia, and G.-y. Zhou, Effect of porous structure on mechanical properties of C/PLA/nano-HA composites scaffold. *Transactions of Nonferrous Metals Society of China*, 2009. 19, Supplement 3(0): p. s748-s751.
130. Pirhonen, E. and P. Törmälä, Coating of bioactive glass 13-93 fibres with biomedical polymers. *Journal of Materials Science*, 2006. 41(7): p. 2031-2036.

131. Matilde, A.D.D., J.C. Nichola, and L.H. Larry, Tensile properties of bioactive fibers for tissue engineering applications. *Journal of Biomedical Materials Research*, 2000. 53(3): p. 199-203.
132. Kim, H.W., H.E. Kim, and J.C. Knowles, Production and Potential of Bioactive Glass Nanofibers as a Next-Generation Biomaterial. *Advanced Functional Materials*, 2006. 16(12): p. 1529-1535.
133. Pirhonen, E., H. Niiranen, T. Niemelä, M. Brink, and P. Törmälä, Manufacturing, mechanical characterization, and <I>in vitro</I> performance of bioactive glass 13-93 fibers. *Journal of Biomedical Materials Research Part B: Applied Biomaterials*, 2006. 77B(2): p. 227-233.
134. Scotchford, C.A., M. Shataheri, P.S. Chen, M. Evans, A.J. Parsons, G.A. Aitchison, C. Efeoglu, J.L. Burke, A. Vikram, S.E. Fisher, and C.D. Rudd, Repair of calvarial defects in rats by prefabricated, degradable, long fibre composite implants. *J Biomed Mater Res A*, 2010. 96(1): p. 230-8.
135. Charvet, J.L., J.A. Cordes, and H. Alexander, Mechanical and fracture behavior of a fiber-reinforced bioabsorbable material for orthopaedic applications. *Journal of Materials Science: Materials in Medicine*, 2000. 11(2): p. 101-109.
136. Borbely, P., K. Gulabivala, and J.C. Knowles, Degradation properties and ion release characteristics of Resilon and phosphate glass/polycaprolactone composites. *Int Endod J*, 2008. 41(12): p. 1093-100.
137. DePolo, W.S. and D.G. Baird, Particulate reinforced PC/PBT composites. I. Effect of particle size (nanotalc versus fine talc particles) on dimensional stability and properties. *Polymer Composites*, 2009. 30(2): p. 188-199.
138. De, S.K. and J.R. White, *Short Fibre-Polymer Composites* 1996: Woodhead Publishing.
139. Krüger, R. and J. Groll, Fiber reinforced calcium phosphate cements – On the way to degradable load bearing bone substitutes? *Biomaterials*, 2012. 33(25): p. 5887-5900.
140. Tsuchida, J., J. Schneider, M.T. Rinke, and H. Eckert, Structure of Ternary Aluminum Metaphosphate Glasses. *The Journal of Physical Chemistry C*. 115(44): p. 21927-21941.
141. Karabulut, M., E. Melnik, R. Stefan, G.K. Marasinghe, C.S. Ray, C.R. Kurkjian, and D.E. Day, Mechanical and structural properties of phosphate glasses. *Journal of Non-Crystalline Solids*, 2001. 288: p. 8-17.
142. Brow, R.K., Review: the structure of simple phosphate glasses. *Journal of Non-Crystalline Solids*, 2000. 263-264: p. 1-28.
143. Lee, Y.K. and S.H. Choi, Novel Calcium Phosphate Glass for Hard-Tissue Regeneration. *J Korean Acad Periodontol*, 2008. 28: p. 273-298.
144. Day, D.E., Z. Wu, C.S. Ray, and P. Hrma, Chemically durable iron phosphate glass wastefoms. *Journal of Non-Crystalline Solids*, 1998. 241(1): p. 1-12.
145. Sales, B.C. and L.A. Boatner, Lead-Iron Phosphate Glass: A Stable Storage Medium for High-Level Nuclear Waste. *Science*, 1984. 226(4670): p. 45-48.

146. Ahmed, I., M. Lewis, I. Olsen, and J.C. Knowles, Phosphate glasses for tissue engineering: Part 1. Processing and characterisation of a ternary-based P_2O_5 -CaO- Na_2O glass system. *Biomaterials*, 2004. 25(3): p. 491-499.
147. Knowles, J.C., K. Franks, and I. Abrahams, Investigation of the solubility and ion release in the glass system K_2O - Na_2O -CaO- P_2O_5 . *Biomaterials*, 2001. 22(23): p. 3091-3096.
148. Vitale-Brovarone, C., G. Novajra, J. Lousteau, D. Milanese, S. Raimondo, and M. Fornaro, Phosphate glass fibres and their role in neuronal polarization and axonal growth direction. *Acta Biomaterialia*, 2012. 8(3): p. 1125-1136.
149. Haque, P., A.J. Parsons, I.A. Barker, I. Ahmed, D.J. Irvine, G.S. Walker, and C.D. Rudd, Interfacial properties of phosphate glass fibres/PLA composites: Effect of the end functionalities of oligomeric PLA coupling agents. *Composites Science and Technology*, 2010. 70(13): p. 1854-1860.
150. Bunker, B.C., G.W. Arnold, and J.A. Wilder, Phosphate glass dissolution in aqueous solutions. *Journal of Non-Crystalline Solids*, 1984. 64(3): p. 291-316.
151. Ropp, R.C., *Inorganic polymeric glasses* 1992: Elsevier.
152. Abou Neel, E.A., I. Ahmed, J. Pratten, S.N. Nazhat, and J.C. Knowles, Characterisation of antibacterial copper releasing degradable phosphate glass fibres. *Biomaterials*, 2005. 26(15): p. 2247-2254.
153. Moss, R.M., D.M. Pickup, I. Ahmed, J.C. Knowles, M.E. Smith, and R.J. Newport, Structural Characteristics of Antibacterial Bioresorbable Phosphate Glass. *Advanced Functional Materials*, 2008. 18(4): p. 634-639.
154. Martin, S.W., Review of the structure of phosphate glasses. *European Journal of Solid State and Inorganic Chemistry*, 1991: p. 163 - 205.
155. Hoppe, U., A structural model for phosphate glasses. *Journal of Non-Crystalline Solids*, 1996. 195(1-2): p. 138-147.
156. Urman, K. and J.U. Otaigbe, New phosphate glass/polymer hybrids--Current status and future prospects. *Progress in Polymer Science*, 2007. 32(12): p. 1462-1498.
157. Abou Neel, E.A., W. Chrzanowski, D.M. Pickup, L.A. O'Dell, N.J. Mordan, R.J. Newport, M.E. Smith, and J.C. Knowles, Structure and properties of strontium-doped phosphate-based glasses. *Journal of The Royal Society Interface*, 2009. 6(34): p. 435-446.
158. Griffith, A.A., *The Phenomena of Rupture and Flow in Solids*. Philosophical Transactions of the Royal Society of London. Series A, Containing Papers of a Mathematical or Physical Character, 1921. 221(582-593): p. 163-198.
159. Ahmed, I., M. Lewis, I. Olsen, and J.C. Knowles, Phosphate glasses for tissue engineering: Part 2. Processing and characterisation of a ternary-based P_2O_5 -CaO- Na_2O glass fibre system. *Biomaterials*, 2004. 25(3): p. 501-507.
160. Simon, V. and H. Mocut, Glass formation and dissolution properties of Na_2O -CaO- P_2O_5 glasses in simulated body fluids. *Romanian Reports in Physics*, 2004. 56(3): p. 424 - 429.

161. Franks, K., I. Abrahams, G. Georgiou, and J.C. Knowles, Investigation of thermal parameters and crystallisation in a ternary CaO-Na₂O-P₂O₅-based glass system. *Biomaterials*, 2001. 22(5): p. 497-501.
162. Samickannian, A., R. Venkatachalam, R. Nallaiyan, and N.B. Abubakkar, Structural and Textural Modifications of Ternary Phosphate Glasses by Thermal Treatment. *International Journal of Applied Glass Science*, 2011. 2(3): p. 222-234.
163. Walter, G., J. Vogel, U. Hoppe, and P. Hartmann, The structure of CaO-Na₂O-MgO-P₂O₅ invert glass. *Journal of Non-Crystalline Solids*, 2001. 296(3): p. 212-223.
164. Brauer, D.S., N. Karpukhina, R.V. Law, and R.G. Hill, Effect of TiO₂ addition on structure, solubility and crystallisation of phosphate invert glasses for biomedical applications. *Journal of Non-Crystalline Solids*, 2010. 356(44-49): p. 2626-2633.
165. Dias, A.G., M.A. Lopes, I.R. Gibson, and J.D. Santos, In vitro degradation studies of calcium phosphate glass ceramics prepared by controlled crystallization. *Journal of Non-Crystalline Solids*, 2003. 330(1-3): p. 81-89.
166. Gao, H., T. Tan, and D. Wang, Dissolution mechanism and release kinetics of phosphate controlled release glasses in aqueous medium. *Journal of Controlled Release*, 2004. 96(1): p. 29-36.
167. Melba, N., G. Maria-Pau, C. Jerome, S. Martínez, G. Avila, and A.P. Josep, Physicochemical Degradation of Titania-Stabilized Soluble Phosphate Glasses for Medical Applications. *Journal of the American Ceramic Society*, 2003. 86(8): p. 1345-1352.
168. Leonardi, E., G. Ciapetti, N. Baldini, G. Novajra, E. VernÃ©, F. Baino, and C. Vitale-Brovarone, Response of human bone marrow stromal cells to a resorbable P₂O₅-SiO₂-CaO-MgO-Na₂O-K₂O phosphate glass ceramic for tissue engineering applications. *Acta Biomaterialia*, 2010. 6(2): p. 598-606.
169. Uo, M., M. Mizuno, Y. Kuboki, A. Makishima, and F. Watari, Properties and cytotoxicity of water soluble Na₂O-CaO-P₂O₅ glasses. *Biomaterials*, 1998. 19(24): p. 2277-2284.
170. Delahaye, F., L. Montagne, G.r. Palavit, J. Claude Touray, and P. Baillif, Acid dissolution of sodium-calcium metaphosphate glasses. *Journal of Non-Crystalline Solids*, 1998. 242(1): p. 25-32.
171. Ahmed, A.A., A.A. Ali, D.A.R. Mahmoud, and A.M. El-Fiqi, Preparation and characterization of antibacterial P₂O₅-CaO-Na₂O-Ag₂O glasses. *Journal of Biomedical Materials Research Part A*, 2011. 98A(1): p. 132-142.
172. Lee, S., A. Obata, and T. Kasuga, Ion release from SrO-CaO-TiO₂-P₂O₅ glasses in Tris buffer solution. *Journal of the Ceramic Society of Japan*, 2009. 117(1369): p. 935-938.
173. Sales, B.C., L.A. Boatner, and J.O. Ramey, Chromatographic studies of the structures of amorphous phosphates: a review. *Journal of Non-Crystalline Solids*, 2000. 263-264: p. 155-166.

174. Hoppe, A., N.S. Güldal, and A.R. Boccaccini, A review of the biological response to ionic dissolution products from bioactive glasses and glass-ceramics. *Biomaterials*, 2011. 32(11): p. 2757-2774.
175. Rigidel, Q. and F. Muñoz, Effect of nitridation on the aqueous dissolution of $\text{Na}_2\text{O-K}_2\text{O-CaO-P}_2\text{O}_5$ metaphosphate glasses. *Acta Biomaterialia*, 2011. 7(6): p. 2631-2636.
176. Navarro, M., M.P. Ginebra, and J.A. Planell, Cellular response to calcium phosphate glasses with controlled solubility. *J Biomed Mater Res A*, 2003. 67(3): p. 1009-15.
177. Abou Neel, E.A., W. Chrzanowski, and J.C. Knowles, Effect of increasing titanium dioxide content on bulk and surface properties of phosphate-based glasses. *Acta Biomaterialia*, 2008. 4(3): p. 523-534.
178. Abou Neel, E. and J. Knowles, Physical and biocompatibility studies of novel titanium dioxide doped phosphate-based glasses for bone tissue engineering applications. *Journal of Materials Science: Materials in Medicine*, 2008. 19(1): p. 377-386-386.
179. Brauer, D.S., C. Rüsel, W. Li, and S. Habelitz, Effect of degradation rates of resorbable phosphate invert glasses on in vitro osteoblast proliferation. *Journal of Biomedical Materials Research Part A*, 2006. 77A(2): p. 213-219.
180. Mohammadi, S.M., I. Ahmed, N. Muja, C. Rudd, M. Bureau, and S. Nazhat, Effect of phosphate-based glass fibre surface properties on thermally produced poly(lactic acid) matrix composites. *Journal of Materials Science: Materials in Medicine*, 2011. 22(12): p. 2659-2672.
181. Parsons, A.J., L.D. Burling, C.A. Scotchford, G.S. Walker, and C.D. Rudd, Properties of sodium-based ternary phosphate glasses produced from readily available phosphate salts. *Journal of Non-Crystalline Solids*, 2006. 352(50-51): p. 5309-5317.
182. Shih, P.Y., S.W. Yung, and T.S. Chin, Thermal and corrosion behavior of $\text{P}_2\text{O}_5\text{-Na}_2\text{O-CuO}$ glasses. *Journal of Non-Crystalline Solids*, 1998. 224(2): p. 143-152.
183. Shih, P.Y., S.W. Yung, and T.S. Chin, FTIR and XPS studies of $\text{P}_2\text{O}_5\text{-Na}_2\text{O-CuO}$ glasses. *Journal of Non-Crystalline Solids*, 1999. 244(2-3): p. 211-222.
184. Parsons, A.J., M. Evans, C.D. Rudd, and C.A. Scotchford, Synthesis and degradation of sodium iron phosphate glasses and their in vitro cell response. *Journal of Biomedical Materials Research Part A*, 2004. 71A(2): p. 283-291.
185. Ahmed, I., C.A. Collins, M.P. Lewis, I. Olsen, and J.C. Knowles, Processing, characterisation and biocompatibility of iron-phosphate glass fibres for tissue engineering. *Biomaterials*, 2004. 25(16): p. 3223-3232.
186. Yu, X., D.E. Day, G.J. Long, and R.K. Brow, Properties and structure of sodium-iron phosphate glasses. *Journal of Non-Crystalline Solids*, 1997. 215(1): p. 21-31.
187. Ahmed, I., A. Parsons, A. Jones, G. Walker, C. Scotchford, and C. Rudd, Cytocompatibility and Effect of Increasing MgO Content in a Range of Quaternary Invert Phosphate-based Glasses. *J Biomater Appl*, 2010. 24(6): p. 555-575.

188. Franks, K., V. Salih, J.C. Knowles, and I. Olsen, *The effect of MgO on the solubility behavior and cell proliferation in a quaternary soluble phosphate based glass system. Journal of Materials Science: Materials in Medicine*, 2002. 13(6): p. 549-556.
189. Feng, S.S., *Nanoparticles of biodegradable polymers for new-concept chemotherapy. Expert Rev Med Devices*, 2004. 1(1): p. 115-25.
190. Liu, H., E.B. Slamovich, and T.J. Webster, *Less harmful acidic degradation of poly(lactico-glycolic acid) bone tissue engineering scaffolds through titania nanoparticle addition. Int J Nanomedicine*, 2006. 1(4): p. 541-5.
191. Tanner, K.E., *Bioactive ceramic-reinforced composites for bone augmentation. J R Soc Interface*, 2010. 7 Suppl 5: p. S541-57.
192. Ehrenfried, L., M. Patel, and R. Cameron, *The effect of tri-calcium phosphate (TCP) addition on the degradation of polylactide-co-glycolide (PLGA). Journal of Materials Science: Materials in Medicine*, 2008. 19(1): p. 459-466.
193. Zhou, H., A. Touny, and S. Bhaduri, *Fabrication of novel PLA/CDHA bionanocomposite fibers for tissue engineering applications via electrospinning. Journal of Materials Science: Materials in Medicine*, 2011. 22(5): p. 1183-1193.
194. Navarro, M., M. Ginebra, J. Planell, S. Zeppetelli, and L. Ambrosio, *Development and cell response of a new biodegradable composite scaffold for guided bone regeneration. Journal of Materials Science: Materials in Medicine*, 2004. 15(4): p. 419-422.
195. Parsons, A., I. Ahmed, M.I.K. Niazi, R.R. Habeb, B. Fitzpatrick, G.S. Walker, I.A. Jones, and C.D. Rudd, *Mechanical and Degradation Properties of Phosphate Based Glass Fibre/PLA Composites with different Fibre Treatment Regimes. Science and Engineering of Composite Materials*, 2010. 17(4): p. 243 - 260.
196. Salih, V., K. Franks, M. James, G.W. Hastings, J.C. Knowles, and I. Olsen, *Development of soluble glasses for biomedical use Part II: The biological response of human osteoblast cell lines to phosphate-based soluble glasses. Journal of Materials Science: Materials in Medicine*, 2000. 11(10): p. 615-620.
197. Bitar, M., V. Salih, V. Mudera, J.C. Knowles, and M.P. Lewis, *Soluble phosphate glasses: in vitro studies using human cells of hard and soft tissue origin. Biomaterials*, 2004. 25(12): p. 2283-2292.
198. Abou Neel, E.A., T. Mizoguchi, M. Ito, M. Bitar, V. Salih, and J.C. Knowles, *In vitro bioactivity and gene expression by cells cultured on titanium dioxide doped phosphate-based glasses. Biomaterials*, 2007. 28(19): p. 2967-2977.
199. Abou Neel, E.A., A.M. Young, S.N. Nazhat, and J.C. Knowles, *A Facile Synthesis Route to Prepare Microtubes from Phosphate Glass Fibres. Advanced Materials*, 2007. 19(19): p. 2856-2862.
200. Choueka, J., J.L. Charvet, H. Alexander, Y.O. Oh, G. Joseph, N.C. Blumenthal, and W.C. LaCourse, *Effect of annealing temperature on the degradation of reinforcing fibers for absorbable implants. J Biomed Mater Res*, 1995. 29(11): p. 1309-15.

201. Cozien-Cazuc, S., A.J. Parsons, G.S. Walker, I.A. Jones, and C.D. Rudd, *Real-time dissolution of $P_{40}Na_{20}Ca_{16}Mg_{24}$ phosphate glass fibers*. *Journal of Non-Crystalline Solids*, 2009. 355(50-51): p. 2514-2521.
202. Cozien-Cazuc, S., A. Parsons, G. Walker, I. Jones, and C. Rudd, *Effects of aqueous aging on the mechanical properties of $P_{40}Na_{20}Ca_{16}Mg_{24}$ phosphate glass fibres*. *Journal of Materials Science*, 2008. 43(14): p. 4834-4839.
203. Feih, S., A. Thrane, and H. Lilholt, *Tensile strength and fracture surface characterisation of sized and unsized glass fibers*. *Journal of Materials Science*, 2005. 40(7): p. 1615-1623.
204. Lin, S.T., S.L. Krebs, S. Kadiyala, K.W. Leong, W.C. LaCourse, and B. Kumar, *Development of bioabsorbable glass fibres*. *Biomaterials*, 1994. 15(13): p. 1057-1061.
205. Haque, P., I.A. Barker, A. Parsons, K.J. Thurecht, I. Ahmed, G.S. Walker, C.D. Rudd, and D.J. Irvine, *Influence of compatibilizing agent molecular structure on the mechanical properties of phosphate glass fiber-reinforced PLA composites*. *Journal of Polymer Science Part A: Polymer Chemistry*, 2010. 48(14): p. 3082-3094.

CHAPTER 3.

PHYSICAL, MECHANICAL, DEGRADATION AND CYTOCOMPATIBILITY PROPERTIES OF BIORESORBABLE FIBRE REINFORCED COMPOSITES

3.1 SUMMARY

In this chapter, bioresorbable phosphate glass fibres (PGF) were used to reinforce PLA. PLA/PGF random mat (RM) and unidirectional (UD) composites were prepared via laminate stacking and compression moulding with fibre volume fractions of ~ 18% and ~ 14% respectively. The composites were degraded in phosphate buffered saline (PBS) at 37°C for up to 95 days. The water uptake and mass change for the UD composites were higher than the RM composites and PLA alone. The crystallinity of the PLA increased during the first few weeks and levelled off. In addition, XRD studies detected a small crystalline peak at 16.6° for PLA sample after 42 days of immersion time.

Initial flexural strength of RM and UD composites was ~ 106 MPa and ~ 115 MPa, whilst the modulus was ~ 6.7 GPa and ~ 9 GPa respectively. After 95 days of immersion in PBS at 37°C, the strength decreased to 48 and 52 MPa respectively, which was assumed to be as a result of fibre-matrix interface degradation. There was no significant change in flexural modulus for the UD composites, whilst the RM composites showed a decrease of ~ 45% to 3.5 GPa after 95 days of degradation in PBS at 37°C. The molecular weight of PLA alone, RM and UD composites decreased linearly with time during degradation due to chain scission of the matrix. Short fibre pull-out length was seen from SEM micrographs of the fractured surface for both RM and UD composites after 95 days of immersion due to degradation of the fibre-matrix interface via hydrolysis. Cytocompatibility studies revealed that both RM and UD composites supported human osteosarcoma cell attachment and maintained > 98% viable cells. They also showed no significant difference when compared with PLA alone or the tissue culture plastic control (Thermanox®) used.

3.2 INTRODUCTION

Over the last few decades, biodegradable polymers such as Poly ϵ -caprolactone (PCL), Poly glycolic acid (PGA), and Poly lactic acid (PLA) have attracted huge interest for use in biomedical applications. PLA is one of the most widely investigated bioresorbable materials due to its use in many different applications such as sutures, pins, plates and screws. However, the mechanical properties of PLA alone are insufficient for some load bearing applications such as screws and plates [1]. Therefore, reinforcement is essential to overcome these limitations, which can be obtained via fabrication of a composite consisting of a bioresorbable polymer (as matrix) and bioceramics (as reinforcement) [2]. The initial mechanical properties for bioresorbable composites (either self-reinforced, particulate and/or fibre reinforced) have been summarised in Table 2-3.

Zhou *et al.* [3] prepared a composite from Poly (L-lactide) (PLLA) and bioactive glass (BG) particulates in weight proportion 90/10 by dissolution in Dichloromethane (DCM). The initial flexural strength and modulus of the composite produced was 153.9 MPa and 3.59 GPa respectively, whilst values of 233 MPa and 3.25 GPa for PLLA alone were achieved. The decrease in initial flexural strength of the composite was stated to be due to void formation created by the absence of chemical adhesion between the polymer and BG particles during composite preparation. The flexural properties dropped by 20% for strength and 62% for modulus after soaking in phosphate-buffered solution (PBS) at 37°C for 20 weeks. The authors also found that the degradation rate of the PLLA/BG composite was slower than that for PLLA alone.

Fabrication of a composite comprising PLA and HA was produced via hot pressing [4] with two kinds of HA (a fine powder and whiskers of 25-30 μm length and 5 μm diameter) used as reinforcement. The initial flexural strength and modulus of an 80 wt% HA composite was 130 MPa and 10 GPa, respectively. The strength decreased rapidly to 60 MPa after only one day immersion in Hank's Balanced Salt Solution (HASS), whilst the modulus decreased slightly over 20 days to 9 GPa.

Mechanical and degradation profiles were investigated for PCL reinforced with 40 volume % of phosphate glass particles (PGP) [5]. Initially, the flexural strength decreased slightly, whilst the modulus was significantly higher than the PCL alone. After 28 days in PBS at 37°C, the mechanical properties for the composites decreased rapidly due to degradation of the filler (PGP) leaving behind a porous PCL structure. This was confirmed via scanning electron microscope (SEM) analysis and mass loss studies.

It is well known that particulate reinforced composites have relatively weaker mechanical properties as compared to other reinforcement morphologies such as fibres. Preliminary mechanical properties of a binary calcium phosphate glass fibre/PCL RM composite were investigated. The flexural strength of the composite was similar to PCL alone (25-30 MPa), whilst the modulus increased with increasing fibre volume fraction to 1 and 2.4 GPa for a 6.4% and 17% volume fraction composite. The flexural modulus for PCL alone was ~0.5 GPa. Mass loss was also monitored and shown to increase from 8% for the lower fibre V_f composite to 20% for the higher V_f samples over a 350 hour time period in deionised water. No mass loss was observed for PCL alone over the course of this study [6]. PCL/phosphate based glass fibre (PGF) reinforced RM composites ($V_f = 18\%$) were also investigated by Mohammadi *et al.* [5, 7] and demonstrated similar initial flexural properties. They compared the mechanical properties of PCL/PGF and PCL/PGP composites since the glass compositions investigated were similar. They concluded that fibre reinforcement effect was greater than that for particulates and they attributed this to high aspect ratio for the fibres leading to high stress transfer from matrix to the fibre reinforcement.

Bioactive glass 1-98 (BaG) UD fibres were also used to reinforce a starch-polycaprolactone (SPCL) polymer. It was found that the bending strength of the composite was 50 MPa (66% higher than the value of SPCL alone). However, the strength reduced to 24 MPa after 2 weeks hydrolysis in PBS at 37°C [8].

The mechanical property retention of composites consisting of PCL with continuous Bioglass fibres (45S5) was investigated by Jiang *et al.* [9]. Surface treatment using

amine silane and propyl silane was applied to the fibres before preparation of the composite using a monomer transfer moulding (MTM) methodology. The amine silane composite had initial properties of 16 GPa for flexural modulus and 200 MPa for flexural strength. These properties decreased to 7 GPa for modulus and 65 MPa for strength after 41 days degradation in deionised water. However, the initial values for the propyl silane treated composite (9 GPa and 130 MPa for modulus and strength respectively) decreased to below 2 GPa and 35 MPa respectively after degradation in water for 41 days.

Mechanical properties of β -Ca(PO₃)₂ fibre reinforced PLA composites were studied in simulated body fluid (SBF) by Kasuga *et al.* [10]. Prior to degradation, the bending strength of the composite was the same as PLA (~50 MPa), whilst the modulus increased from 3 GPa for PLA alone to 5-6 GPa for the composite. After 90 days degradation in SBF, the flexural strength of PLA and the composite decreased to ~ 5 MPa and ~ 25 MPa, respectively.

Ahmed *et al.* [11] produced PGF fibre reinforced PLA composite, with 14% fibre volume fraction. Its initial flexural properties were 90 MPa for strength and 5 GPa for modulus. The strength and modulus decreased to 40 MPa and 1 GPa respectively after degradation in deionised water at 37°C for 6 weeks. However, properties at intermediate time points were not evaluated. Recently, Ahmed *et al.* [12] investigated degradation and mechanical retention for PLA/PGF composite with range of fibre volume (from 20 to 45 %) fraction and fibre geometries. The initial flexural strength and modulus for RM composite increased to reach ~ 120 MPa and ~ 10 GPa with increasing fibre volume fraction to ~ 45 %. The initial flexural properties for UD composite were ~ 130 MPa for strength and ~ 11.5 GPa for modulus for ~ 24 % fibre volume fraction composites. The composites lost ~ 50 and 80 % of their initial strength and modulus after 14 days of degradation in deionised water at 37°C which might be attributed to degradation of fibre/matrix interface and fibres. Afterwards, no significant change was seen till the end of the study at 42 days. Percentage mass loss for the composites also increased with increasing fibre volume fraction. Most of previous attempts at particulate and

fibre-reinforced composites based on PBG showed a rapid loss in mechanical properties when exposed to water.

In this study, PLA/PGF composites were produced and evaluated with different fibre geometries (chopped random mat versus unidirectional continuous fibres). Their degradation and mechanical properties were investigated over 95 days along with the effect of degradation on thermal properties and density. In addition, cytocompatibility studies were also conducted. Composites based on fixed 50 mol % P_2O_5 have previously been published, which were shown to degrade far too rapidly for application. In this study, fibres from phosphate based glasses PBG's with fixed 40 mol % P_2O_5 were produced which have much better mechanical and biocompatible properties as compared to 50 mol % P_2O_5 formulations previously investigated [13-15].

3.3 MATERIALS AND METHODOLOGY

3.3.1 Phosphate Glass and Fibre Production

Phosphate glass was produced using NaH_2PO_4 , $CaHPO_4$, $FePO_4 \cdot 2H_2O$, P_2O_5 and $MgHPO_4 \cdot 3H_2O$ as starting materials (Sigma Aldrich, UK). The precursors were weighed according to the compositions (50 P_2O_5 -40CaO-5Na₂O-5Fe₂O₃ in mol% - denoted as P50) and (40 P_2O_5 -24MgO-16CaO-16 Na₂O-4Fe₂O₃ in mol% - denoted as P40). The salt mixtures were loaded into a 100 ml volume Pt/5% Au crucible type BC 18 (Birmingham Metal Co., UK) and placed into a furnace for 30 minutes at 350°C (for drying). The crucible was then transferred to another furnace at 1100°C for 90 minutes (for melting). The molten glass was then poured directly onto a steel plate and left to cool to room temperature. The glass was kept in a desiccator until fibre production.

Continuous fibres with ~15 μm diameter (the minimum fibre diameter can be produced) were produced via melt-draw spinning at ~1100°C and ~1600 rpm using a dedicated in-house facility (see Figure 3-1). Diameter of the fibres manufactured can be controlled via the speed of the drum rotation (see Figure 3-2). The fibres were

annealed for 90 minutes at -5°C below the glass transition temperature T_g ($T_g = 490^{\circ}\text{C}$ (for P50) and $T_g = 479^{\circ}\text{C}$ (for P40)) prior to use [15-18].

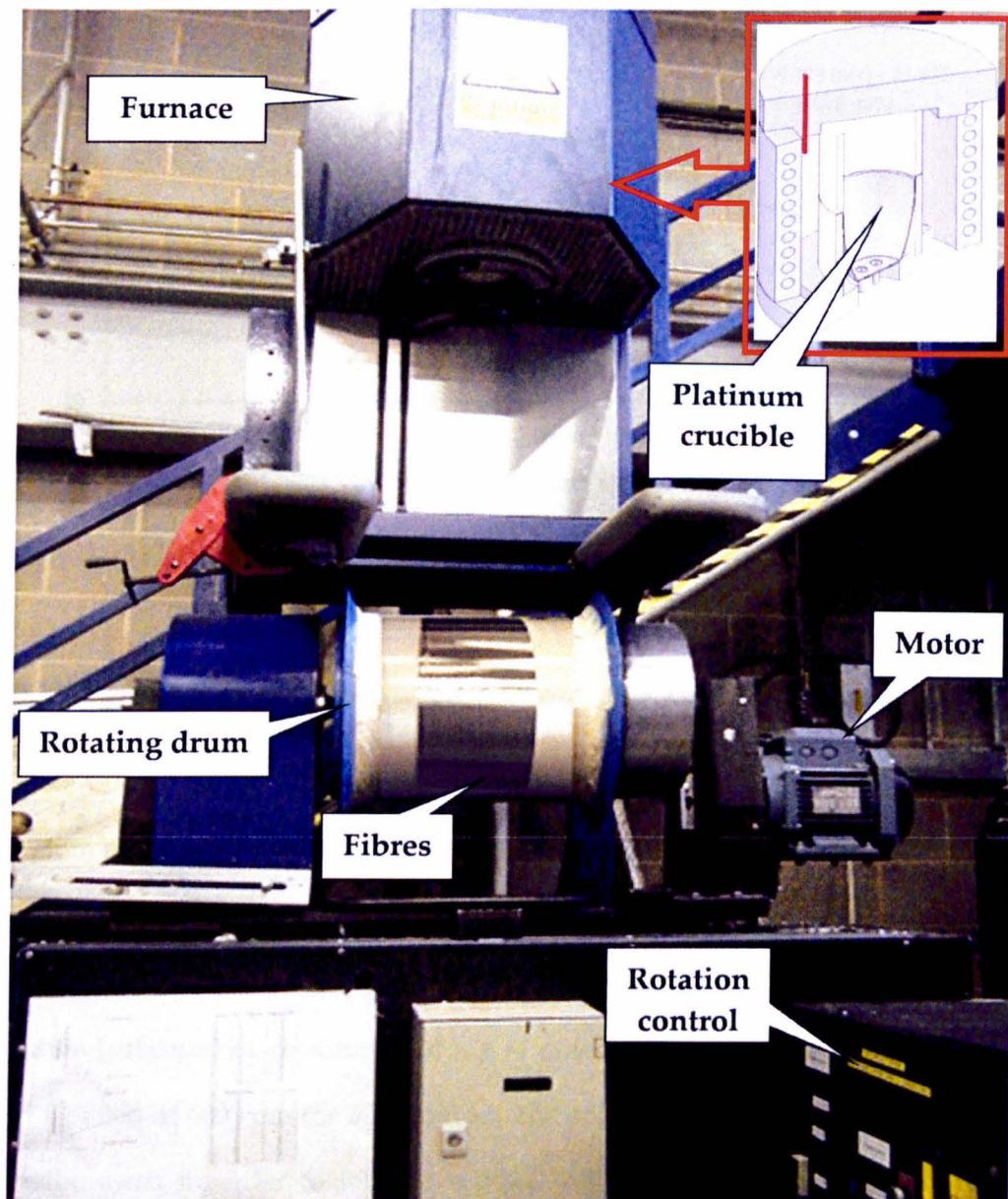


Figure 3-1: Melt-spinning rig for pulling phosphate based glass fibres.

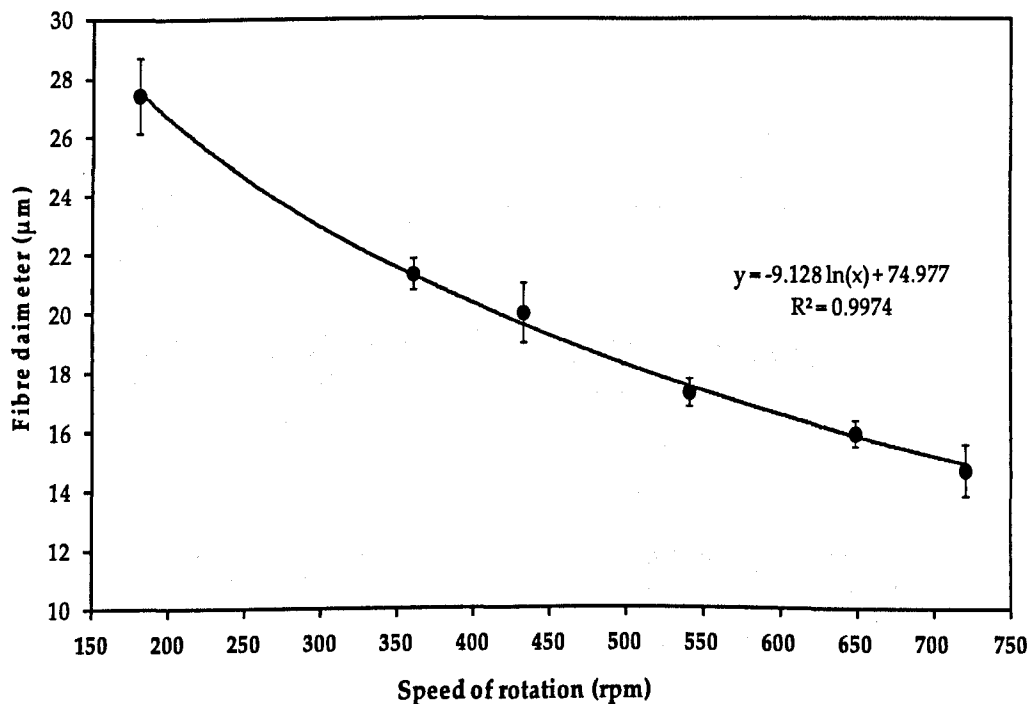


Figure 3-2: The change in fibre diameter against speed of rotation.

3.3.2 Preparation of non-woven random and continuous unidirectional fibre mats

Random non-woven mats (RM) were prepared from 10mm chopped fibres by using slurry deposition apparatus (see Figure 3-3). The fibres were separated into 3g batches and dispersed in a Cellosize (hydroxyethyl cellulose) (Univar Ltd, UK) solution (prepared by dissolution of 11g of powder into 4 litres of deionised water and agitated at 600 rpm for 30 minutes). The solution was strained through a fine metallic mesh in order to remove residual cellosize granules. Fibres were then added to the solution and stirred for 10 minutes at the same rate before extraction by the mesh strainer. The random mats (see Figure 3-4-a) formed were rinsed with deionised water to remove any residual binder before being dried at 50°C for 30 minutes.



Figure 3-3: Laboratory setup for preparing phosphate glass fibre random mats.

The unidirectional (UD) fibre mats (see **Figure 3-4-b**) were produced from continuous 180 mm fibre bundles aligned together (manually) and bound using Cellosize solution. The produced UD mats were also washed carefully with deionised water and dried for 30 minutes at 50°C.

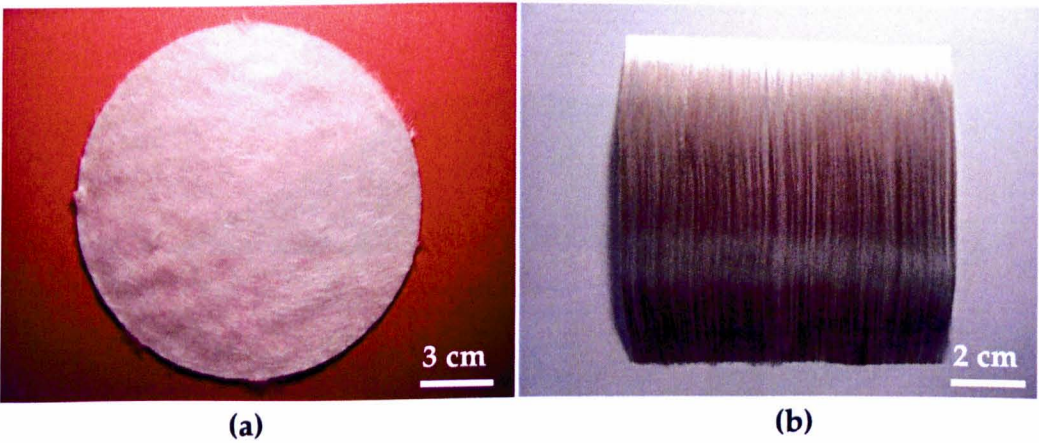


Figure 3-4: Images for the prepared (a) random mat (RM) and (b) unidirectional mat (UD).

3.3.3 Composite production

PLA films (approx 0.2 mm thick) were prepared by compression moulding 5g batches of PLA resin pellets (Resin 3251-D NatureWorks® average Mw ~90,000-120,000). The PLA pellets were dried in a vacuum oven at 50°C for 48 hours before use. The pellets were placed between two metallic plates and heated to 210°C in a press for 10 mins, before being pressed at 3 bar for 30 sec. The plates were then cooled immediately by transferring to a room temperature press at the same pressure.

Both RM and UD composites were prepared via a film stacking process (see **Figure 3-5**). The PLA films were stacked alternately with RMs in a 170mm diameter, 2 mm thick mould cavity between two metallic plates (see **Figure 3-6**). This stack was then heated in the press for 15 mins at 210°C and pressed for 15 mins at 38 bar. The plates were transferred to a second press for cooling to room temperature at 38 bar for 15mins. The same protocol was applied for the UD composite except that the mould cavity had dimensions of 160 mm x 160 mm x 2 mm (see **Figure 3-6**). The resulting laminated composites (see **Figure 3-7**) were cut into 40 mm length x 15 mm width samples for physical testing using a band saw. The fibre volume and mass fractions of the composites were obtained using the matrix burn off method, according to the standard test method ASTM D2584-94 [19]. See **Table 3-1** for details of the composites produced in this study.

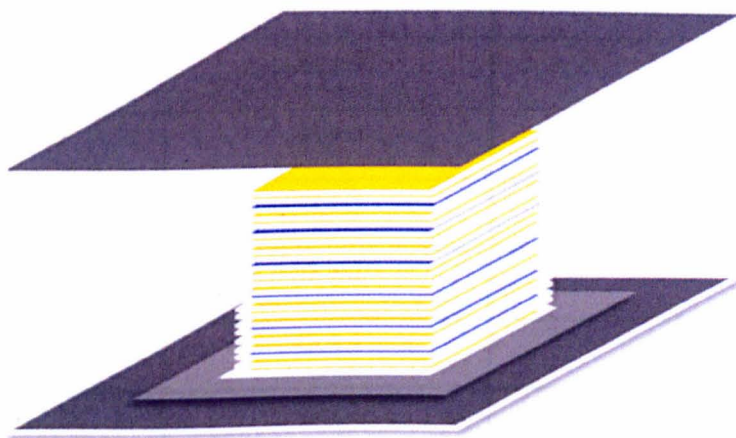


Figure 3-5: Schematic diagram for film stacking process.

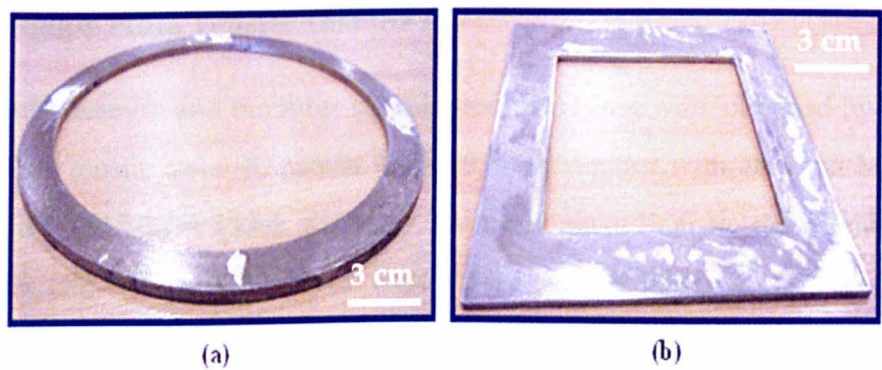


Figure 3-6: Photographs of the moulds used in this study (a) circular shim for random mat composites (RM) and (b) square shim for unidirectional composites (UD)

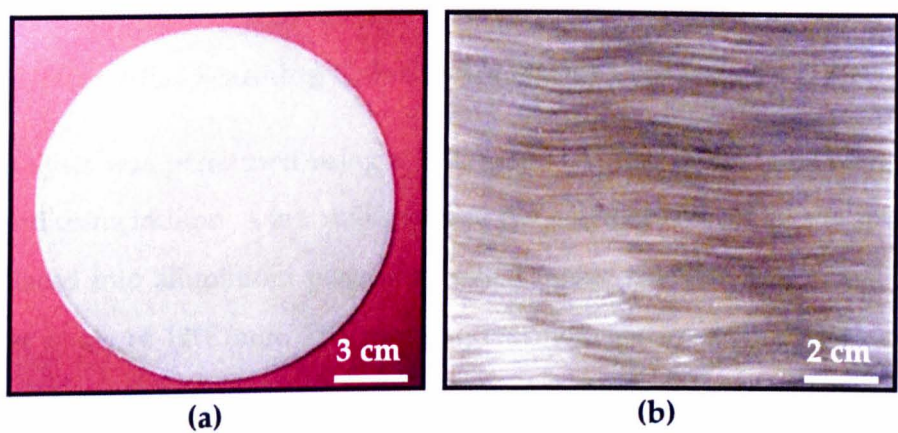


Figure 3-7: Photographs of the prepared (a) RM and (b) UD composites.

Table 3-1: Fibre volume fractions, mass fractions and sample codes for the composites.

Composite Code	Fibre mass fraction (%)	Fibre volume fraction (V_f %)
PLA	N/A	N/A
P40 RM	34 ± 4	18 ± 3
P40 UD	26 ± 3	14 ± 2
P40 RM H	52 ± 3	28 ± 1
P40 UD H	52 ± 2	28 ± 1
P50 RM H	45 ± 4	24 ± 3
P50 UD H	45 ± 2	24 ± 2

P40 RM, P40 UD and H refer to a PLA-PBG random mat, unidirectional fibre-reinforced composites and high fibre volume fraction.

3.3.4 Single Fibre Tensile Test (SFTT)

The tensile strength and modulus for the produced fibres were obtained by using a single fibre tensile tester (Diastron LEX-810 Tensile tester with attached Mitutoyo Series 544 LSM-500S Laser diameter monitor) according to the standard BS ISO11566 [20]. At least 20 fibres were tested with a gauge length of 25 mm. Phosphate based glass fibre (PGF) are essentially brittle and Weibull distribution is an accepted statistical tool used to characterise the failure mode of brittle fibres. In this study, Weibull parameters were obtained from the tensile strength data calculated using Minitab® 15 (version 3.2.1).

3.3.5 Differential Scanning Calorimetry (DSC)

DSC analysis was performed using a DSC Q10 (TA Instrument, USA) which was calibrated using indium. A few milligrams of the polymer and composite specimens were placed into aluminium pans and heated under nitrogen between 40°C and 190°C at a rate of 10°C/min. The resulting thermograms were analysed using TA instrument universal analysis 2000 software version 4.3A to determine the percentage of crystallinity (X_c %). The crystallinity percentage was calculated using *Equation 3-1* [21].

$$\chi (\%) = \frac{\Delta H_m - \Delta H_c}{\Delta H_m^o} \times 100 \quad \text{Equation 3-1}$$

where ΔH_m and ΔH_c are the melting and crystallisation enthalpy (determined from area under melting and crystallisation peaks in DSC thermogram), whilst ΔH_m^o is the melting enthalpy for 100% crystalline PLA (93.1 J/g) [1, 22].

3.3.6 X-Ray Diffraction (XRD)

The X-ray diffraction (XRD) measurements were performed for PLA using a D500 diffractometer (SIEMENS). CuK α radiation ($\lambda = 0.154$ nm) was used at voltage of 40 kV and current of 25 mA. The samples were scanned using a step-scanning method with a step-size of 0.05° and 2 s intervals in the range from 2° to 50° of the diffraction angle (2θ).

3.3.7 Pycnometry

Density of the specimens was measured using a Micromeritics AccuPyc 1330 helium pycnometer (Norcross, GA, USA). During the test, the helium pressure was set to 21 psi with a purging time of approximately 15 min. The measurements were conducted at room temperature and a relative humidity of 50%. Triplicate specimens were run for each sample (see **Figure 3-12**).

3.3.8 Degradation Studies

The degradation study of the specimens produced was performed according to the standard BS EN ISO 10993-13:2010 [23]. Specimens of PLA, RM and UD composites were placed into 30 ml glass vials. The vials were filled with phosphate buffered saline (PBS) (pH =7.4±0.2) and maintained at a temperature of 37°C. Since PBS was used as degradation medium, it was expected that degradation via hydrolysis would occur and as such enzymatic degradation was not considered in this study. At various time points the specimens were extracted and blot dried before weight measurements were obtained. The samples were placed back into vials with fresh PBS solution. At each time point, replicates (n = 6) of each sample were measured and the average reported. The data was plotted as percentage water uptake (W) and mass (M) change against time (see **Figure 3-14** and **Figure 3-15**).

The percentage change in mass (M), water uptake (W) and mass loss (M_L) was determined using the following equations:

$$M = \frac{m - m_i}{m_i} \times 100 \quad (\%) \quad \text{Equation 3-2}$$

$$W = \frac{m - m_d}{m_d} \times 100 \quad (\%) \quad \text{Equation 3-3}$$

$$M_L = \frac{m_d - m_i}{m_i} \times 100 \quad (\%) \quad \text{Equation 3-4}$$

Where m is the mass of degraded sample measured at time t , m_i is the initial mass of the sample and m_d is the mass of degraded sample after drying at 50°C for three days.

3.3.9 Mechanical properties

The initial flexural strength and modulus were evaluated by flexural (three-point bending) tests using a Hounsfield Series S testing machine. These measurements were done according to the standards BS EN ISO 14125:1998 [24] and BS 2782-10:1977 [25]. A crosshead speed of 1 mm/min and a 1 kN load cell was used. The measurements were conducted on wet samples to simulate mechanical properties of the composite within *in-vitro* conditions. The measurements were carried out in triplicate.

The mechanical testing was conducted according to the standards utilising the minimum number of replicates ($n = 3$). The reason for using this minimum number of samples was mainly due to lack of large quantities of PBG fibres to manufacture more composite specimens for all of the tests conducted. In addition, the spread of error between the replicates was considered sufficiently small that $n = 3$ was deemed suitable for the tests conducted.

3.3.10 Gel Permeation Chromatography (GPC)

The weight average molecular weight (M_w) of PLA in the specimens (PLA, P40 RM and P40 UD composites) was determined using Gel Permeation Chromatography (GPC). GPC was performed using a refractive index (RI) detector with HPLC grade chloroform (Fisher Scientific, U.K.) as the eluent. Analysis was performed at 40°C with a flow rate of 1 ml/min through two PLgel Mixed-C columns with a calibration range of 5000 – 300,000 Da calibrated with poly (styrene) narrow standards. All GPC equipment and standards were supplied by Polymer Laboratories (Varian Inc). GPC data was analysed using the Cirrus GPC Offline software package version 3.0.

3.3.11 Scanning Electron Microscopy (SEM)

Specimens were sputter-coated with carbon and examined using a JEOL 6400 SEM with an accelerating voltage of 10KV in secondary electron mode (SE).

3.3.12 Preliminary Cytocompatibility Studies (Cell Viability and Live Dead Staining)

This study was performed in collaboration with Professor Jonathan Knowles group, UCL, Eastman Dental Institute. Human osteosarcoma cell lines (HOS) were used for

this study to assess the biocompatibility of both random (P40 RM) and unidirectional (P40 UD) composites in comparison to PLA and a positive tissue culture plastic control (Thermanox®). Samples were sterilised using UV for 1 h on each side, and then pre-incubated in growth medium [Dulbecco's modified Eagles Medium (DMEM, Gibco), containing 10% fetal calf serum and a 1% penicillin and streptomycin solution (Gibco)] for 4 hours. Cells were cultured on material surface at a density of 3×10^4 /cm² in 4 well culture plates and left for 30 minutes before adding the growth medium. Cultured samples were then kept at 37°C in a humidified atmosphere incubator containing 5% CO₂. The growth medium was changed at day 3 of culture.

Cell viability was determined for 5 replicates (n = 5) at day 1 and 4 of culture by incubating the cultured samples for 1 h in standard growth medium containing 1 µl/ml calcein AM to stain live cells green and propidium iodide to stain any dead cells red. The assessment of cell viability in three dimensions was performed using confocal laser scanning microscopy (CLSM; Bio-Rad, USA) as previously described (Ahmed *et al.* [11]).

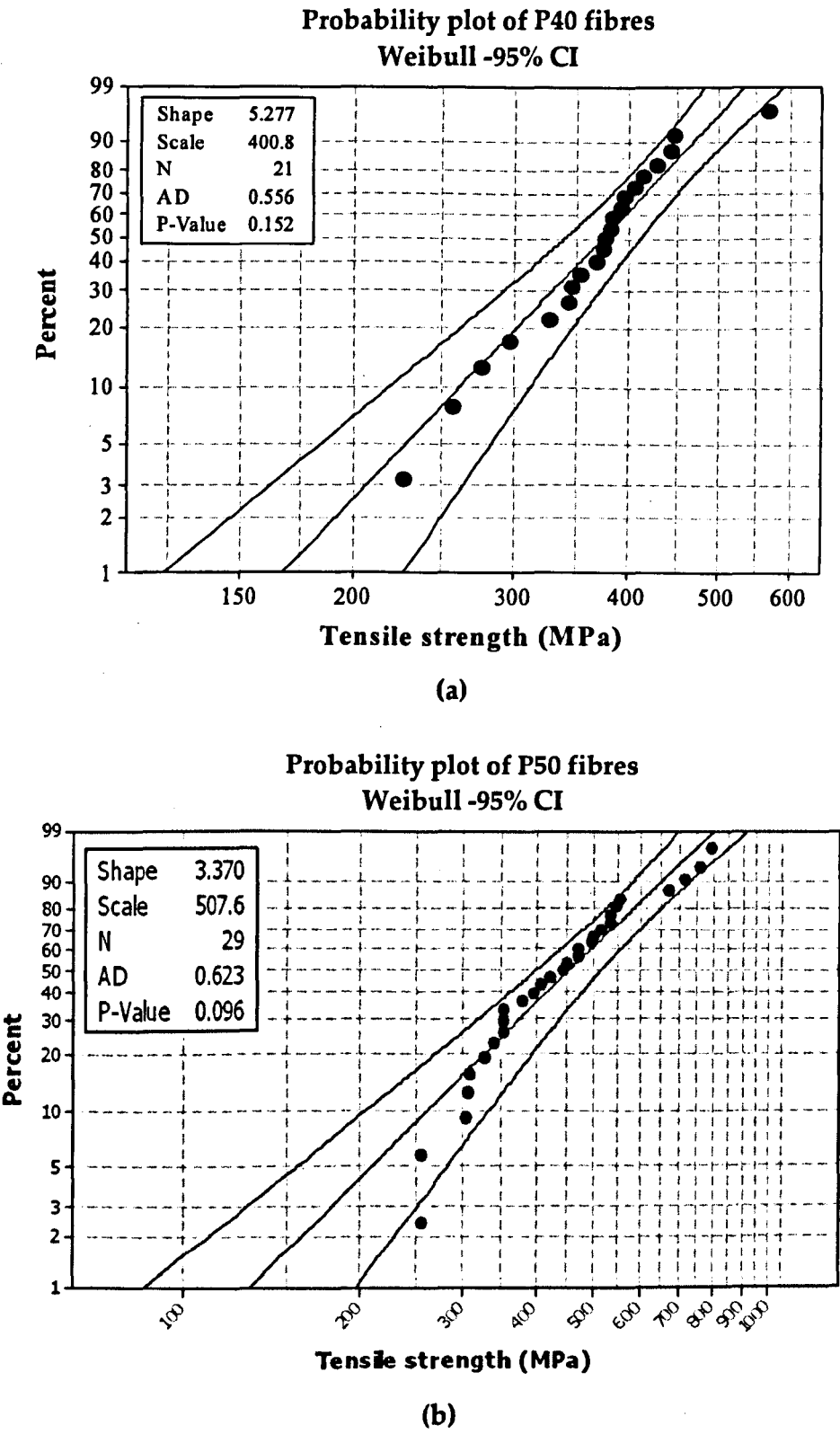
3.3.13 Statistical analysis

One way ANOVA test followed by the Tukey's multiple comparison test was conducted for the results using GraphPad prism software (v. 5). Significance was determined at the 95% level of significance. All data are expressed as mean ± standard error.

3.4 RESULTS

3.4.1 Tensile properties

The average tensile strength and modulus of the used fibres were 370 ± 74 MPa and 62 ± 4 GPa (for P40 fibres) and 456 ± 110 MPa and 52 ± 2 GPa (for P50 fibres) respectively. The high standard errors for the tensile strength observed were probably due to the presence of flaws on the fibre surface after annealing. The Weibull scale and shape parameters were ~ 401 and ~ 5.28 (P40) and ~ 508 and ~ 3.37 (P50) [11] respectively (see Figure 3-8 a and b). As-prepared P40 PBG fibres exhibited a clean smooth surface (see Figure 3-9).



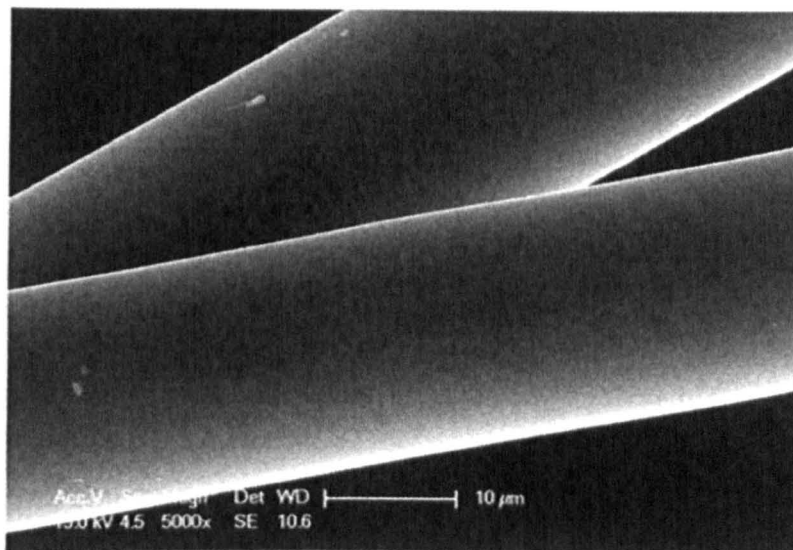


Figure 3-9: SEM micrograph of as-prepared phosphate based glass fibres.

3.4.2 Crystallinity and density

DSC traces were conducted for all samples and **Figure 3-10** shows thermograms for PLA alone, P40 RM and P40 UD composites before degradation. The crystallinity of PLA was measured using DSC during the degradation period as shown in **Figure 3-11**. The initial crystallinity of the PLA was approximately 8 %. The crystallinity increased to ~ 16 % after degradation for 2 weeks in PBS. Subsequently, their values showed a plateau ($P > 0.05$) at around 15 % till the end of degradation study at 95 days. However, determination of the crystallinity for the composites (P40 RM and P40 UD) was difficult to determine as this was dependent mainly on the fraction of PLA with the specimen. Furthermore, the fibre volume fraction can vary considerably between the specimens and the DSC samples which are very small (a few milligrams). Therefore, the amount of PLA within each of the DSC composite samples is very difficult to control. The crystallinity of composites followed similar trends to the PLA profile.

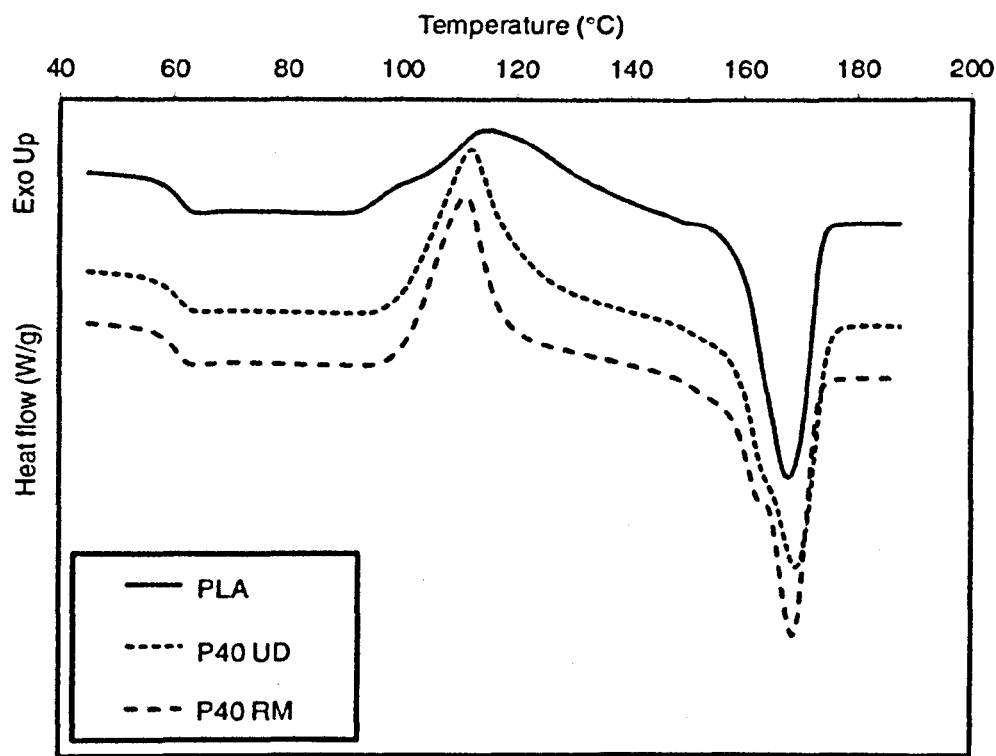


Figure 3-10: DSC traces for PLA alone, P40 RM and P40 UD composites before degradation.

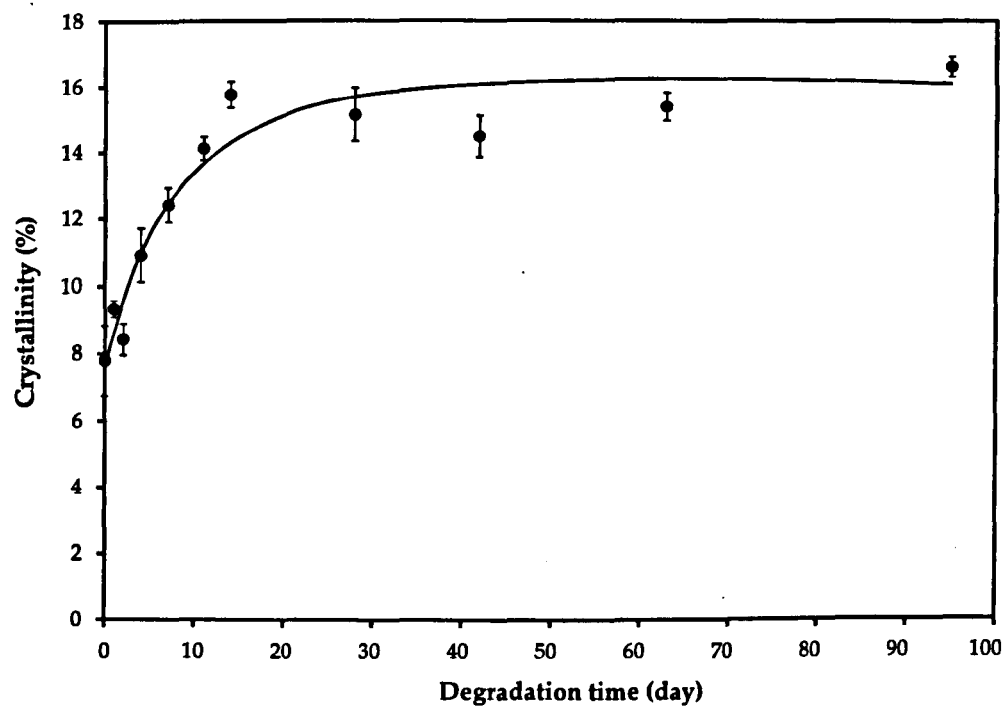


Figure 3-11: The percentage change of PLA crystallinity (measured using DSC) with time during degradation in PBS at 37 °C.

As seen from **Figure 3-12**, the density of PLA alone increased slightly from 1.235 to 1.243 g/cm³ after 2 weeks and then remained absolutely stable ($P > 0.05$) until the end of degradation study in PBS at 37°C. Density of P40 UD and RM composites before and after degradation remained the same at ~ 1.44 g/cm³. During the degradation study, the density of the P40 UD composite was higher than that for P40 RM, however the values plateaued ($P > 0.05$) equally towards the end of the study.

3.4.3 X- Ray Diffraction (XRD)

Figure 3-13 shows the XRD pattern of PLA before and after degradation for 42 and 95 days in PBS at 37°C. It is clear from the initial profile (at day 0) for PLA alone that this polymer grade is mostly amorphous. However, after degradation for 42 and 95 days, a small peak was seen at ~ 16.6 ° with Miller indices of (200) and (110) [26].

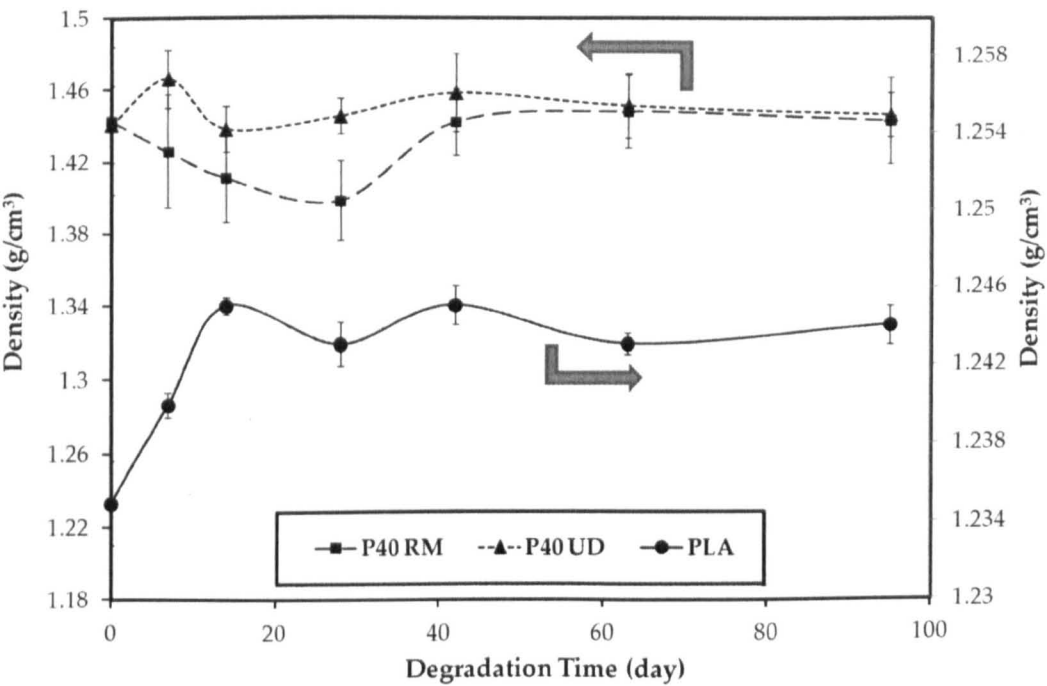


Figure 3-12: The density change of PLA, RM, and UD composites with time during degradation in PBS at 37°C. The arrows indicate the axes for density values for PLA and composites.

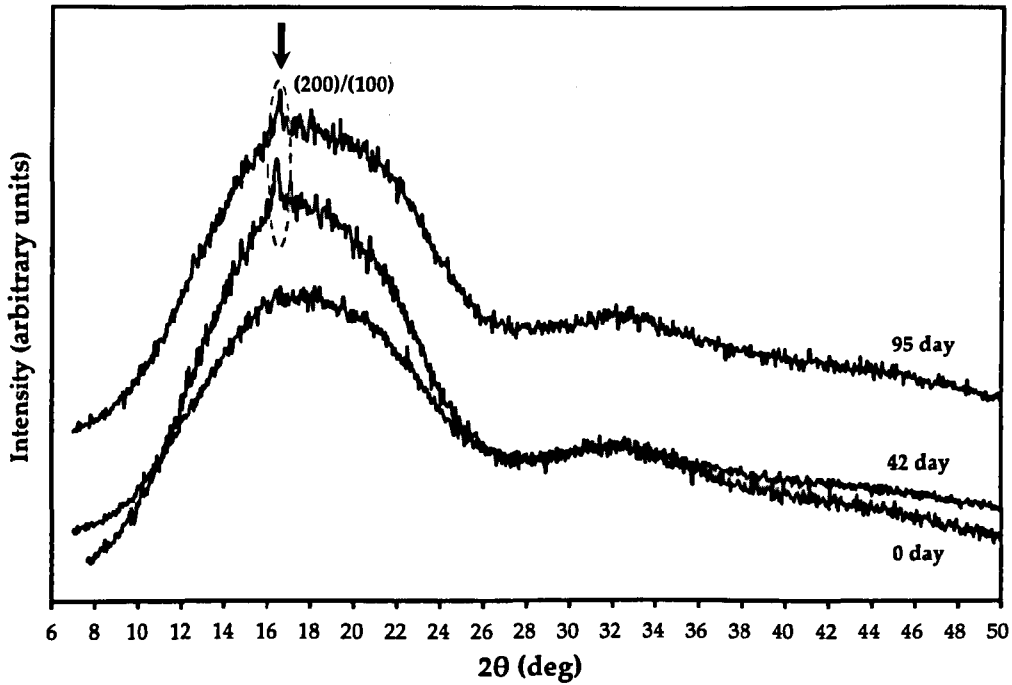


Figure 3-13: XRD patterns of PLA before and after degradation in PBS at 37°C.

3.4.4 Degradation study

Water uptake and mass loss percentages versus time are plotted in Figure 3-14, where it can be seen that for PLA alone, P40 RM, and P40 UD composites water absorption increased rapidly during the first two days to ~ 0.85 %, 0.65 %, and 0.85 %, respectively. After these initial two days of immersion, it was found that the PLA stabilised around 0.85 % for the remainder of the study. The water uptake for P40 RM and P40 UD continued to increase linearly to ~ 1.4 % and ~ 1.6 % respectively after 95 days of degradation (see Figure 3-14). The mass loss for PLA alone hardly changed, whilst the RM and UD composites only lost ~ 0.7 % and ~ 0.4 % of their initial mass respectively after 95 days of degradation.

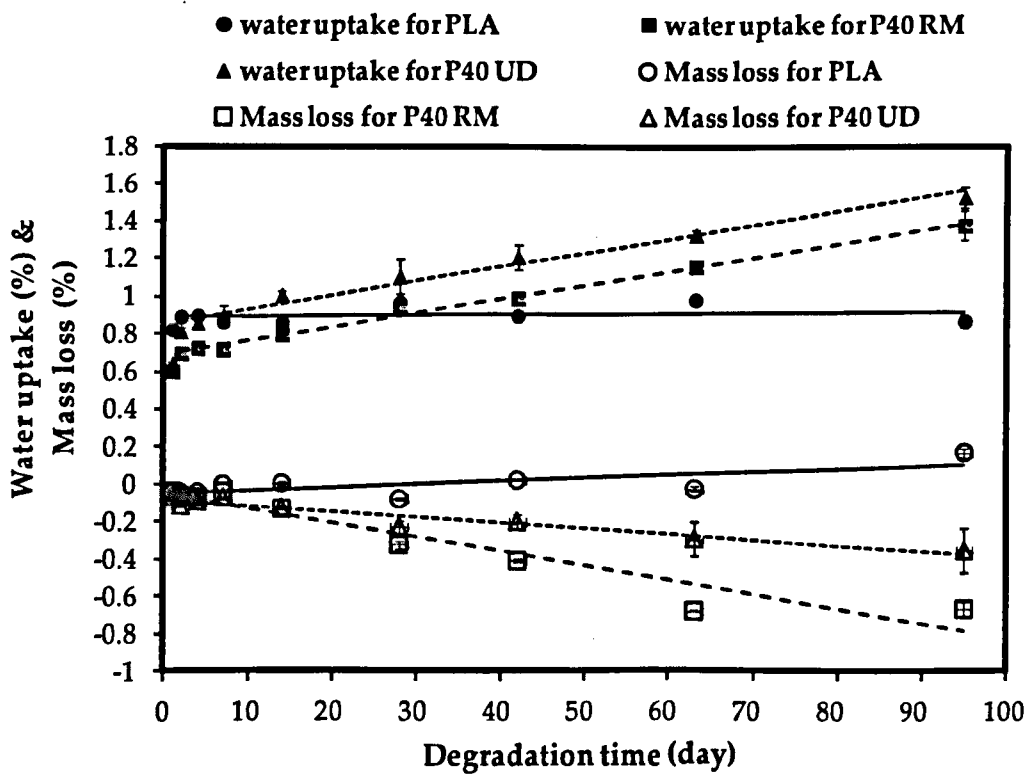


Figure 3-14: Water uptake percentage and mass loss change of PLA, RM, and UD composites over immersion time in PBS at 37°C. (Closed symbols are for water uptake and opened symbols are for mass loss).

Figure 3-15 shows the percentage mass change profile for PLA alone and for P40 RM and UD composites as a function of time (95 days). During the initial phase, the mass gradually increased until it reached saturation after two days as shown in the inset graph. The percentage mass change of all samples remained relatively constant over the duration of the study. The approximate plateau values were 0.85 % for PLA alone and ~ 0.95 % for P40 UD composite, whereas the mass change of P40 RM composite fluctuated around 0.65%.

pH analysis of the degradation media is shown in Figure 3-16. From this figure, it is seen that the pH values slightly varied around 7.5 which was close to the starting value of the immersion solution (PBS). The pH traces obtained for all three samples investigated were identical (and overlapped on the graph).

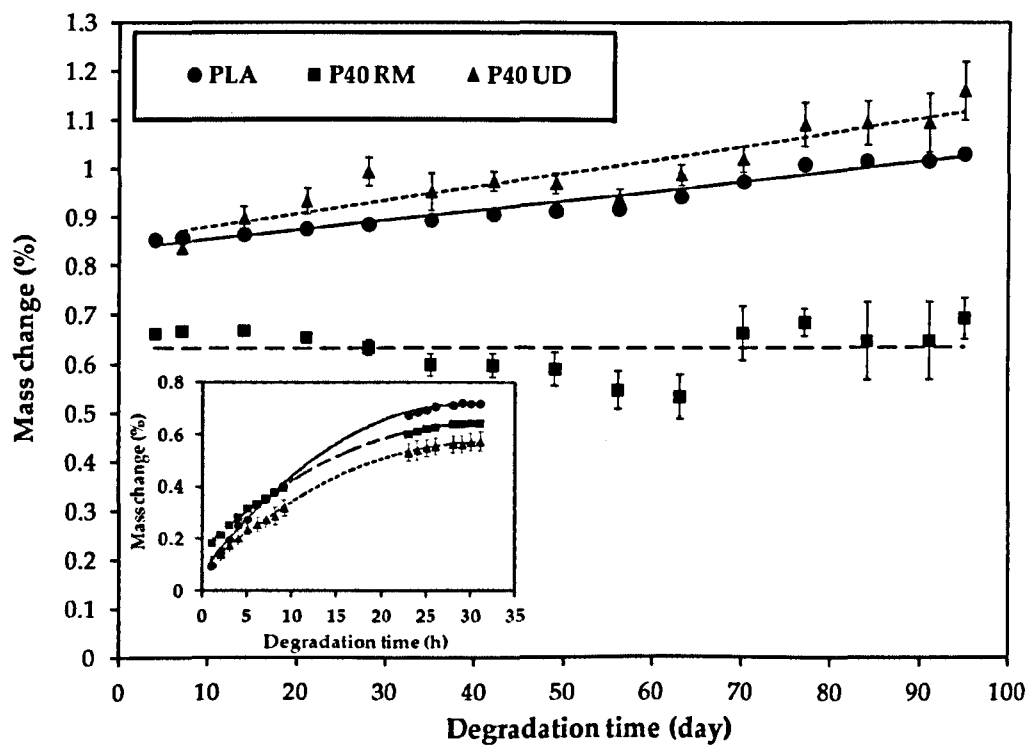


Figure 3-15: The percentage change in wet mass of PLA, RM, and UD composites during immersion in PBS at 37°C. (The inset graph shows data for the first 32 h).

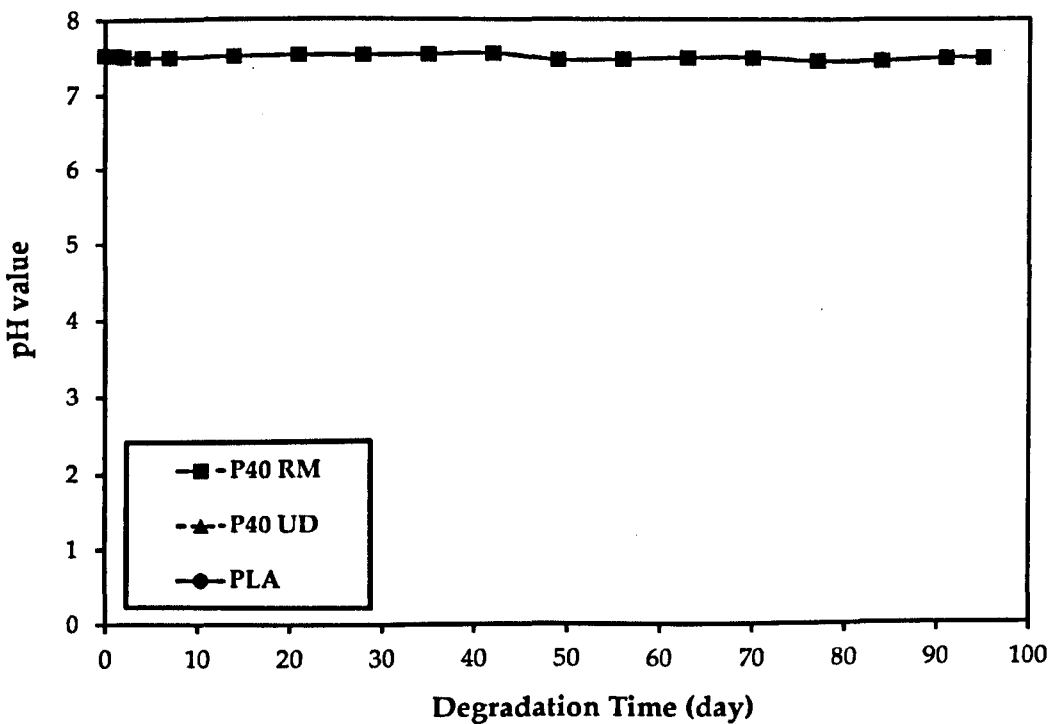


Figure 3-16: pH value change for PBS during the degradation process in PBS at 37°C for PLA alone, RM, and UD composites.

3.4.5 Flexural properties

Flexural strength is plotted against time in **Figure 3-17**, where it can be seen that the initial flexural strength of PLA alone was improved by the inclusion of PGF reinforcement. PLA alone provided strength of ~ 90 MPa, with P40 RM providing ~106 MPa and P40 UD ~ 115 MPa. The flexural modulus also increased from ~ 3.8 GPa for PLA to ~ 6.8 GPa and ~ 9 GPa for RM and UD composites respectively (see **Figure 3-18**).

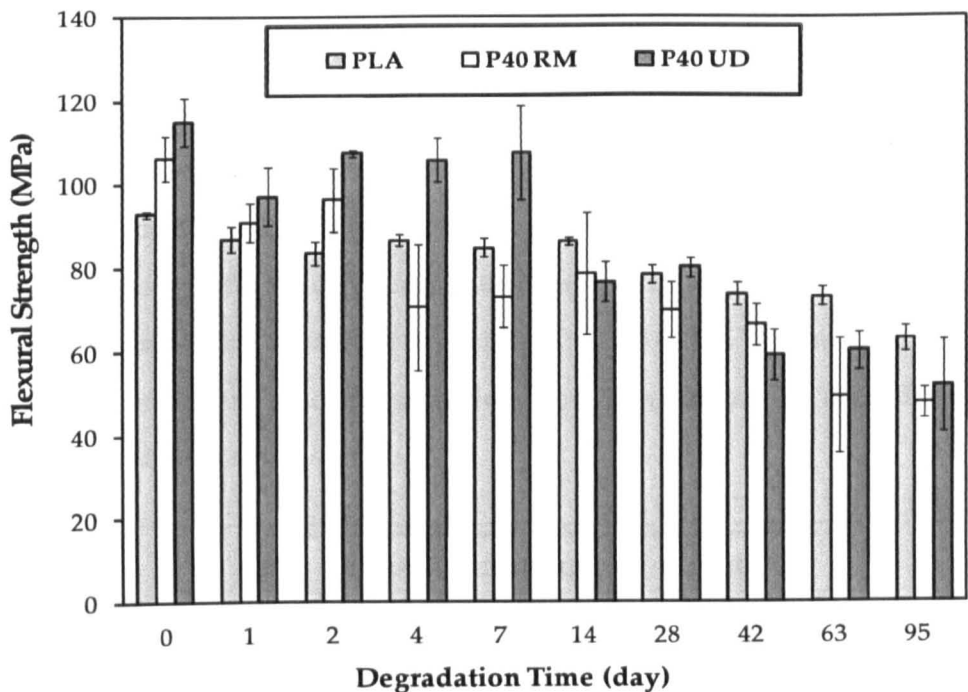


Figure 3-17: Flexural strength vs time for PLA, RM, and UD composites. (Samples measured wet after immersion in PBS at 37°C.

The PLA, RM and UD composite specimens were degraded in PBS for 95 days at 37°C. Flexural tests were conducted on these samples at varying time points to ascertain mechanical property retention over time.

For the P40 UD composite, it was seen that the flexural strength remained constant ($P > 0.05$) up till the 7 days time point after which the strength decreased significantly ($P < 0.05$) by 30 % to ~ 75 MPa. A further decrease in the flexural strength for the UD composite was observed and reached a value of ~ 50 MPa after

95 days immersion in PBS at 37°C. During the first two weeks, the flexural strength of P40 RM composite decreased from 106 MPa to 75 MPa, whilst no significant ($P > 0.05$) change was seen for PLA alone. An additional gradual reduction in the strength of PLA and P40 RM composite was seen to ~ 60 MPa and ~ 50 MPa respectively, by the end of the study (95 days).

The initial flexural modulus for P40 UD was ~9 GPa after which slight increase to ~ 10 GPa was seen up till the 7 days time point. After 2 weeks the modulus showed a plateau at around 10 GPa ($P > 0.05$) for the remainder duration of the study. The flexural modulus of PLA alone remained constant ($P > 0.05$) at ~3.8 GPa during the study period. However, the modulus for the RM composite maintained a value of 6.8 GPa for 2 weeks before reducing by 30% ($P < 0.01$) to ~ 4.5 GPa, after which it remained relatively constant. **Figure 3-19** shows stress-strain curves for P40 UD and P40 RM composites. Before degradation, the fracture of the samples were regarded to be brittle ,whilst after 95 days of degradation in PBS at 37°C, the samples became more ductile as a result of the plasticisation effect of water and the short fibre pull out observed at the fracture surface.

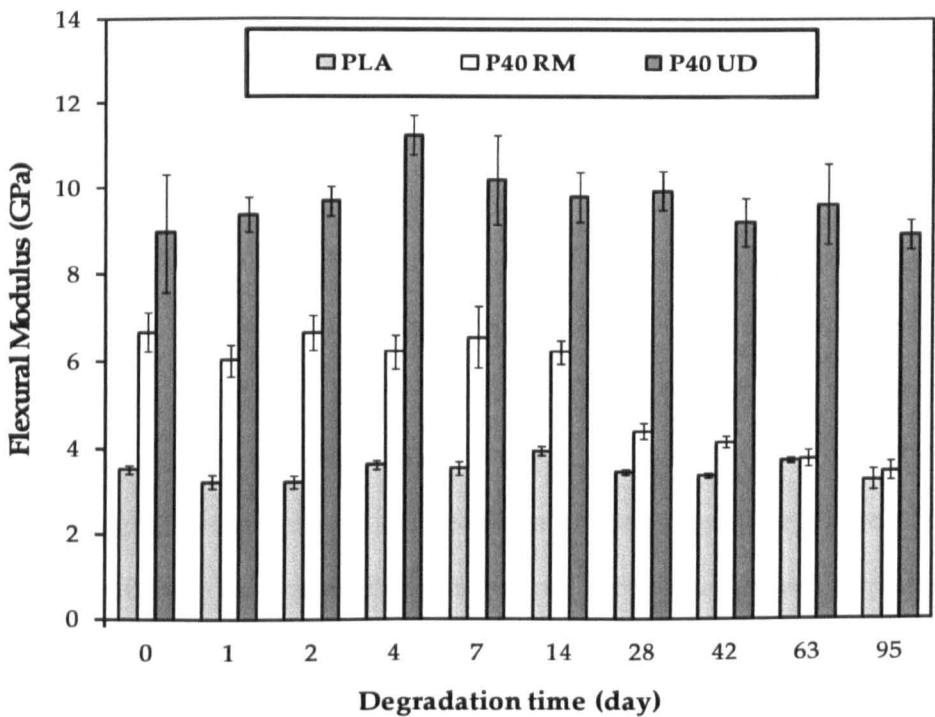


Figure 3-18: The flexural modulus against degradation time for PLA, RM, and UD composites. (Samples measured wet after immersion in PBS at 37°C).

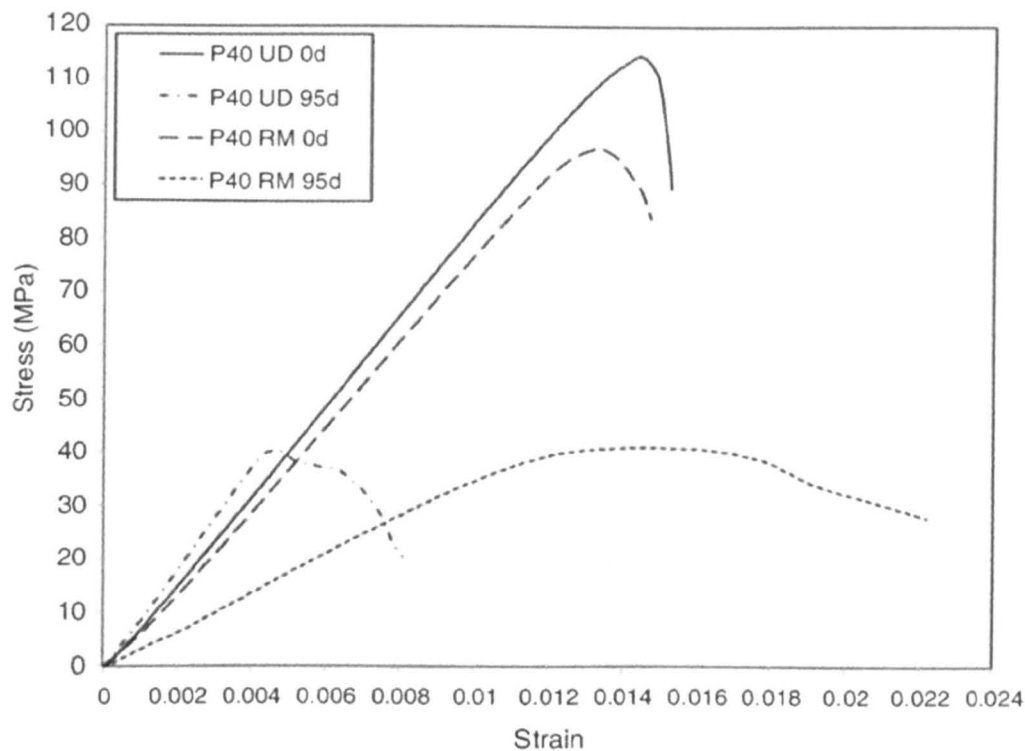


Figure 3-19: Stress–strain curves for P40 UD and P40 RM composites before (0d) and after 95 (95d) days of degradation in PBS at 37°C.

Figure 3-20 shows the flexural strength and modulus for RM and UD composites based on P40 and P50 fibres. The flexural properties for the composites increased by increasing the fibre volume fraction as expected [27]. The flexural strength and modulus for P40 UD H ($V_f \sim 28\%$) increased by $\sim 100\%$ in comparison with P40 UD ($V_f \sim 14\%$) as the fibre volume fraction doubled (i.e. followed the rule of mixture). Conversely, the flexural modulus for P40 RM H was slightly greater than that P40 RM, whilst the strength decreased from 106 MPa for P40 RM to ~ 91 for P40 RM H. This was suggested to be due to the breakage of the fibres during processing of composites with high fraction of chopped random fibres. The flexural properties for P50 composites were lower than P40 composite which was not only caused by the slight decrease in the fibre volume fraction but also due to the lower mechanical properties particularly the modulus of the P50 fibres in comparison to P40 fibres.

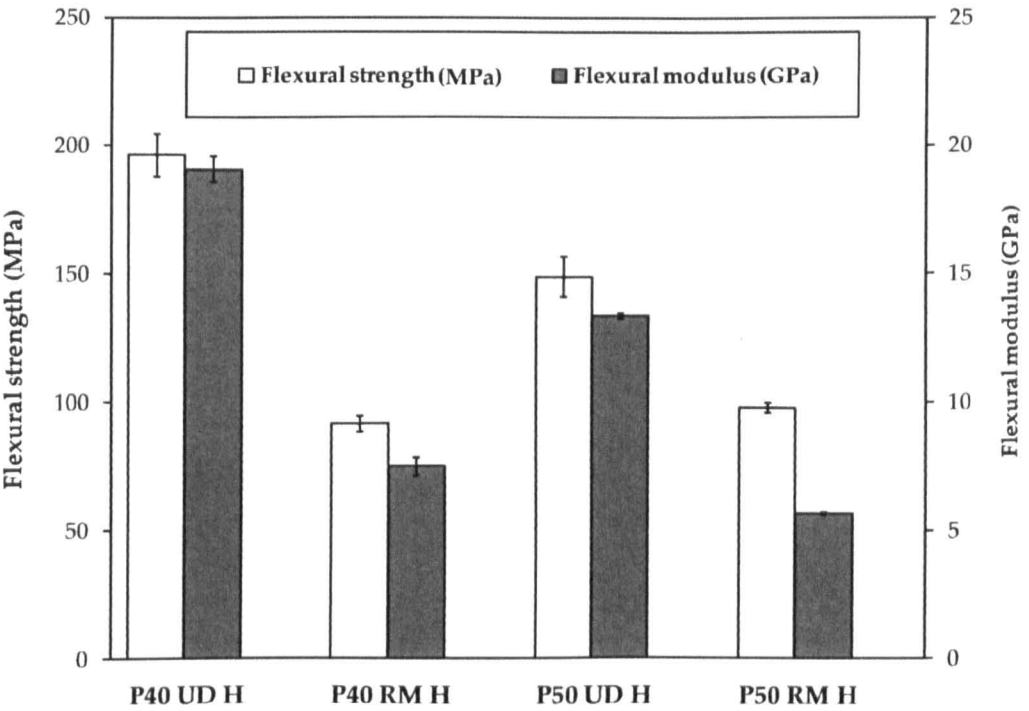


Figure 3-20: Flexural properties for composites with high fibre volume fraction. Two different fibre architecture (RM and UD) and composition (P40 and P50) were used in this study.

3.4.6 Molecular weight change with the time

Figure 3-21 shows molecular weight profiles for the three samples investigated over time. The molecular weight percentage of PLA alone, P40 RM, and P40 UD composites decreased linearly during the degradation process. From the linear fitting, it was found that the gradients were -0.0117, -0.0093, and -0.0124 for PLA alone, P40 RM, and P40 UD respectively. However, no significant differences ($P > 0.05$) in the molecular weight were seen between all specimens.

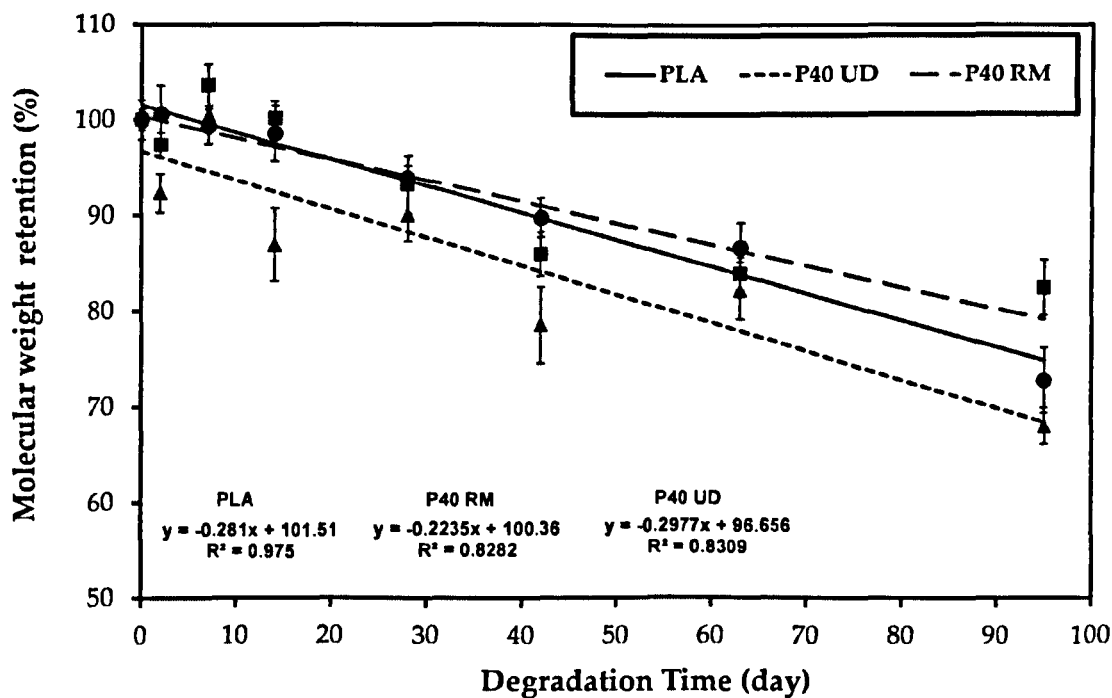


Figure 3-21: The change in weight average molecular weight of PLA, RM, and UD composites, over time.

3.4.7 SEM Analysis

Figure 3-22 shows the fractured surface for PLA, P40 RM and P40 UD composite specimens. Figure 3-22 a, c, and e represent the samples before degradation and Figure 3-22 b, d, and f illustrate the specimens after 95 days of degradation in PBS at 37°C.

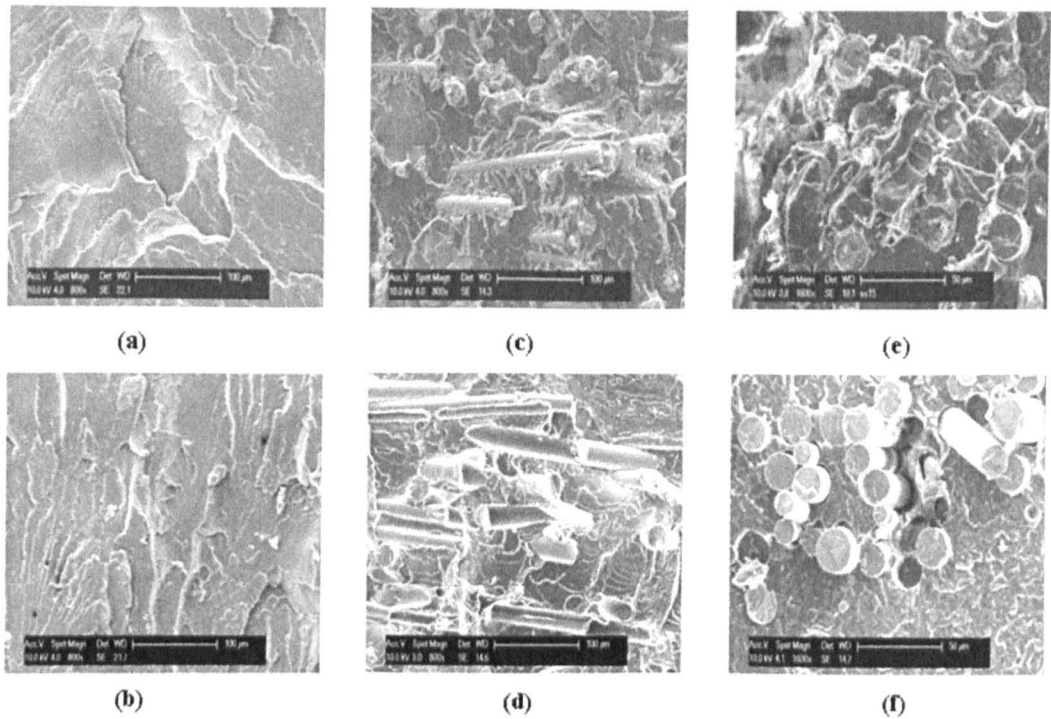


Figure 3-22: SEM micrographs of a fractured surface of (a) PLA before degradation, (b) PLA after 95days of degradation in PBS at 37°C, (c) P40 RM composite before degradation, (d) P40 RM composite after 95days of degradation in PBS at 37°C, (e) P40 UD composite before degradation, (d) P40 UD composite after 95days of degradation in PBS at 37°C. A scale bar for PLA and P40 RM represents 100 µm and is 50 µm for P40 UD specimens.

3.4.8 Cytocompatibility Studies

Figure 3-23 shows confocal laser scanning images of live/dead stained HOS cells attached to the surface of random and UD composites in comparison with PLA and Thermanox® control. After 1 day in culture, cells were scattered on the surfaces of the samples. PLA and P40 RM appeared to support more cell numbers in comparison with positive control and P40 UD surfaces. At 4 days, however, cells were compacted on all surfaces with no significant differences from those grown on the positive control surface. All samples maintained more than 98% viable cells on their surfaces with the cells exhibiting typical osteoblastic morphology.

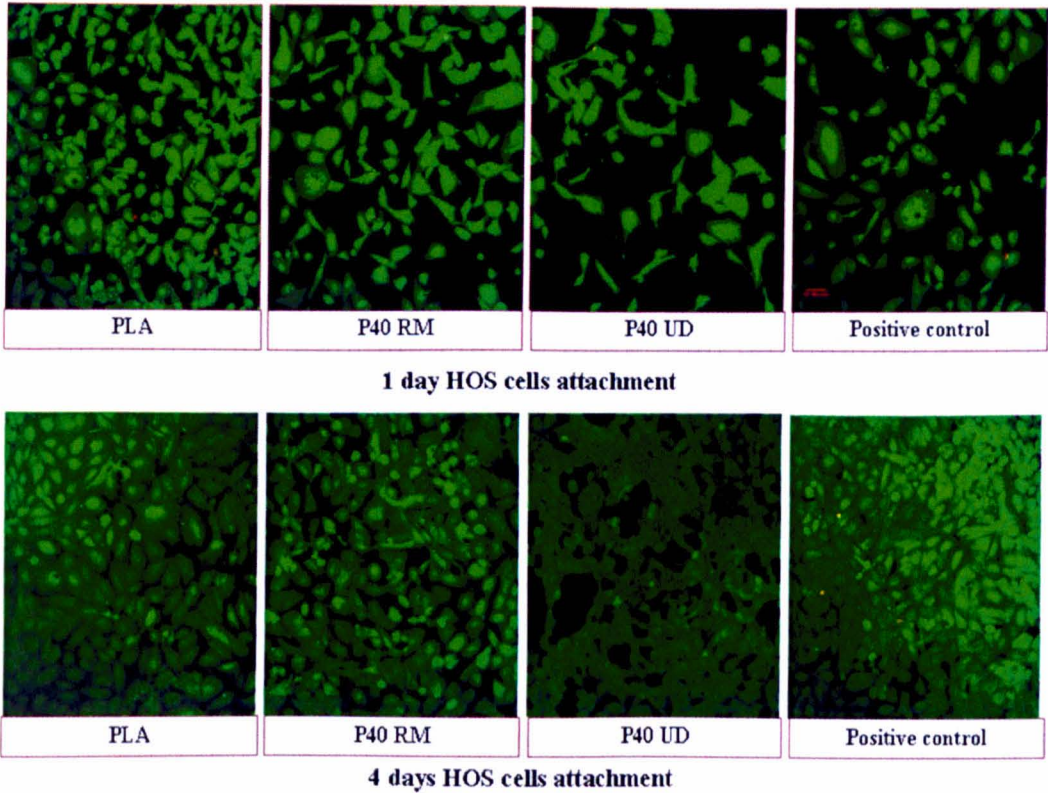


Figure 3-23: Cytocompatibility assessment of Pure PLA, P40 RM and P40 UD composites. Cell viability was conducted over 1day and 4 days. Magnification of images is 20X.

3.5 DISCUSSION

The ideal material for bone fracture fixation would be bioresorbable to eliminate the need for surgical removal if required (as removal of metal plates is routine practice in Europe). This would then also allow for stress to be transferred to the healing bone over the course of the repair process in order to prevent bone atrophy. It should also be robust enough to withstand the implantation process. Fibre reinforcement of polymers is known to increase their mechanical properties and make the composite more ductile than the polymer alone. This ductile behaviour of fibre-reinforced composites (FRC) is able to prevent sudden failure of the implants which can create serious consequences for the patient [2]. In addition, if the reinforcing phase (i.e. fibres) were made from bioresorbable phosphate-based glass, they could promote bone healing via the release of specific ions to aid or accelerate the healing process [28].

Two different compositions of PBG fibres fixed with 50 mol% P_2O_5 (P50) and 40 mol% P_2O_5 (P40) were used in this chapter. Ahmed *et al.* [29] investigated a range of ternary phosphate based glasses with fixed 45, 50 and 55 mol% P_2O_5 and the degradation rates obtained ranged from $2.83 \times 10^{-3} \text{ g.cm}^{-2}.\text{h}^{-1}$ to $1.56 \times 10^{-4} \text{ g.cm}^{-2}.\text{h}^{-1}$. Quaternary phosphate glasses containing iron oxide (which has a strong reinforcing effect in these glasses) were also investigated [30] with degradation rates for these glasses ranging from $4.5 \times 10^{-4} \text{ g.cm}^{-2}.\text{h}^{-1}$ to $2.5 \times 10^{-5} \text{ g.cm}^{-2}.\text{h}^{-1}$. The P40 PBG formulation investigated in this study ($40P_2O_5$ - $24MgO$ - $16CaO$ - $16Na_2O$ - $4Fe_2O_3$ in mol%) has a degradation rate of approximately $3 \times 10^{-6} \text{ g.cm}^{-2}.\text{h}^{-1}$. However, obtaining fibres from fixed 40 mol% P_2O_5 formulations proved to be extremely difficult. The reason for this and for the differences in their degradation profiles is suggested to be due to their structure. PBG formulations with fixed 50 mol% P_2O_5 are reported to have an infinite chain structure (i.e. Q^2) [31-33], whereas glasses with fixed 40 mol% P_2O_5 had much shorter chains (i.e. a mixture of Q^1 's and Q^2 's with reported ratios of ~ 56 to ~ 44 respectively) revealing a depolymerising effect with a decrease in phosphate content [29, 34]. These shorter chains are able to pack together tighter creating more durable glasses with a tensile modulus greater than that for P50 fibres (62 vs 52 GPa). The increase in tensile strength for P50 fibres in comparison with the P40 fibres was suggested to be due to the infinite linear chain structure with the PO_4 units in the phosphate backbone aligned and oriented in the direction of fibre pull. It is also suggested that due to this mixture of Q^1 's and Q^2 's within their structure, fibres are difficult to produce as during the drawing process fibres continuously break, most probably when having encountered the end of a (Q^1) chain [29, 35]. Conversely, P50 formulations are relatively easy to draw due to their structure due to infinite Q^2 structure [31-33].

PGF when tested sustain little or no plastic deformation up to the point of failure, signifying their brittle nature. The failure stress mostly depends on the presence of flaws. As the population of flaws occur randomly along the length of the fibres, a large variation in strength is observed. The Weibull distribution statistically resolves this situation. The Weibull scale parameter states the most probable strength and the shape parameter characterises the distribution of strength of the fibres.

3.5.1 Polymer and Composite Degradation Studies

The degree of crystallinity within a polymer can have a significant effect on its properties such as modulus, strength, water sorption and degradation. From **Figure 3-11**, it was seen that the crystallinity for PLA increased during the initial 14 days after which a plateau was observed for the duration of the study. This increase in crystallinity with degradation was firstly suggested to be due to the fact that during the degradation process of semi-crystalline polymers, the amorphous phase degrades faster than the crystalline phase. Secondly, it is possible that additional crystallisation occurred as a result of the increase in the mobility of polymer chains, due either to the plasticisation effect of water and/or the reduction in molecular weight of the polymer [36]. Zhou *et al.* [37] also investigated the degradation properties of PLLA and found an increase in crystallinity during the initial stages of degradation which then decreased. They ascribed this decrease to the degradation of the crystalline phase as a result of hydrolysis.

Polymer morphology has a significant role in the degradation of polymers due to the difference in amorphous and crystalline domains. In this study, XRD was used to examine crystallinity change during the degradation process. As seen in **Figure 3-13**, a small peak was detected at $\sim 16.6^\circ$ after 42 days of immersion in PBS at 37°C . This peak was then also seen at 95 days (see **Figure 3-13**). The appearance of this peak was indicative of an increase in the crystallinity [36]. This peak was also seen and characterised by Zhou *et al.* [37] who investigated XRD of PLLA as a function of degradation time in PBS.

The increase in crystallinity was also suggested as the main reason for the increase in density observed for PLA alone. The density of the crystalline phase in PLA is higher than that of the amorphous phase [38]. However, there was a large difference in the density between PLA alone and the fibre-reinforced composites (FRC's), due to the addition of glass fibre (2.7 g/cm^3). The variation seen between the P40 RM and P40 UD composites may be due to variation in the fibre distribution within the composites.

Water uptake percentage of P40 UD composites was higher than that for P40 RM (Figure 3-14). This suggested that the water diffusion through RM composite was slower than the UD composite. Composites usually absorb more water than pure polymers and water absorption of poorly impregnated FRC's can be higher than well impregnated fibre composites. Four types of degradation for fibre reinforced composites in water are known. Physical degradation, such as swelling; degradation of the matrix; degradation of the bonding interfaces between the fibres and matrix and weakening of the fibre strength [39]. Water wicking at the fibre/matrix interface is also known to play a significant role in the degradation of composites, especially resorbable fibre reinforced composites. Wicking is a form of capillary action between fibre and matrix as a result of interface degradation. These capillaries can decrease the mechanical strength of FRCs and amount of water uptake for composites would decrease as the fibres impregnation with the polymer matrix improved [40-43].

The water uptake of PLA showed saturation at around 0.9 % after 4 days of immersion in PBS at 37°C, whilst for the composites; a continual increase was seen. It was suggested that this increase may be due to continuous degradation of the interface between the fibres and matrix [44].

Figure 3-15 showed that the wet mass change of P40 UD was higher than that for P40 RM composites and this was suggested to be due to the discontinuous nature of the fibres, inhibiting the wicking effect and/or making them less prone to wicking [45]. The influence of fibre architecture on diffusion of water was demonstrated by Arnold *et al.* [46]. They found that water diffused along the fibres faster than in other directions [47].

There was not a significant change in the pH of PBS for PLA alone, P40 RM and P40 UD during the degradation process (Figure 3-16). The pH of the degradation media for PLA alone and the composites remained relatively neutral for the duration of the study. Ahmed *et al.* [13] studied the degradation behaviour of PBGs of similar formulations (i.e. fixed 40 mol% P₂O₅). They found that the pH of the immersion solution remained relatively neutral for the duration of the study (700 hour).

Ruffieux *et al.* [48] prepared rods from PDLLA and β -tri-calcium phosphate (TCP) composite and studied the degradation in PBS at 37°C. They also did not observe any considerable change in the pH up to 30 weeks of degradation time.

3.5.2 Mechanical properties

However, the fibre volume for P40 UD composite was low (~ 14%). It was greater than the critical fibre volume fraction V_{crit} (above which the mechanical strength of composite is higher than the matrix alone).

$$V_{crit} = \frac{\sigma_m^* - \sigma'_m}{\sigma_f^* - \sigma'_m} \quad \text{Equation 3-5}$$

where σ_m^* , σ_f^* and σ'_m are ultimate tensile stress of the matrix (~ 55.7 MPa for PLA), scale parameter of the Weibull analysis for the fibres (400.8 and 507.6 MPa for P40 and P50 fibres respectively) and tensile stress of the matrix (~ 11.2 MPa for PLA) at the failure strain of the fibres [49, 50]. Therefore, the critical fibre fraction for P40 and P50 composites was determined as ~ 11.5 % and ~ 9 % respectively.

As seen from Figure 3-17 and Figure 3-18 the flexural strength decreased with time during the degradation process, whilst no significant change in the modulus was observed. Similar findings were also seen by Bunsell *et al.* [47] and Shao *et al.* [51] who studied the effect of hydrolysis of polyethylene terephthalate/E-glass fibre (PET/GF) composites on mechanical properties. They found that the strength decreased dramatically with time, whilst the modulus was not affected.

Pegoretti *et al.* [52] investigated long-term effects of aging in water on the flexural properties of commercial dental polymer composites. This composite consisted of bisphenol A glycidyl methacrylate (Bis-GMA) resin diluted with triethylene glycol dimethacrylate (TEGDMA) and reinforced with long E-glass fibres. They found that the modulus was unaffected; however, the strength reduced over time. They suggested that the degradation of the fibre/matrix interface mainly affected the ultimate properties such as strength, whilst elastic properties such as the modulus were only slightly affected at low deformation.

The reduction in flexural strength for the composites and PLA in this study was suggested to be due to the existence of water within the sample which can act as a plasticiser. In addition, water can also cause degradation of the fibre-matrix interface creating poor stress transfer efficiency. Flexural strength is also known to depend on the failure mode. The strength will be lower if the failure involved compression, micro-buckling or shear splitting [42, 53].

The reduction in mechanical strength can also be due to polymer chain scission caused by hydrolysis. Plotting the flexural strength properties against molecular weight change, a linear relationship was seen. As molecular weight decreased, the strength decreased. However, the modulus profiles did not show any specific relationship with molecular weight which agreed with Kajorncheappunngam *et al.* [54] who also saw that the strength of glass-reinforced epoxy decreased as a result of chain scission within the composite matrix and the modulus was not affected.

The increase in chain scission during degradation is clear from the reduction in molecular weight with time seen in Figure 3-21. The molecular weight loss for P40 UD composite was slightly higher than for P40 RM and PLA alone. The P40 UD composite absorbed water more than P40 RM and also degraded faster, potentially increasing the rate of chain scission.

Figure 3-22 a and b show the fractured surface morphology of PLA alone. After degradation (Figure 3-22 b), some ripples were observed [55]. The fibre-matrix interface can be seen in the SEM micrographs of the composites before and after degradation in Figure 3-22 c and f. For the P40 RM and P40 UD composites, the fractured surfaces before degradation show no fibre pull-out whereas after degradation, short fibre pull-out was observed which is indicative of loss of interface properties due to de-bonding of the fibres from the matrix [54, 56].

Live/dead staining gives an indication of cell morphology and how cells are attached to the underlying surface. It could also be used quantitatively to calculate the live/dead cell ratio. As inferred from Figure 3-23, the cell number increased with time. Similar findings were reported for PCL/PBG and PLA/PBG composites [7, 11, 57]. The observed cytocompatibility could be associated with the absence of acidic

degradation products that can adversely affect cell attachment and viability. This was confirmed by pH measurement where the pH of the degradation medium remained relatively neutral.

PLA composites reinforced with P40 PBG fibres have shown retention of their properties for much longer periods than previously investigated composites produced using P50 PBG fibres [11]. Thus, P40 PBG fibre composites are much more suitable for bone fixation applications than the previously investigated composites. However, further work is required here to control the degradation process, which could be made possible via the use of coupling/sizing agents to improve the fibre-matrix interface. Parsons *et al.* [14, 58, 59] and Papia *et al.* [17, 18] found that initial interfacial shear strength (IFSS) between PLA and PBG fibres doubled after treatment of the fibres with coupling agents such as Glycerol-2-phosphate disodium pentahydrate (GP). However, IFSS decreased rapidly close to the control samples (i.e. untreated fibres) after soaking in water for 3 days at 37°C. Thus, further improvements for these coupling agents will be essential in order to enhance their resistance to aqueous attack.

The flexural properties P40 UD H (~ 20 GPa of modulus and ~ 200 MPa of strength) were very close to the upper limit of the mechanical properties of cortical bone. The increase in properties of the composites was attributed to an increase in fibre volume fraction to ~30 %. Therefore, composites with fibre volume fraction of ~30 % or even higher should be considered for preparation of composite rods and screws in following chapters.

3.6 CONCLUSIONS

Mechanical and degradation properties were investigated for PLA reinforced with PGF. Random fibre mat (RM) and unidirectional (UD) fibre distributions were evaluated in this study. The RM composite contained ~ 18 % of fibre volume fraction and the UD composite contained ~ 14%. During degradation studies in PBS at 37°C water uptake for RM and UD was ~ 1.4 % and 1.5 % respectively after 95 days. Mass change studies showed a plateau for PLA alone, P40 RM and P40 UD composite at ~ 0.85 %, ~ 0.65 % and ~ 0.95 % respectively. The density profiles for

the composites were around 1.44 g/cm³. The crystallinity increased with time during the degradation process and a small peak was detected by XRD as indication for the increase in crystallinity. The composites absorbed more water than the PLA alone due to loss of the interface between matrix and fibres. The degradation of the fibre-matrix interface was also seen from SEM micrographs. The strength of the composites decreased from ~ 115 MPa for UD and ~ 106 MPa for RM to ~ 50 MPa after immersion in PBS at 37°C for 95 days whilst the modulus remained constant. In addition, the mechanical properties for composites increased by increasing the fibre volume fraction to match the mechanical properties of the cortical bone. Cytocompatibility studies showed that cell numbers increased with time. The combination of PLA and fibre formulation used in this study showed property retention for much longer than previously investigated composites. In the following chapters, composites with higher fibre volume fraction (~ 30 %) would be used for preparation of rods and screws.

3.7 REFERENCES

1. Navarro, M., M.P. Ginebra, J.A. Planell, C.C. Barrias, and M.A. Barbosa, *In vitro degradation behavior of a novel bioresorbable composite material based on PLA and a soluble CaP glass*. *Acta Biomaterialia*, 2005. 1(4): p. 411-419.
2. Brauer, D., C. Rüssel, S. Vogt, J. Weisser, and M. Schnabelrauch, *Degradable phosphate glass fiber reinforced polymer matrices: mechanical properties and cell response*. *Journal of Materials Science: Materials in Medicine*, 2008. 19(1): p. 121-127.
3. Zhou, Z., Q. Yi, X. Liu, L. Liu, and Q. Liu, *In vitro degradation behaviors of Poly-l-lactide/bioactive glass composite materials in phosphate-buffered solution*. *Polymer Bulletin*, 2009.
4. Russias, J., E. Saiz, R.K. Nalla, K. Gryn, R.O. Ritchie, and A.P. Tomsia, *Fabrication and mechanical properties of PLA/HA composites: A study of in vitro degradation*. *Materials Science and Engineering: C*, 2006. 26(8): p. 1289-1295.
5. Mohammadi, S.M., I. Ahmed, B. Marelli, C. Rudd, M.N. Bureau, and S.N. Nazhat, *Modulation of polycaprolactone composite properties through incorporation of mixed phosphate glass formulations*. *Acta Biomaterialia*, 2010. 6(8): p. 3157-3168.
6. Ahmed, I., A.J. Parsons, G. Palmer, J.C. Knowles, G.S. Walker, and C.D. Rudd, *Weight loss, ion release and initial mechanical properties of a binary calcium phosphate glass fibre/PCL composite*. *Acta Biomaterialia*, 2008. 4(5): p. 1307-1314.
7. Mohammadi, M.S., I. Ahmed, N. Muja, S. Almeida, C.D. Rudd, M.N. Bureau, and S.N. Nazhat, *Effect of Si and Fe doping on calcium phosphate glass fibre reinforced*

- polycaprolactone bone analogous composites. *Acta Biomater*, 2012. 8(4): p. 1616-1626.
8. Jukola, H., L. Nikkola, M.E. Gomes, F. Chiellini, M. Tukiainen, M. Kellomäki, E. Chiellini, R.L. Reis, and N. Ashammakhi, Development of a bioactive glass fiber reinforced starch–polycaprolactone composite. *Journal of Biomedical Materials Research Part B: Applied Biomaterials*, 2008. 87B(1): p. 197-203.
 9. Jiang, G., M.E. Evans, I.A. Jones, C.D. Rudd, C.A. Scotchford, and G.S. Walker, Preparation of poly([epsilon]-caprolactone)/continuous bioglass fibre composite using monomer transfer moulding for bone implant. *Biomaterials*, 2005. 26(15): p. 2281-2288.
 10. Kasuga, T., S.-Y. Ozaki, T. Hayakawa, M. Nogami, Y. Abe, and Y. Ota, Mechanical properties of polylactic acid composites containing β -Ca(PO₃)₂ fibers in simulated body fluid. *Journal of Materials Science Letters*, 1999. 18(24): p. 2021-2023.
 11. Ahmed, I., P.S. Cronin, E.A. Abou Neel, A.J. Parsons, J.C. Knowles, and C.D. Rudd, Retention of mechanical properties and cytocompatibility of a phosphate-based glass fiber/polylactic acid composite. *Journal of Biomedical Materials Research Part B: Applied Biomaterials*, 2009. 89B(1): p. 18-27.
 12. Ahmed, I., I. Jones, A. Parsons, J. Bernard, J. Farmer, C. Scotchford, G. Walker, and C. Rudd, Composites for bone repair: phosphate glass fibre reinforced PLA with varying fibre architecture. *Journal of Materials Science: Materials in Medicine*, 2011. 22: p. 1825 - 1834.
 13. Ahmed, I., A. Parsons, A. Jones, G. Walker, C. Scotchford, and C. Rudd, Cytocompatibility and Effect of Increasing MgO Content in a Range of Quaternary Invert Phosphate-based Glasses. *J Biomater Appl*, 2010. 24(6): p. 555-575.
 14. Parsons, A.J., I. Ahmed, P. Haque, B. Fitzpatrick, M.I.K. Niazi, G.S. Walker, and C.D. Rudd, Phosphate Glass Fibre Composites for Bone Repair. *Journal of Bionic Engineering*, 2009. 6(4): p. 318-323.
 15. Cozien-Cazuc, S., A. Parsons, G. Walker, I. Jones, and C. Rudd, Effects of aqueous aging on the mechanical properties of P40Na20Ca16Mg24 phosphate glass fibres. *Journal of Materials Science*, 2008. 43(14): p. 4834-4839.
 16. Cozien-Cazuc, S., A.J. Parsons, G.S. Walker, I.A. Jones, and C.D. Rudd, Real-time dissolution of P40Na20Ca16Mg24 phosphate glass fibers. *Journal of Non-Crystalline Solids*, 2009. 355(50-51): p. 2514-2521.
 17. Haque, P., I.A. Barker, A. Parsons, K.J. Thurecht, I. Ahmed, G.S. Walker, C.D. Rudd, and D.J. Irvine, Influence of compatibilizing agent molecular structure on the mechanical properties of phosphate glass fiber-reinforced PLA composites. *Journal of Polymer Science Part A: Polymer Chemistry*, 2010. 48(14): p. 3082-3094.
 18. Haque, P., A.J. Parsons, I.A. Barker, I. Ahmed, D.J. Irvine, G.S. Walker, and C.D. Rudd, Interfacial properties of phosphate glass fibres/PLA composites: Effect of the end functionalities of oligomeric PLA coupling agents. *Composites Science and Technology*, 2010. 70(13): p. 1854-1860.
 19. ASTM D2584-94, Standard Test Method for Ignition Loss of Cured Reinforced Resins 1994.

20. BS ISO 11566 (1996). *Carbon Fiber – Determination of the Tensile Properties of Single-filament Specimens*, Geneva, Switzerland, International Standard. .
21. Ahmed, J., J. Zhang, Z. Song, and S. Varshney, Thermal properties of polylactides. *Journal of Thermal Analysis and Calorimetry*, 2009. 95(3): p. 957-964.
22. Lee, T.H., F.Y.C. Boey, and K.A. Khor, On the determination of polymer crystallinity for a thermoplastic PPS composite by thermal analysis. *Composites Science and Technology*, 1995. 53(3): p. 259-274.
23. BS EN ISO 10993-13:2010, *Biological evaluation of medical devices. Identification and quantification of degradation products from polymeric medical devices*
24. BS EN ISO 14125 (1998). *Fiber Reinforced Plastic Composites—Determination of Flexural Properties*, Geneva, Switzerland, International Standard.
25. BS 2782 – 10: Method 1005 (1977). *Methods of Testing Plastics: Glass Reinforced Plastics - Determination of Flexural properties. Three Point Method*. Geneva, Switzerland, International Standard.
26. Iannace, S., A. Maffezzoli, G. Leo, and L. Nicolais, Influence of crystal and amorphous phase morphology on hydrolytic degradation of PLLA subjected to different processing conditions. *Polymer*, 2001. 42(8): p. 3799-3807.
27. Abdulmajeed, A.A., T.O. Nāārhi, P.K. Vallittu, and L.V. Lassila, The effect of high fiber fraction on some mechanical properties of unidirectional glass fiber-reinforced composite. *Dental Materials*, 2011. 27(4): p. 313-321.
28. Knowles, J.C. and G.W. Hastings, In vitro and in vivo investigation of a range of phosphate glass-reinforced polyhydroxybutyrate-based degradable composites. *Journal of Materials Science: Materials in Medicine*, 1993. 4(2): p. 102-106.
29. Ahmed, I., M. Lewis, I. Olsen, and J.C. Knowles, Phosphate glasses for tissue engineering: Part 1. Processing and characterisation of a ternary-based P2O5-CaO-Na2O glass system. *Biomaterials*, 2004. 25(3): p. 491-499.
30. Ahmed, I., C.A. Collins, M.P. Lewis, I. Olsen, and J.C. Knowles, Processing, characterisation and biocompatibility of iron-phosphate glass fibres for tissue engineering. *Biomaterials*, 2004. 25(16): p. 3223-3232.
31. Abou Neel, E.A., A.M. Young, S.N. Nazhat, and J.C. Knowles, A Facile Synthesis Route to Prepare Microtubes from Phosphate Glass Fibres. *Advanced Materials*, 2007. 19(19): p. 2856-2862.
32. Abou Neel, E.A., I. Ahmed, J.J. Blaker, A. Bismarck, A.R. Boccaccini, M.P. Lewis, S.N. Nazhat, and J.C. Knowles, Effect of iron on the surface, degradation and ion release properties of phosphate-based glass fibres. *Acta Biomaterialia*, 2005. 1(5): p. 553-563.
33. Abou Neel, E.A., V. Salih, and J.C. Knowles, 1.117 - Phosphate-Based Glasses, in *Comprehensive Biomaterials*, D. Editor-in-Chief: Paul, Editor 2011, Elsevier: Oxford. p. 285-297.

34. Carta, D., J.C. Knowles, M.E. Smith, and R.J. Newport, *Synthesis and structural characterization of P_2O_5 -CaO- Na_2O sol-gel materials*. *Journal of Non-Crystalline Solids*, 2007. 353(11-12): p. 1141-1149.
35. Walter, G., J. Vogel, U. Hoppe, and P. Hartmann, *The structure of CaO- Na_2O -MgO- P_2O_5 invert glass*. *Journal of Non-Crystalline Solids*, 2001. 296(3): p. 212-223.
36. Buchanan, F.J., ed. *Degradation Rate of Bioresorbable Materials Prediction and Evaluation*. ed. C. Press 2008, Woodhead Cambridge. 320.
37. Zhou, Z., Q. Yi, L. Liu, X. Liu, and Q. Liu, *Influence of Degradation of Poly-L-lactide on Mass Loss, Mechanical Properties, and Crystallinity in Phosphate-Buffered Solution*. *Journal of Macromolecular Science, Part B: Physics*, 2009. 48(2): p. 309-317.
38. Zhang, R. and P.X. Ma, *Synthetic nano-fibrillar extracellular matrices with predesigned macroporous architectures*. *J Biomed Mater Res*, 2000. 52(2): p. 430-8.
39. Sekine, H., K. Shimomura, and N. Hamana, *Strength Deterioration and Degradation Mechanism of Glass Chopped Reinforced Plastics in Water Environment*. *JSME international journal*. , 1988. 31(3): p. 619-626.
40. Wan, Y.Z., Y.L. Wang, X.H. Xu, and Q.Y. Li, *In vitro degradation behavior of carbon fiber-reinforced PLA composites and influence of interfacial adhesion strength*. *Journal of Applied Polymer Science*, 2001. 82(1): p. 150-158.
41. Michael, A.S., C.C. Chu, and A.A. Ida, *Fiber-matrix interface studies on bioabsorbable composite materials for internal fixation of bone fractures. I. Raw material evaluation and measurement of fiber - matrix interfacial adhesion*. *Journal of Biomedical Materials Research*, 1997. 36(4): p. 469-477.
42. Lassila, L.V.J., T. Nohrström, and P.K. Vallittu, *The influence of short-term water storage on the flexural properties of unidirectional glass fiber-reinforced composites*. *Biomaterials*, 2002. 23(10): p. 2221-2229.
43. Väkiparta, M. and P.K. Vallittu, *Flexural Properties of Glass Fibre Reinforced Composite with Partially Biodegradable Polymer Matrix*. *Macromolecular Symposia*, 2007. 253(1): p. 88-93.
44. Shen, L., H. Yang, J. Ying, F. Qiao, and M. Peng, *Preparation and mechanical properties of carbon fiber reinforced hydroxyapatite/polylactide biocomposites*. *Journal of Materials Science: Materials in Medicine*, 2009. 20(11): p. 2259-2265.
45. Zimmerman Mark, C., H. Alexander, J.R. Parsons, and P.K. Bajpai, *The Design and Analysis of Laminated Degradable Composite Bone Plates for Fracture Fixation, in High-Tech Fibrous Materials 1991*, American Chemical Society. p. 132-148.
46. Arnold J. C., Alston S., K. F., Dauhoo S., Adams R., and O. R., *Design Optimisation of Carbon Fibre Epoxy Composites Operating in Humid Atmospheres*. , in *Composites UK - 10th Annual Conference: Innovation in Composites 2010*: Birmingham, UK.

47. Bunsell, A.R. and J. Renard, *Fundamentals of fibre reinforced composite materials* 2005: Institute of Physics Publishing.
48. Ruffieux, K., A. Dell'Agosti, B. Riesen, and E. Wintermantel, *Influence of Calcium Phosphates on the Degradation of Poly Lactic Acid for Medical Implants*. *Biomedizinische Technik/Biomedical Engineering*, 1996. 41(s1): p. 420-421.
49. Bowen, C.R., A.C. Dent, L.J. Nelson, R. Stevens, M.G. Cain, and M. Stewart, *Failure and volume fraction dependent mechanical properties of composite sensors and actuators*. *Proceedings of the Institution of Mechanical Engineers, Part C: Journal of Mechanical Engineering Science*, 2006. 220(11): p. 1655-1663.
50. Pan, N., *Theoretical determination of the optimal fiber volume fraction and fiber-matrix property compatibility of short fiber composites*. *Polymer Composites*, 1993. 14(2): p. 85-93.
51. Shao, Y. and S. Kouadio, *Durability of Fiberglass Composite Sheet Piles in Water*. *J. Compos. Constr.* 6, 280 (2002); , 2002. 6: p. 280 - 287.
52. Pegoretti, A. and C. Migliaresi, *Effect of hydrothermal aging on the thermo-mechanical properties of a composite dental prosthetic material*. *Polymer Composites*, 2002. 23(3): p. 342-351.
53. Dhakal, H.N., Z.Y. Zhang, and M.O.W. Richardson, *Effect of water absorption on the mechanical properties of hemp fibre reinforced unsaturated polyester composites*. *Composites Science and Technology*, 2007. 7-8: p. 1674-1683.
54. Kajorncheappunngam, S., R.K. Gupta, and H.V.S. GangaRao, *Effect of Aging Environment on Degradation of Glass-Reinforced Epoxy*. *Journal of Composites for Construction*, 2002. 6(1): p. 61 - 69.
55. Debra, D.W.-C., A.K. Julia, M.M. Darinda, and L. Cho Hui, *In vitro flexural properties of hydroxyapatite and self-reinforced poly(L-lactic acid)*. *Journal of Biomedical Materials Research Part A*, 2006. 78A(3): p. 541-549.
56. Liao, K., C.R. Schultheisz, and D.L. Hunston, *Effects of environmental aging on the properties of pultruded GFRP*. *Composites Part B: Engineering*, 1999. 30(5): p. 485-493.
57. Mohammadi, S.M., I. Ahmed, N. Muja, C. Rudd, M. Bureau, and S. Nazhat, *Effect of phosphate-based glass fibre surface properties on thermally produced poly(lactic acid) matrix composites*. *Journal of Materials Science: Materials in Medicine*, 2011. 22(12): p. 2659-2672.
58. Parsons, A.J., I. Ahmed, N. Han, R. Felfel, and C.D. Rudd, *Mimicking Bone Structure and Function with Structural Composite Materials*. *Journal of Bionic Engineering*, 2010. 7(Supplement 1): p. S1-S10.
59. Parsons, A., I. Ahmed, M.I.K. Niazi, R.R. Habeb, B. Fitzpatrick, G.S. Walker, I.A. Jones, and C.D. Rudd, *Mechanical and Degradation Properties of Phosphate Based Glass Fibre/PLA Composites with different Fibre Treatment Regimes*. *Science and Engineering of Composite Materials*, 2010. 17(4): p. 243 - 260.

CHAPTER 4.

BIORESORBABLE PHOSPHATE GLASS FIBRE- REINFORCED COMPOSITE RODS: PREPARATION AND MECHANICAL TESTING

4.1 SUMMARY

This chapter investigates the use of novel phosphate-glass fibre reinforced rods as resorbable intramedullary nails. Random and unidirectional fibres were moulded into composite rods via a forging process at 90°C. Rods produced using non-woven chopped strand random fibre mats (RM) showed little improvement in mechanical strength in comparison to the unreinforced polylactic acid (PLA) rods. This was suggested to be due to fibre breakage during the manufacturing process; the length of the fibres decreased from 10 mm (initial) to ~1.2 mm. Modulus and stiffness values for P50 RM rods were higher than those for the PLA rods which could be due to orientation of the fibres during the rod manufacturing process. Rods produced using long fibres parallel to the length of the rod (UD) displayed superior mechanical properties, not only against the PLA rods but also in comparison to cortical bone. Maximum flexural, shear and compressive strengths recorded were 242 MPa, 87 MPa and 400 MPa respectively. A flexural modulus of 25 GPa was achieved, with shear and compressive stiffness values of 6 kN. mm⁻¹ and 21.5 kN. mm⁻¹ respectively. These unidirectionally reinforced phosphate glass fibre PLA composite rods have huge potential to be used as intramedullary fixation devices.

4.2 INTRODUCTION

Intramedullary (IM) rods are used as internal fracture fixation devices in long bones, such as the femur and tibia and their first ever use was reported in the 1940s [1]. IM nails or rods are commonly inserted into the medullary cavity and locked distally and proximally using screws to provide rotational and compressive stability

for the fracture. These rods have advantages over other methods of fixation in that they provide a gradual sharing of the load rather than a bridging effect across a short distance, a small surgical procedure is required, length and alignment of the bone is preserved and there is no requirement for long-term immobilisation [2-4]. During the initial stages of the bone healing process, the majority of the load must be supported by the rods. Therefore, their initial mechanical properties should be sufficient for this purpose in order to prevent fixation failure [2].

Commercial IM nails are usually made of metals such as stainless steel and titanium [5]. Difficulties can be encountered during the removal procedure for such devices, such as re-fracture of the bone due to bone formation around the rods [6, 7]. Moreover, metallic bone fixation devices have disadvantages such as corrosion and significantly higher stiffness than bone, which could cause bone resorption [8, 9]. Bioresorbable IM rods could potentially overcome these complications if they were made to be fully resorbable (thus removal surgery would not be required), biocompatible, able to accelerate or facilitate tissue healing and if their mechanical properties could be engineered to transfer stress to the bone gradually, allowing for progressive healing [10-13].

Relatively poor mechanical properties for load-bearing applications are the main limitation for use of these bioresorbable polymers by themselves [14]. Reinforcement of these polymers is one method which could produce a device with mechanical properties matching that of cortical bone (which ranges between 6 – 20 GPa for Young's modulus and 90 – 140 MPa for flexural strength) [15]. Törmälä *et al.* [16] stated that the modulus of bone fixation devices should be close to the modulus of cortical bone, to allow potentially for controlled micromotions of the fixed bone fragments in order to accelerate bone remodelling. Various methods have been explored in order to enhance the mechanical properties of polymeric rods such as self-reinforcement [17-24] and particulate reinforcement (using Hydroxyapatite (HA), Calcium phosphate (CaP)) [25-30].

Self-reinforced polyglycolic acid (SR-PGA) rods have been prepared by sintering PGA sutures (Dexon) in a cylindrical mould and pressing (500 – 800 bar) at 205°C -

232°C for 3 to 7 min. The mechanical properties of the rods were ~ 225 MPa for shear strength and ~12 GPa and ~365 MPa for flexural modulus and strength respectively [19]. The flexural strength and modulus for SR-PLA (self-reinforced poly-lactic acid) rods in the literature ranged from 160 - 270 MPa and from 3.5 – 13 GPa respectively [8, 17, 31-33] depending on the draw ratio and chemical composition of the PLA. Their shear and compressive strengths reported were ~ 100 MPa and ~ 80 MPa respectively [17, 31].

Composite rods of un-calcined and un-sintered hydroxyapatite (u-HA) particles (20, 30, 40, 50 weight %) and poly-L-lactide (PLLA) were produced via a forging process (compression moulding followed by machining treatment) [34]. It was seen that bending, tensile and compressive moduli increased (by ~70 %, 20 % and 30 % respectively) with an increasing weight fraction of u-HA (from 20 % to 50 %). Bending and shear strengths of the rods increased slightly with u-HA weight fraction, whilst tensile strength decreased by ~ 50 % with increasing HA.

Poly-L-lactide (PLLA) rods reinforced with 40 % hydroxyapatite have been reported with properties of ~ 270 MPa for flexural strength and ~ 10 GPa for modulus [25-27, 34]. Flexural properties for particulate composite rods based on PLA and 25 % calcium phosphate have been reported to be in the range of 120 MPa for strength and 4.3 GPa modulus [29].

A more recent approach for reinforcing biodegradable polymer matrices has been to use resorbable phosphate based glass fibres (PGF) to produce totally bioresorbable composites [15, 35-45]. Phosphate based glasses have many unique properties as mentioned previously in Chapter 2. Composite plates based on PLA and PGF were produced with different fibre content and lay-up geometries. As an example, Brauer *et al.* [35] and Parsons *et al.* [36] reported flexural properties for unidirectional composites with fibre volume fraction (V_f) ~ 30% and ~ 55% as 115 MPa and 170 MPa for strength and 16 GPa and 15 GPa for modulus respectively. Ahmed *et al.* [15] reported that PLA reinforced with chopped strand random PGF mats (V_f ~14 %) showed properties of 90 MPa and 5 GPa for bending strength and modulus respectively.

In this chapter, fibre reinforced composites based on PGF and PLA were prepared. Two different compositions of PGF were used. PBG with fixed 50 mol % P_2O_5 (P50) was selected initially for preparing composites due to its ease of fibre manufacture. As a large quantity of fibres was required to conduct the initial experiments and normalisation of manufacture method for composite rods, this formulation was selected. PBG fibres with 40 mol % P_2O_5 (P40) were then utilised due to their superior mechanical, degradation and biocompatibility properties [46]. The composites were prepared with different fibre architecture (random and unidirectional) and rods were then manufactured via forging process. Mechanical tests (flexural, shear and compression) were performed in order to assess the competence of the materials for use as intramedullary fixation devices. The Rule of Mixtures was used to predict Young's modulus for the composites that were manufactured as a means of assessing the effectiveness of the rods manufacturing process.

4.3 MATERIALS AND METHODS

4.3.1 Composites production

Random (RM) and unidirectional (UD) fibre reinforced composite plates were manufactured using phosphate-based glass fibres (PGF) as reinforcement and PLA as matrix. Two different fibre compositions were used; $40P_2O_5 - 24MgO - 16CaO - 16Na_2O - 4Fe_2O_3$ in mol% (denoted as P40) and $50P_2O_5 - 40CaO - 5Na_2O - 5Fe_2O_3$ in mol% (denoted as P50). The manufacturing process for the composites was discussed previously in sections 3.3.1, 3.3.2 and 3.3.3.

4.3.2 Composite Rod Production

PLA, P50 RM, P50 UD and P40 UD composite rods were prepared by thermomechanical deformation (forging) at $\sim 90^\circ C$ using a custom mould (see Figure 4-1). The composite laminates and pure PLA plates were cut into pieces of 100 mm length \times 4.5 mm width \times 3.5 mm height using a band saw and were placed

into the cavity of the mould. The rod processing (forging) window for PLA and the composites was selected to be greater than the T_g and lower than the crystallisation temperature (see **Figure 4-2**) for PLA to prevent crystallisation of the matrix. The mould was then placed into an oven at 210°C and left for 9 mins. Change in specimen temperature against elapsed time in the oven at 210°C (see **Figure 4-3**) showed that 9 mins were sufficient to heat the specimens within the mould to ~ 90°C. After heating, the mould was transferred to a cold press, formed into shape under pressure and cooled for 5 mins at 15 bar. Images of the prepared PLA, P40 RM, P50 UD and P40 UD composite rods can be seen in **Figure 4-4**. Continuous unidirectional (UD) and in plane chopped strand random mat (RM) fibres within the composite rods were parallel to their longitudinal axis. The fibre volume and mass fractions of the composite rods were obtained using the matrix burn off method according to the standard test method (ASTM D2584-94) [47]. See **Table 4-1** for details of the rods produced in this chapter with their respective sample codes.

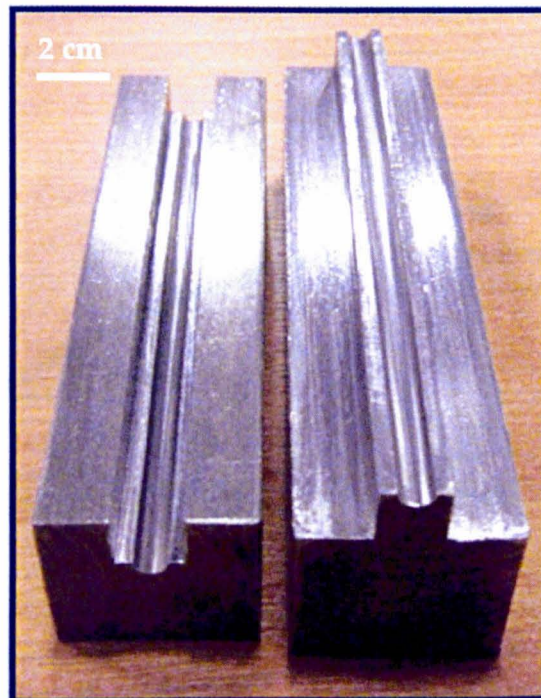


Figure 4-1: *Photograph of the mould used in this study for forging PLA and composite bars into rods.*

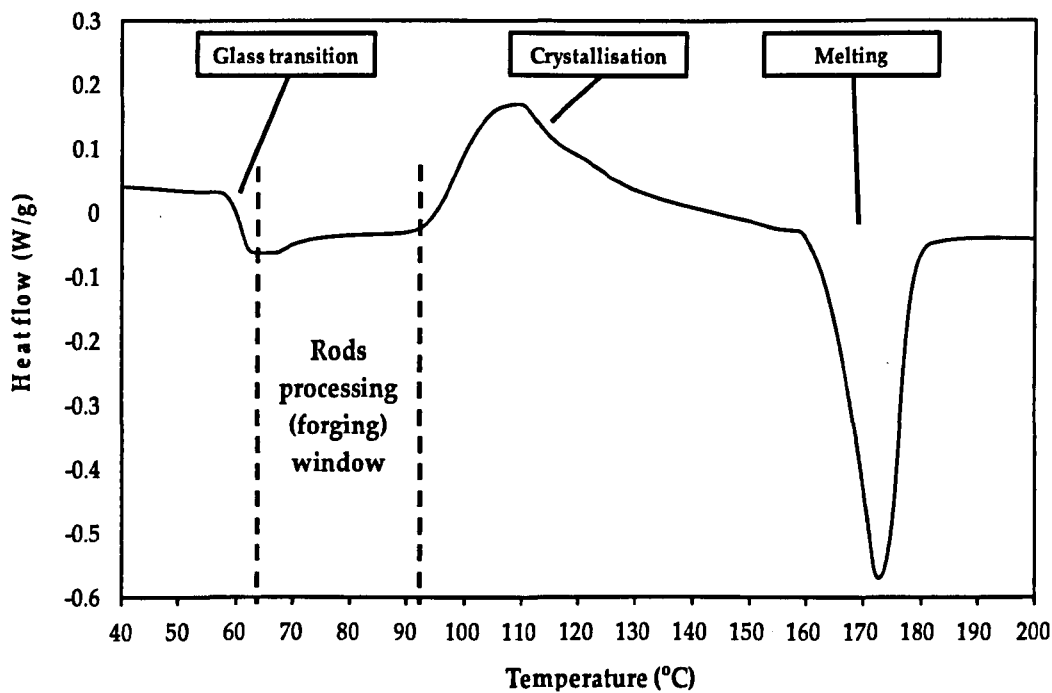


Figure 4-2: DSC trace for PLA plate over temperature range from 40°C to 200°C.

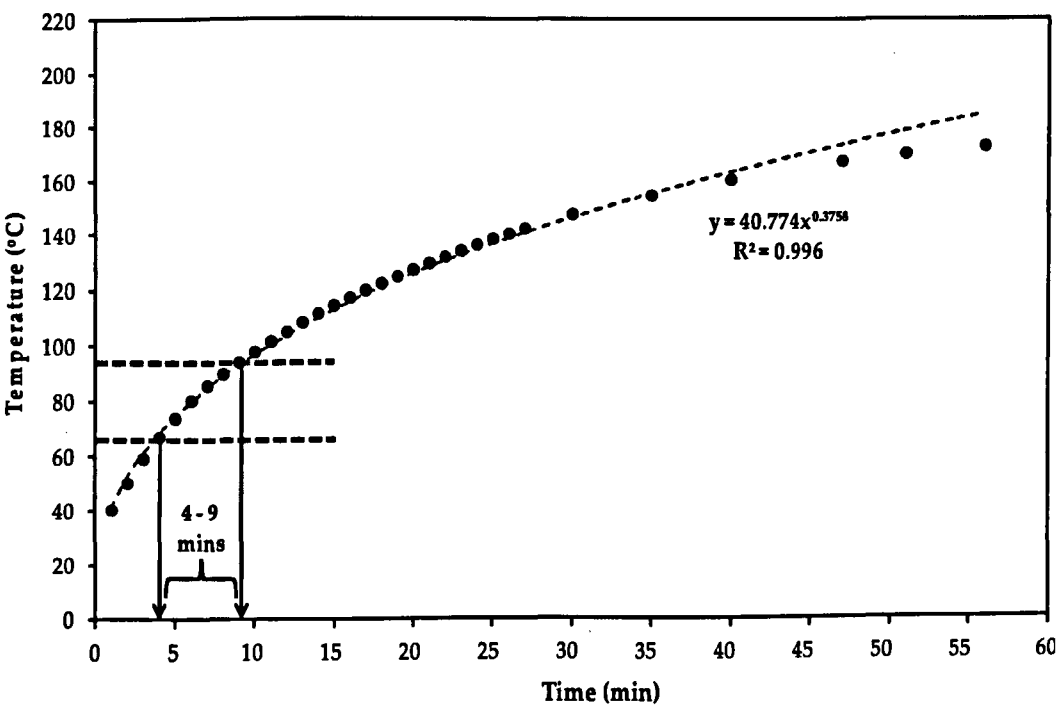


Figure 4-3: Change in temperature of PLA plate against elapsed time in oven at 210°C.

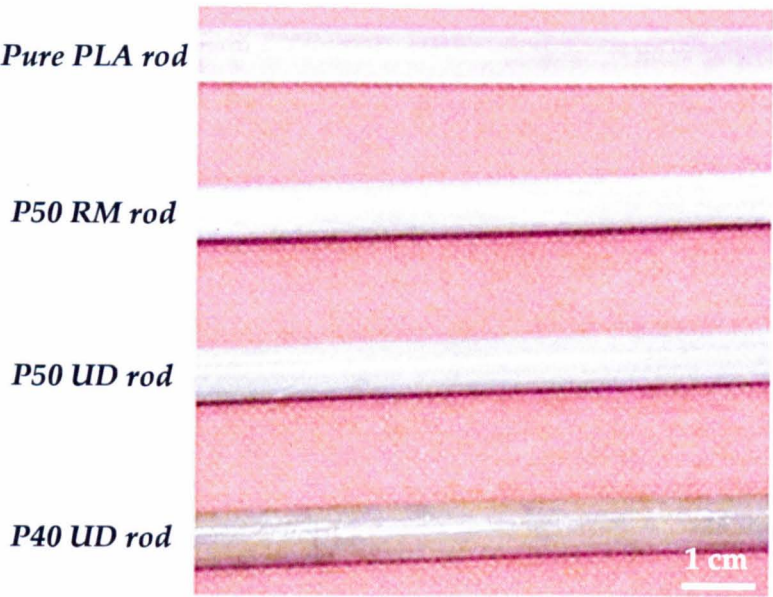


Figure 4-4: Images for the manufactured PLA, P40 RM, P50 UD and P40 UD composite rods.

Table 4-1: Sample codes for the specimens investigated in this chapter, with associated fibre volume and mass fractions.

Sample code	Specimen	Fibre mass fraction (%)	Fibre volume fraction V_f (%)
PLA	Pure PLA rods	-	-
P50 RM	P50 random mat composite rods	51 ± 5	32 ± 5
P50 UD	P50 unidirectional composite rods	50 ± 2	31 ± 2
P40 UD	P40 unidirectional composite rods	56 ± 2	37 ± 2

4.3.3 Mechanical tests

4.3.3.1 *Flexural test*

The flexural strength and modulus properties were evaluated by flexural (three-point bend) testing using a Hounsfield Series S testing machine. The measurements were performed according to the standard BS 2782-10: Method 1008B:1996 [48]. Here, the two supports should have a notch in the middle with diameter equal to the diameter of the rods. These notches in both supports are required to eliminate rotational movement of the rods during testing. Displacement was measured from the crosshead of the machine travelling at 1 mm/min and force was recorded using a 1 kN load cell. The rod diameter was measured at the mid-span using vernier callipers to accuracy of 0.01 mm and the measurements were conducted in triplicate ($n = 3$). Specimen dimensions were 80 mm length and 4 mm diameter.

4.3.3.2 *Double shear test*

The shear strength and stiffness values for PLA alone, P50 RM, P50 UD and P40 UD composite rods were measured using a modified double shear test (see Figure 4-5) according to the standards BS 2782-3:Methods 340A and 340B:1978 [49] and ASTM D7617M-11 [50]. The crosshead speed of the machine was 5 mm/min and the load cell capacity was 25kN. The measurements were carried out in triplicate ($n = 3$). The shear strength τ was calculated using the following equation;

$$\tau = \frac{F}{2A} \quad \text{Equation 4-1}$$

where F is the force at fracture and A is the cross-sectional area of the test rod. Shear stiffness was evaluated as the maximum gradient of the linear portion in the shear load – deflection plot (see Figure 4-6). Specimen dimensions were 30 mm length and 4 mm diameter.

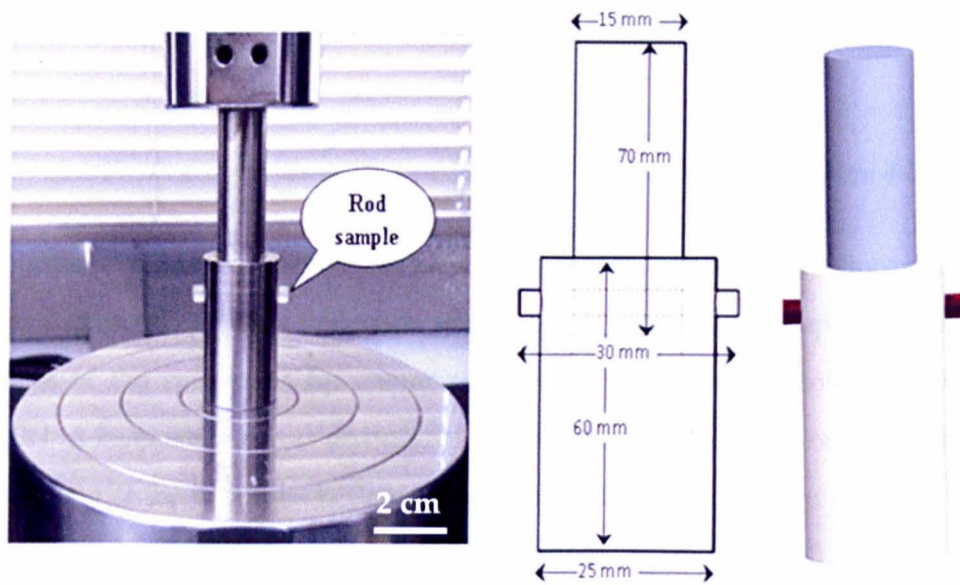


Figure 4-5: Double shear test tool used for shear tests.

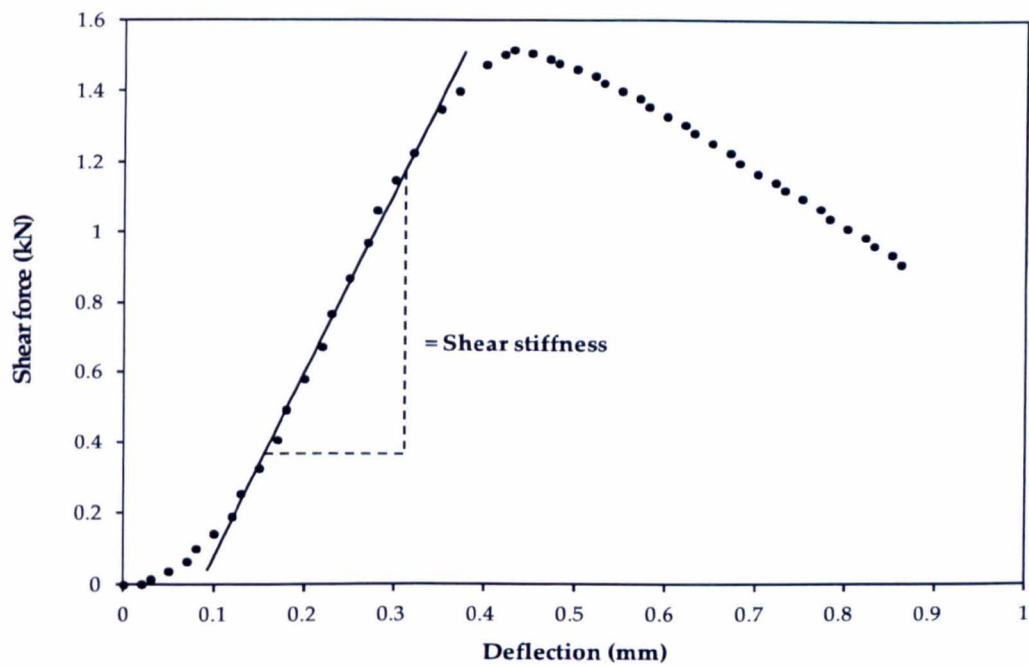


Figure 4-6: Applied force versus deflection during the double shear test for rods.

4.3.3.3 Compression test

The compressive strength and stiffness values were determined using an Instron 5969 and the calculations were performed according to the standard BS ISO 3597-3: 2003 [51]. A crosshead speed of 5 mm/min and a 25 kN load cell were used with

measurements conducted in triplicate ($n = 3$). The compressive strength σ was given by

$$\sigma = \frac{F}{A}$$

Equation 4-2

Compressive stiffness was taken to be the maximum gradient of the linear portion in the compressive load – deflection graph (see Figure 4-7). The upper and lower surfaces of the specimens for compression testing should be absolutely flat and parallel. A bespoke tool was manufactured with a hole (of dimensions equal to the dimensions of the samples) to flatten the ends of the specimens (by polishing with sand papers) and ensure reproducibility and to avoid potential discrepancies associated with sample preparation for testing. Specimen dimensions were 10 mm length and 4 mm diameter.

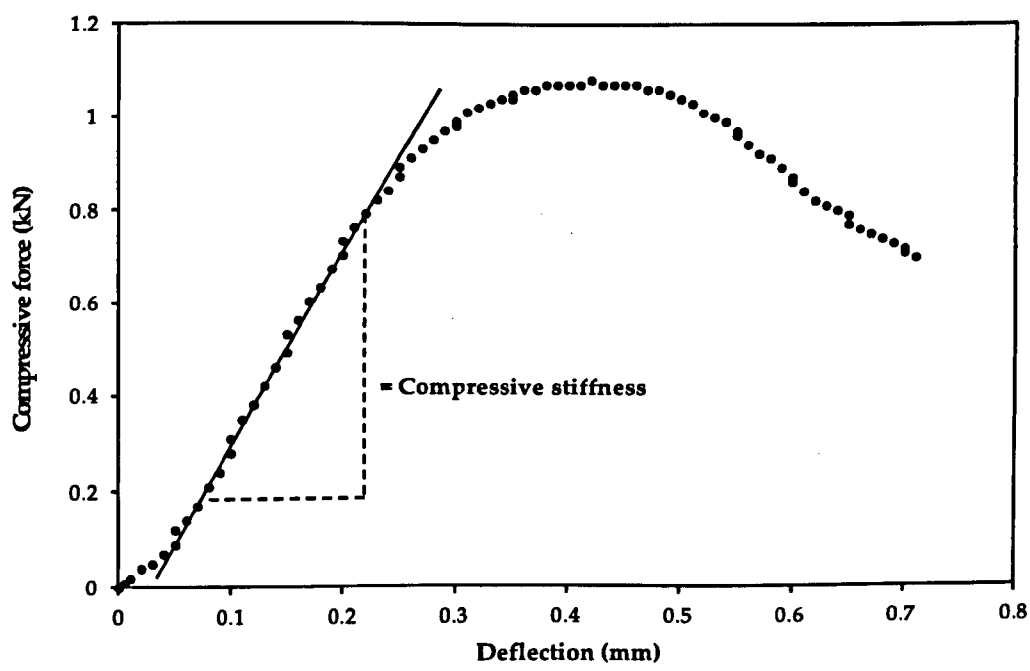


Figure 4-7: Applied compressive force against deflection.

Statistical analysis was conducted for the mechanical tests using one-way ANOVA as mentioned previously in section 3.3.13.

4.3.3.4 *Extracted fibre length measurement*

Chopped strand random fibres were extracted from composite bars (30 mm (length) x 4.5 mm (width) x 3.5 mm (thickness)) and rods (30 mm (length) x 4 mm (diameter)) via a burn-off method at 450°C for 3 hours. The extracted fibres remained aggregated and so acetone was used as a medium to disperse them. The fibres were left in acetone for one hour, after which the solution was cast into a glass Petri dish and left until the solvent had evaporated. Images were captured using a Zeiss optical microscope operating with Image-Pro Plus software version 6.3. The length distribution of the extracted fibres was measured using Image J 1.42q software. A total of 1000 fibres were measured and the number average and weight average length of the distribution was determined using the following equations [52].

Number average length,

$$L_N = \frac{\sum N_i L_i}{\sum N_i} \quad \text{Equation 4-3}$$

Weight average length,

$$L_W = \frac{\sum N_i L_i^2}{\sum N_i L_i} \quad \text{Equation 4-4}$$

where N_i is the number of fibres of length L_i .

4.3.3.5 *Fibre orientation*

Two pieces of P50 RM bar (cut from the laminates produced) and two pieces of the forged rod were cast into resin and polished to a fineness of 1 micron. Images for the cross-sections were captured by using a Zeiss optical microscope. Images obtained were analysed using Image J 1.42q software. The images were converted into binary (black and white colours) images; black colour represented the fibres whereas the white indicated the composite matrix. A total of 2000 fibres were measured for each sample and the out of plane orientation angle (the inclination angle of the fibres) was calculated using the following equation, assuming a 2D laminar structure.

$$\theta = \arccos \left(\frac{b}{a} \right)$$

Equation 4-5

where θ , b and a are angular eccentricity, minor and major diameters for the ellipse, respectively [53, 54].

4.3.3.6 Scanning Electron Microscopy (SEM)

Freeze fractured specimens were sputter-coated with carbon and examined using a JEOL 6400 SEM with an accelerating voltage of 10kV in secondary electron mode (SE).

4.3.3.7 Rule of Mixtures

Young’s modulus for a fibre reinforced composite is given by:

$$E = \eta_L \eta_o E_f V_f + E_m (1 - V_f)$$

Equation 4-6

where η_L is fibre length correction factor (~ 1 for fibres longer than 10 mm and 0.9 for fibres longer than 1 mm) and η_o is orientation efficiency factor ($\eta_o = 1$ for unidirectional and $\eta_o = 0.375$ for in-plane random composites) [55]. Using the properties of fibres and matrix and the fibre volume fraction (see Table 4-2), it is possible to predict Young’s modulus values for the composites.

Table 4-2: Rule of mixtures input data.

Sample	Matrix Young’s Modulus (E_m) GPa	Fibre Young’s Modulus (E_f) GPa	Fibre length correction factor (η_L)	Orientation efficiency factor (η_o)
P50 RM	3.8	52	0.9	0.375
P50 UD	3.8	52	1	1
P40 UD	3.8	62	1	1

4.4 RESULTS

4.4.1 Flexural properties

Figure 4-8 shows flexural strength and modulus values for PLA, P50 RM, P50 UD and P40 UD composite rods. The flexural strength for P50 RM composite rods was slightly lower (not significant, $P > 0.05$) than PLA, whilst, P50 UD and P40 UD were significantly higher ($P < 0.05$) than PLA by approximately 40 % and 100 % respectively. The flexural modulus values for P50 RM, P50 UD and P40 UD composite rods were three, five and six times that for PLA.

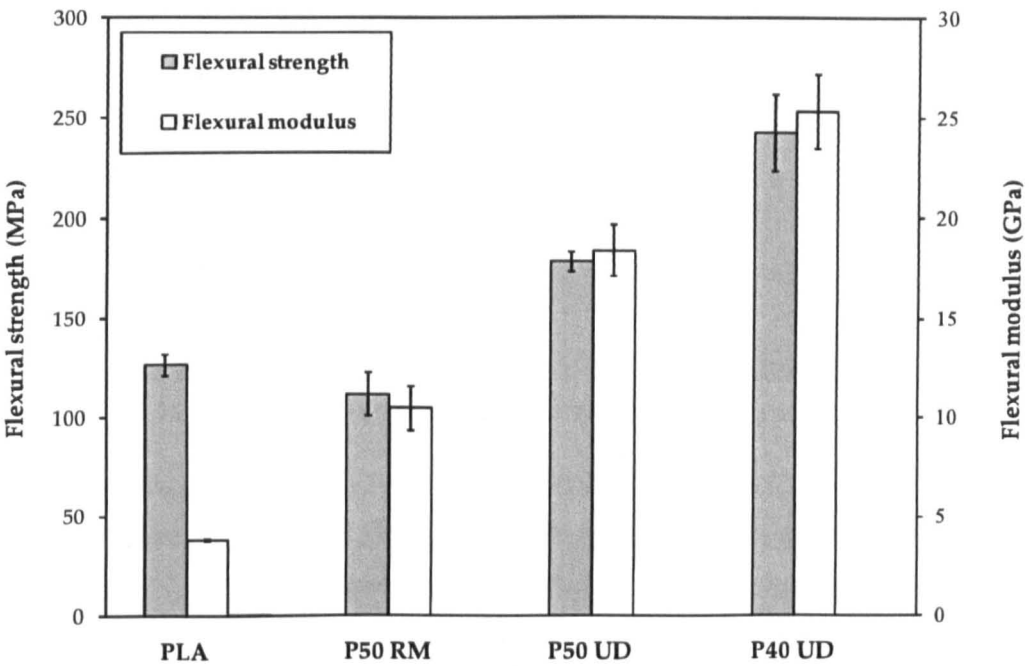


Figure 4-8: Flexural properties for PLA, P50 RM, P50 UD and P40 UD composite rods. The test was conducted for dry samples in triplicate at room temperature (~ 20°C). Sample dimensions were 80 mm length and 4 mm diameter. Young’s moduli for P50 and P40 fibres were ~ 52 GPa and ~ 62GPa respectively.

4.4.2 Shear Properties

The shear strength and stiffness values for PLA, P50 RM, P50 UD and P40 UD composite rods are shown in Figure 4-9. The shear strength for PLA was ~ 47 MPa

and increased by ~ 10, 25 and 40 MPa for P50 RM, P50 UD and P40 UD composite rods respectively. No significant difference ($P > 0.05$) was seen between PLA and P50 RM rods, whilst the other composite rods were significantly ($P < 0.05$) higher than PLA alone. The shear stiffness values for P50 UD and P40 UD composite rods were higher ($P < 0.05$) than those of the PLA and P50 RM rods.

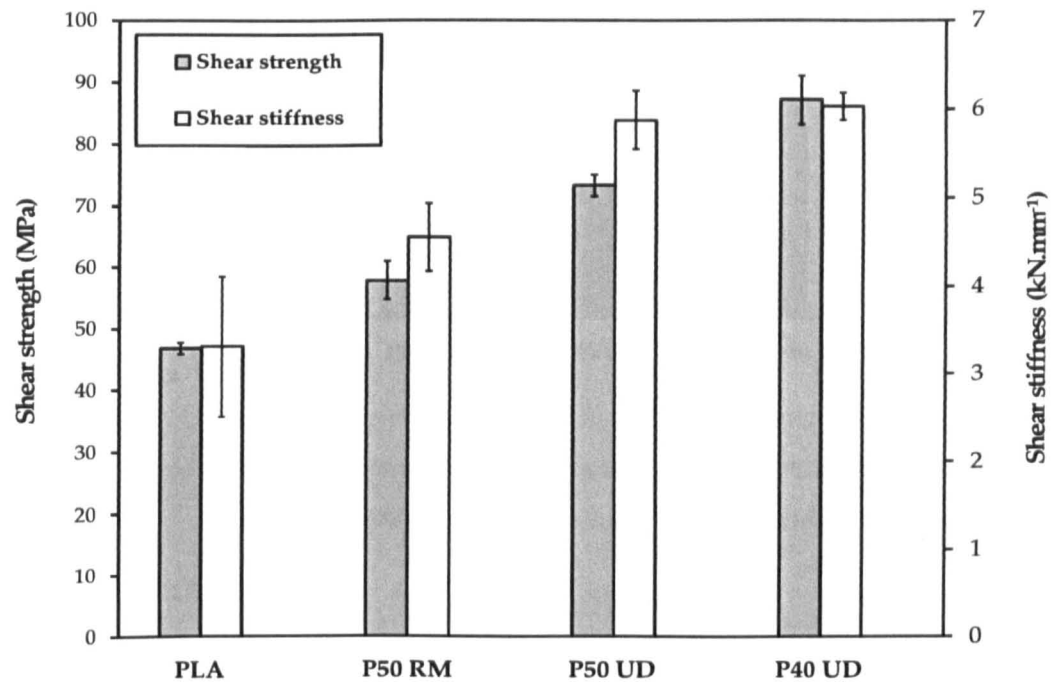


Figure 4-9: Shear properties for PLA, P50 RM, P50 UD and P40 UD composite rods. The test was conducted for dry samples in triplicate at room temperature (~ 20°C). Sample dimensions were 30 mm length and 4 mm diameter.

4.4.3 Compressive properties

Figure 4-10 illustrates the compressive properties obtained for PLA, P50 RM, P50 UD and P40 UD composite rods. The compressive strength for P50 RM rods was slightly higher (not significant, $P > 0.05$) than PLA rods whereas the stiffness was around 80% higher ($P < 0.05$) than for PLA. For P50 UD and P40 UD composite rods, the strength and stiffness values increased by 350% and 450% in comparison to the unreinforced PLA rods.

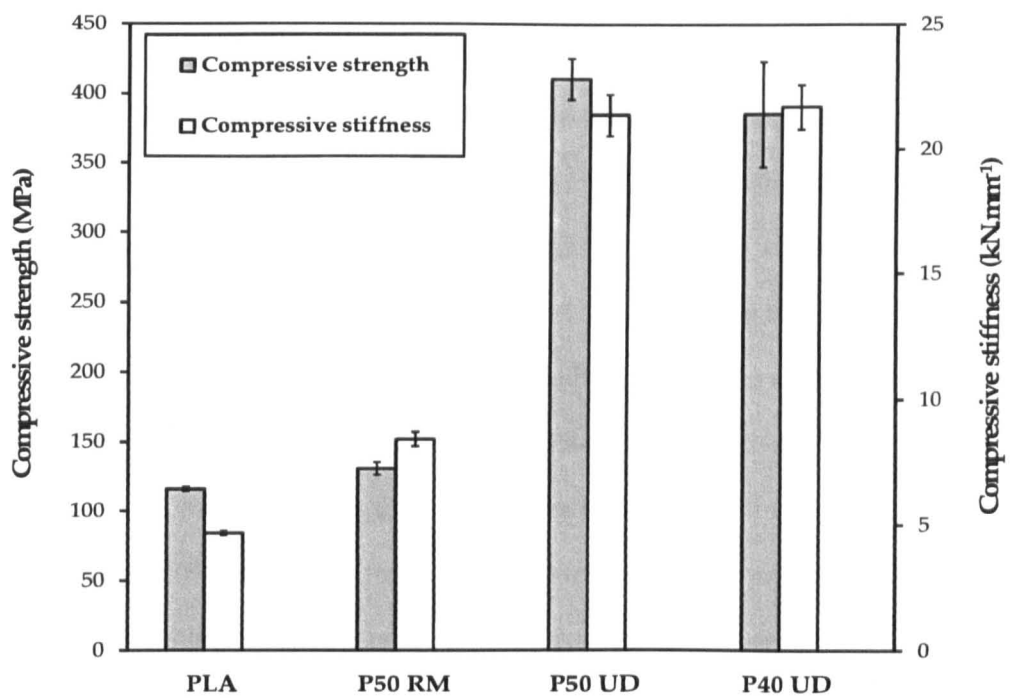


Figure 4-10: *Compressive properties for PLA, P50 RM, P50 UD and P40 UD composite rods. The test was conducted for dry samples in triplicate at room temperature (~ 20°C). Sample dimensions were 10 mm height and 4 mm diameter.*

4.4.4 SEM analysis

SEM micrographs for the fractured cross-section of P50 RM, P50 UD and P40 UD composite rods are provided in **Figure 4-11**. The fracture surfaces revealed that the fibres were well dispersed and excellent wet-out of the fibres had been achieved, with minimal fibre pull-out demonstrating good impregnation of the fibres.

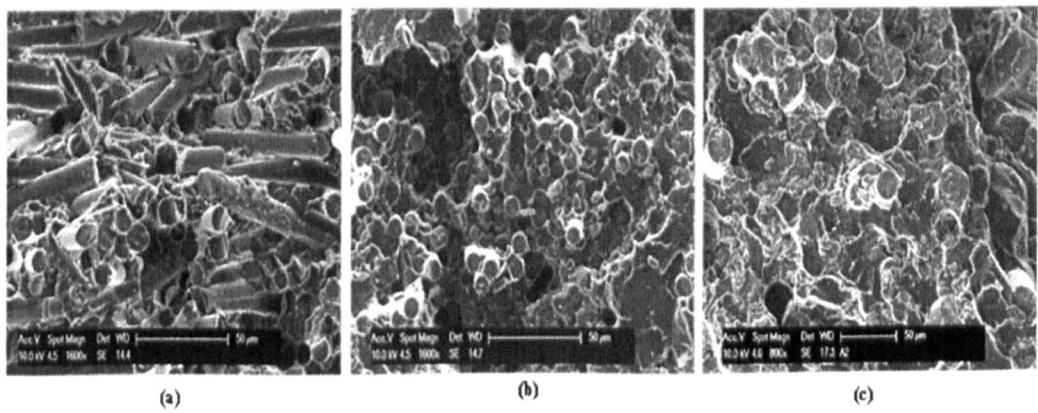


Figure 4-11: *SEM micrographs of freeze fractured surfaces for (a) P50 RM rod, (b) P50 UD rod and (c) P40 UD rod. Scale bars for all micrographs represent 50 µm.*

4.4.5 Fibre length and orientation analysis

Figure 4-12 shows images of fibres that were extracted from the composite rods and bars using the burn off method at 450°C for 3h. The fibres within the UD composite rods remained continuous, whilst fibre breakage could be observed for the RM composites. The breakage for fibres within the RM rods was more significant than the RM composite bars. The fibre length distributions for the extracted fibres from composite bars and rods are shown in Figure 4-13 and Figure 4-14. The majority of the fibres were between a length ranging between ~ 1.0 – 3.0 mm and the number average length (Equation 4-3) for the fibres extracted from composite bars and rods were approximately ~ 1.5 mm and 1.2 mm respectively. The weight average length (Equation 4-4) for the fibres was ~ 2.4 mm and 2 mm for RM bar and rod. For UD composite bars and rods, the extracted fibres were still continuous for the full length of the specimens investigated.

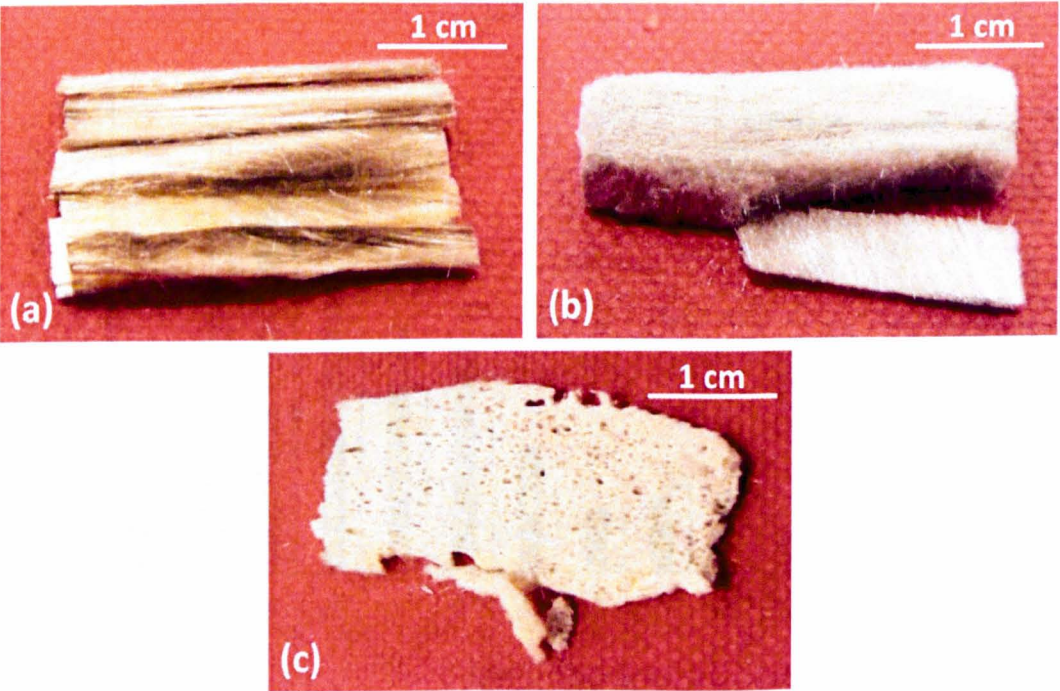


Figure 4-12: Photographs for the extracted fibres after burn off from (a) UD composite rod, (b) RM composite bar and (c) RM composite rod.

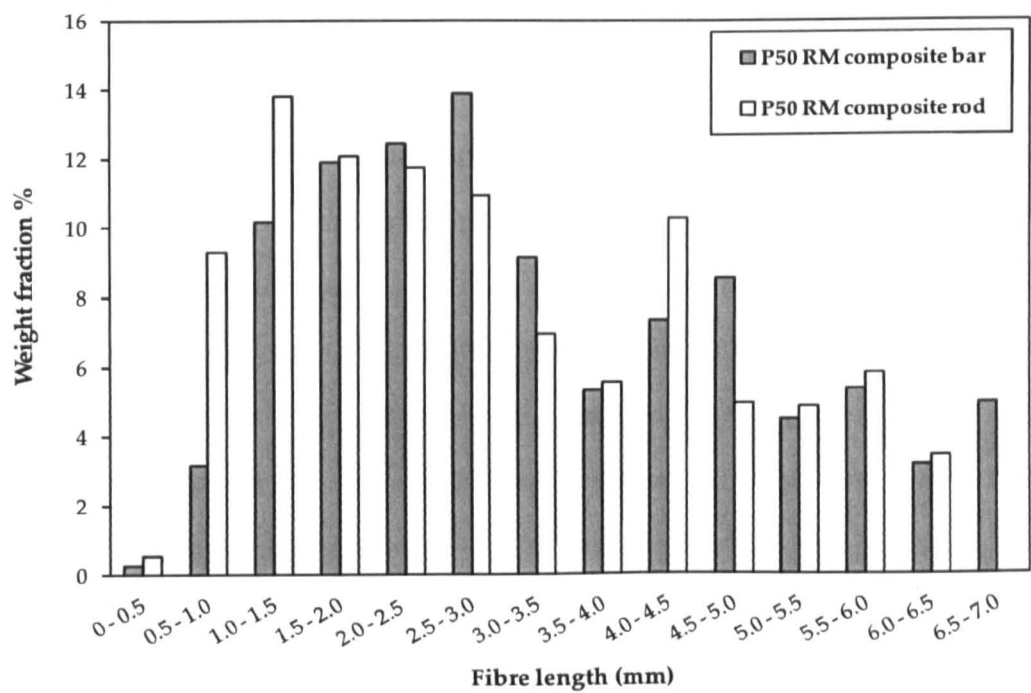


Figure 4-13: Weight average length distribution of the extracted fibres from the P50 RM composite bar (30 mm (length) x 4.5 mm (width) x 3.5 mm (thickness)) and rod (30 mm (length) x 4 mm (diameter)).

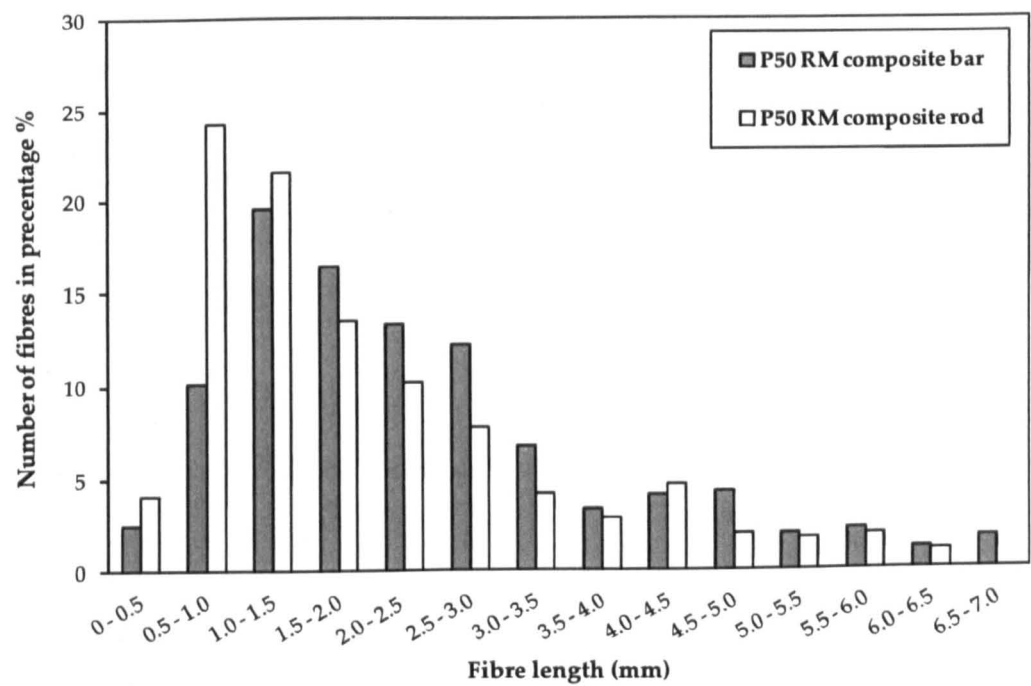


Figure 4-14: Number average length distribution of the extracted fibres from the P50RM composite bar (30 mm (length) x 4.5 mm (width) x 3.5 mm (thickness)) and rod (30 mm (length) x 4 mm (diameter)).

Figure 4-15 shows thresholded optical images of polished cross-sections of the P50 RM bar and rod specimens that were used to determine fibre orientation and distribution. For the P50 RM bar, the cross-sections for the fibres were seen to be ellipsoidal with small aspect values and a wide range of cross-section aspect ratios (the ratio of minor to major axes of the ellipse). With the rod, the cross-section aspect ratios were closer to unity (circular) and less variable, suggesting minimal rearrangement of the fibres within the rods during the forging process. From Figure 4-16, it can be seen that the orientation angles for the rod were lower than that for the bar. The spread of fibre orientation angles throughout 90° was due to in plane random distribution of fibre throughout the composite.

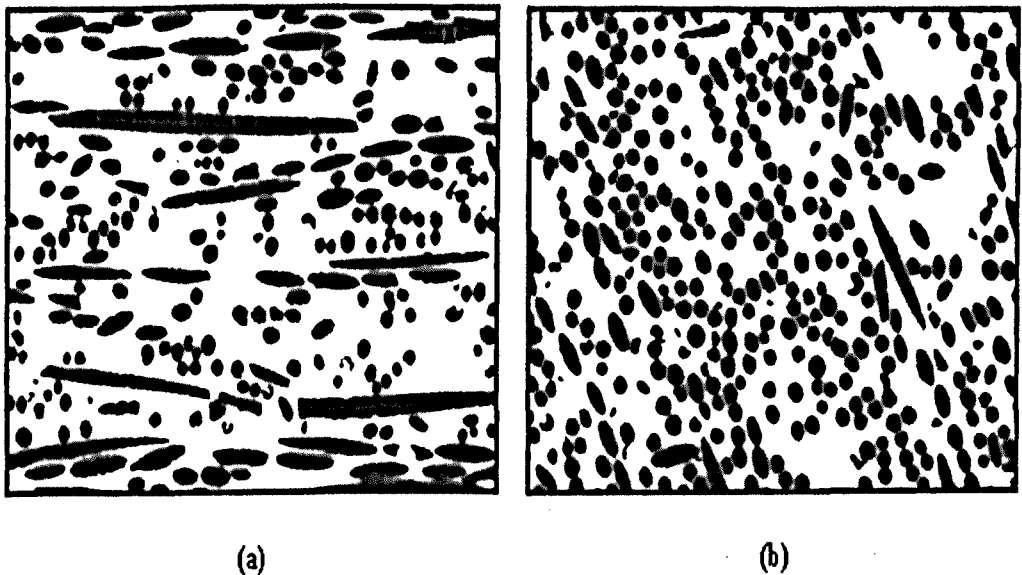


Figure 4-15: *Optical binary images (5X) of polished cross-sections for (a) P50 RM bar and (b) P50 RM rod obtained via optical microscope.*

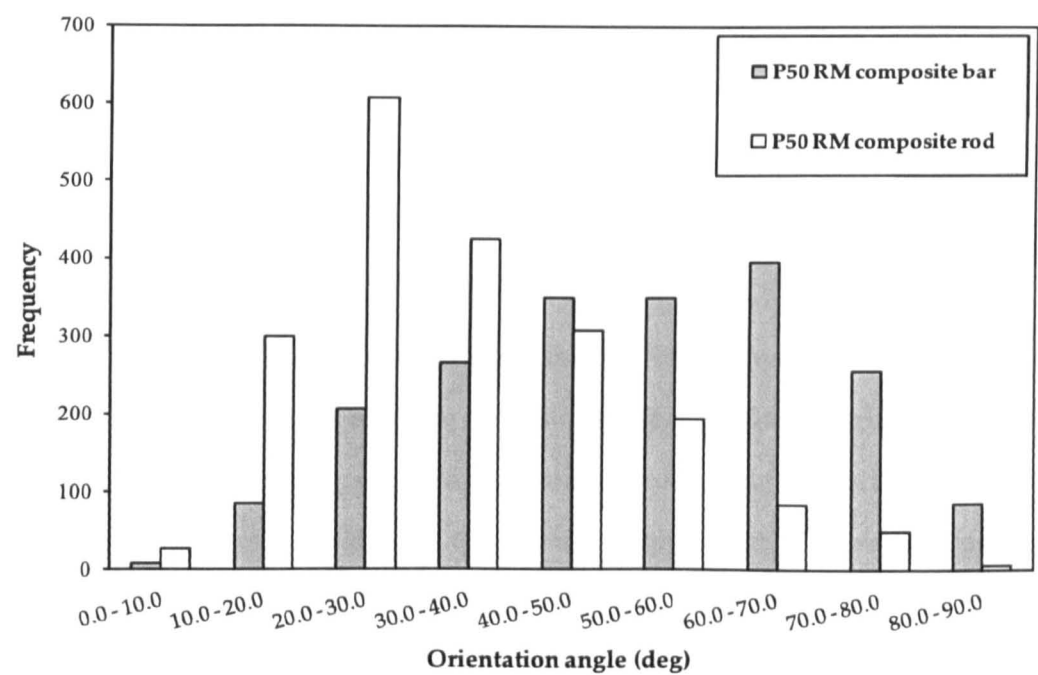


Figure 4-16: Orientation angle distribution for P50 RM composite bar and rod.

4.5 DISCUSSION

The ideal intramedullary rods should be totally bioresorbable, have excellent biocompatibility and provide adequate initial mechanical properties (to support majority of the load during the initial stages of bone healing) that diminish gradually over time, transferring load to the healing bone [56].

The percentage improvements in compressive properties for UD rods in comparison to the pure PLA rods were greater than those for the flexural and shear properties. This was suggested to be due to the influence of the fibre and fibre/matrix interface (i.e. the direction of fibre/matrix interface comparing to the direction of applied load). The interface is more significant for the compressive properties as the load is applied in the direction of the parallel fibres. For the flexural and double shear tests, the load applied was perpendicular to the fibre direction and therefore the interface was not directly responsible for transferring load between the two constituent materials. Rijdsdijk *et al.* [57] investigated the effect of adding 10 wt% Maleic-anhydride-modified polypropylene (mPP) as a potential coupling agent on the flexural, shear and compressive properties of polypropylene

(PP) reinforced with continuous unidirectional E-glass fibres. They found flexural and interlaminar shear strength had increased by ~ 30 % of their initial values, whilst the compressive strength had increased from 250 MPa to 396 MPa (~ 60 %). They concluded that the compressive strength of the composites was governed by the fibre/matrix interface (i.e. interface-dominant property).

Flexural, compressive and shear strength for P50 RM composites were similar to that of the PLA alone. This could be attributed to fibre breakage during the various stages of production: i.e. random mat preparation; composite production; cutting of and forging the bars. According to the extracted fibre length distribution from P50 RM composite bars and rod, it was seen that the fibre length had decreased from 10 mm (initial length) to ~ 1.0 – 3.0 mm (see Figure 4-13 and Figure 4-14). Given the relative similarity of the two distributions it would appear that majority of the damage was caused during the initial chopped strand random fibre mat fabrication process and composite pressing, though there was also evidence of further damage during the rod forging process used.

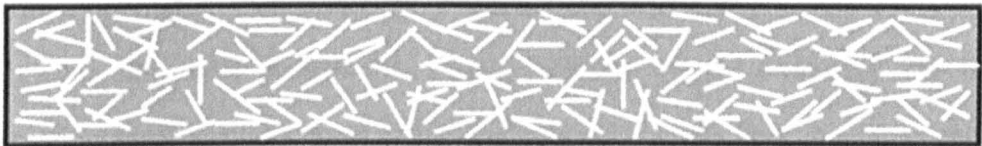
Ahmed *et al.* [43] reported that fibre length within chopped strand random fibre mat (RM) composites had decreased from 10 mm (initial length) to ~ 3 mm due to collision damage with the stirring impeller blade during the fibre dispersion stage in the RM manufacturing process. The number average length obtained for the extracted fibres from the bars and rods were approximately 1.5 mm and 1.2 mm respectively. The average length of the fibres within the P50 RM rods was higher than the critical fibre length (around 0.7 mm [43]), therefore some fibre reinforcing effect should have been conferred. It was found that the mechanical properties for discontinuous fibre reinforced composites increase as fibre length increases [58-60].

Ahmed *et al.* [43] investigated the flexural properties for P50 RM ($V_f = 30\%$) and P50 UD ($V_f = 23.5\%$) composite plates. The reported flexural properties were lower than those obtained in the present study. The flexural strengths were 105 MPa and 129 MPa and the moduli were 8.4 GPa and 11.5 GPa for RM and UD composites

respectively. The increase in mechanical properties seen from the current study was suggested to be due to two aspects; chain orientation of the matrix [34] and reorientation of the short PGF fibres within the RM composites during the rod manufacturing process (see **Figure 4-17**).



(a)



(b)

Figure 4-17: Schematic representation of the change in fibre orientation during rods manufacture (a) P50 RM plate and (b) P50 RM rod. Fibre reorientation (i.e, more fibres near to parallel with the extension axis) can be seen within the forged rods

Prior investigations revealed that the flexural strength and modulus values for plates (or bars) for this grade of PLA were ~ 90 MPa and ~ 3.8 GPa respectively (see Chapter 3). In this chapter the strength of the PLA rods increased to ~125 MPa, whilst the modulus remained at ~ 3.8 GPa. The increase in observed flexural strength was due likely to polymer chain orientation as a result of the thermomechanical deformation process [21, 22, 24]. The SEM micrographs in **Figure 4-18 a** and **b** show some evidence for chain orientation from the cross-section of the PLA rod in comparison with the plate. It is well know that the processing of polymers below their melting temperature can result in chain orientation.

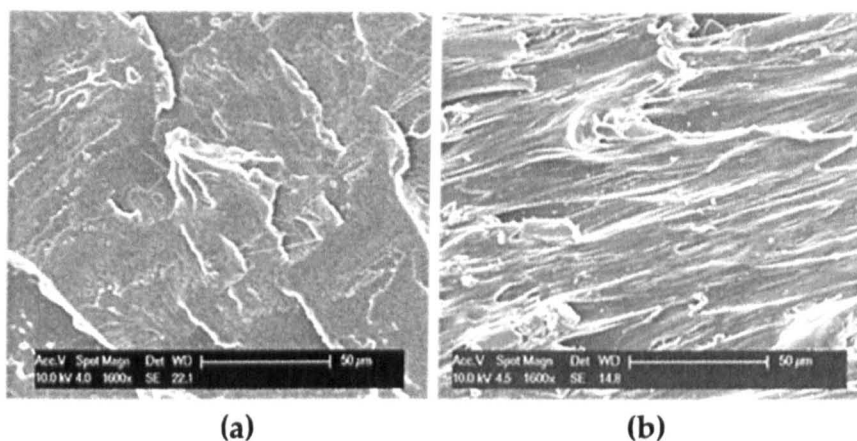


Figure 4-18: SEM micrographs of a freeze fractured surface for (a) PLA plate and (b) PLA forged rod. PLA rod showed chain orientation.

The fibre orientation distribution for P50 RM composite bars and rods was derived from their ellipsoidal profiles (see **Figure 4-15** and **Figure 4-16**) [53]. The fibre orientation angle varies from 0° to 90° and depends on the fibre directions. When the fibres were parallel to the rod axis, the cross-section for the fibres was circular and the angle was equal to 0° . The cross-section for the fibres becomes linear when the fibres are perpendicular to the rod axis and then the orientation angle will be 90° (see **Figure 4-19**). Between 0° and 90° , the cross-sections of the fibres are ellipsoids with aspect ratios greater than 0 and less than 1. Fibre orientation usually occurs during the processing of short fibre composites as a result of extensional and shear flows. The fibres tend to rotate towards the direction of extension (axis of the rods) and the fibre alignment depends mainly on the degree of extension and physical properties of the matrix (see **Figure 4-17**) [55]. Slight fibre orientation was seen for composite bars and was attributed to squeeze flow of the melting polymer during compression moulding [61, 62]. Similar finding was presented by Yang *et al.* [63] via investigation of the flexural properties of discontinuous random composite (PCL/PGF) at different angles. However, variation in flexural strength and modulus over the angles was not significant ($P > 0.05$) which is indicative of homogenous distribution of the fibres at macroscopic level.

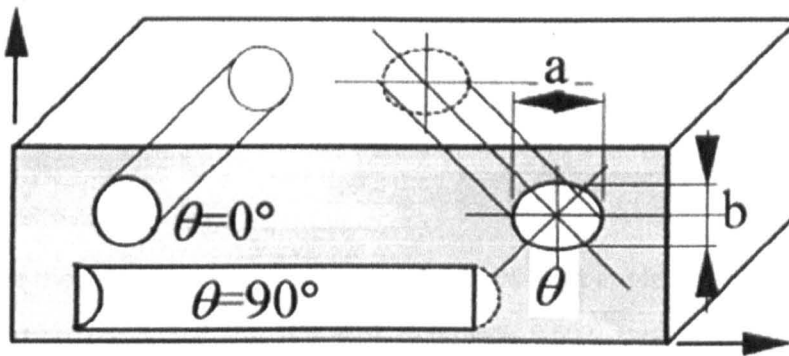


Figure 4-19: Schematic diagram for possible shapes of fibre cross-sections at the polished surface (grey plane)[54].

It is well known that the rule of mixture is applicable for prediction of tensile properties. Flexural modulus is directly proportional to the tensile modulus; however, a function of the span to thickness ratio should be employed. Shorter span to thicknesses result in higher shear stresses through the thickness of the sample, resulting in lower flexural moduli, as reported in [64]. Tensile and flexural properties for PLA/PGF composites were investigated previously in [44]. Tensile and flexural moduli were 12 ± 2 GPa and 9 ± 2 GPa using a span to thickness ratio of 16:1 (the difference was considered to be statistically insignificant using the students t-test). Thus, the rule of mixture was applied to predict the flexural modulus for the composite rods in the current study.

There was no appreciable difference between experimental and theoretical flexural modulus values for P50 UD and P40 UD composite rods (see **Table 4-3**). Theoretical values were calculated using the Rule of Mixture (**Equation 4-5**). This was indicative of complete fibre impregnation and a strong fibre/matrix interface and potentially an improvement of the matrix properties via thermomechanical deformation. For P50 RM composite rods, the theoretical value was lower than the experimental value, which could be due to using the theoretical standard value of 0.375 as the orientation efficiency factor. The orientation factor for the P50 RM rods should be higher than 0.375 due to the alignment of the short fibres along the extension axis during the shaping of the rods (see **Figure 4-16**). The actual orientation factor for the P50 RM rods was determined by applying the fibre

orientation distribution which was determined previously via the following equation [65];

$$\eta_o = \sum_{i=1}^{I=n} a_i \cos^4 \theta_i$$

Equation 4-7

where a_i is the fibre fraction which has the orientation angle θ_i . It was found that the orientation factor for the P50 RM rods was 0.502. By using this value, the theoretical flexural modulus was calculated to be 9 ± 2 GPa, which was similar to the experimental value (11 ± 2 GPa). Therefore, the measured flexural modulus for P50 RM composites was improved via fibre alignment and chain orientation of the matrix (PLA).

Table 4-3: Comparison between the experimental and theoretical flexural modulus for PLA/PBG fibre reinforced composites.

Sample code	Experimental flexural modulus (GPa)	Theoretical flexural modulus range (GPa)
P50 RM	11 ± 2	6.3 – 8
P50 UD	18 ± 2	17.6 – 19.5
P40 UD	25 ± 3	24.2 – 26.5

In the present study, a new method was applied to manufacture fibre-reinforced composite rods based on PLA and PBG fibres with different fibre geometry (UD and RM). This method provided improved mechanical properties for the PLA and composite rods in comparison to the plates made via the conventional compression moulding process. It was also found that the method of rod manufacture had a similar influence of “hot drawing” at small draw ratios due to the chain orientation and fibre alignment observed within the rods. After determination of the actual orientation factor for RM composite rods, it was found that the rule of mixtures was applicable for prediction of the mechanical properties for the RM and UD composites that were produced. Further investigations such as mechanical retention *in vitro* and *in vivo* are required to understand the performance of the rods as

intramedullary fixation devices. *In vitro* degradation and mechanical properties retention for the rods produced will be covered in the following chapter.

4.6 CONCLUSIONS

Totally bioresorbable fibre reinforced composite rods were manufactured via forging process. Their initial mechanical properties obtained were similar to that for cortical bone. These resorbable composite rods can be used potentially as intramedullary (IM) fixation devices in order to align and stabilise bone fractures. Flexural modulus values for P50 and P40 UD rods were ~450 % and ~ 600 % higher in comparison to pure PLA rods. Compressive properties for UD composite rods were four times higher than the PLA, whilst the shear properties increased slightly (~ 50 % to ~ 80 % greater than the PLA values). The method used for preparing the rods (forging) improved the mechanical properties for the matrix as well as the composites. This method had a similar effect to the drawing process at low draw ratios for the matrix. Both the orientation of the polymer chains in the matrix and the fibre rearrangement were suggested to be responsible for the improvement of the mechanical properties, especially the flexural modulus. It was also found that the rule of mixtures was applicable for the UD and RM composites when using the actual orientation factor derived from the fibre orientation distribution.

4.7 REFERENCES

1. Stannard, J.P., L. Bankston, L.A. Futch, G. McGwin, and D.A. Volgas, *Functional outcome following intramedullary nailing of the femur: a prospective randomized comparison of piriformis fossa and greater trochanteric entry portals*. *J Bone Joint Surg Am*, 2011. 93(15): p. 1385-91.
2. Eveleigh, R.J., *A review of biomechanical studies of intramedullary nails*. *Medical Engineering & Physics*, 1995. 17(5): p. 323-331.
3. Weinstein, A.M., A.J. Clemow, W. Starkebaum, M. Milicic, J.J. Klawitter, and H.B. Skinner, *Retrieval and analysis of intramedullary rods*. *J Bone Joint Surg Am*, 1981. 63(9): p. 1443-8.
4. Toms, A.D., R.L. Morgan-Jones, and R. Spencer-Jones, *Intramedullary femoral nailing: removing the nail improves subjective outcome*. *Injury*, 2002. 33(3): p. 247-249.

5. Lewis, D., C. Lutton, L. Wilson, R. Crawford, and B. Goss, Low cost polymer intramedullary nails for fracture fixation: a biomechanical study in a porcine femur model. *Archives of Orthopaedic and Trauma Surgery*, 2009. 129(6): p. 817-822.
6. Star, A.M., R.P. Whittaker, H.M. Shuster, J. Duda, and E. Menkowitz, Difficulties during removal of fluted femoral intramedullary rods. *J Bone Joint Surg Am*, 1989. 71(3): p. 341-344.
7. Bombaci, H. and M. Gorgec, Difficulty in removal of a femoral intramedullary nail: the geometry of the distal end of the nail. *Yonsei Med J*, 2003. 44(6): p. 1083-6.
8. Matsusue, Y., T. Yamamuro, M. Oka, Y. Shikinami, S.-H. Hyon, and Y. Ikada, In vitro and in vivo studies on bioabsorbable ultra-high-strength poly(L-lactide) rods. *Journal of Biomedical Materials Research*, 1992. 26(12): p. 1553-1567.
9. Viljanen, J., H. Pihlajamäki, J. Kinnunen, S. Bondestam, and P. Rokkanen, Comparison of absorbable poly-L-lactide and metallic intramedullary rods in the fixation of femoral shaft osteotomies: an experimental study in rabbits. *Journal of Orthopaedic Science*, 2001. 6(2): p. 160-166.
10. An, Y.H., S.K. Woolf, and R.J. Friedman, Pre-clinical in vivo evaluation of orthopaedic bioabsorbable devices. *Biomaterials*, 2000. 21(24): p. 2635-2652.
11. Roure, P., W.Y. Ip, W. Lu, S.P. Chow, and S. Gogolewski, Intramedullary Fixation by Resorbable Rods in a comminuted Phalangeal fracture Model. A Biomechanical Study *The Journal of Hand Surgery: Journal of the British Society for Surgery of the Hand*, 1999. 24(4): p. 476-481.
12. Tunc, D., Orientruded polylactide based body-absorbable osteosynthesis devices: A short review. *Journal of Biomaterials Science, Polymer Edition*, 1996. 7: p. 375-380.
13. Rokkanen, P.U., O. Böstman, E. Hirvensalo, E.A. Mäkelä, E.K. Partio, H. Päätiälä, S. Vainionpää, V. Kimmo, and P. Törmälä, Bioabsorbable fixation in orthopaedic surgery and traumatology. *Biomaterials*, 2000. 21(24): p. 2607-2613.
14. Hoffmann, J., K. Friedrich, M. Evgstatiev, and U. Finkc, A Totally Bioresorbable Fibrillar Reinforced Composite System: Structure and Properties. *International Journal of Polymeric Materials*, 2001. 50(3): p. 469 - 482.
15. Ahmed, I., P.S. Cronin, E.A. Abou Neel, A.J. Parsons, J.C. Knowles, and C.D. Rudd, Retention of mechanical properties and cytocompatibility of a phosphate-based glass fiber/polylactic acid composite. *Journal of Biomedical Materials Research Part B: Applied Biomaterials*, 2009. 89B(1): p. 18-27.
16. Törmälä, P., M. Huttunen, N. Ashammakhi, M. Tukiainen, H. Ylänen, M. Hupa, and M. Kellomäki, Bioabsorbable and Bioactive Composite Material and A method for Manufacturing the Composite, Patent US 2010/0121463 A1, 2010.
17. Majola, A., S. Vainionpää, P. Rokkanen, H.M. Mikkola, and P. Törmälä, Absorbable self-reinforced polylactide (SR-PLA) composite rods for fracture fixation: strength and strength retention in the bone and subcutaneous tissue of rabbits. *Journal of Materials Science: Materials in Medicine*, 1992. 3(1): p. 43-47.

18. Pihlajamäki, H., E.A. Mäkelä, N. Ashammakhi, J. Viljanen, H. Päätiälä, P. Rokkanen, T. Pohjonen, P. Törmälä, and A. Joukainen, *Strength retention of drawn self-reinforced polyglycolide rods and fixation properties of the distal femoral osteotomies with these rods. An experimental study on rats. Journal of Materials Science: Materials in Medicine*, 2002. 13(4): p. 389-395.
19. Törmälä, P., J. Vasenius, S. Vainionpää, J. Laiho, T. Pohjonen, and P. Rokkanen, *Ultra-high-strength absorbable self-reinforced polyglycolide (SR-PGA) composite rods for internal fixation of bone fractures: In vitro and in vivo study. Journal of Biomedical Materials Research*, 1991. 25(1): p. 1-22.
20. Vasenius, J., S. Vainionpää, K. Vihtonen, M. Mero, J. Mikkola, P. Rokkanen, and P. Törmälä, *Biodegradable self-reinforced polyglycolide (SR-PGA) composite rods coated with slowly biodegradable polymers for fracture fixation: strength and strength retention in vitro and in vivo. Clinical Materials*, 1989. 4(4): p. 307-317.
21. Lim, J.Y., S.H. Kim, S. Lim, and Y.H. Kim, *Improvement of Flexural Strengths of Poly(L-lactic acid) by Solid-State Extrusion, 2. Extrusion Through Rectangular Die. Macromolecular Materials and Engineering*, 2003. 288(1): p. 50-57.
22. Weiler, W. and S. Gogolewski, *Enhancement of the mechanical properties of polylactides by solid-state extrusion : I. Poly(-lactide). Biomaterials*, 1996. 17(5): p. 529-535.
23. Törmälä, P., T. Pohjonen, and P. Rokkanen, *Ultrahigh-strength self-reinforced polylactide composites and their surgical applications. Macromolecular Symposia*, 1997. 123(1): p. 123-131.
24. Ferguson, S., D. Wahl, and S. Gogolewski, *Enhancement of the mechanical properties of polylactides by solid-state extrusion. II. Poly(L-lactide), poly(L/D-lactide), and poly(L/DL-lactide). J Biomed Mater Res*, 1996. 30(4): p. 543-51.
25. Hasegawa, S., S. Ishii, J. Tamura, T. Furukawa, M. Neo, Y. Matsusue, Y. Shikinami, M. Okuno, and T. Nakamura, *A 5-7 year in vivo study of high-strength hydroxyapatite/poly(l-lactide) composite rods for the internal fixation of bone fractures. Biomaterials*, 2006. 27(8): p. 1327-1332.
26. Furukawa, T., Y. Matsusue, T. Yasunaga, Y. Shikinami, M. Okuno, and T. Nakamura, *Biodegradation behavior of ultra-high-strength hydroxyapatite/poly (-lactide) composite rods for internal fixation of bone fractures. Biomaterials*, 2000. 21(9): p. 889-898.
27. Paul, J.P., *Strength requirements for internal and external prostheses. Journal of Biomechanics*, 1999. 32(4): p. 381-393.
28. Ashammakhi, N., A.M. Gonzalez, P. Törmälä, and I.T. Jackson, *New resorbable bone fixation. Biomaterials in craniomaxillofacial surgery: present and future. European Journal of Plastic Surgery*, 2004. 26(8): p. 383-390.
29. Li Liao, Lin Chen, Ai-Zheng Chen, Xi-Ming Pu, Yun-Qing Kang, Ya-Dong Yao, Xiao-Ming Liao, Zhong-bing Huang, and G.-F. Yin, *Preparation and characteristics of novel poly-L-lactide/ β -calcium metaphosphate fracture fixation composite rods. J. Mater. Res. , 2007. 22(12): p. 3324 - 3329.*

30. Ruffieux, K., A. Dell'Agosti, B. Riesen, and E. Wintermantel, *Influence of Calcium Phosphates on the Degradation of Poly Lactic Acid for Medical Implants. Biomedizinische Technik/Biomedical Engineering*, 1996. 41(s1): p. 420-421.
31. Niemelä, T., H. Niiranen, M. Kellomäki, and P. Törmälä, *Self-reinforced composites of bioabsorbable polymer and bioactive glass with different bioactive glass contents. Part I: Initial mechanical properties and bioactivity. Acta Biomaterialia*, 2005. 1(2): p. 235-242.
32. Saikku-Bäckström, A., R.M. Tulamo, T. Pohjonen, P. Törmälä, J.E. Rähä, and P. Rokkanen, *Material properties of absorbable self-reinforced fibrillated poly-96L/4 D-lactide (SR-PLA96) rods; a study in vitro and in vivo. Journal of Materials Science: Materials in Medicine*, 1999. 10(1): p. 1-8.
33. Haltia, A.-M., K. Lähteenkorva, P. Törmälä, A. Helminen, J. Tuominen, J. Seppälä, S. Veittola, and J. Ahvenlammi, *Self-reinforcement and hydrolytic degradation of amorphous lactic acid based poly(ester-amide), and of its composite with sol-gel derived fibers. Journal of Materials Science: Materials in Medicine*, 2002. 13(10): p. 903-909.
34. Shikinami, Y. and M. Okuno, *Bioresorbable devices made of forged composites of hydroxyapatite (HA) particles and poly-L-lactide (PLLA): Part I. Basic characteristics. Biomaterials*, 1999. 20(9): p. 859-877.
35. Brauer, D., C. Rüssel, S. Vogt, J. Weisser, and M. Schnabelrauch, *Degradable phosphate glass fiber reinforced polymer matrices: mechanical properties and cell response. Journal of Materials Science: Materials in Medicine*, 2008. 19(1): p. 121-127.
36. Parsons, A.J., I. Ahmed, P. Haque, B. Fitzpatrick, M.I.K. Niazi, G.S. Walker, and C.D. Rudd, *Phosphate Glass Fibre Composites for Bone Repair. Journal of Bionic Engineering*, 2009. 6(4): p. 318-323.
37. Lin, S., S. Krebs, A. Nazre, and R. King, *Totally Bioabsorbable composites, in 39th International SAMPE Symposium 1994. p. 1981 - 1985.*
38. Parsons, A.J., I. Ahmed, N. Han, R. Felfel, and C.D. Rudd, *Mimicking Bone Structure and Function with Structural Composite Materials. Journal of Bionic Engineering*, 2010. 7(Supplement 1): p. S1-S10.
39. Ahmed, I., A.J. Parsons, G. Palmer, J.C. Knowles, G.S. Walker, and C.D. Rudd, *Weight loss, ion release and initial mechanical properties of a binary calcium phosphate glass fibre/PCL composite. Acta Biomaterialia*, 2008. 4(5): p. 1307-1314.
40. Zhengke, W. and H. Qiaoling, *Preparation and properties of three-dimensional hydroxyapatite/chitosan nanocomposite rods. Biomedical Materials*, 2010. 5(4): p. 045007.
41. Mohammadi, S.M., I. Ahmed, B. Marelli, C. Rudd, M.N. Bureau, and S.N. Nazhat, *Modulation of polycaprolactone composite properties through incorporation of mixed phosphate glass formulations. Acta Biomaterialia*, 2010. 6(8): p. 3157-3168.

42. Parsons, A., I. Ahmed, M.I.K. Niazi, R.R. Habeb, B. Fitzpatrick, G.S. Walker, I.A. Jones, and C.D. Rudd, *Mechanical and Degradation Properties of Phosphate Based Glass Fibre/PLA Composites with different Fibre Treatment Regimes*. *Science and Engineering of Composite Materials*, 2010. 17(4): p. 243 - 260.
43. Ahmed, I., I. Jones, A. Parsons, J. Bernard, J. Farmer, C. Scotchford, G. Walker, and C. Rudd, *Composites for bone repair: phosphate glass fibre reinforced PLA with varying fibre architecture*. *Journal of Materials Science: Materials in Medicine*, 2011. 22: p. 1825 - 1834.
44. Haque, P., *Oligomeric PLA Coupling Agents for Phosphate Glass Fibres/PLA Composites*, in *Division of Materials, Mechanics & Structures, Faculty of Engineering* 2011, University of Nottingham.
45. Han, N., I. Ahmed, A.J. Parsons, L. Harper, C.A. Scotchford, B.E. Scammell, and C.D. Rudd, *Influence of screw holes and gamma sterilization on properties of phosphate glass fiber-reinforced composite bone plates*. *J Biomater Appl*, 2011.
46. Ahmed, I., C.A. Collins, M.P. Lewis, I. Olsen, and J.C. Knowles, *Processing, characterisation and biocompatibility of iron-phosphate glass fibres for tissue engineering*. *Biomaterials*, 2004. 25(16): p. 3223-3232.
47. ASTM D2584-94, *Standard Test Method for Ignition Loss of Cured Reinforced Resins* 1994.
48. BS 2782-10:Method 1008B:1996, ISO 3597-2:1993, *Methods of testing plastics. Glass reinforced plastics. Determination of flexural strength on rods made of roving-reinforced resin*
49. BS 2782-3:Methods 340A and 340B:1978, *Methods of testing plastics. Mechanical properties. Determination of shear strength of moulding material. Determination of shear strength of sheet material*
50. ASTM D7617 / D7617M - 11: *Standard Test Method for Transverse Shear Strength of Fiber-reinforced Polymer Matrix Composite Bars* 2011.
51. BS ISO 3597-3: 2003, *Textile-glass-reinforced plastics. Determination of mechanical properties on rods made of roving-reinforced resin. Determination of compressive strength*
52. Wong, K.H., S.J. Pickering, and C.D. Rudd, *Recycled carbon fibre reinforced polymer composite for electromagnetic interference shielding*. *Composites Part A: Applied Science and Manufacturing*, 2010. 41(6): p. 693-702.
53. Clarke, A.R. and C.N. Eberhardt, *Microscopy Techniques for Materials Science* 2002: Woodhead Publishing.
54. Neves, N.M., G. Isdell, A.S. Pouzada, and P.C. Powell, *On the effect of the fiber orientation on the flexural stiffness of injection molded short fiber reinforced polycarbonate plates*. *Polymer Composites*, 1998. 19(5): p. 640-651.
55. Hull, D. and T.W. Clyne, *An Introduction to Composite Materials Cambridge Solid State Science Series* 1981, Cambridge.

56. Törmälä, P., T. Pohjonen, and P. Rokkanen, *Bioabsorbable polymers: materials technology and surgical applications. Proceedings of the Institution of Mechanical Engineers - H*, 1998. 212(2): p. 101 - 111.
57. Rijdsdijk, H.A., M. Contant, and A.A.J.M. Peijs, *Continuous-glass-fibre-reinforced polypropylene composites: I. Influence of maleic-anhydride-modified polypropylene on mechanical properties. Composites Science and Technology*, 1993. 48(1-4): p. 161-172.
58. Fu, S.-Y. and B. Lauke, *Effects of fiber length and fiber orientation distributions on the tensile strength of short-fiber-reinforced polymers. Composites Science and Technology*, 1996. 56(10): p. 1179-1190.
59. Takagi, H. and Y. Ichihara, *Effect of Fiber Length on Mechanical Properties of "Green" Composites Using a Starch-Based Resin and Short Bamboo Fibers. JSME International Journal Series A Solid Mechanics and Material Engineering*, 2004. 47(4): p. 551-555.
60. Garoushi, S.K., L.V. Lassila, and P.K. Vallittu, *Short fiber reinforced composite: the effect of fiber length and volume fraction. J Contemp Dent Pract*, 2006. 7(5): p. 10-7.
61. Dweib, M.A., C.F. Vahlund, and C.M. Ó Brádaigh, *Fibre structure and anisotropy of glass reinforced thermoplastics. Composites Part A: Applied Science and Manufacturing*, 2000. 31(3): p. 235-244.
62. Nilsson, G., M.L. Ericson, and J. Anders Holmberg, *Flow induced fiber orientation in compression molded glass mat thermoplastics. Polymer Composites*, 2000. 21(6): p. 1007-1013.
63. Yang, J., *Preparation and characterisation of a bioresorbable phosphate glass fibre reinforced poly(ϵ -caprolactone) composite*, 2007, University of Nottingham: Nottingham. p. 187.
64. Tolf, G.r. and P. Clarin, *Comparison between flexural and tensile modulus of fibre composites. Fibre Science and Technology*, 1984. 21(4): p. 319-326.
65. Bunsell, A.R., *Developments in the Science and Technology of Composite Materials: Sixth European Conference on Composite Materials 1993*: Woodhead.

CHAPTER 5.

DEGRADATION, MECHANICAL PROPERTY RETENTION, ION RELEASE AND CYTOCOMPATIBILITY ASSESSMENT OF PLA/PGF COMPOSITE RODS

5.1 SUMMARY

This study investigated totally bioresorbable composite rods manufactured using a thermomechanical deformation method at $\sim 90^{\circ}\text{C}$. Phosphate glass fibres (P50 and P40 formulations) were used to reinforce PLA. The initial mechanical properties for unidirectionally reinforced (P50 UD and P40 UD) composite rods were significantly higher than for PLA alone as reported previously in CHAPTER 4. The mechanical properties of the composite rods decreased initially after immersion in PBS for 3 days. Afterwards, P40 UD rods maintained their mechanical properties for the duration of the study up to 63 days. The decrease in mechanical properties observed was attributed to a combination of the plasticisation effect of water and degradation of the fibre/matrix interface, with subsequent constancy being attributed to the chemical durability of the P40 fibres. Further reduction in mechanical properties was seen for P50 composite rods due to rapid degradation of P50 fibres. Moreover, this was the main reason attributed for the increased mass loss and water uptake for the composite rods ($\sim 16\%$), whilst the P40 UD rods only lost $\sim 1\%$ of their initial mass by the end of the study period.

The ion release and degradation profiles for the composites investigated showed similar trends. The amount of sodium and orthophosphate ions released were greater in comparison to the other cations and anions detected (namely calcium, magnesium, pyrophosphate, tripolyphosphate and cyclic trimetaphosphate). The trends observed were attributed to low Dietzal's field strength for the Na^{+} in comparison with Mg^{2+} and Ca^{2+} and breakdown of longer chain polyphosphates into orthophosphate units. P40 composites exhibited good cytocompatibility to human

mesenchymal stem cells (MSCs), which was suggested to be due to the low degradation rate of P40 fibres.

5.2 INTRODUCTION

A lot of interest has recently been directed towards the use of bioresorbable composites for manufacturing internal bone fracture fixation devices such as plates, screws, pins and rods [1]. Several studies have investigated self-reinforced polylactic acid (SR-PLA) and self-reinforced polyglycolic acid (SR-PGA) rods as internal fixation devices [2, 3]. The reported initial mechanical properties for SR-PGA rods were ~ 225 MPa for shear strength and ~ 12 GPa and ~ 365 MPa for flexural modulus and strength respectively. After 6 weeks degradation in phosphate buffer saline (PBS) solution at 37°C, the shear strength decreased to ~ 40 MPa and the flexural modulus and strength decreased to 1GPa and ~ 10 MPa respectively [2]. SR-PLLA rods were also prepared using the same process, however; the SR-PLLA rods had lower initial mechanical properties (~ 270 MPa for bending strength and ~ 100 MPa for shear strength) in comparison to SR-PGA rods however retained their mechanical properties for longer periods (~10 MPa for bending strength and ~ 5 MPa for shear strength after 38 and 48 weeks *in vivo* respectively [4]. Törmälä *et al.* [5] also investigated the mechanical properties of self-reinforced composites and ceramic fibre (longer than 150µm such as hydroxyapatite), calcium phosphate and bioactive glass reinforced composites.

Hydroxyapatite (HA) and calcium phosphate particulate reinforced poly lactic acid (PLLA) composite rods have also been investigated [6-11]. Shikinami *et al.* [6] found that PLLA and PLLA/HA (20 wt%) rods maintained their initial bending strengths (~ 250 MPa) for approximately three months during degradation studies in PBS at 37°C. Whilst, rods with higher weight fraction of HA (30 – 50 wt%) decreased gradually from ~ 270 to ~ 140 MPa with time up to 52 weeks [6]. Biocompatibility for PLLA/HA rods was examined via *in vivo* experiments using a rabbit femur model for 52 weeks [8]. The rods were implanted into the medullary canals of the

femurs through their knees. No inflammatory reactions were reported from this study.

Attempts have also been made to combine the advantages of both the previous two methods, i.e. using self-reinforcement in addition to also incorporating osteoconductive particles such as bioactive glass 13-93 (BaG) in order to accelerate bone healing [12-14]. Niemela *et al.* [13] investigated the initial mechanical properties for SR-PLA rods reinforced with 0 % to 50 wt% of BaG particles. They found the initial flexural, shear and compressive strength decreased gradually with increasing BaG content. They ascribed this reduction in mechanical properties to the formation of pores, discontinuity of the structure and the absence of chemical bonds between the BaG particles and PLA. However, improvement in bioactivity was reported for these BaG particle reinforced specimens as precipitation of calcium phosphate was observed on the composite surface after 4 days of immersion in PBS at 37°C.

Fibre reinforcement is another common method employed to enhance strength and stiffness of polymers, although this approach is uncommon with degradable systems due to limitations in appropriate reinforcement materials. Phosphate glass fibres (PGF) have been investigated for this purpose. Biocompatibility for fibre reinforced composites (PCL/PGF and PCL/45S5 Bioglass) was examined by Scotchford *et al.* [15] via implantation into the skulls of rats. No inflammation was seen for either composite for the duration of the study at 26 weeks. Moreover, new bone formed below the composite implant, which was confirmed using micro-computed tomography (μ -CT) [16, 17]. This new bone growth was not observed with the control samples (PCL alone). Moreover, PCL/PGF showed increase in the bone formation in comparison to Bioglass composite. Thus, it was surmised that PGF composites were capable of promoting new bone formation.

Ion release profiles for phosphate based glasses (PBGs) were previously investigated for bulk glass, fibres and composites [18-33]. Since the degradation rate

for PGFs is greater than bulk glass of the same composition, ion release rates for fibres were expected to be higher than for the bulk glasses. Abou Neel *et al.* [27] also investigated the effect of fibre diameter and chemical durability of the glass with ion release rates. They found that the amount of ions released decreased via addition of Fe_2O_3 at the expense of Na_2O within PBG glass formulations. This effect was attributed to formation of Fe-O-P bonds which have high resistance to hydration in comparison to P-O-P. The amounts of ions released increased with reduced fibre diameters which were suggested to be due to the increase in surface area per volume ratio [24, 27].

Ion release rates for the composites were mainly controlled via glass composition, quantity and geometry and not due to the matrix [25]. Mohammadi *et al.* [28, 32, 33] investigated ion release for PLA and PCL reinforced with PBG (P_2O_5 – CaO – SiO_2 – Fe_2O_3) fibres and particles. No significant difference in rates of ion release was observed between PLA/PGF and PCL/PGF composites with the same fibre volume fraction (18%) as expected. In contrast, particulate composites of the same glass composition showed higher amounts of ion release in comparison to fibre reinforced composites. This was attributed to increase in volume fraction of PBG particles (40%) and surface area in comparison with the fibre-reinforced composites.

Degradation and mechanical property retention (flexural, shear and compression) for PLA, P50 RM, P50 UD and P40 UD composite rods are investigated over a 63 day period in the current chapter. Glass of a similar composition to P40 fibres was investigated previously and showed a lower degradation rate and good cytocompatibility in comparison to P50 formulation [34, 35]. Ion release rates and cytocompatibility for the composite rods manufactured were also investigated and correlated with degradation profiles. Since these composite rods have potential applications as IM nails, human mesenchymal stem cells (MSCs) were used for cytocompatibility testing (in collaboration with Dr Virginie Sotille, Centre for Biomolecular Sciences, University of Nottingham).

5.3 MATERIALS AND METHODS

5.3.1 Composite Rod Production

PLA, P50 RM, P50 UD, P40 UD and P40 UD/RM (70/30) rods were manufactured as previously mentioned in sections 4.3.1 and 4.3.2. The PLA films were stacked alternately with UDs and RMs for UD/RM mix composites. See Table 5-1 for details of the rods produced in this study with their respective sample codes.

Table 5-1: Sample codes for the specimens investigated in this chapter, with associated fibre volume and mass fractions.

<i>Sample code</i>	<i>Specimen</i>	<i>Fibre mass fraction (%)</i>	<i>Fibre volume fraction V_f (%)</i>
PLA	Pure PLA rods	-	-
P40 RM	P40 random mat fibres composite rods	48 ± 4	29 ± 4
P40 UD	P40 unidirectional composite rods	56 ± 2	37 ± 2
P50 RM	P50 random mat composite rods	51 ± 5	32 ± 5
P50 UD	P50 unidirectional composite rods	50 ± 2	31 ± 2
P40 UD/RM (70/30)	P40 70 % unidirectional/ 30 % random mat (by weight) composite rods	50 ± 3	31 ± 3

5.3.2 Degradation study

The degradation study of the rods produced was performed according to the procedure mentioned previously in section 3.3.8. Dimensions of the rod specimens were 40 mm length and 4 mm diameter. 50 ml vials were used to accommodate the

rods. The percentage wet mass change (M_w), mass loss (M_L) and water uptake (W) were determined using *Equation 3-2*, *Equation 3-3* and *Equation 3-4*

5.3.3 Gel Permeation Chromatography (GPC)

The weight average molecular weight (M_w) of PLA in the specimens (PLA, P50 RM, P50 UD and P40 UD composite rods) was determined using Gel Permeation Chromatography (GPC) as mentioned previously in section 3.3.10.

5.3.4 Mechanical tests

Flexural, double shear and compression tests for PLA, P50 RM, P50 UD and P40 UD rods were performed as previously mentioned in sections 4.3.3.1, 4.3.3.2 and 4.3.3.3. The measurements were applied on wet samples. At various time points the specimens were extracted from the degradation medium (PBS) at 37°C and blot dried before testing.

5.3.5 Cumulative Ion Release Study

PLA and, P50 RM, P50 UD and P40 UD rods (6 mm diameter) were prepared and cut into discs of 2 mm height. These samples were degraded in 25 ml of deionised water for 1, 2, 3, 8, 10, 14, 17, 20, 24, 28 days, which was then analysed using ion chromatography for cation and anion release (in collaboration with Professor Jonathan Knowles group, UCL, Eastman Dental Institute).

5.3.5.1 Cation Release

An ICS-1000 ion chromatography system (Dionex, UK) was used for measurements of cation release. Na^+ , Ca^{2+} and Mg^{2+} cations can be detected simultaneously by using this technique. A 20 mM Methanesulfonic acid (BDH, UK) solution was used as the eluent. In this method, cations were eluted using 4 x 250 mm IonPac(r) CS12A separator columns, a 25-ml sample loop, and a Cation Self-Regenerating Suppressor (CSRS). All results were calculated against a seven-point calibration curve using the predefined calibration routine. Calibration solutions were prepared from a six-cation standard stock solution (Dionex, UK). The following standard dilutions were

prepared: 200, 100, 50, 25, 12.5, 6.25, and 3.125 ppm. Data analysis was performed using the Chromeleon software package (version 6.0).

5.3.5.2 Anion Release

The phosphate anion measurements were obtained using a Dionex ICS-2500 ion chromatography system (Dionex, UK), consisting of a gradient pump with a 25-ml sample loop. In this method, polyphosphates were eluted using 4 x 250 mm IonPac(r) AS16 anion exchange columns packed with anion exchange resin. A Dionex ASRS(r) (Anion Self-Regenerating Suppressor) was used at 223 mA. The Dionex EG40 eluent generator equipped with a KOH (potassium hydroxide) cartridge was used in conjunction with the ASRS(r). The sample run time was set for 20 min. The gradient program started from 30 mM KOH, and after 2 min increased from 30 to 60 mM KOH over 11 ½ min, and remained there for 2 min. After this, it decreased down to 30 mM for 2 min. The Chromeleon software package was used for data analysis. Only four reagents were commercially available for the preparation of standards - sodium phosphate tribasic (Na_3PO_4), trisodium trimetaphosphate ($\text{Na}_3\text{P}_3\text{O}_9$), pentasodium tripolyphosphate ($\text{Na}_5\text{P}_3\text{O}_{10}$), (Sigma, UK) and tetrasodium pyrophosphate ($\text{Na}_4\text{P}_2\text{O}_7$) (BDH, UK). A 100 ppm working solution containing all of the above four reagents was prepared, from which serially diluted 50, 20, 10, and 5 ppm standard solutions were obtained. Higher phosphate group containing reagents (i.e. P₄ or above) were not commercially available.

5.3.6 Biological assessment

This study was performed in collaboration with Dr Virginie Sotille, Centre for Biomolecular Sciences, University of Nottingham. In order to evaluate the cytocompatibility of the composite samples and their effect on cell differentiation, GFP-labelled human marrow-derived mesenchymal stem cells (hMSCs) were seeded onto composite discs and cultured for up to 3 weeks. PLA, P40 RM, P40 UD and P40 UD/RM (70/30) composite discs of 2 mm thickness and 6 mm diameter

were used for biological assessment. The cells were seeded onto polished cross sections of the composite discs to with roughness coefficients of approximately 2 μm .

5.3.6.1 Cell culture

Human mesenchymal stem cells (MSCs) labelled with green fluorescent protein (GFP) were grown as previously described [36, 37]. Briefly, cells were maintained in a medium containing Dulbecco's Modified Eagle Medium (DMEM) supplemented with 10% fetal calf serum (FCS), 1 mM L-glutamine, 1% nonessential amino acids and antibiotics (Invitrogen, Paisley, UK). Before cell seeding, the composite samples were transferred to a 48-well plate, sterilised in 70% ethanol and subsequently allowed to air-dry overnight in a sterile environment. Cells were harvested with Trypsin/EDTA, pelleted and seeded in the medium at 30×10^4 cells/well. Cell seeding was monitored after 48 hours using a fluorescent stereomicroscope (Leica) and the medium was changed every 3 days. After 5 days, medium was changed and cells were treated for a further 15 days in order to evaluate the ability of cells to undergo osteogenic differentiation.

5.3.6.2 Quantification of cell metabolism and differentiation

For cell metabolic activity measurements, samples were analysed using an Alamar blue assay (AbD Serotec, UK) according to the manufacturer's instructions. Fluorescence was measured in triplicate using a Bio-TEK FLx800 micro-plate reader at 530/25 nm excitation, 590/35 nm emission. For differentiation analysis, samples were washed with PBS and fixed in 4% (v/v) paraformaldehyde at room temperature for 15 min. Mineralisation was measured as previously described [38]. Briefly, fixed wells were incubated with 1% Alizarin-Red S solution for 15 min, and mineral deposition was quantified by extraction of the incorporated stain [39] before absorbance measurement using a plate reader (BioTek ELx800, Fisher Scientific, Loughborough, UK) in triplicate. Measurements of alkaline phosphatase activity were performed in triplicate using SIGMAFAST pNPP reagents (Sigma)

according to the manufacturer's instructions. At least 5 replicates of each sample were measured and the average reported.

Statistical analysis was conducted using one-way ANOVA as mentioned previously in section 3.3.13.

5.3.7 Scanning Electron Microscopy (SEM)

Specimens were sputter-coated with carbon and examined using a JEOL 6400 SEM with an accelerating voltage of 10kV in secondary electron mode (SE). SEM analysis was applied to the cross-section of the fractured rods.

5.4 RESULTS

5.4.1 Degradation study

Figure 5-1 shows the percentage wet mass change for PLA, P50 RM, P50 UD and P40 UD composite rods against time in PBS at 37°C. The wet mass increased initially by ~ 0.8% for PLA, P50 RM and P50 UD after 1 day. The PLA rods maintained a constant weight for the duration of the study (approximately 2 months), whilst the P50 composite rods remained at ~ 0.8 % for 14 days after which a gradual decrease to -6 % is observed for the P50 RM rods. The mass change for the P50 UD rods increased to ~ 3.5 % at 21 days before decreasing to -4 % over the course of the study. Percentage of wet mass for P40 UD rods increased initially to ~ 0.4 % at 14 days and then decreased gradually to reach ~ - 0.4 % at the end of the study.

pH change for PBS against time during the degradation studies is shown in Figure 5-2. The pH value for PLA and P40 UD rods remained neutral as expected during the degradation period (63 days). For P50 composite rods, pH remained constant (~ 7.4) for 7 days and then decreased to ~ 5 after 14 and 28 days for P50 RM and P50 UD rods respectively. A gradual increase was seen after these time intervals for both P50 RM and P50 UD rods to approximately pH 7 towards the end of the study.

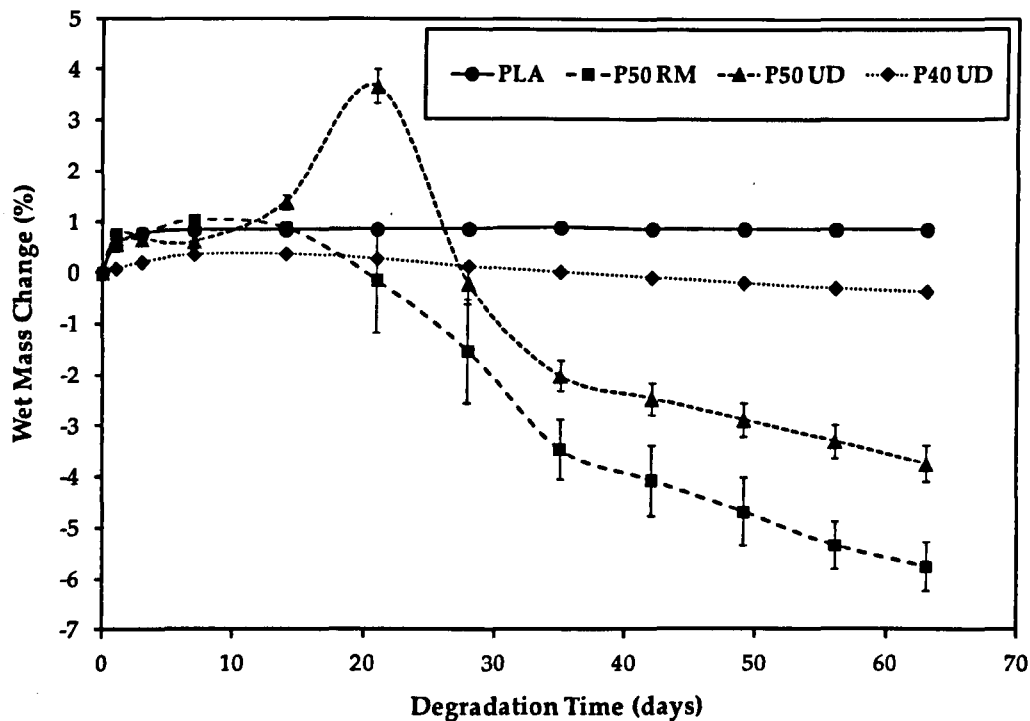


Figure 5-1: The percentage change in wet mass of PLA, P50 RM, P50 UD and P40 UD composite rods immersed in PBS at 37°C.

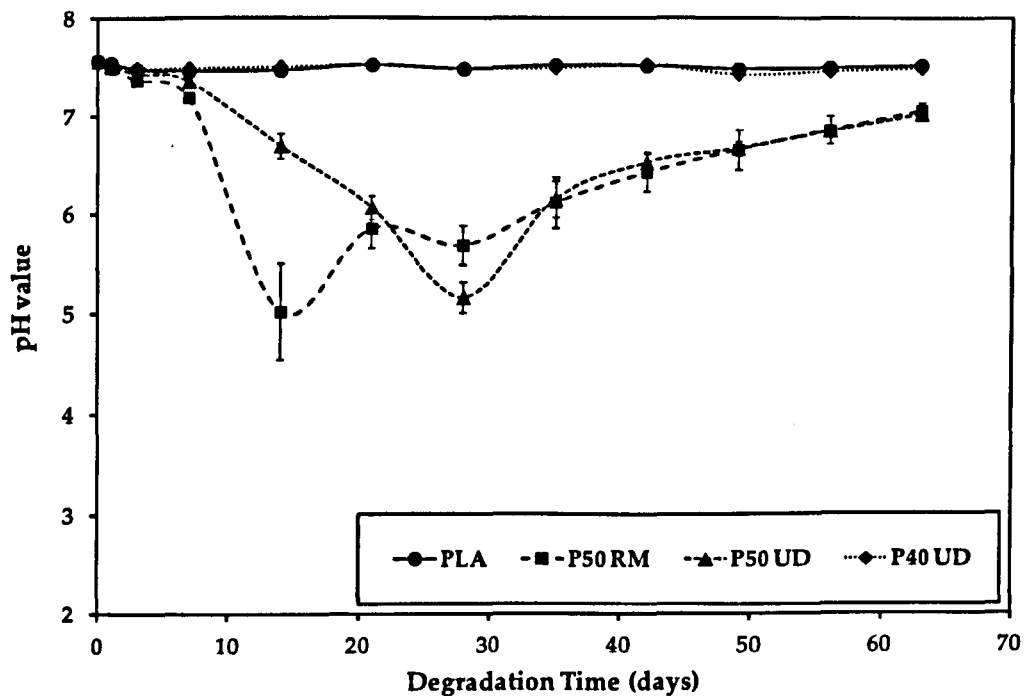


Figure 5-2: pH change for PBS during immersion in PBS at 37°C for PLA alone, P50 RM, P50 UD and P40 UD composite rods.

Figure 5-3 and **Figure 5-4** illustrate the percentage change in mass loss and the media (PBS) uptake for pure PLA, P50 RM, P50 UD and P40 UD rods. The PLA rods did not reveal any mass loss during this study (at 63 days), whilst for the P50 RM and P50 UD rods respectively, the percentage mass loss was around 0.2% up until the 7 and 14 day interval and increased to ~ 15 % towards the end of the study. A gradual increase was seen in mass loss for P40 UD rods over time to reach ~ 1.1 % after 63 days in PBS at 37°C. No statistically significant change in mass loss ($P > 0.05$) was seen between the 3 and 14 day interval for the P40 UD rods and after 42 days for P50 UD and RM rods. Media uptake for the PLA and P40 UD rods increased initially to ~ 0.8 % after 3 days and then remained stable for the duration of the study (see **Figure 5-4**). The P50 RM and P50 UD rods showed a huge increase in media uptake to ~ 15 % and ~ 17 % respectively after 63 days of immersion in PBS at 37°C.

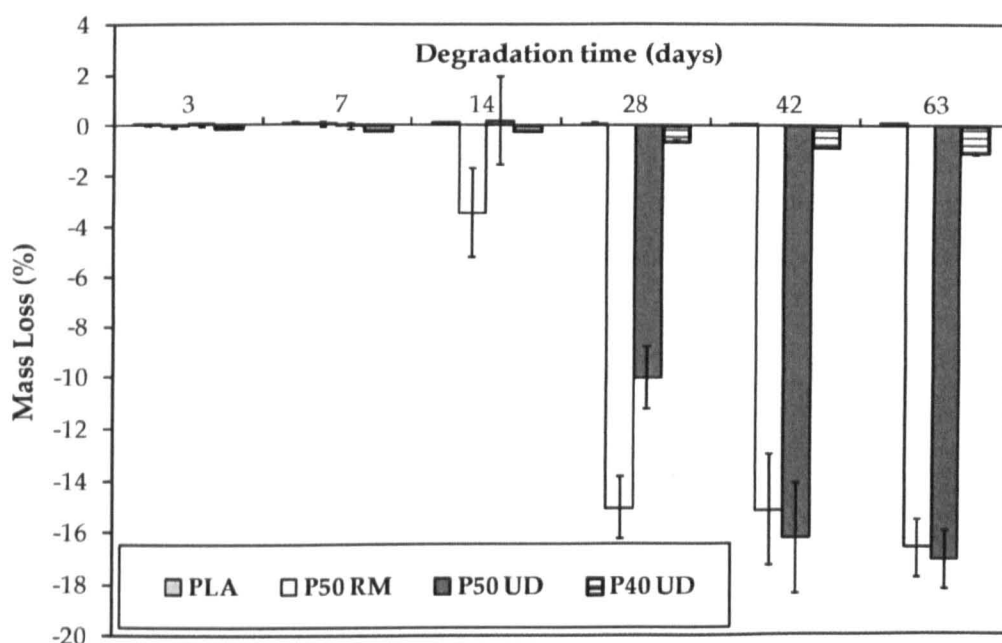


Figure 5-3: The percentage change in mass loss with time for PLA alone, P50 RM, P50 UD and P40 UD composite rods during degradation in PBS at 37°C.

From **Figure 5-5**, the change in molecular weight retention can be seen for PLA, P50 RM, P50 UD and P40 UD composite rods against degradation time. No statistically significant difference ($P > 0.05$) in retention of molecular weight change was observed among the rods investigated during the degradation period. The

molecular weight for all rod samples decreased gradually with time to 82 % after 63 days of immersion in PBS at 37°C.

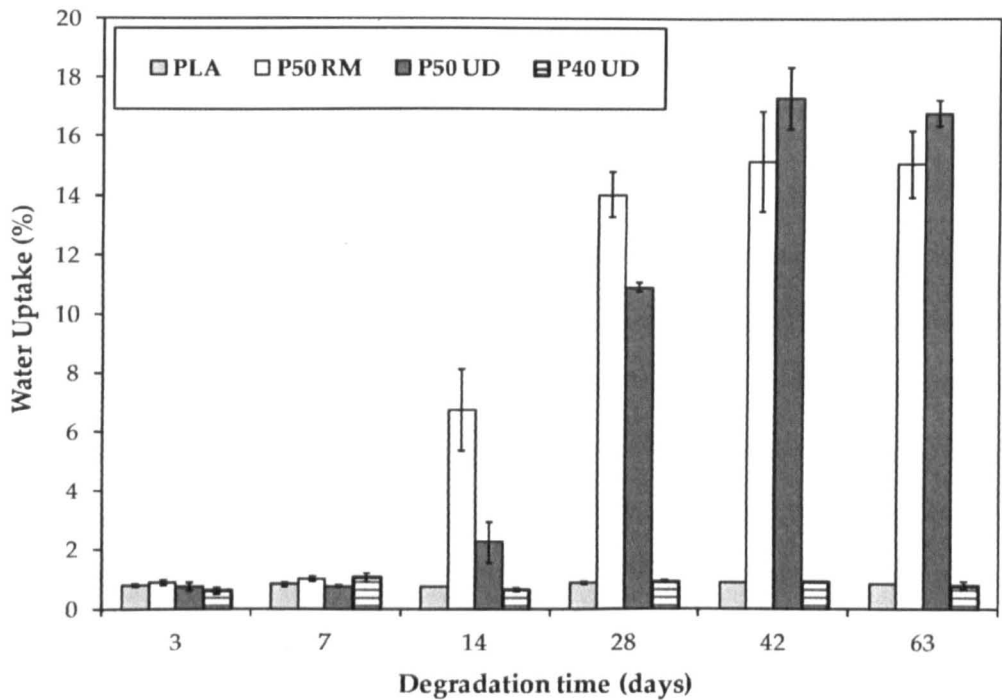


Figure 5-4: The percentage change in water uptake with time for PLA alone, P50 RM, P50 UD and P40 UD composite rods during degradation in PBS at 37°C.

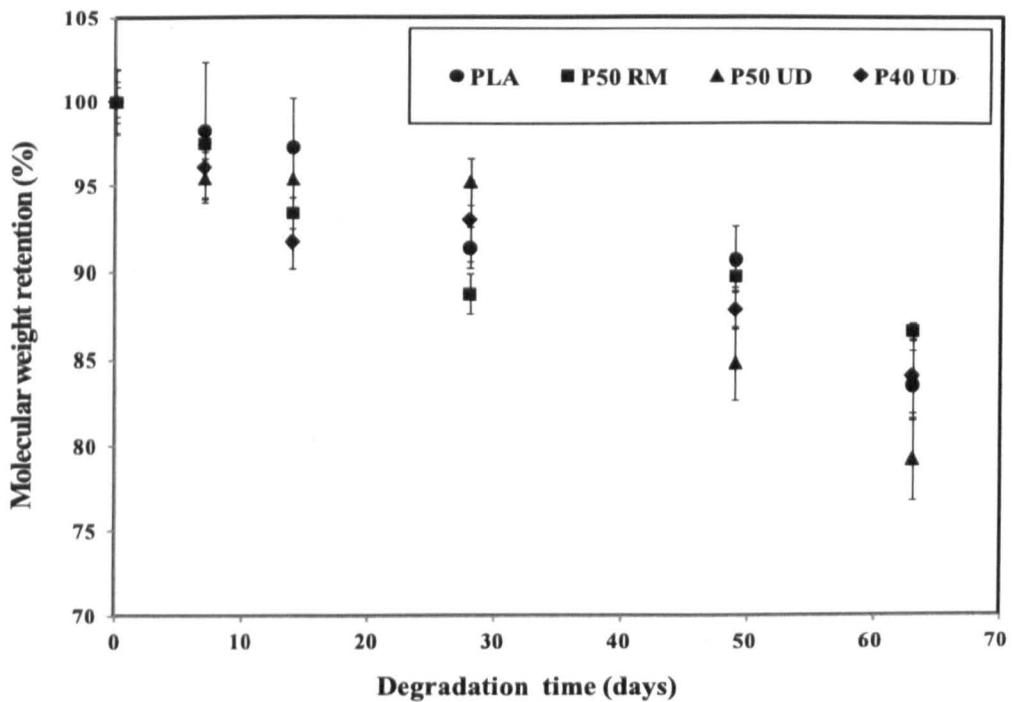


Figure 5-5: Molecular weight retention for PLA, P50 RM, P50 UD and P40 UD composite rods over time during degradation in PBS at 37°C, ascertained using GPC.

5.4.2 Mechanical properties

From Figure 5-6 and Figure 5-7, it can be seen that the flexural strength and modulus decreased with time during degradation. Unidirectional (P50 UD and P40 UD) fibre reinforced composite rods had approximately 50 % and 100 % higher initial flexural strength as compared to PLA and P50 RM composite rods (see section 4.4.1 for the initial flexural properties for rods). No significant change was observed in the flexural strength for the PLA rods until the 42 day interval after which a decrease to ~ 85 MPa (at 63 days) was seen, whereas the modulus remained constant over the entire degradation period. The wet flexural strength and modulus for P50 UD and P40 UD rods was around 30 % less than the initial dry values after 3 days of degradation, whilst the P50 RM rods lost around 50 % of their initial properties. The P50 composite rods maintained their strength and modulus for 4 days before their strength profiles decreased gradually to ~ 35 MPa. The flexural modulus for the P50 UD rods decreased to ~ 6 GPa and the P50 RM samples remained in the region of 3 GPa for the duration of the study. No statistical significant difference ($P > 0.05$) in flexural strength for P50 RM and P50 UD rods was seen after 42 days of immersion in PBS. The strength and modulus for P40 UD rods remained at ~ 95 MPa and ~ 14 GPa until the 42 day interval followed by a decrease to 80 MPa and 10.5 GPa respectively at the final time point of the study (63 days). However, the differences in strength and modulus values between 7 and 63 days were not statistically significant ($P > 0.05$).

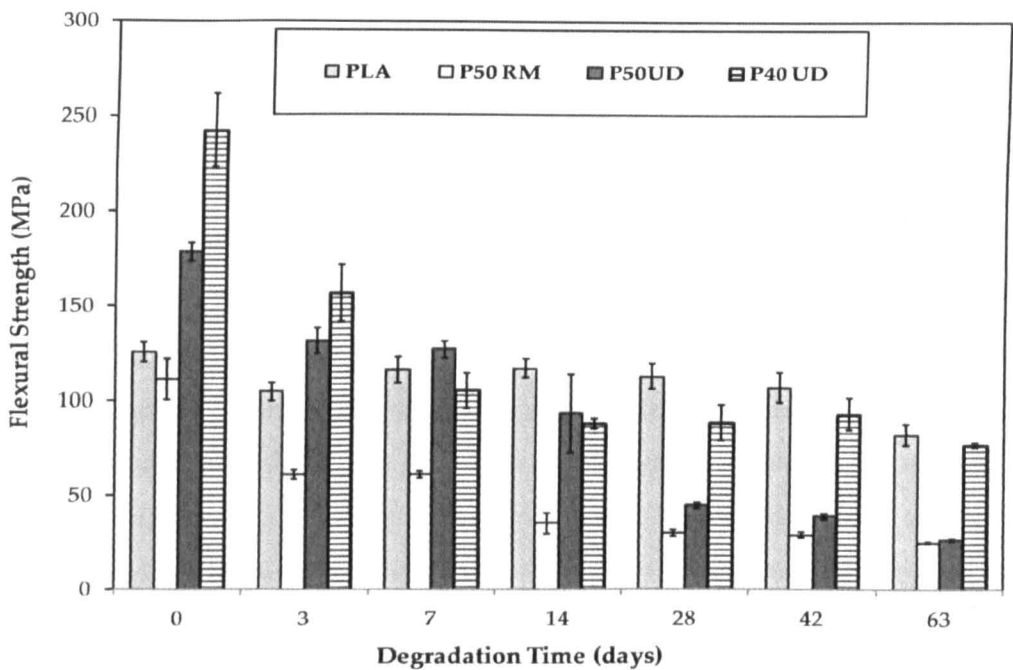


Figure 5-6: Flexural strength versus time for PLA, P50 RM, P50 UD and P40 UD rods. Samples measured wet after immersion in PBS at 37°C. Sample dimensions were 80 mm length and 4 mm diameter.

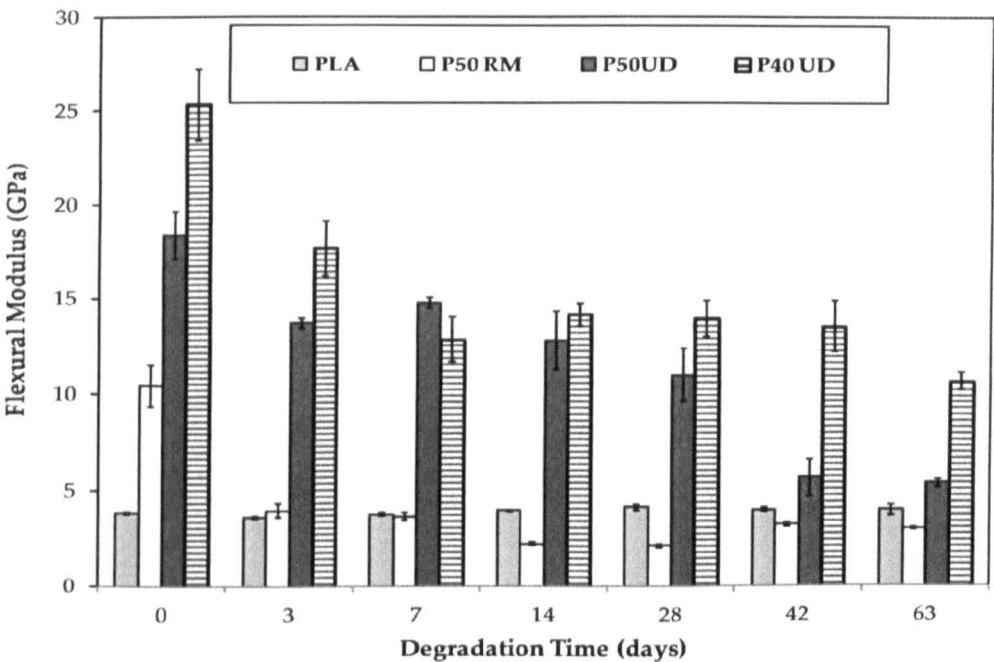


Figure 5-7: Flexural modulus over time for PLA, P50 RM, P50 UD and P40 UD rods. Samples measured wet after immersion in PBS at 37°C.

The change in shear strength and stiffness against time during degradation in PBS at 37°C for the samples investigated is shown in **Figure 5-8** and **Figure 5-9**. Initial shear strength for P50 RM, P50 UD and P40 UD rods was ~ 20, ~ 60 and ~ 90 %

greater than for PLA alone, respectively. The P50 and P40 composite rods showed ~ 80 and ~ 40 % increase in initial shear stiffness in comparison to PLA. After 3 days of immersion in PBS at 37°C, the shear strength and stiffness for the UD composite rods decreased by ~ 30 % in comparison to their initial values, whilst P50 RM remained stable at ~ 4.5 KN.mm⁻¹. P50 RM and P50 UD rods maintained shear strength at 30 and 55 MPa for 7 days. Further decrease in strength (~ 22 and 18 MPa) was seen at the end of the study. The shear stiffness for P50 composite rods decreased rapidly during the first two weeks after which a gradual decrease to ~ 0.7 KN.mm⁻¹ was observed for both the UD and RM samples towards the end of the study (see **Figure 5-9**). The shear strength for P40 UD rods decreased slightly to reach ~ 50 MPa at day 14 and remained constant ($P > 0.05$) until the final 63 day interval, whilst the stiffness fluctuated between 2.2 and 3.2 kN.mm⁻¹ and this change was noted to not be statistically significant ($P > 0.05$). No significant change in shear strength was observed for the PLA rods and the shear stiffness remained at approximately 3.2 kN.mm⁻¹ until the 42 day interval after which a decrease to ~ 2.2 kN.mm⁻¹ was seen at 63 days. Again, no statistically significant difference ($P > 0.05$) in shear strength was noticed for the P50 RM and P50 UD rods after 28 days of degradation in PBS at 37°C.

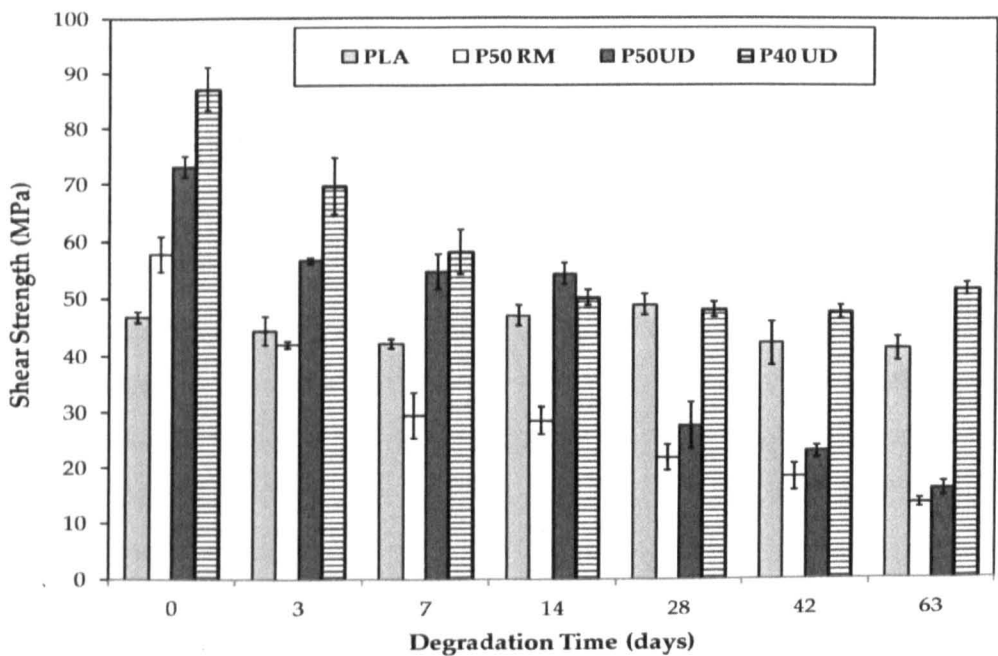


Figure 5-8: Shear strength change against time for PLA, P50 RM, P50 UD and P40 UD rods. Samples were measured wet after immersion in PBS at 37°C. Sample dimensions were 30 mm length and 4 mm diameter.

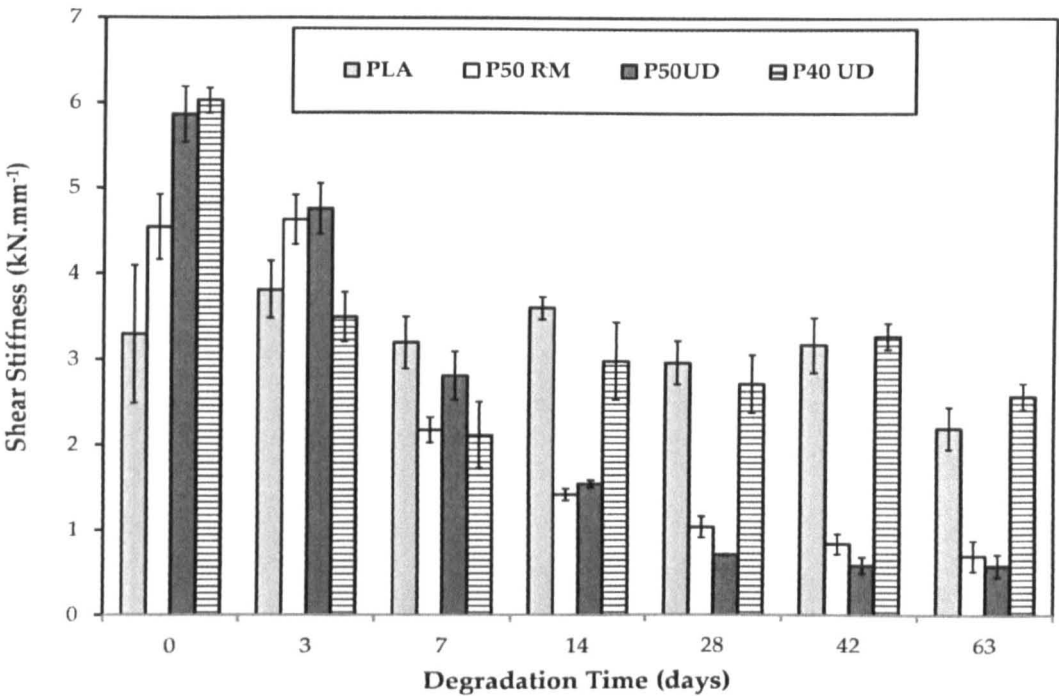


Figure 5-9: The shear stiffness against degradation time for PLA, P50 RM, P50 UD and P40 UD rods. Samples measured wet after immersion in PBS at 37°C.

Figure 5-10 and **Figure 5-11** show the change in compressive strength and stiffness for PLA and composite rods over time at 37°C in PBS. The initial compressive strength for P50 RM, P50 UD and P40 UD rods was ~ 130, 400 and 370 MPa before degradation. A sudden decrease in compressive strength for UD rods to ~ 130 and ~ 200 MPa after 3 days immersion in PBS was observed for P50 UD and P40 UD which remained constant until the 14 day interval after which a further decrease to ~ 50 MPa and ~ 110 MPa was seen. The compressive strength for the P50 RM rods decreased to ~ 100 MPa and maintained this level until the 14 day interval after which a gradual decrease to ~ 50 MPa was seen. Compressive strength and stiffness for PLA remained constant at ~ 120 MPa for strength and ~ 5 kN.mm⁻¹ stiffness for the duration of the study (see **Figure 5-11**). However, the compressive stiffness for P50 RM, P50 UD and P40 UD rods decreased from ~ 8, 21 and 22 kN.mm⁻¹ to ~ 5, 11 and 15 kN.mm⁻¹ after 3 days of degradation. P50 composite rods remained at this level for a further 4 days before they gradually decreased again to ~ 4 kN.mm⁻¹ after 63 days. As seen in **Figure 5-11**, no statistically significant difference ($P > 0.05$) in compressive strength and stiffness was observed between P50 RM and P50 UD composite rods after 3 days. From day 14 onwards, the compressive properties for

P40 UD rods stabilised ($P > 0.05$) between ~ 100 MPa and ~ 120 MPa (for strength) and between ~ 8 kN.mm⁻¹ and ~ 11 kN.mm⁻¹ (for stiffness).

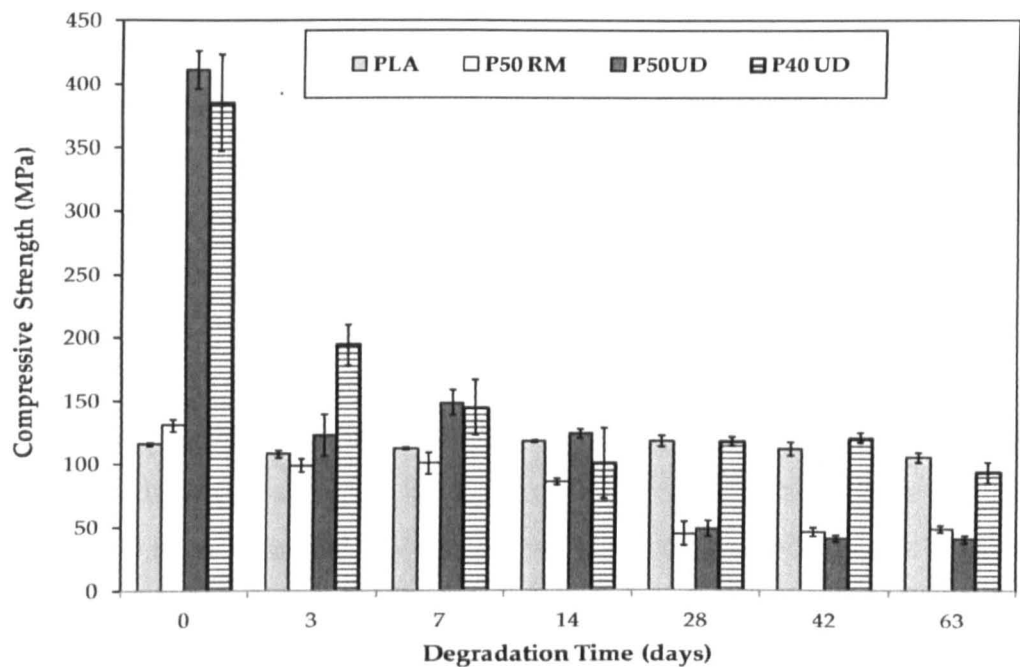


Figure 5-10: Compressive strength change against time for PLA, P50 RM, P50 UD and P40 UD rods. Samples measured wet after immersion in PBS at 37°C. Sample dimensions were 10 mm height and 4 mm diameter.

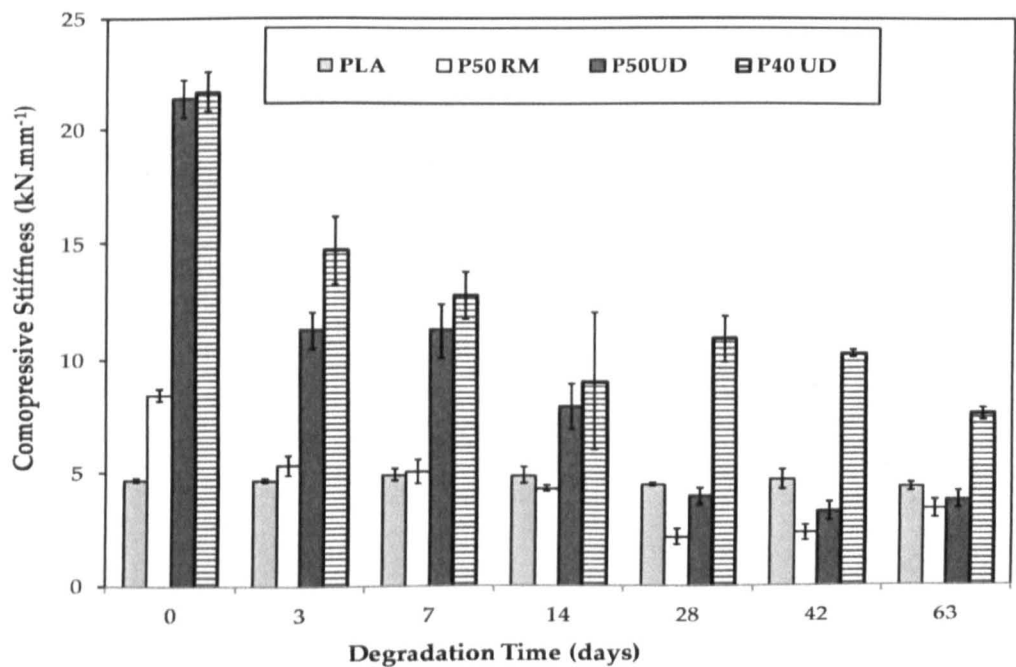
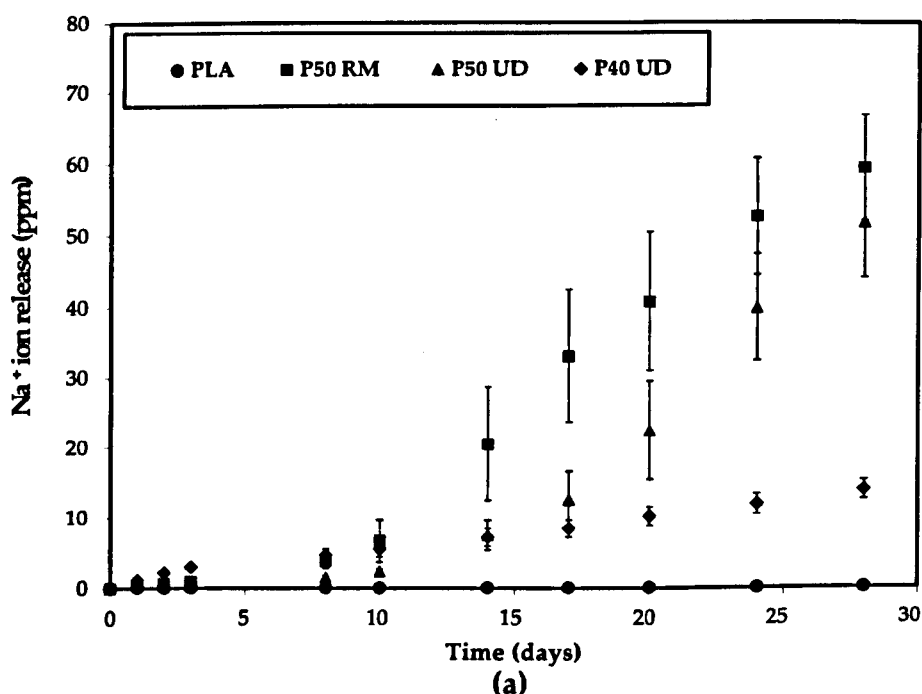


Figure 5-11: Compressive stiffness change against time for PLA, P50 RM, P50 UD and P40 UD rods. Samples measured wet after immersion in PBS at 37°C.

5.4.3 Ion release

Figure 5-12 and Figure 5-13 shows cations and anions release profiles from P50 RM, P50 UD and P40 UD composites. PLA alone was used as control and showed zero ion release as expected. The total amount of anions released were greater than the cations released. The release of both cations and anions from P40 UD composites followed an approximately linear relationship with time for the duration of the study (28 days). Sodium (Na^+), calcium (Ca^{2+}) and magnesium (Mg^{2+}) cations reached ~ 14 , ~ 11 and ~ 6 ppm (respectively), whilst the orthophosphate (PO_4^{3-}), pyrophosphate ($\text{P}_2\text{O}_7^{4-}$), tripolyphosphate ($\text{P}_3\text{O}_{10}^{5-}$) and cyclic trimetaphosphate ($\text{P}_3\text{O}_9^{3-}$) anion levels were ~ 50 , ~ 35 , ~ 15 and ~ 2 ppm respectively, after 28 days of immersion in deionised water. Ion release profiles for P50 composites could be divided into two stages; first 10 days and the rest of the study (from day 10 to day 28). During the first stage, the amount of cations and anions released increased slowly to reach approximately 10 % of the final values recorded. After the 10 day interval, the rate of ion release increased linearly with time (up till day 28). For P50 composites, higher amounts of Ca^{2+} and PO_4^{3-} ions were released in comparison to the other cations and anions investigated. Linear profiles for the $\text{P}_2\text{O}_7^{4-}$ and $\text{P}_3\text{O}_{10}^{5-}$ ions were observed which were almost identical over the duration of the study.



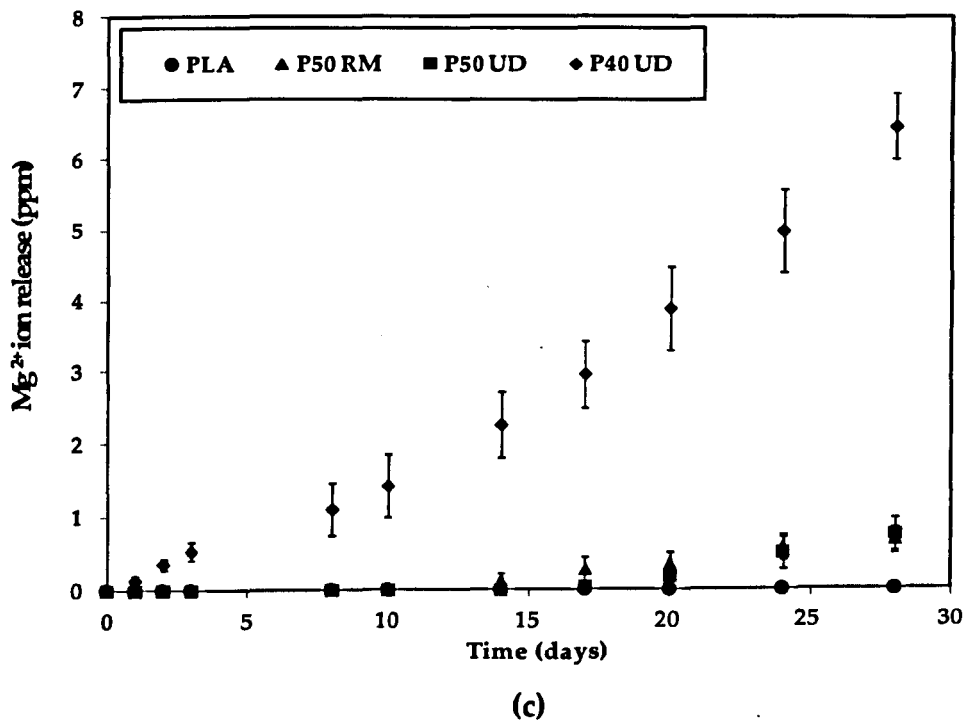
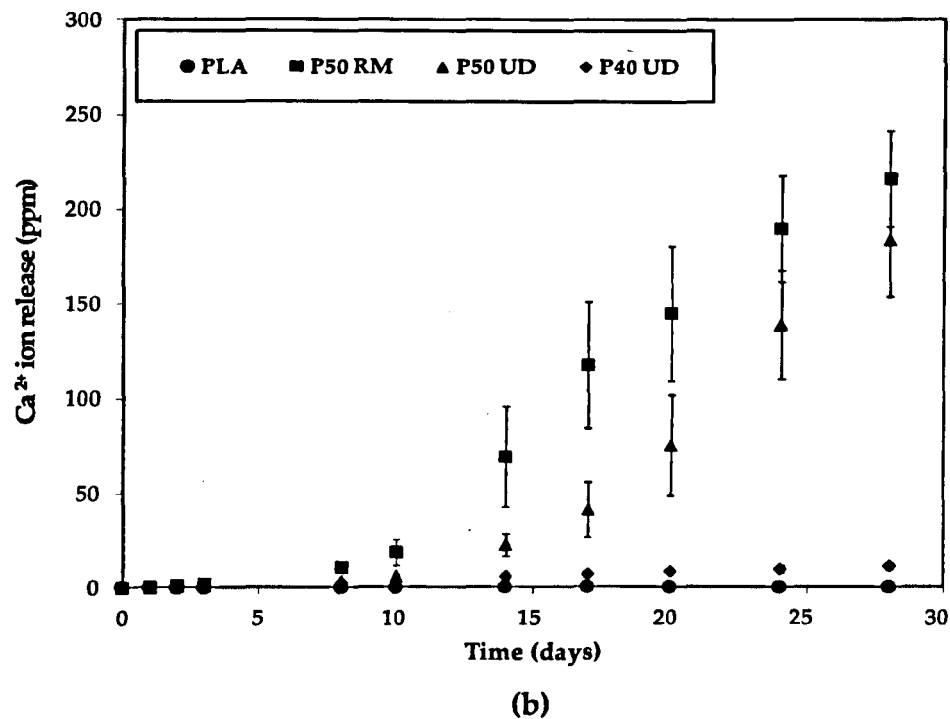
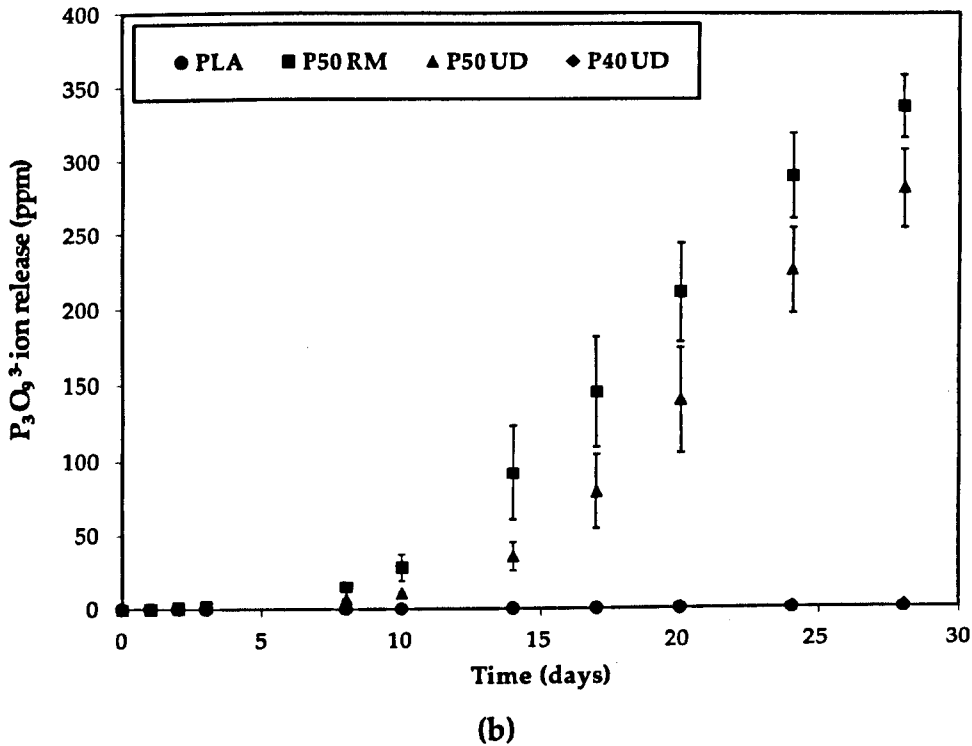
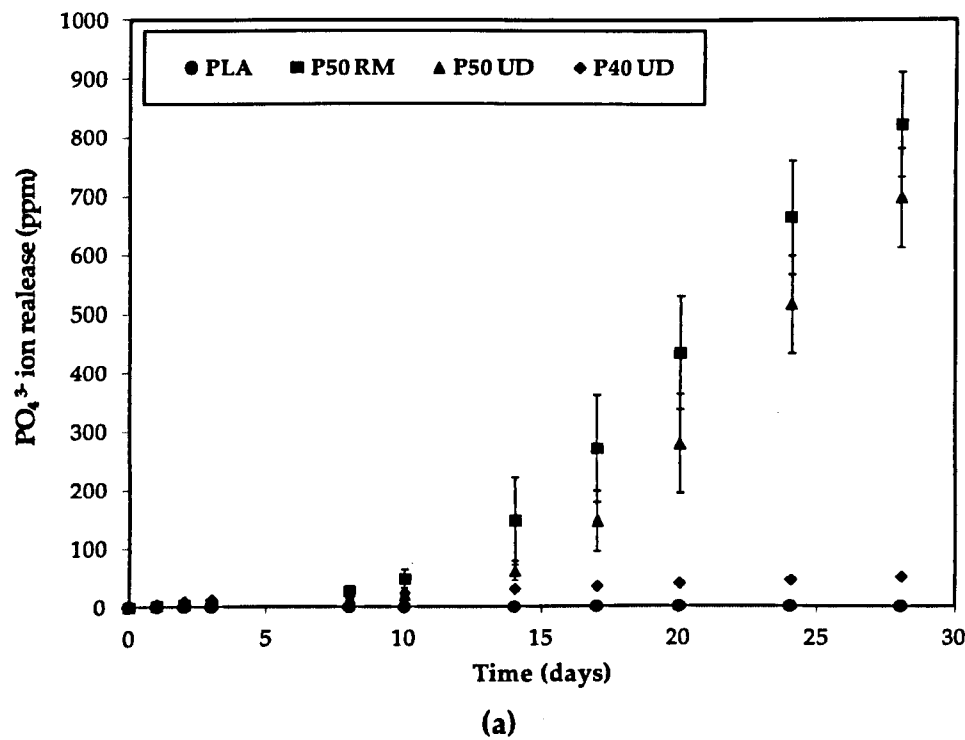


Figure 5-12: Cumulative cations ion release versus time for PLA, P50 RM, P50 UD and P40 UD composite discs: (a) Sodium (Na^+), (b) Calcium (Ca^{2+}) and (c) Magnesium (Mg^{2+}).



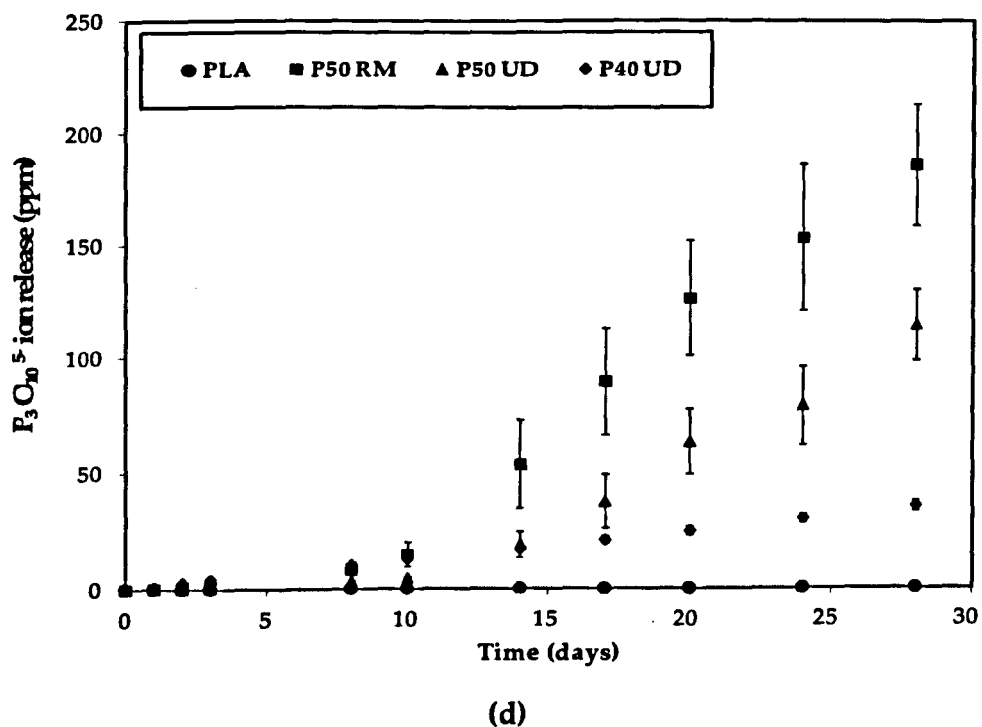
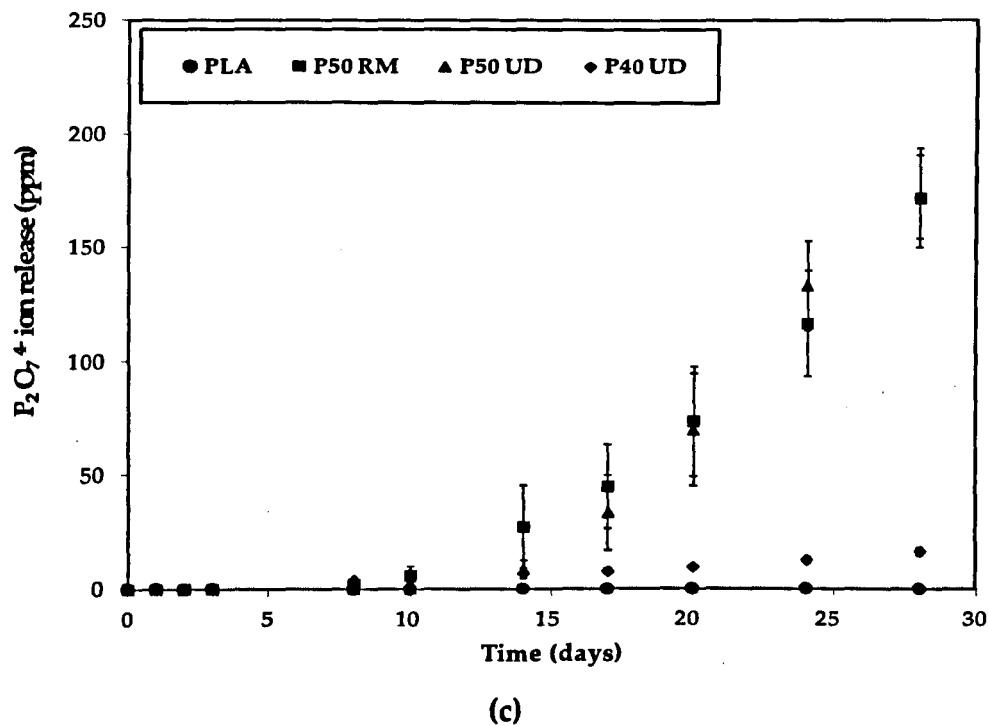


Figure 5-13: Cumulative anions ion release versus time for PLA, P50 RM, P50 UD and P40 UD composite discs: (a) Orthophosphate ($P_4O_4^{3-}$), (b) Cyclic Trimetaphosphate ($P_3O_9^{3-}$), (c) Pyrophosphate ($P_2O_7^{4-}$) and (d) Tripolyphosphate ($P_3O_{10}^{5-}$).

5.4.4 Cytocompatibility testing

Cell seeding assessed after 48h using fluorescence stereomicroscopy showed similar cells attachment for PLA and composite specimens (see **Figure 5-14**). Further observation at day 5 highlighted that the number of cells on the composite samples seemed to have increased due to proliferation. Comparison of composite samples revealed that the P40 RM seemed to sustain a marginally higher cell number than the other samples (PLA, P40 UD and P40 UD/RM). After 5 days, the medium was changed in the culture wells with alternate wells receiving fresh medium and the well plates were then incubated for a further 15 days.

The relative cell proliferation on the composites (P40 RM, P40 UD and P40 UD/RM) was evaluated at day 20 using the Alamar blue assay (**Figure 5-15-a**). This revealed a relatively homogeneous cellular response on the samples, with the P40 RM samples appearing to show slightly higher values in comparison to PLA, P40 UD and P40 UD/RM composites. However, the differences were not statistically significant ($P > 0.05$).

The cellular response to PLA and P40 composites was also assessed in terms of differentiation by measuring both the alkaline phosphatase activity (see **Figure 5-15-b**) and the Alizarin red-stained mineral deposition (see **Figure 5-15-c**, **Figure 5-16**). **Figure 5-16** shows optical images of Alizarin red staining of cell-seeded specimens and the stained nodules highlighting the deposited minerals (CaP). No significant difference ($P > 0.05$) in cell differentiation was observed amongst the samples ((P40 RM, P40 UD and P40 UD/RM) (see **Figure 5-15-b**). Although, no significant difference ($P > 0.05$) was seen in Alizarin red-stained assay between the composite specimens, these were found to be significantly greater than for PLA alone ($P < 0.0001$).

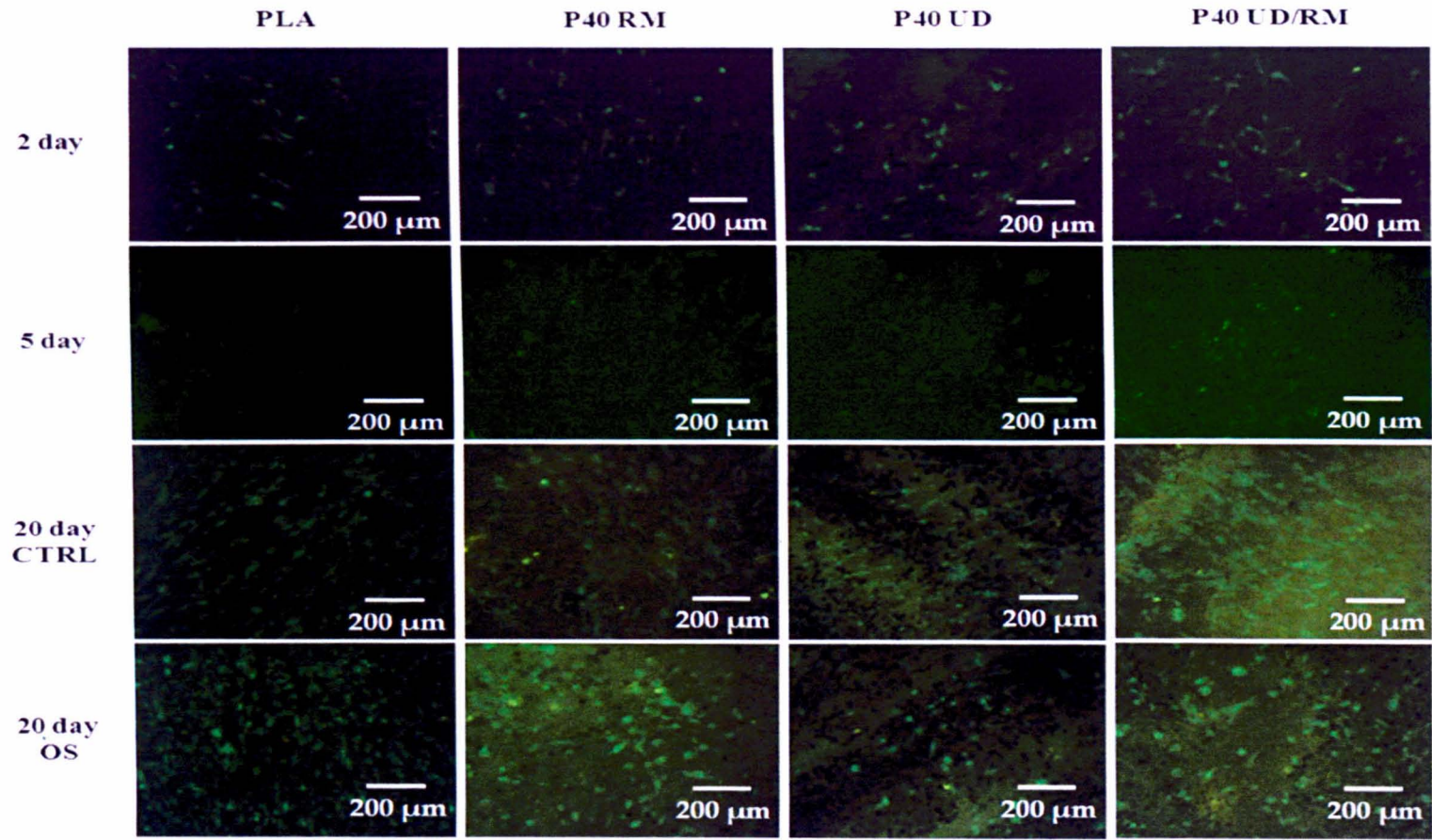
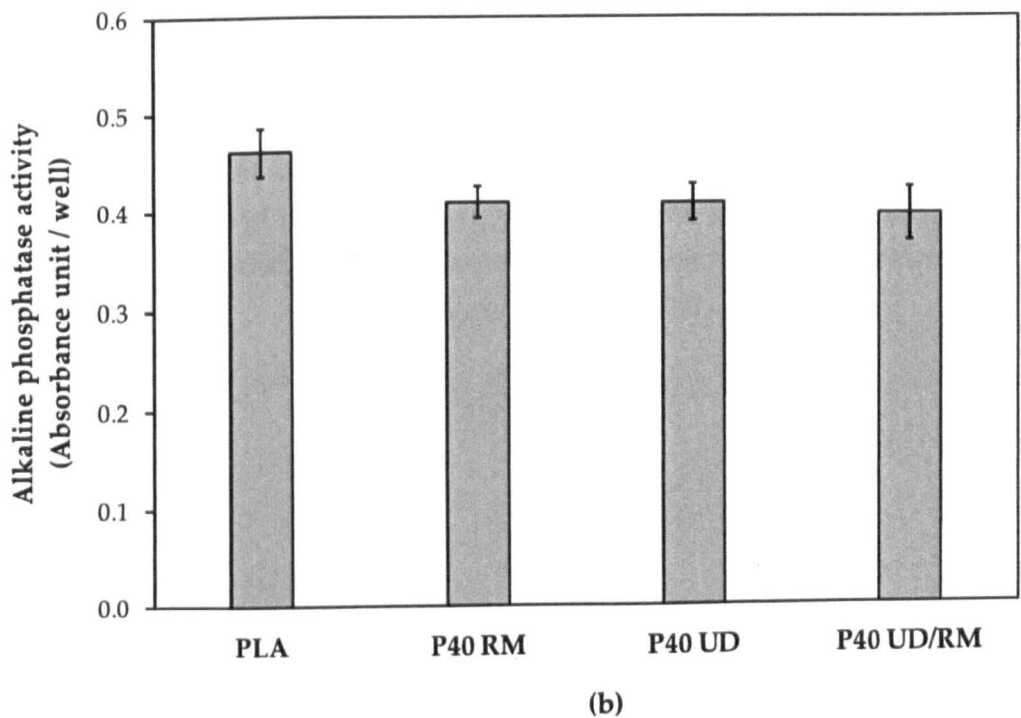
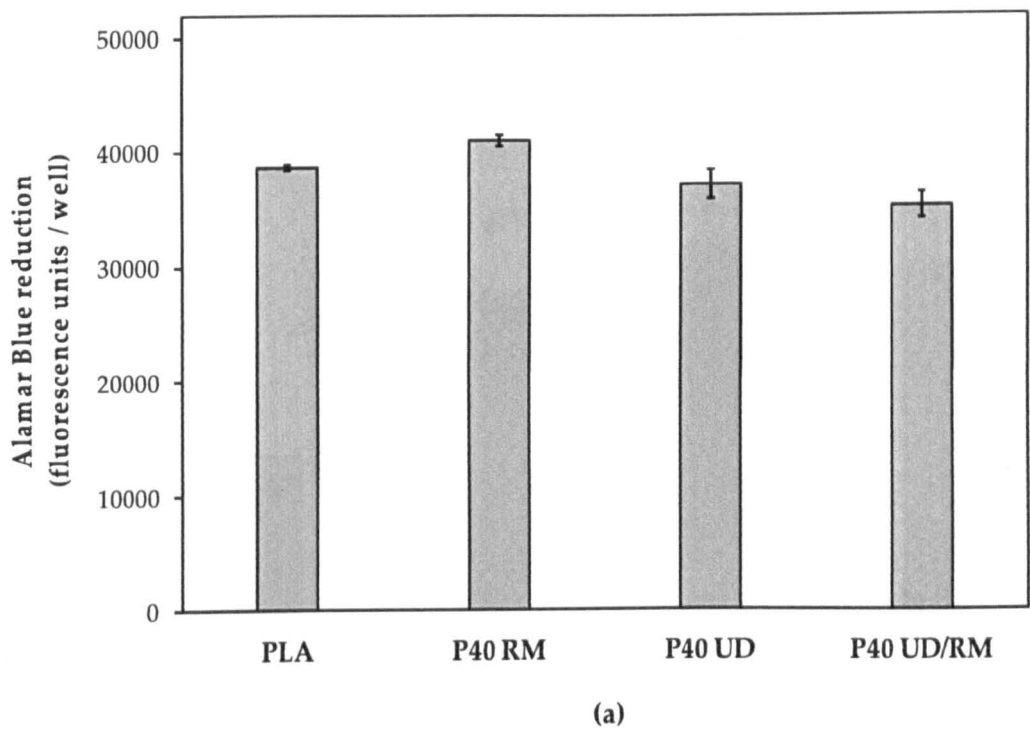


Figure 5-14: *Cytocompatibility assessment for PLA, P40 RM, P40 UD and P40 UD/RM composite. MSC cell attachment and growth of live cells (green) were visualised under a GFP-stereomicroscope over 2-day, 5-day and 20-day time points.*



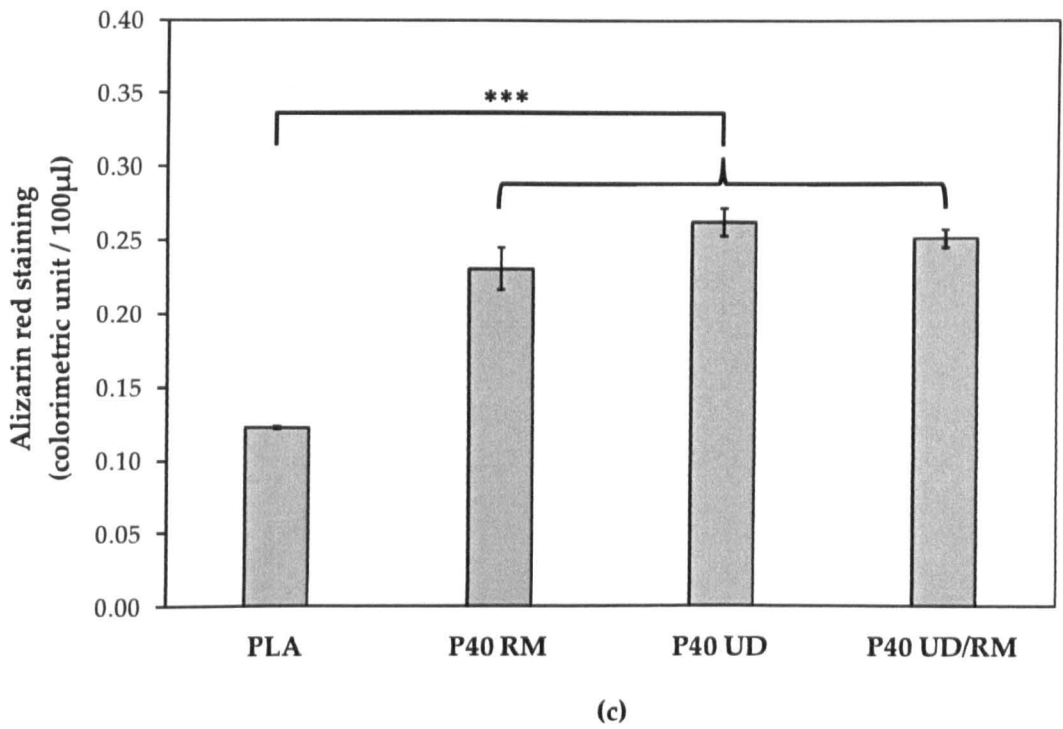


Figure 5-15: Comparison of MSC proliferation and differentiation response on different composites after 20 day immersion in cell culture media. (a) Alamar blue assay showing the metabolic activity observed for MSC cultured on the different composites. (b) MSC differentiation analysed by alkaline phosphatase activity and (c) Alizarin red staining showing the osteogenic response for composites. No statistical significant difference ($P > 0.05$) in cell proliferation and differentiation was seen between PLA and composites and *** is extremely significant ($P < 0.0001$).

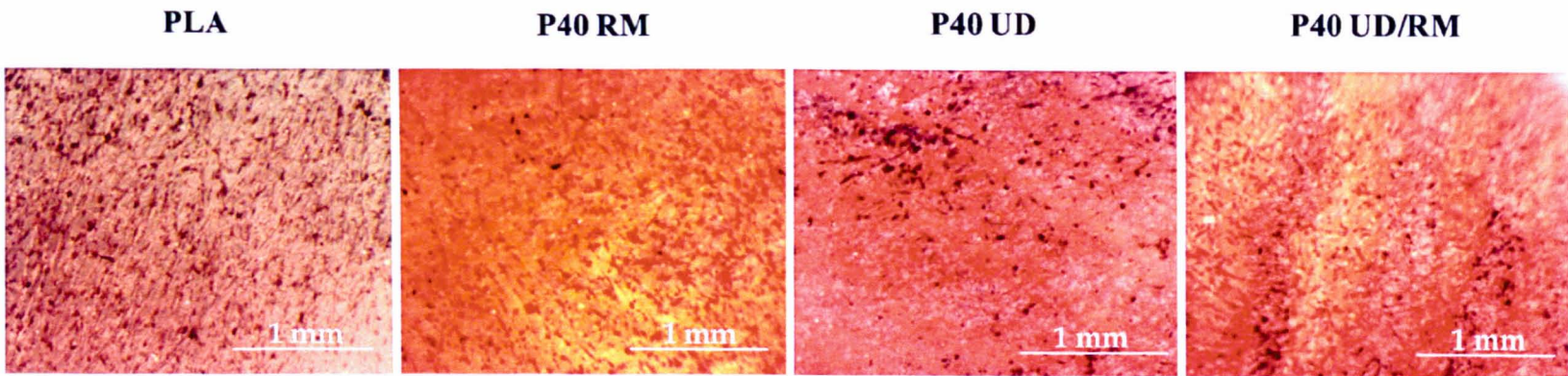


Figure 5-16: Optical images for Alizarin red staining of cell-seeded PLA, P40 RM, P40 UD and P40 UD/RM composites.

5.5 DISCUSSION

The composite rods investigated in this chapter have a potential to be used as intramedullary (IM) fixation devices to align and stabilise fractures. IM rods are inserted into the bone marrow canal of the long bones such as the femur or tibia [40] and have advantages over other methods of fixation which enable them to share the load with the bone rather than just supporting the bone.

Percentage of wet mass for composite rods increased initially during the first 14 days and then decreased gradually (Figure 5-1). The initial increase was suggested to be due to water absorption during the saturation period. Afterwards, P40 UD rods exhibited a gradual decrease in the wet mass which was attributed to gradual degradation of the fibre/matrix interface and slight degradation of the fibres. Increase in wet mass for P50 UD rods at day 20 was ascribed to swelling of the specimens. The decrease in wet mass change of P50 RM and P50 UD (Figure 5-1) composite rods after 3 and 4 weeks were suggested to be due to rapid degradation of fibres as seen from the SEM micrographs (see Figure 5-17). pH was relatively neutral as expected for the pure PLA rods, whilst a decrease in pH was observed for P50 RM and P50 UD composite rods after the 14 day interval. The decrease was suggested to be due to the release of phosphate ions into solution producing acidic compounds such as phosphoric acid (H_3PO_4) [41]. pH of the degradation medium for P40 UD rods remained stable (~ 7.5) until the end of the study at 63 days. This was attributed to the fact that PBS is buffer capable of compensating for small changes in pH. Degradation of fibre/matrix interface and fibres was the main reason for the gradual increase in mass loss and media uptake for the composite rods (see Figure 5-3 and Figure 5-4). Reduction of the molecular weight during degradation was attributed to chain scission of the PLA matrix via hydrolysis.

The initial reduction in mechanical properties (flexural, shear and compression) for composite rods after immersion in PBS was suggested to be due to the plasticisation effect of water and degradation of the fibre/matrix interface. The plasticisation effect of water is temporary and can be removed by drying, whilst degradation of the fibre/matrix interface has a permanent effect [42, 43]. The mechanical tests were restricted to wet specimens (i.e. immediately after having removed the samples from the media and blot drying them) to acquire the actual mechanical properties of the composites under simulated *in vitro* conditions.

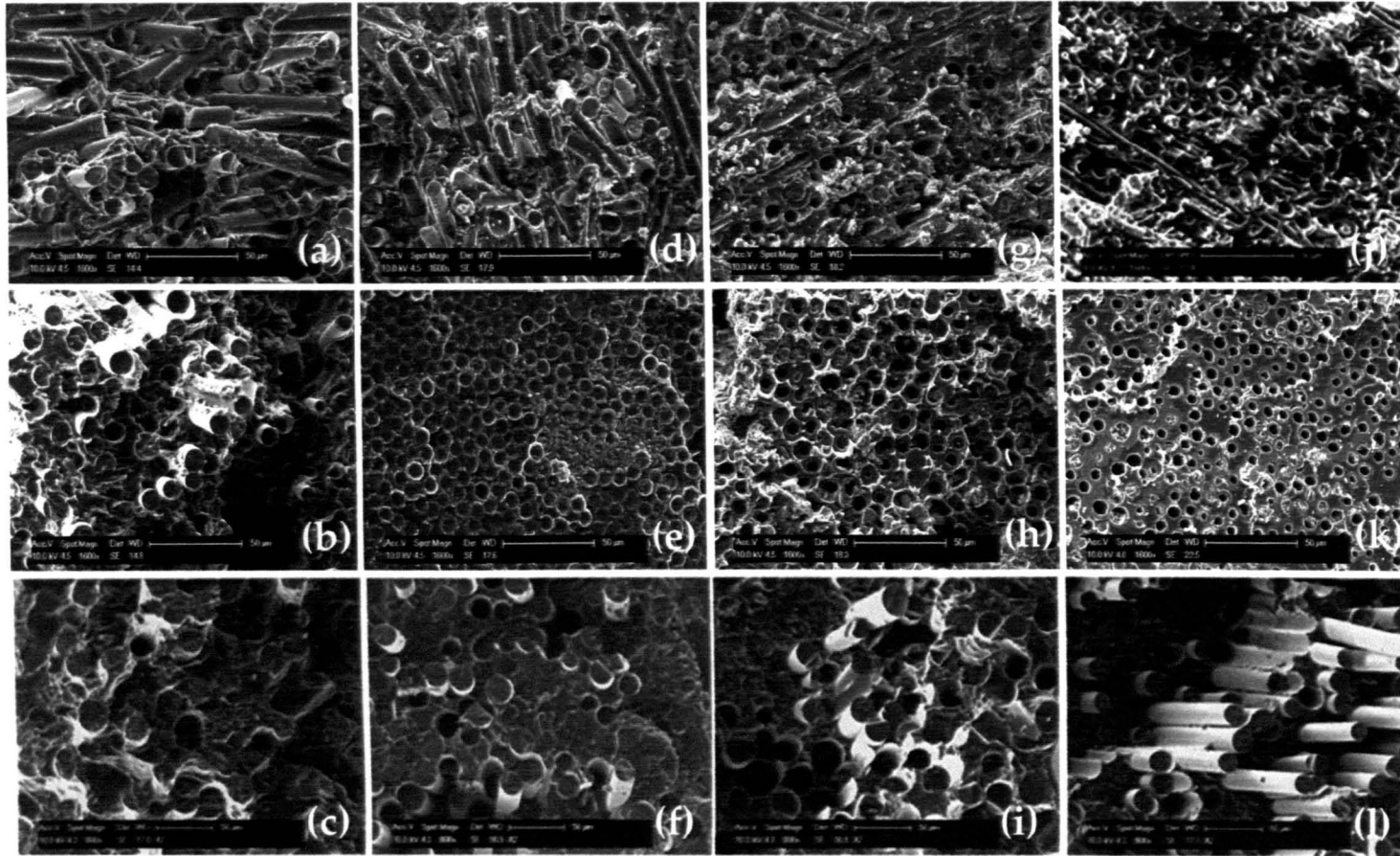


Figure 5-17: SEM micrographs of a freeze fractured surface for P50 RM, P50 UD and P40 UD composite rods (a), (b) and (c) before degradation, (d), (e) and (f) after 2 weeks of degradation in PBS at 37°C, (g), (h) and (i) after 4 weeks of degradation in PBS at 37°C, and (j), (k) and (l) after 9 weeks of degradation in PBS at 37°C. Scale bars for all micrographs represent 50 µm.

Haltia *et al.* [44] investigated hydrolytic degradation for self-reinforced poly(ester-amide) rods in PBS at 37°C and reported that degradation at the fibre/matrix interface is faster than that in the matrix. The diffusion of PBS through the fibre/matrix interface accelerated the degradation of the matrix by hydrolysis. They also stated that degradation at the core of the rods was faster than that at the surface as a result of increased carboxylic end-groups in the centre of the rods. This phenomenon has also been reported for PLA rods [44].

The strength of the interface depends on the type of mechanical test to be conducted (i.e. the direction of load application with respect to the direction of the interface or the fibres). Therefore, the interface has a significant effect on the compressive properties due to the direction of load applied especially if parallel to the fibres. For the flexural and double shear tests, the load applied was perpendicular to the fibre direction. As seen from **Figure 5-10** and **Figure 5-11**, a sudden decrease in compressive properties was seen after 3 days for the UD rods which could have been due to plasticisation of the fibre/matrix interface by the media. Another reason was the failure mode before degradation (i.e. the non-degraded dry samples), where the failure modes seen were either buckling or edge failure (see **Figure 5-18** below). Whereas after 3 days of immersion in PBS (wet sample), the failure modes were replaced by crushing or splitting which was suggested to be due to the weak interface (see **Figure 5-18** below). The failure modes were determined according to the standard BS ISO 3597-3: 2003 [45].

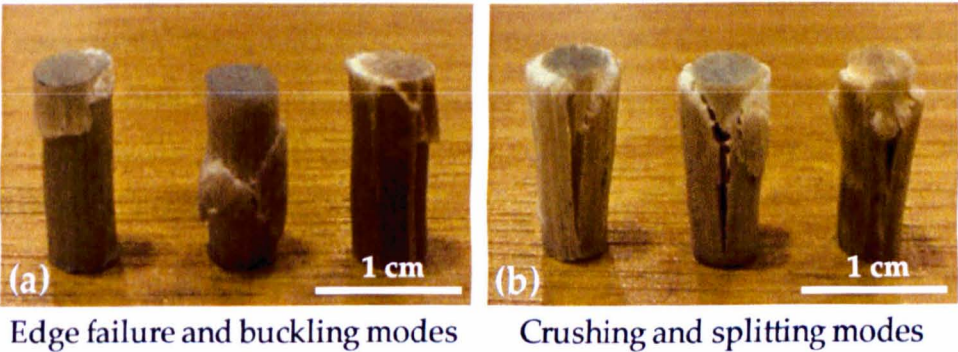


Figure 5-18: Representative failure modes observed for P50 UD, P50 RM and P40 UD composite rods after compression test; (a) before degradation and (b) after 7 days of degradation in PBS at 37°C.

A further decrease in the mechanical properties for P50 RM and P50 UD rods was seen after 2 weeks which was attributed to degradation of the fibre matrix interface. After 28 days of degradation, the mechanical strength for the composite rods was ~ 50 % of the strength of pure PLA due to creation of a porous structure owing to degradation of the fibres. In contrast, the mechanical properties for P40 UD rods remained stable (after 7 days of degradation) at values similar to those of cortical bone for the remaining duration of the study. This was attributed to the chemical durability of the P40 fibres in comparison to P50 Fibres.

The shear property measurement arrangement used in this study (see Figure 4-5), measured the shear effects in perpendicular direction to the long axis of the rod. This mode of loading was selected as it was similar to the load applied by bone fragments at the bone fracture position [4]. Pietrzak *et al.* [46] manufactured pins from an oriented copolymer of 82 % PLLA and 18 % PGA and tested shear stiffness using the arrangement used in this study. They found that the initial shear stiffness for pins of 3.2 mm diameter was 3.47 kN.mm⁻¹ which was close to the results obtained for pure PLA rods (4 mm diameter) in this chapter. P50 RM and P50 UD composite rods had ~ 200 % higher initial shear stiffness as compared to PLA.

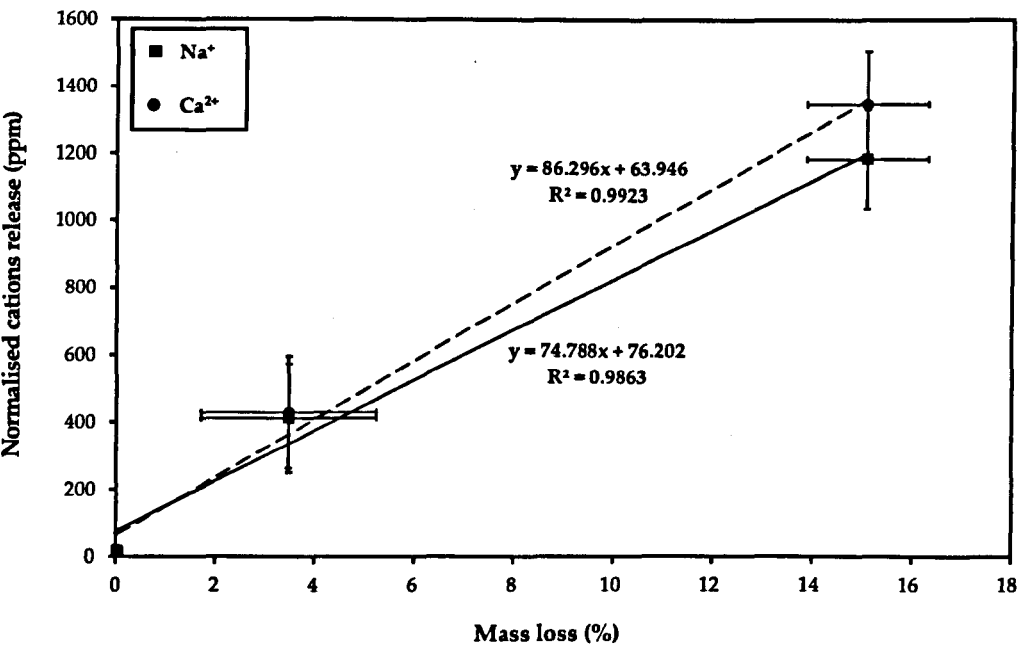
The reduction in mechanical properties after degradation in PBS agreed with the findings of Lin *et al.* [47]. They prepared composites of PLLA reinforced with calcium phosphate glass fibres with fibre volume fraction ~ 55 % and their initial flexural bending strength and modulus of the composites was ~ 350 MPa and ~ 28 GPa respectively. These properties decreased to ~ 84 MPa for strength and ~ 3.8 GPa for Modulus (which were similar to the flexural properties of PLA alone) after 1 week of degradation in PBS at 37°C. They also referred the decrease observed to breakdown of the fibre/matrix interface.

The degradation of the fibre/matrix interface by water can be seen from the SEM micrographs (see Figure 5-17) of the cross-sections of freeze fractured rod samples before and after degradation in PBS at 37°C. Before degradation, the fibres within the composites were fully covered with the PLA matrix and this was indicative of good fibre impregnation due to sufficient wet-out and a strong interface (see Figure 5-17 a, b and c). After 2 weeks of immersion in PBS at 37°C, the P50 and P40 fibres

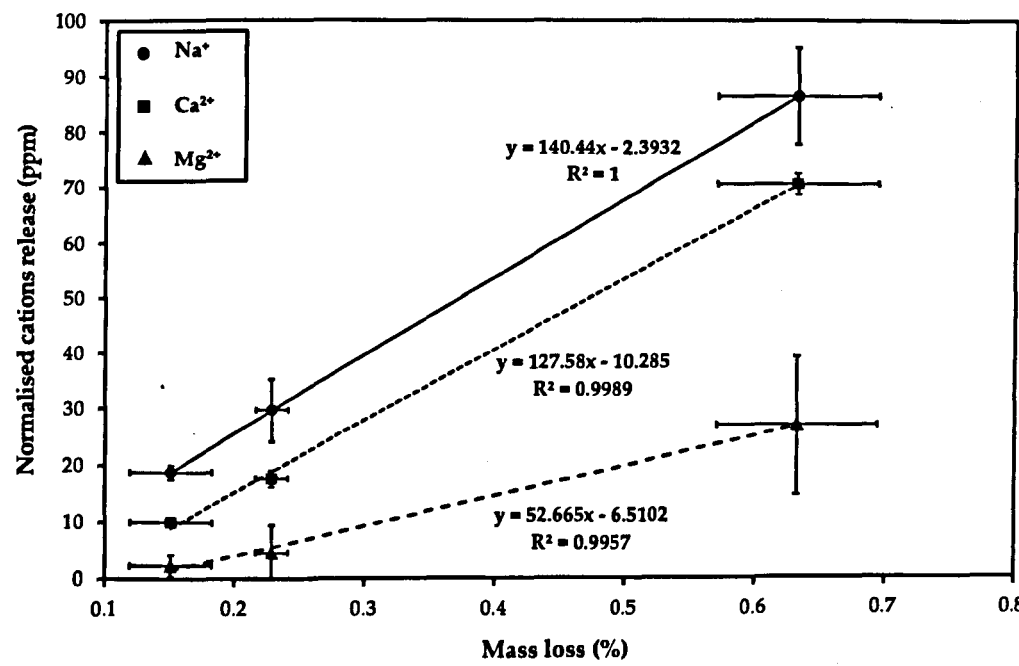
appeared to be intact as the fibres were still present (see Figure 5-17 d, e and f). After 4 weeks immersion in PBS, the P50 fibres within P50 RM and P50 UD rods had degraded from the core out and hollow chambers could be seen (see Figures 14e and f). The fibres in samples P50 RM and P50 UD rods leached out into solution after 6 and 9 weeks respectively, leaving behind a very porous structure with remnants of fibre in places (Figure 5-17 j and k). Conversely, the P40 fibres were still present after 9 weeks of degradation in PBS. Furthermore, short fibre pull-out and clean fibre surfaces were observed, which was attributed to the degradation of the fibre/matrix interface (see Figure 5-17 l).

Similar findings to P50 fibres were obtained by Abou Neel *et al.* [48]. It was suggested that these pores and channels could also facilitate a speedier breakdown of the remaining PLA matrix itself. The formation of hollow fibres within the composites was suggested to be due to hydrolysis of long P-O-P chains (Q^2 species) into shorter chains (Q^1 and Q^0) [2]. These short chains then leached out to the surrounding medium leaving behind porous microtubes. It could also be due to more water attacking the ends of the fibres rather than their surface which is slightly protected by polymer.

Ion release profiles for composite rods correlated extremely well with the mass loss profiles (see Figure 5-19 and Figure 5-20) [20, 25, 33], demonstrating a linear relationship between mass loss and ion release. However, the ion release and degradation studies were conducted independently for the rods using different media (deionised water for ion release and PBS for degradation) and as such a comparison must be considered with caution. Similar findings were presented previously for PCL/PGF composites by Ahmed *et al.* [31]. It was difficult to correlate pH with ion release as the degradation medium was different. Furthermore, it is well known that PBS is capable of compensating for small changes in the pH of the medium to maintain it around 7.4. However, a clear link can be seen between pH and anion release profiles for P50 composites (see Figures 5-2 and 5-13). Reduction in pH for P50 composite rods started at day 10 of degradation and similarly anion release. Moreover, pH for P50 RM rods at day 14 was lower than that for P50 UD rods and amounts of anion released at the same day for P50 RM were greater than P50 UD rods.

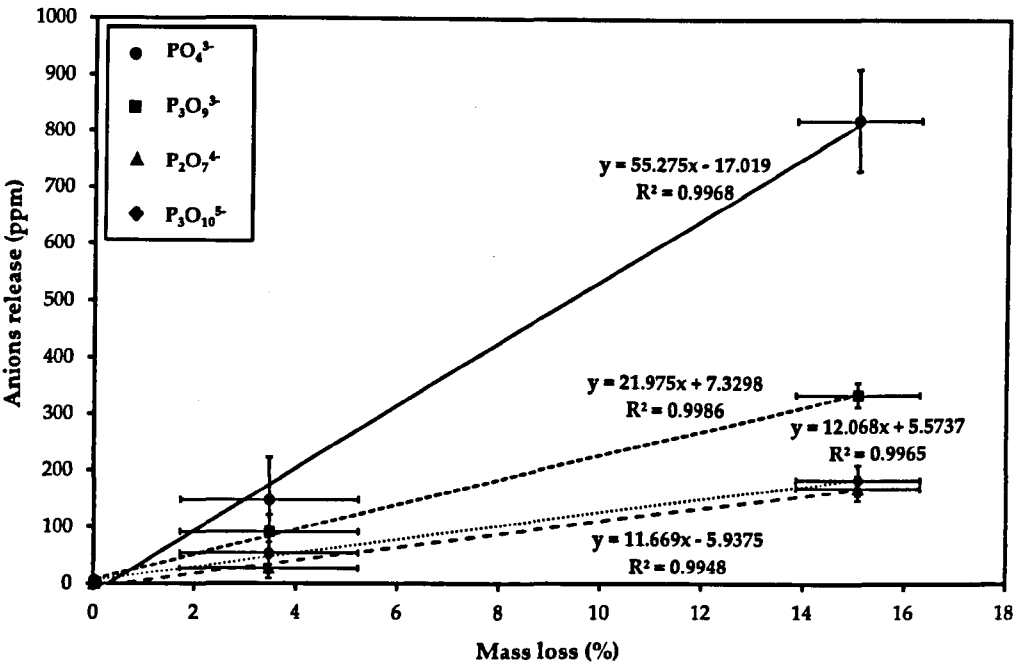


(a)

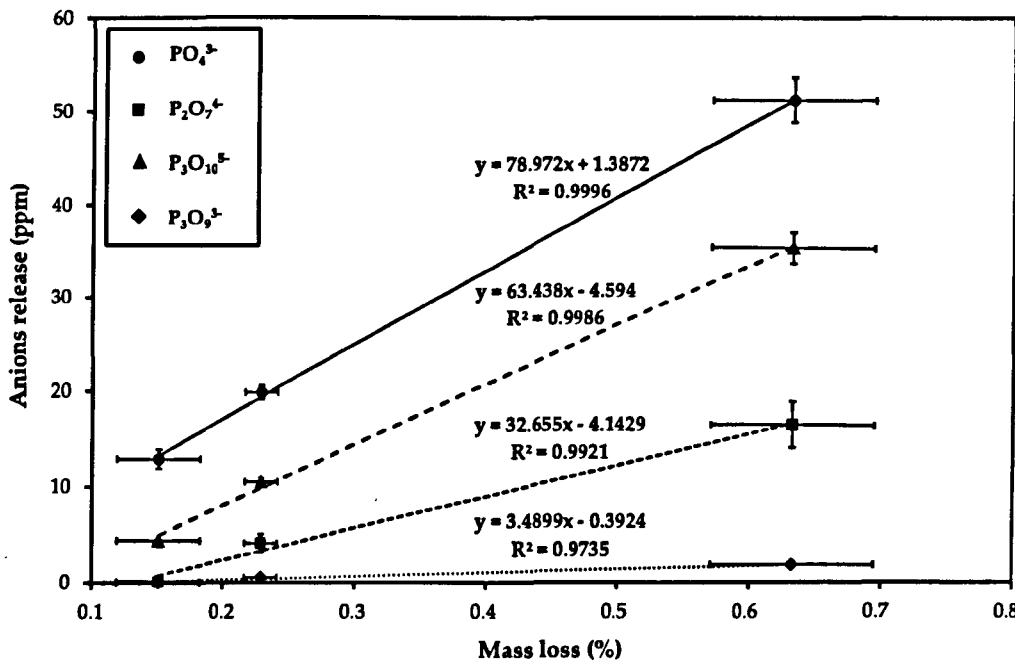


(b)

Figure 5-19: Change in molar normalised cation release at different time points against mass loss for composite rods (a) P50 RM and (b) P40 UD composite rods. Molar normalisation was calculated via dividing of amount of released cations by the molar concentration of the cation with the glass composition (0.16, 0.16 and 0.24 for Na, Ca and Mg respectively).



(a)



(b)

Figure 5-20: Change in anion release at different time points against mass loss for composite rods (a) P50 RM and (b) P40 UD composite rods.

Ion release tests can be performed by either changing the medium at every time point (cumulative method) or by using a static medium (i.e. without changing the medium till the end of the study). Cumulative ion release was conducted in the current study in order to avoid precipitation effects of degradation products [20, 27] that could have given incorrect values and incomparable results with the degradation studies. Lower degradation and ion release rates for P40 composites in comparison to P50 composites [29, 30] were suggested to be due to their high chemical durability. The durability of the P40 composition was attributed to lower phosphate content and presence of Mg^{2+} which can enable cross-linking between phosphate chains [49]. The structure of phosphate glasses with low P_2O_5 content (40 mol% or below) have also been referred to as 'invert glasses' [34, 50, 51]. Invert phosphate glasses have low degradation rates and less acidic products in aqueous media due to a decrease in the fraction of Q^2 species [51, 52]. P50 formulations have been reported to have an infinite Q^2 chain structure which can be highly susceptible to hydration followed by hydrolysis [53]. Whereas the P40 glass composition has much shorter chains (i.e. a mixture of Q^1 's and Q^2 's) [18, 52]. These shorter chains are able to pack together tighter creating more durable glasses [49, 52]. Dissolution rates for P50 and P40 glass formulations in distilled water at 37°C were reported to be approximately $3 \times 10^{-5} \text{ g.cm}^{-2}.\text{h}^{-1}$ and $3 \times 10^{-6} \text{ g.cm}^{-2}.\text{h}^{-1}$ respectively [35].

The content of calcium and sodium oxide within the P40 glass fibre formulation was the same (16 mol% of each). Sodium released in slightly higher quantities in comparison to the calcium, which was suggested to be due to the fact that Ca^{2+} ions have a stronger cross-linking effect and ionic field strength than Na^+ [27]. The amount of Mg^{2+} ions released were lower than Ca^{2+} , even though there was more Mg in the glass. This was also attributed to the field strength effect as shown in **Figure 5-21**. Rates of released cations (determined from the gradient of the line between amounts of cation released and time) for P50 and P40 composites decreased as the field strength of the cation increased. Dietzal's field strength (ratio of valence (Z) to the square of ionic distance (a^2) for oxides) for Na^+ , Ca^{2+} , Mg^{2+} and Fe^{3+} is 0.19, 0.33, 0.45 and 0.76 \AA^{-2} [54].

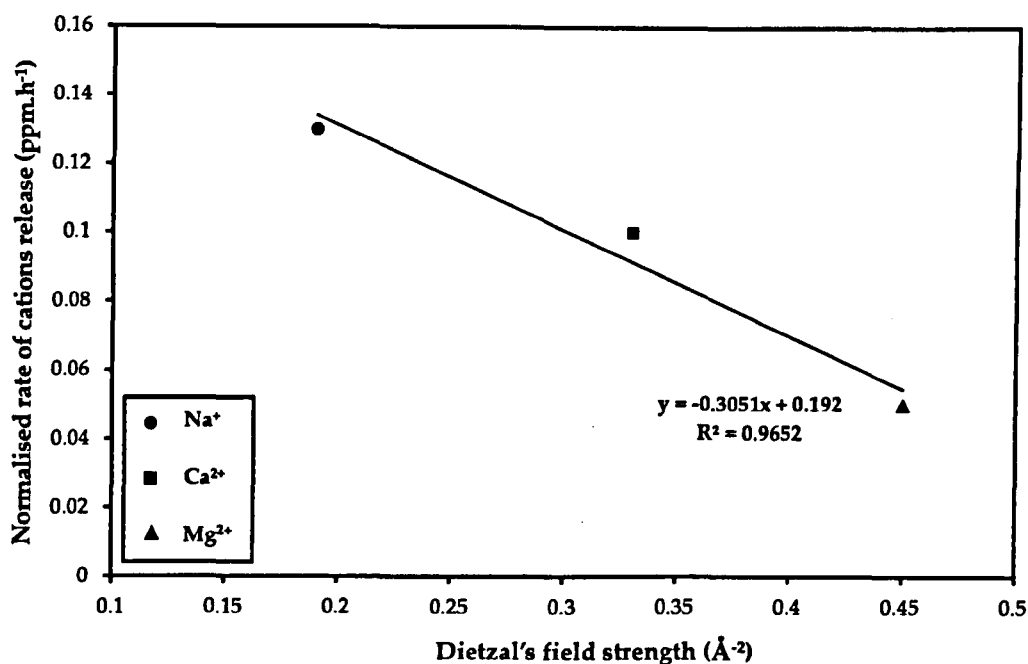


Figure 5-21: Molar normalised rate of cations released (Na⁺, Ca²⁺ and Mg²⁺) versus Dietzal's field strength. Molar normalisation was calculated via dividing of rate of released cations by the molar concentration of the cation with the glass composition (0.16, 0.16 and 0.24 for Na, Ca and Mg respectively).

Types and amount of ions released depend mainly on composition and chemical durability of the glass. PO₄³⁻ anion release data were higher than that seen for the rest of the anions investigated for all specimens investigated. This higher amount of released PO₄³⁻ ions was suggested to be due to the breakdown of the longer chain polyphosphates in solution prior to analysis, as PO₄³⁻ is the final breakdown product of these phosphate chains [24, 31].

Ahmed *et al.* [19-21] found that P₃O₉³⁻ was the highest released anionic species for a range of ternary phosphate glasses (with fixed 45, 50 and 55 mole % P₂O₅). They ascribed these higher release levels of P₃O₉³⁻ anions to the structure of the glass which contained significant amounts of unbranched or ring P₃O₉³⁻. Abou Neel *et al.* [27] reported similar findings for ternary glasses with similar compositions. Conversely, it was found that the amount of PO₄³⁻ became greater than P₃O₉³⁻ after addition of 5 mol % Fe₂O₃ at the expense of Na₂O [24, 27]. Borbely *et al.* [29] and Alani *et al.* [30] also reported the dominance of PO₄³⁻ ions over the rest of the anions investigated in PCL composites reinforced with P50 fibres (similar to the

compositions of the P50 fibres used in this chapter) and they ascribed this to the degradation of the long phosphate chains. Moreover, it was reported that the amount of all ions released decreased as the content of Fe_2O_3 increased [30].

In this study, the rate of PO_4^{3-} ions released as seen in Figure 5-13 was greater in comparison to the other anions and cations investigated, indicating a rapid breakdown of the phosphate glass network. Release of PO_4^{3-} was also suggested to be responsible for the drop in pH during the degradation process (see Figure 5-2) due to formation of phosphoric acid (H_3PO_4) [25, 31]. Furthermore, $\text{P}_3\text{O}_9^{3-}$ anion completely disappeared for P40 UD rods which could be due to shortening chain structure in glass because of increased levels of network modifiers. This confirmed that the quantity and type of releasing ions were sensitive to the glass composition as well as the chemical durability. Therefore, it could be summarised that phosphate glasses can have predictable and controllable ion release profiles based on their composition.

A slow ion release rate for P50 UD and P50 RM composite rods over the first 3 days was attributed to water absorption during the saturation period [25] (see Figure 5-1). Afterwards, the P50 rods showed a higher and linear rate of release for all anions and cations investigated. This was suggested to be due to controlled and continuous ion diffusion from the glass fibres as a result of degradation of the fibres after saturation of the matrix with water.

Ca^{2+} ions play a crucial role in the chemical durability of the glass composition. This was seen by Ahmed *et al.* [18] and Bunker *et al.* [55], who observed that the degradation rate for phosphate glass decreased as the amount of Ca^{2+} increased. Ca^{2+} ions can form a chelating structure via ionic bonds between two PO_4^{3-} chains producing strong P-O-P bonds. Fe_2O_3 content also has a significant positive effect on the durability of these glass fibres which has been attributed to formation of hydration resistant Fe-O-P bonds [27]. Parsons *et al.* [56] found that the effect of metal addition on degradation rate of the phosphate glasses was in the order of $\text{Fe} > \text{Mg} > \text{Ca}$.

It was also found that the dissolution rate of phosphate glasses has a direct influence on their biological performance, as their biocompatibility is enhanced when the dissolution rate decreases [34, 57-62]. Ahmed *et al.* [35] showed that for an immortal muscle precursor cell line proliferation and differentiation for iron phosphate glass fibres ($\text{P}_2\text{O}_5 - \text{CaO} - \text{Na}_2\text{O}$) were enhanced via incorporation of iron (Fe_2O_3) due to an increase in the glass durability [27, 35]. The cell culture studies conducted here were applied to PLA and P40 composite samples and P50 fibre composites have been studied previously [41]. Cytocompatibility for composites based on PLA and annealed and non-annealed P50 fibres ($V_f \sim 13\%$) using an osteoblast cell line (MG63) for 7 days were investigated previously by Ahmed *et al.* [41]. They found that the annealed fibre reinforced composites as well as PLA alone showed higher cell viability than non-annealed fibre composites. They ascribed this to the slower degradation rate of the annealed fibres in comparison with non-annealed fibres. Thus, it was expected that the P40 composites should have better cytocompatibility in comparison with the P50 composites due to their lower degradation rate.

The mechanical properties of RM composites were not greatly improved in comparison to PLA alone. Therefore, UD composites would be potential materials for use as intramedullary nails. However, PLA/PGF composites have potential application not only for intramedullary nailing but also as bone plates and screws. Moreover, Han *et al.* [63] demonstrated that the drilling of screw holes into UD composite plates caused extensive damage (cracks, delamination) around the screw-holes. They found that the damage was eliminated by using random fibre mats at the surface of the composites instead of pure UD composites. Thus, the biocompatibility tests were conducted on P40 composites with different fibre architecture (RM, UD and UD/RM) to assess the effect of fibre distribution and degradation on the biocompatibility of the composites.

MSC cell differentiation on the P40 composites in this chapter was demonstrated by alkaline phosphatase (ALP) (see **Figure 5-15-b**). No statistically significant

difference was found for cell proliferation and differentiation between the different specimens (PLA, P40 RM, P40 UD and P40 UD/RM). Since mineralisation is an essential process for new bone formation [64], deposition of calcium phosphate on the specimens was quantified using alizarin red staining. P40 composites showed a higher deposition of calcium phosphate (CaP) in comparison with PLA (see Figure 5-15-c). This could suggest the possible ability of phosphate glass fibres to stimulate new bone formation via CaP deposition during degradation. This finding was seen by Scotchford *et al.* [15] for PCL/PGF during in vivo study.

Based on the mechanical, ion release, degradation and biocompatibility properties observed above, the P40 composite would be a potential material for intramedullary application. However, enhancement of the fibre/matrix interface is indispensable in helping to maintain the initial mechanical properties for a longer period, which is desirable for bone fixation implants. The interface could be improved by coating the fibres with coupling agent prior to use in composites manufacturing.

5.6 CONCLUSIONS

The wet flexural, shear and compressive strengths for P40 UD rods decreased by ~ 30 %, ~ 20 % and ~ 50 % of the initial dry values after 3 days. Afterwards, the P40 composites rods maintained their mechanical properties at a similar range to that of cortical bone until the end of study at 63 days. The mechanical properties for the P50 rods decreased rapidly below that for the pure PLA rods which remained constant. The initial reduction in the mechanical properties for composite rods was attributed to water plasticisation effect. The fibres within the P50 rods started to degrade after 21 – 28 days and the fibre morphology resembled microtubes as seen from the SEM micrographs. The composite rods became porous structures after degradation which was the main reason suggested for the decrease in mechanical properties and mass.

Rates of degradation and ion release for P40 UD rods were slower than that for P50 composite rods due to the enhanced durability of P40 fibres. Percentages of mass loss and water uptake for P50 and P40 composite rods were approximately 17 %

and 1 % respectively. Cation and anion release rates were well correlated with mass loss profiles for all composite rods. The amount of ions released and mass loss increased linearly over time until the end of the study. Sodium ions were released in the largest amount from the glass, whilst the orthophosphate ion was released in the largest quantities. P40 composite rods exhibited good cytocompatibility due to the high chemical durability of P40 fibres. The amount of calcium phosphate (CaP) deposition was greater for the composites than PLA, although cell activity was similar.

5.7 REFERENCES

1. Hoffmann, J., K. Friedrich, M. Eustatiev, and U. Finkc, *A Totally Bioresorbable Fibrillar Reinforced Composite System: Structure and Properties*. *International Journal of Polymeric Materials*, 2001. 50(3): p. 469 - 482.
2. Törmälä, P., J. Vasenius, S. Vainionpää, J. Laiho, T. Pohjonen, and P. Rokkanen, *Ultra-high-strength absorbable self-reinforced polyglycolide (SR-PGA) composite rods for internal fixation of bone fractures: In vitro and in vivo study*. *Journal of Biomedical Materials Research*, 1991. 25(1): p. 1-22.
3. Pertti, T., R. Pentti, L. Juha, T. Markku, and V. Seppo, *Material for osteosynthesis devices*, U.S. Patent, Editor 1988: United States.
4. Majola, A., S. Vainionpää, P. Rokkanen, H.M. Mikkola, and P. Törmälä, *Absorbable self-reinforced polylactide (SR-PLA) composite rods for fracture fixation: strength and strength retention in the bone and subcutaneous tissue of rabbits*. *Journal of Materials Science: Materials in Medicine*, 1992. 3(1): p. 43-47.
5. Törmälä, P., M. Huttunen, N. Ashammakhi, M. Tukiainen, H. Ylänen, M. Hupa, and M. Kellomäki, *Bioabsorbable and Bioactive Composite Material and A method for Manufactureing the Composite*, Patent US 2010/0121463 A1, 2010.
6. Shikinami, Y. and M. Okuno, *Bioresorbable devices made of forged composites of hydroxyapatite (HA) particles and poly-L-lactide (PLLA): Part I. Basic characteristics*. *Biomaterials*, 1999. 20(9): p. 859-877.
7. Hasegawa, S., S. Ishii, J. Tamura, T. Furukawa, M. Neo, Y. Matsusue, Y. Shikinami, M. Okuno, and T. Nakamura, *A 5-7 year in vivo study of high-strength hydroxyapatite/poly(l-lactide) composite rods for the internal fixation of bone fractures*. *Biomaterials*, 2006. 27(8): p. 1327-1332.
8. Furukawa, T., Y. Matsusue, T. Yasunaga, Y. Shikinami, M. Okuno, and T. Nakamura, *Biodegradation behavior of ultra-high-strength hydroxyapatite/poly (-lactide) composite rods for internal fixation of bone fractures*. *Biomaterials*, 2000. 21(9): p. 889-898.

9. Paul, J.P., *Strength requirements for internal and external prostheses. Journal of Biomechanics*, 1999. 32(4): p. 381-393.
10. Li Liao, Lin Chen, Ai-Zheng Chen, Xi-Ming Pu, Yun-Qing Kang, Ya-Dong Yao, Xiao-Ming Liao, Zhong-bing Huang, and G.-F. Yin, *Preparation and characteristics of novel poly-L-lactide/ β -calcium metaphosphate fracture fixation composite rods. J. Mater. Res. , 2007. 22(12): p. 3324 - 3329.*
11. Ruffieux, K., A. Dell'Agosti, B. Riesen, and E. Wintermantel, *Influence of Calcium Phosphates on the Degradation of Poly Lactic Acid for Medical Implants. Biomedizinische Technik/Biomedical Engineering*, 1996. 41(s1): p. 420-421.
12. Niemelä, T., H. Niiranen, and M. Kellomäki, *Self-reinforced composites of bioabsorbable polymer and bioactive glass with different bioactive glass contents. Part II: In vitro degradation. Acta Biomaterialia*, 2008. 4(1): p. 156-164.
13. Niemelä, T., H. Niiranen, M. Kellomäki, and P. Törmälä, *Self-reinforced composites of bioabsorbable polymer and bioactive glass with different bioactive glass contents. Part I: Initial mechanical properties and bioactivity. Acta Biomaterialia*, 2005. 1(2): p. 235-242.
14. Niiranen, H., T. Pyhälä, P. Rokkanen, M. Kellomäki, and P. Törmälä, *In vitro and in vivo behavior of self-reinforced bioabsorbable polymer and self-reinforced bioabsorbable polymer/bioactive glass composites. Journal of Biomedical Materials Research Part A*, 2004. 69A(4): p. 699-708.
15. Scotchford, C.A., M. Shataheri, P.S. Chen, M. Evans, A.J. Parsons, G.A. Aitchison, C. Efeoglu, J.L. Burke, A. Vikram, S.E. Fisher, and C.D. Rudd, *Repair of calvarial defects in rats by prefabricated, degradable, long fibre composite implants. J Biomed Mater Res A*, 2010. 96(1): p. 230-8.
16. Parsons, A.J., I. Ahmed, N. Han, R. Felfel, and C.D. Rudd, *Mimicking Bone Structure and Function with Structural Composite Materials. Journal of Bionic Engineering*, 2010. 7(Supplement 1): p. S1-S10.
17. Efeoglu, C., J.L. Burke, A.J. Parsons, G.A. Aitchison, C. Scotchford, C. Rudd, A. Vikram, and S.E. Fisher, *Analysis of calvarial bone defects in rats using microcomputed tomography: potential for a novel composite material and a new quantitative measurement. British Journal of Oral and Maxillofacial Surgery*, 2009. 47(8): p. 616-621.
18. Ahmed, I., M. Lewis, I. Olsen, and J.C. Knowles, *Phosphate glasses for tissue engineering: Part 1. Processing and characterisation of a ternary-based P_2O_5 - CaO - Na_2O glass system. Biomaterials*, 2004. 25(3): p. 491-499.
19. Ahmed, I., A.J. Parsons, C.D. Rudd, S.N. Nazhat, J.C. Knowles, P. Guerry, and M.E. Smith, *Comparison of phosphate-based glasses in the range $50P_2O_5$ - $(50-x)CaO$ - xNa_2O prepared using different precursors. Glass Technology - European Journal of Glass Science and Technology Part A*, 2008. 49(2): p. 63 - 72.

20. Ahmed, I., M.P. Lewis, S.N. Nazhat, and J.C. Knowles, Quantification of anion and cation release from a range of ternary phosphate-based glasses with fixed 45 mol% P₂O₅. *J Biomater Appl*, 2005. 20(1): p. 65-80.
21. Ahmed, I., M.P. Lewis, and J.C. Knowles, Quantification of anions and cations from ternary phosphate based glasses with fixed 50 and 55 mol% P₂O₅ using ion chromatography. 2005. 46: p. 547 - 557.
22. Knowles, J.C., K. Franks, and I. Abrahams, Investigation of the solubility and ion release in the glass system K₂O-Na₂O-CaO-P₂O₅. *Biomaterials*, 2001. 22(23): p. 3091-3096.
23. Franks, K., V. Salih, J.C. Knowles, and I. Olsen, The effect of MgO on the solubility behavior and cell proliferation in a quaternary soluble phosphate based glass system. *Journal of Materials Science: Materials in Medicine*, 2002. 13(6): p. 549-556.
24. Patel, A. and J. Knowles, Investigation of silica-iron-phosphate glasses for tissue engineering. *Journal of Materials Science: Materials in Medicine*, 2006. 17(10): p. 937-944.
25. Georgiou, G., L. Mathieu, D.P. Pioletti, P.E. Bourban, J.A.E. Manson, J.C. Knowles, and S.N. Nazhat, Polylactic acid-phosphate glass composite foams as scaffolds for bone tissue engineering. *Journal of Biomedical Materials Research Part B: Applied Biomaterials*, 2007. 80B(2): p. 322-331.
26. Prabhakar, R.L., S. Brocchini, and J.C. Knowles, Effect of glass composition on the degradation properties and ion release characteristics of phosphate glass--polycaprolactone composites. *Biomaterials*, 2005. 26(15): p. 2209-2218.
27. Abou Neel, E.A., I. Ahmed, J.J. Blaker, A. Bismarck, A.R. Boccaccini, M.P. Lewis, S.N. Nazhat, and J.C. Knowles, Effect of iron on the surface, degradation and ion release properties of phosphate-based glass fibres. *Acta Biomaterialia*, 2005. 1(5): p. 553-563.
28. Mohammadi, S.M., I. Ahmed, B. Marelli, C. Rudd, M.N. Bureau, and S.N. Nazhat, Modulation of polycaprolactone composite properties through incorporation of mixed phosphate glass formulations. *Acta Biomaterialia*, 2010. 6(8): p. 3157-3168.
29. Borbely, P., K. Gulabivala, and J.C. Knowles, Degradation properties and ion release characteristics of Resilon and phosphate glass/polycaprolactone composites. *Int Endod J*, 2008. 41(12): p. 1093-100.
30. Alani, A., J.C. Knowles, W. Chrzanowski, Y.L. Ng, and K. Gulabivala, Ion release characteristics, precipitate formation and sealing ability of a phosphate glass-polycaprolactone-based composite for use as a root canal obturation material. *Dent Mater*, 2009. 25(3): p. 400-10.
31. Ahmed, I., A.J. Parsons, G. Palmer, J.C. Knowles, G.S. Walker, and C.D. Rudd, Weight loss, ion release and initial mechanical properties of a binary calcium phosphate glass fibre/PCL composite. *Acta Biomaterialia*, 2008. 4(5): p. 1307-1314.

32. Mohammadi, M.S., I. Ahmed, N. Muja, S. Almeida, C.D. Rudd, M.N. Bureau, and S.N. Nazhat, *Effect of Si and Fe doping on calcium phosphate glass fibre reinforced polycaprolactone bone analogous composites*. *Acta Biomater*, 2012. 8(4): p. 1616-1626.
33. Mohammadi, S.M., I. Ahmed, N. Muja, C. Rudd, M. Bureau, and S. Nazhat, *Effect of phosphate-based glass fibre surface properties on thermally produced poly(lactic acid) matrix composites*. *Journal of Materials Science: Materials in Medicine*, 2011. 22(12): p. 2659-2672.
34. Ahmed, I., A. Parsons, A. Jones, G. Walker, C. Scotchford, and C. Rudd, *Cytocompatibility and Effect of Increasing MgO Content in a Range of Quaternary Invert Phosphate-based Glasses*. *J Biomater Appl*, 2010. 24(6): p. 555-575.
35. Ahmed, I., C.A. Collins, M.P. Lewis, I. Olsen, and J.C. Knowles, *Processing, characterisation and biocompatibility of iron-phosphate glass fibres for tissue engineering*. *Biomaterials*, 2004. 25(16): p. 3223-3232.
36. Rashidi, H., S. Strohbiecker, L. Jackson, S. Kalra, A.J. Blake, L. France, C. Tufarelli, and V. Sottile, *Differences in the Pattern and Regulation of Mineral Deposition in Human Cell Lines of Osteogenic and Non-Osteogenic Origin*. *Cells Tissues Organs*, 2011.
37. Sottile, V., A. Thomson, and J. McWhir, *In vitro osteogenic differentiation of human ES cells*. *Cloning Stem Cells*, 2003. 5(2): p. 149-55.
38. Rashidi, H., S. Strohbiecker, L. Jackson, S. Kalra, A.J. Blake, L. France, C. Tufarelli, and V. Sottile, *Differences in the Pattern and Regulation of Mineral Deposition in Human Cell Lines of Osteogenic and Non-Osteogenic Origin*. *Cells Tissues Organs*, 2011: p. 484 - 494.
39. Gregory, C.A., W.G. Gunn, A. Peister, and D.J. Prockop, *An Alizarin red-based assay of mineralization by adherent cells in culture: comparison with cetylpyridinium chloride extraction*. *Anal Biochem*, 2004. 329(1): p. 77-84.
40. Chad Munro, M.C., *Intramedullary rod with vent*, 2010: USA.
41. Ahmed, I., P.S. Cronin, E.A. Abou Neel, A.J. Parsons, J.C. Knowles, and C.D. Rudd, *Retention of mechanical properties and cytocompatibility of a phosphate-based glass fiber/polylactic acid composite*. *Journal of Biomedical Materials Research Part B: Applied Biomaterials*, 2009. 89B(1): p. 18-27.
42. Michael, A.S. and C.C. Chu, *Fiber-matrix interface studies on bioabsorbable composite materials for internal fixation of bone fractures. II. A new method using laser scanning confocal microscopy*. *Journal of Biomedical Materials Research*, 1997. 37(3): p. 353-362.
43. Bergeret, A., L. Ferry, and P. Ienny, *Influence of the fibre/matrix interface on ageing mechanisms of glass fibre reinforced thermoplastic composites (PA-6,6, PET, PBT) in a hygrothermal environment*. *Polymer Degradation and Stability*, 2009. 94(9): p. 1315-1324.

44. Haltia, A.-M., K. Lähteenkorva, P. Törmälä, A. Helminen, J. Tuominen, J. Seppälä, S. Veittola, and J. Ahvenlammi, Self-reinforcement and hydrolytic degradation of amorphous lactic acid based poly(ester-amide), and of its composite with sol-gel derived fibers. *Journal of Materials Science: Materials in Medicine*, 2002. 13(10): p. 903-909.
45. BS ISO 3597-3: 2003, Textile-glass-reinforced plastics. Determination of mechanical properties on rods made of roving-reinforced resin. Determination of compressive strength
46. Pietrzak, W.S., D.S. Caminear, and S.V. Perns, Mechanical characteristics of an absorbable copolymer internal fixation pin. *The Journal of Foot and Ankle Surgery*, 2002. 41(6): p. 379-388.
47. Lin, S., S. Krebs, A. Nazre, and R. King, Totally Bioabsorbable composites, in 39th International SAMPE Symposium 1994. p. 1981 - 1985.
48. Abou Neel, E.A., A.M. Young, S.N. Nazhat, and J.C. Knowles, A Facile Synthesis Route to Prepare Microtubes from Phosphate Glass Fibres. *Advanced Materials*, 2007. 19(19): p. 2856-2862.
49. Parsons, A.J., I. Ahmed, C.D. Rudd, G.J. Cuello, E. Pellegrini, D. Richard, and M.R. Johnson, Neutron scattering and ab initio molecular dynamics study of cross-linking in biomedical phosphate glasses. *Journal of Physics: Condensed Matter*, 2010. 22(48): p. 485403 -485411.
50. Brauer, D.S., N. Karpukhina, R.V. Law, and R.G. Hill, Effect of TiO₂ addition on structure, solubility and crystallisation of phosphate invert glasses for biomedical applications. *Journal of Non-Crystalline Solids*, 2010. 356(44-49): p. 2626-2633.
51. Brow, R.K., Review: the structure of simple phosphate glasses. *Journal of Non-Crystalline Solids*, 2000. 263-264: p. 1-28.
52. Walter, G., J. Vogel, U. Hoppe, and P. Hartmann, The structure of CaO-Na₂O-MgO-P₂O₅ invert glass. *Journal of Non-Crystalline Solids*, 2001. 296(3): p. 212-223.
53. Abou Neel, E.A., D.M. Pickup, S.P. Valappil, R.J. Newport, and J.C. Knowles, Bioactive functional materials: a perspective on phosphate-based glasses. *Journal of Materials Chemistry*, 2009. 19(6): p. 690-701.
54. Sales, B.C., L.A. Boatner, and J.O. Ramey, Chromatographic studies of the structures of amorphous phosphates: a review. *Journal of Non-Crystalline Solids*, 2000. 263-264: p. 155-166.
55. Bunker, B.C., G.W. Arnold, and J.A. Wilder, Phosphate glass dissolution in aqueous solutions. *Journal of Non-Crystalline Solids*, 1984. 64(3): p. 291-316.
56. Parsons, A.J., L.D. Burling, C.A. Scotchford, G.S. Walker, and C.D. Rudd, Properties of sodium-based ternary phosphate glasses produced from readily available phosphate salts. *Journal of Non-Crystalline Solids*, 2006. 352(50-51): p. 5309-5317.

57. Abou Neel, E. and J. Knowles, *Physical and biocompatibility studies of novel titanium dioxide doped phosphate-based glasses for bone tissue engineering applications*. *Journal of Materials Science: Materials in Medicine*, 2008. 19(1): p. 377-386-386.
58. Brauer, D.S., C. Rüssel, W. Li, and S. Habelitz, *Effect of degradation rates of resorbable phosphate invert glasses on in vitro osteoblast proliferation*. *Journal of Biomedical Materials Research Part A*, 2006. 77A(2): p. 213-219.
59. Hoppe, A., N.S. Güldal, and A.R. Boccaccini, *A review of the biological response to ionic dissolution products from bioactive glasses and glass-ceramics*. *Biomaterials*, 2011. 32(11): p. 2757-2774.
60. Salih, V., K. Franks, M. James, G.W. Hastings, J.C. Knowles, and I. Olsen, *Development of soluble glasses for biomedical use Part II: The biological response of human osteoblast cell lines to phosphate-based soluble glasses*. *Journal of Materials Science: Materials in Medicine*, 2000. 11(10): p. 615-620.
61. Uo, M., M. Mizuno, Y. Kuboki, A. Makishima, and F. Watari, *Properties and cytotoxicity of water soluble Na₂O-CaO-P₂O₅ glasses*. *Biomaterials*, 1998. 19(24): p. 2277-2284.
62. Navarro, M., M.P. Ginebra, and J.A. Planell, *Cellular response to calcium phosphate glasses with controlled solubility*. *J Biomed Mater Res A*, 2003. 67(3): p. 1009-15.
63. Han, N., I. Ahmed, A.J. Parsons, L. Harper, C.A. Scotchford, B.E. Scammell, and C.D. Rudd, *Influence of screw holes and gamma sterilization on properties of phosphate glass fiber-reinforced composite bone plates*. *J Biomater Appl*, 2011.
64. Maeno, S., Y. Niki, H. Matsumoto, H. Morioka, T. Yatabe, A. Funayama, Y. Toyama, T. Taguchi, and J. Tanaka, *The effect of calcium ion concentration on osteoblast viability, proliferation and differentiation in monolayer and 3D culture*. *Biomaterials*, 2005. 26(23): p. 4847-4855.

CHAPTER 6.

PREPARATION AND CHARACTERISATION OF BIORESORBABLE SCREWS BASED ON PLA AND PBG FIBRES

6.1 SUMMARY

In trauma and orthopaedic surgery, screws can be used to fix fracture plates to bone segments or to fix bone fractures directly without plates, depending on the type and location of the fracture. Bioresorbable screws are required to overcome the complications of metallic screws currently in use. Removal of metallic screws after the bone has healed is a serious issue that can lead to refracture at site due to the presence of screw holes. Phosphate based glass fibres were used to reinforce poly lactic acid (PLA) in order to produce unidirectionally aligned (UD) and combined unidirectional plus randomly distributed (UD/RM) composite screws (P40 UD and P40 UD/RM) via thermomechanical deformation method. The maximum flexural and push-out properties for the composite screws (P40 UD and P40 UD/RM) increased by almost 100 % in comparison with the PLA screws. Whilst the pull-out strength and stiffness of the headless composite screws were ~ 80 % (strength) and ~ 130 % (stiffness) higher than for PLA, those with heads exhibited properties lower than those for PLA alone as a result of failure at the head. An increase in the maximum shear load and stiffness for the composite screws (~ 30 % and ~ 40 %) in comparison to the PLA screws was also observed. Maximum torque for the PLA screws was ~ 1000 mN.m, whilst the composite screws were slightly lower. Water uptake and mass loss for the composite screws increased gradually to reach ~ 1.25 % and ~ 1.1 % respectively, after 42 days of degradation in PBS at 37°C. The mechanical properties for the composite screws decreased initially after 3 days of degradation and this reduction was ascribed to the degradation of the fibre/matrix interface. Afterwards, a plateau was observed for the mechanical properties (flexural, shear and pull-out) which were maintained for the duration of the study

at 42 days. This was attributed to the chemical durability of the fibre and stability of the matrix properties during degradation.

6.2 INTRODUCTION

Researchers and clinicians have investigated a range of different fixation techniques (internal and external) to address bone fractures resulting from trauma. Approaches to fixation have included the use of screws, pins, rods and plates. A screw and plate system is the most commonly used for internal fixation of bone fractures to stabilise bone fragments [1].

Fixation devices like plates and screws are made commonly of Titanium, Cobalt chromium alloys and Stainless steel. Metallic screws are used commonly to restore the normal function of bone at fracture sites due to their mechanical properties and stability. However, complications can arise with the use of metallic implants such as requirements for removal operations, allergic responses, corrosion, MRI interference, long term infection issues and have also been known to cause bone atrophy as a result of the mismatch between the mechanical properties of bone and metal (causing stress shielding) [2]. Use of bioresorbable materials could potentially eliminate all of the drawbacks associated with metals. Mechanical properties of bone screws based on bioresorbable polymers alone are not adequate to fix bone fractures except in relatively low load bearing applications such as the face or skull (i.e. craniomaxillofacial) fractures. Bioresorbable screws have been manufactured from self-reinforced [2-9] and particulate [10, 11] composites.

Insertion torque and pull-out strength for screws depend on the size of the pre-drilled hole in the bone sample. However, Gantous *et al.* [12] determined that increasing the size of the hole by up to 80 % of the outer diameter of the screws did not influence the pull-out strength significantly which was suggested to be due to the ratio of the core to outer diameter of the screws. Battula *et al.* [13] reported that the insertion torque and pull-out strength of self-tapping Synthes stainless steel cortical screws (3.5 mm diameter) decreased by ~ 30 % of the initial values (~ 500

mN.m and ~ 1.5 kN) as the hole size increased from 70 % to 80 % of the outer diameter of the screw. They suggested that this decrease was due to the use of an osteoporotic bone model.

In vitro and *in vivo* degradation were investigated for SR-PLLA screws (4.5 mm diameter) by Suuronen *et al.* [5]. They found that the shear strength for these screws decreased from 110 MPa (before degradation) to 3.3 MPa and 4.2 MPa after 48 weeks of *in vitro* and *in vivo* degradation. They also reported an approximate 30 % and 40 % loss of the initial shear strength values after 12 weeks of *in vitro* and *in vivo* studies respectively. The strength loss *in vivo* was faster than that *in vitro* during the whole period. They attributed this to enzymatic degradation and movements of the animals used. Similar findings were demonstrated by Pohjonen *et al.* [7] for compression moulded and machine cut SR-PLA 4.5 and 3.5 mm screws.

Maximum shear and pull-out load retention for screws (composed of PLLA/PGA (18/82) copolymer) were investigated during *in vitro* degradation in PBS at 37°C using a synthetic bone model (polyurethane foam). The initial maximum shear and pull-out load reported was 218.5 N and 197 N, respectively. Shear strength remained constant for 8 weeks with pull-out remaining constant for 2 weeks. After which, they lost more than 90 % of their initial properties by 12 weeks [14].

Shikinami *et al.* [10] manufactured mini-screws of dimensions 2/1.6/1/8 mm (major/minor diameter/pitch/length) by forging and machining PLLA/HA and compared their mechanical properties with pure PLLA and titanium (Ti) screws of the same size. Pull-out strengths recorded were 134 N, 162 N and 198 N for PLLA/HA, PLLA and Ti screws respectively. The ultimate torsional load for PLLA and PLLA/HA screws was similar (7.5 N) and 20 % of that for the Ti screws. They also found that the maximum torsional load for PLLA/HA screws remained constant for 20 weeks and thereafter decreased gradually to 3 N after 50 weeks of degradation in PBS at 37°C.

PLA/PGF composite plates and rods have been investigated previously for their degradation and mechanical retention properties in Chapters 3, 4 and 5. However, the focus of this chapter was investigation of totally bioresorbable composite screws based on PLA and PGF prepared using two different fibre architectures, fully unidirectional (UD) and a combination of UD and random mats (UD/RM) with ~ 30 % fibre volume fraction. *In vitro* degradation and mechanical retention (Flexural, shear and pull-out) properties were investigated up to 42 days in phosphate buffer solution (PBS) at 37°C.

Different mechanisms of failure were reported during fixation by screws such as screw pullout, screw fracture by bending or torsion and bone failure due to increasing stress concentration especially for metallic screws [15, 16]. From these various modes of failure it is necessary to assess potential new screw types using varying methods including; maximum pull-out, flexural, shear and torque to identify potential modes of failure.

6.3 MATERIALS AND METHODOLOGY

6.3.1 Composite Production

Unidirectional (UD) and unidirectional/randomly combined fibre mat (UD/RM) composite plates were manufactured using phosphate-based glass fibres (PGF) as reinforcement and PLA as matrix. PGFs with a composition of 40P₂O₅ - 24MgO - 16CaO - 16Na₂O - 4Fe₂O₃ in mol% (denoted as P40) were used in this chapter. Manufacture process for composites was previously mentioned in sections 3.3.1, 3.3.2 and 3.3.3.

6.3.2 Method of screw manufacture

PLA, P40 UD/RM (70/30) and P40 UD composite screws were prepared via a thermomechanical deformation (forging method) using composite bars. Continuous unidirectional (UD) and in plane chopped strand random mat fibres (RM) within

the manufactured composite screws were parallel to their longitudinal axis. The laminated composites and pure PLA plates produced were cut into 40 mm length x 6.5 mm width x 4.5 mm height, using a band saw and placed into the cavity of a specially made mould to manufacture screws (see **Figure 6-1-a**). The mould was heated in the press for 10 mins at 90°C and then pressed for 30 sec at 3 bar. The side of the mould was compressed via a screw threaded rod at the end of the composite bar into the square head of the screws. Afterwards, the mould was transferred to another cold press for cooling under 3 bar for 5 mins. The finished screws had dimensions of 6 mm outer diameter, 4.75 mm core diameter and 32 mm length (see **Figure 6-1-b**) and **Figure 6-2**). The fibre volume and mass fractions of the composite screws were obtained using the matrix burn off method, according to the ASTM standard test method (ASTM D2584-94) [17]. See **Table 6-1** for details of the screws produced in this study.

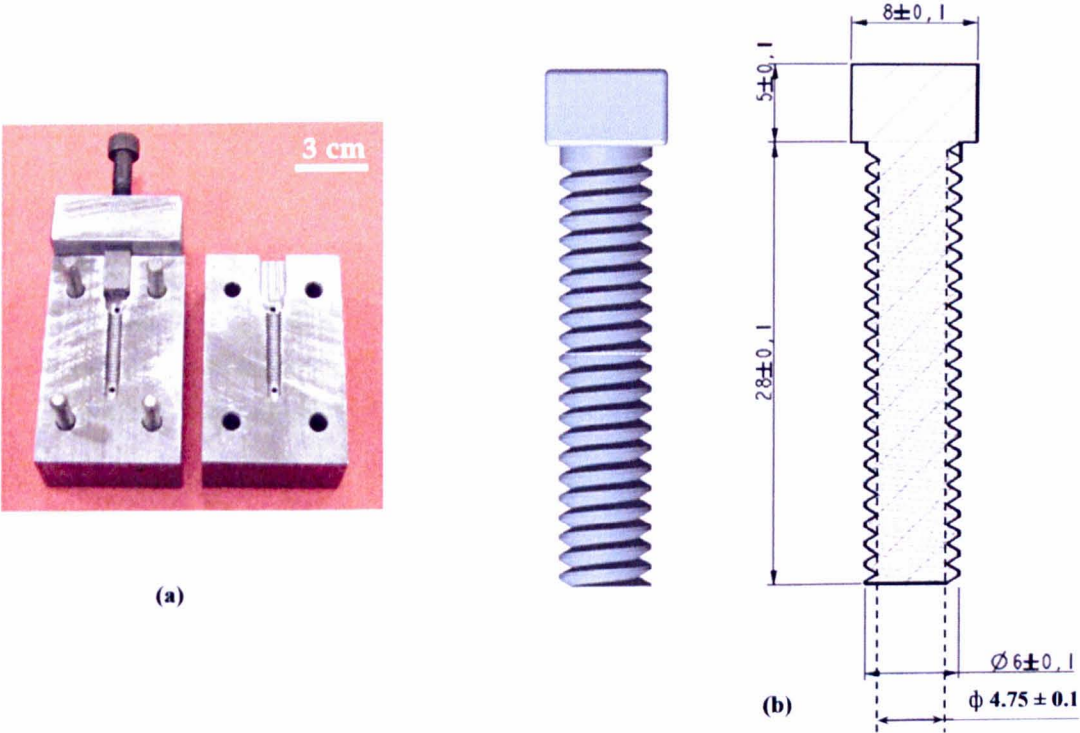


Figure 6-1: (a) *Photograph of the mould used for manufacturing screws* and (b) *Dimensions (mm) of the produced screws.*

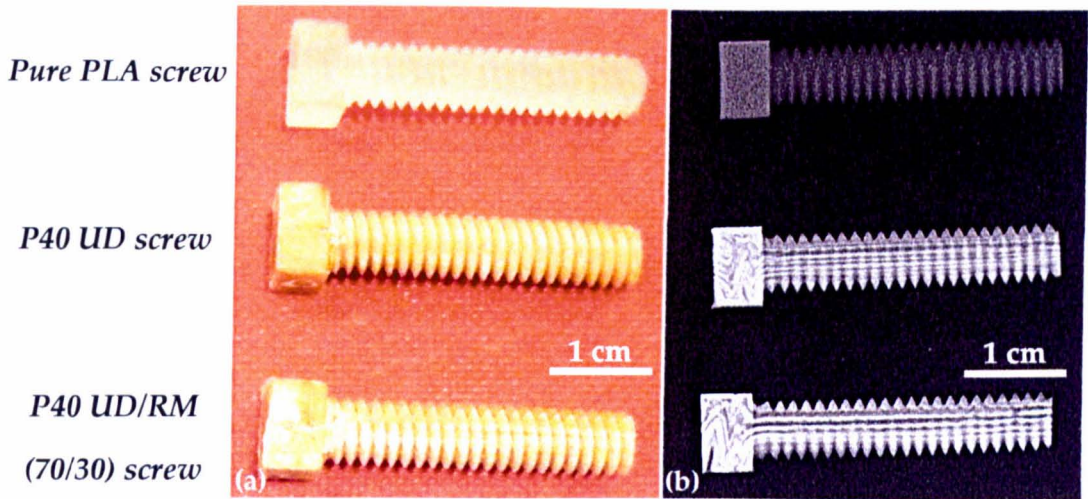


Figure 6-2: (a) Optical and (b) X-ray photographs for PLA, P40 UD and P40 UD/RM screws used in this chapter.

Table 6-1: Fibre volume, mass fractions and sample codes for the specimens investigated in this chapter.

Sample code	Specimen	Fibre mass fraction (%)	Fibre volume fraction V_f (%)
PLA	Pure PLA screws	-	-
P40 UD/RM	P40 unidirectional 70 % / random mat 30 % composite screws	50 ± 3	31 ± 3
P40 UD	P40 unidirectional composite screws	50 ± 2	31 ± 2

6.3.3 Mechanical tests for screws

6.3.3.1 Flexural testing

The maximum flexural load and stiffness for screws were evaluated by flexural (three-point bending) tests using a Hounsfield Series S testing machine at room temperature ($\sim 20^{\circ}\text{C}$). A crosshead speed of 5 mm/min and a 1 kN load cell was used. The support span was 20 mm and radii for loading applicator and supports

were 2.5 mm. The maximum flexural load was the maximum value recorded during the test and the stiffness was the maximum gradient in the load – deflection plot (see Figure 6-4). Measurements were conducted in triplicate ($n = 3$).

6.3.3.2 Pull-out test

The axial pull-out strength and stiffness were determined using an Instron 5969 according to the standard ASTM F 2502-05 [18] using a modified setup (see Figure 6-3-a for equipment used). The screw was inserted to a depth of 15 mm (i.e. 60%) of the total length of the screw-thread into a tapped stainless steel test block. The loading fixture was made of stainless steel bar with a slot to house the screw head. The fixture was perfectly aligned with the longitudinal axis of the screw and attached to the load frame of the Instron testing machine. A crosshead speed of 5 mm/min and a 25 kN load cell was used. The measurements were carried out in triplicate ($n = 3$). The axial pull-out strength was taken to be the maximum load reached during the test. The type of failure was also reported. The pull-out test was applied also for headless screws in a thread to thread test after insertion of 30 % (7.5 mm) of the overall thread length into each tapped jaw (see Figure 6-3-b for the setup used). Furthermore, push-out test was conducted on whole and headless screws (see Figure 6-3-c and Figure 6-3-b) using the variables mentioned previously. The pull-out and push-out stiffness were taken to be the maximum gradient of the linear portion in the load – deflection plot (see Figure 6-4).

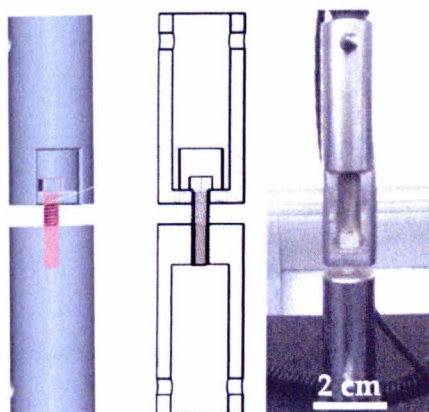
6.3.3.3 Double shear test

The maximum shear load and stiffness for PLA alone, P40 UD/RM (70/30) and P40 UD composite screws were measured using a modified double shear test according to the standard BS 2782-3:Methods 340A and 340B:1978 [19] and ASTM D7617M-11 [20]. The testing arrangements for the double shear test were reported previously (see section 4.3.3.2). The crosshead speed of the machine was 5 mm/min and the load cell capacity was 5 kN. The maximum shear load and stiffness were determined as the maximum load recorded during the test and the maximum gradient in the load – deflection plot (see Figure 6-4). The measurements were carried out in triplicate ($n = 3$).

6.3.3.4 Torsional testing

The maximum torque, stiffness and breaking angle were measured for the screws produced according to the standard ASTM F 2502-05 [18] using torque arrangements (see **Figure 6-3-d**) attached to an Instron 3367. A tensile force was converted into torque by using a rotating wheel mounted onto a bearing stand. Calibration was performed in order to convert the axial deflection into a rotation angle. The crosshead speed of the machine was 5 mm/sec, which equated to 1 revolution per minute (RPM) according to the calibration and the load cell capacity was 33 kN. According to the standard, the gauge length should be 20 % (~ 6 mm) of the total thread length as the screws are fully threaded. The maximum torque is represented by the highest recorded value of the torque during the test and the breaking angle was the rotation angle at the maximum torque. Torsional stiffness was determined as the maximum gradient in the torsional load – angle plot. The measurements were carried out in triplicate ($n = 3$).

Neither natural bone nor synthetic bone models were used in this study. Metallic tools were applied in order to determine the optimum mechanical properties of the screws and eliminate variability which exists in natural bone and potentially in bone model materials. All tests were carried out at room temperature (~ 20°C).



(a)

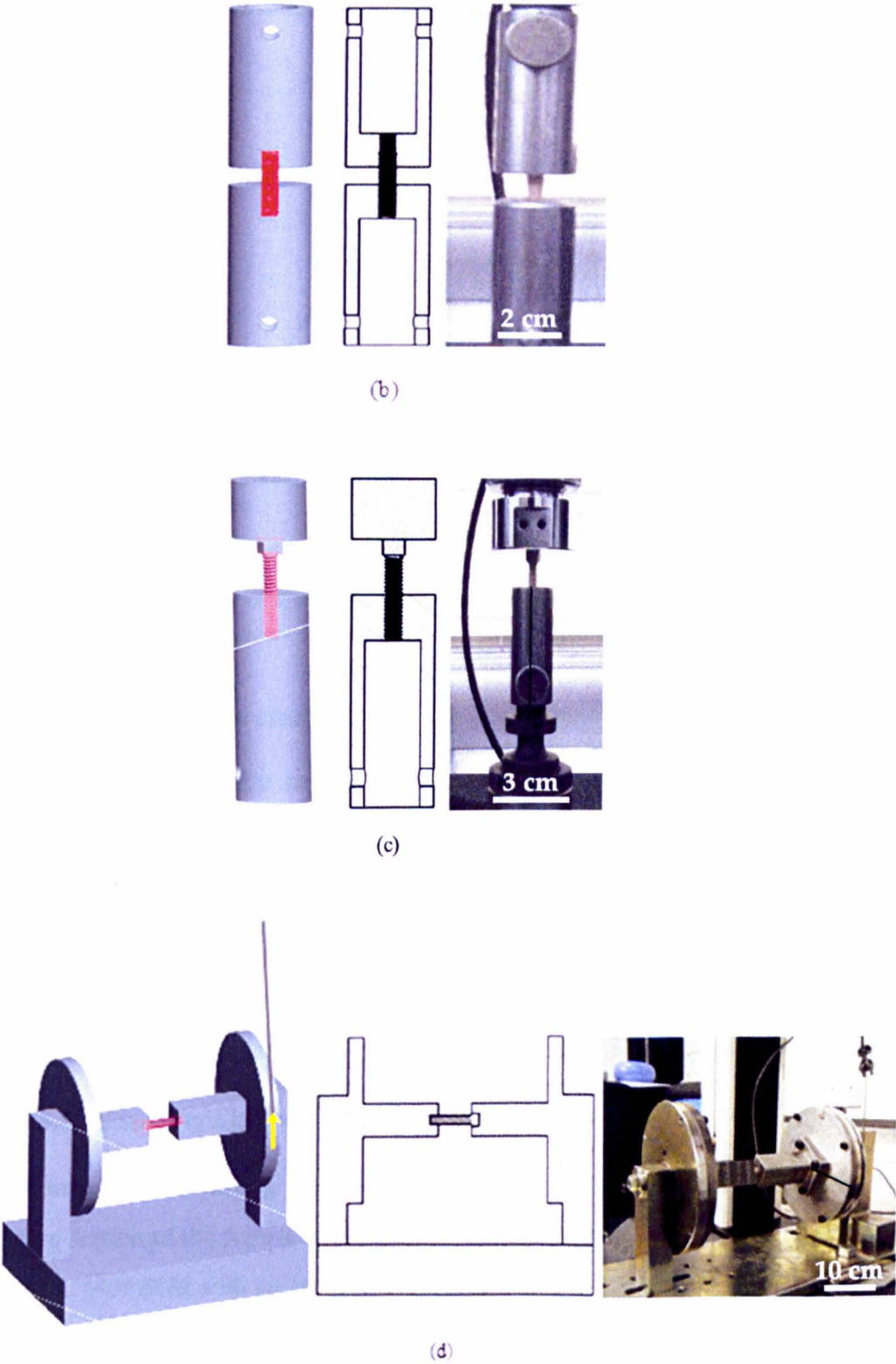


Figure 6-3: Mechanical testing setup for (a) Screw pull-out, (b) headless screw pull-out and push-out, (c) screw push-out and (d) torsional test.

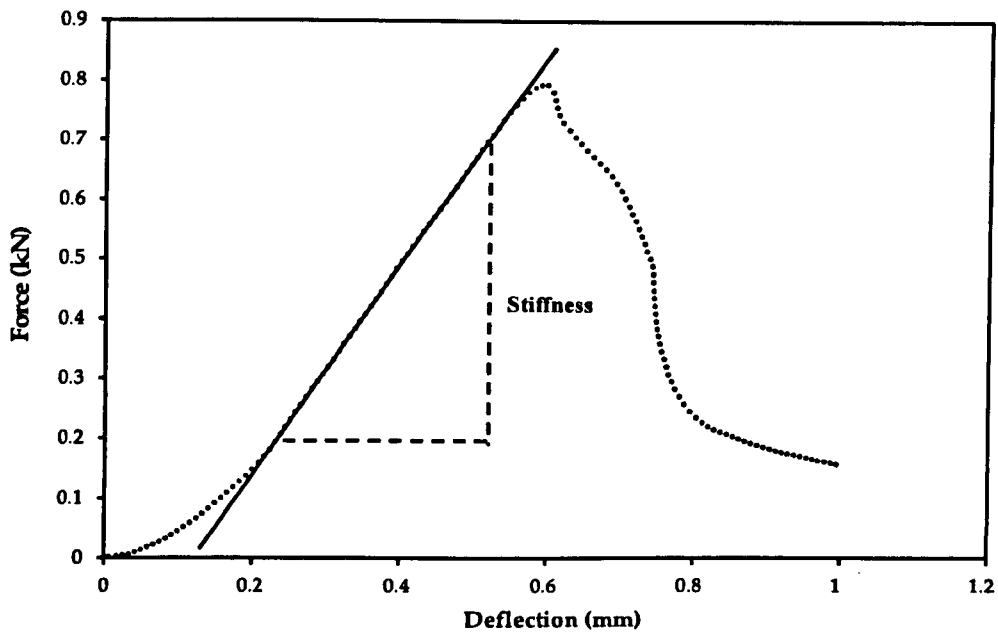


Figure 6-4: Example of applied force against deflection plot during different mechanical tests for screws. The stiffness was determined as the maximum gradient of the linear portion of the force-deflection curve.

6.3.3.5 Degradation study

The degradation study of the screws produced was done according to the procedure mentioned previously in section 3.3.8. The percentage wet mass change (M_w), mass loss (M_L) and water uptake (W) were determined using Equation 3-2, Equation 3-3 and Equation 3-4

Statistical analysis was conducted for the degradation and mechanical tests using one-way ANOVA as mentioned previously in section 3.3.13.

6.3.3.6 Scanning Electron Microscopy (SEM)

Fractured screws during the flexural test were examined via SEM investigation. Cross-section of the screws were sputter-coated with platinum and examined using a JEOL 6400 SEM with an accelerating voltage of 10 kV in secondary electron mode (SE).

6.4 RESULTS

6.4.1 Initial Mechanical properties

Figure 6-5 shows the maximum flexural load and stiffness for PLA, P40 UD and P40 UD/RM composite screws. The flexural load and stiffness values for P40 UD were double ($P < 0.001$) that for pure PLA screws. For P40 UD/RM screws, the maximum load and stiffness were ~ 75 % (significant, $P < 0.05$) and ~ 100 % (significant, $P < 0.001$) higher than the PLA screws (~ 190 N and ~ 200 N.mm⁻¹) respectively.

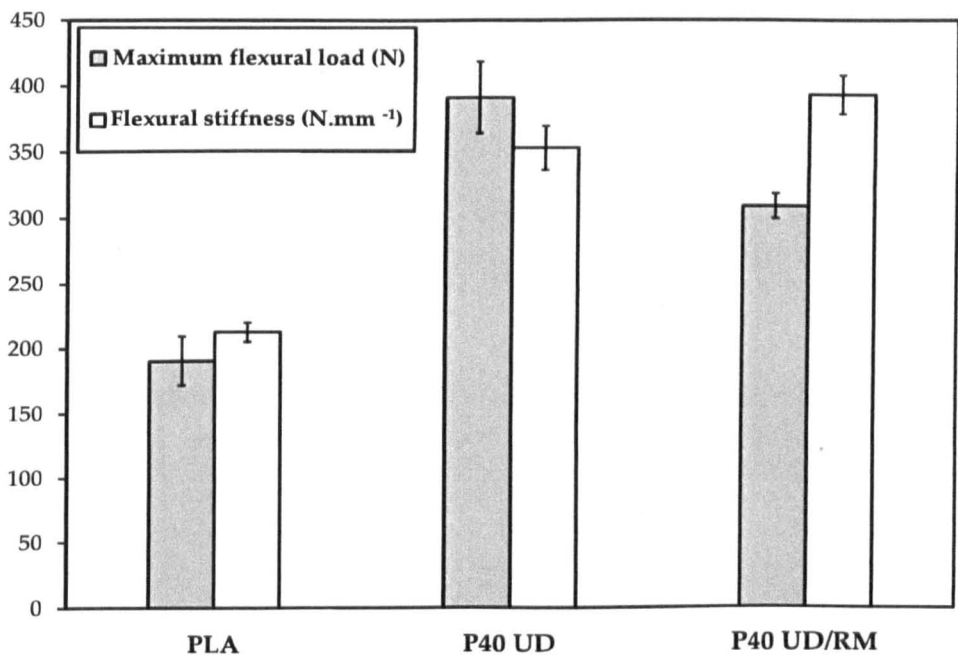


Figure 6-5: Flexural load to failure and stiffness for PLA, P40 UD and P40 UD/RM screws.

Axial pull-out strength and stiffness for PLA and composite screws are shown in Figure 6-6. The pull-out strength and stiffness for PLA screws were ~ 0.9 kN and ~ 1.7 kN.mm⁻¹. P40 UD and P40 UD/RM composite screws had slightly higher (not significant, $P > 0.05$) pull-out stiffness with lower strength (significant, $P < 0.05$) than that for PLA screws. The axial pull-out strength for headless PLA screws was very

similar to that of the screws with heads and their stiffness was slightly higher (~ 2 kN.mm⁻¹) (see **Figure 6-7**). For P40 UD headless screws, the pull-out strength and stiffness increased by ~ 80 % ($P < 0.05$) and ~ 130 % ($P < 0.001$) in comparison to the PLA headless screws. The pull-out strength for P40 UD/RM headless screws was similar to the PLA ($P > 0.05$) and the stiffness was around 75 % ($P < 0.001$) higher than for the headless PLA screws.

Figure 6-8 and **Figure 6-9** show the maximum push-out strength and stiffness for PLA, P40 UD and P40 UD/RM composite screws, with and without heads. Screws with heads recorded significantly higher ($P < 0.001$) push-out properties than the headless screws. The push-out stiffness values for the composite screws both with and without heads were approximately twice ($P < 0.001$) those obtained for the PLA screws (~ 2.8 kN.mm⁻¹). The maximum push-out loads for the P40 UD and P40 UD/RM screws were ~ 70 % (significant, $P < 0.05$) higher than those of the PLA.

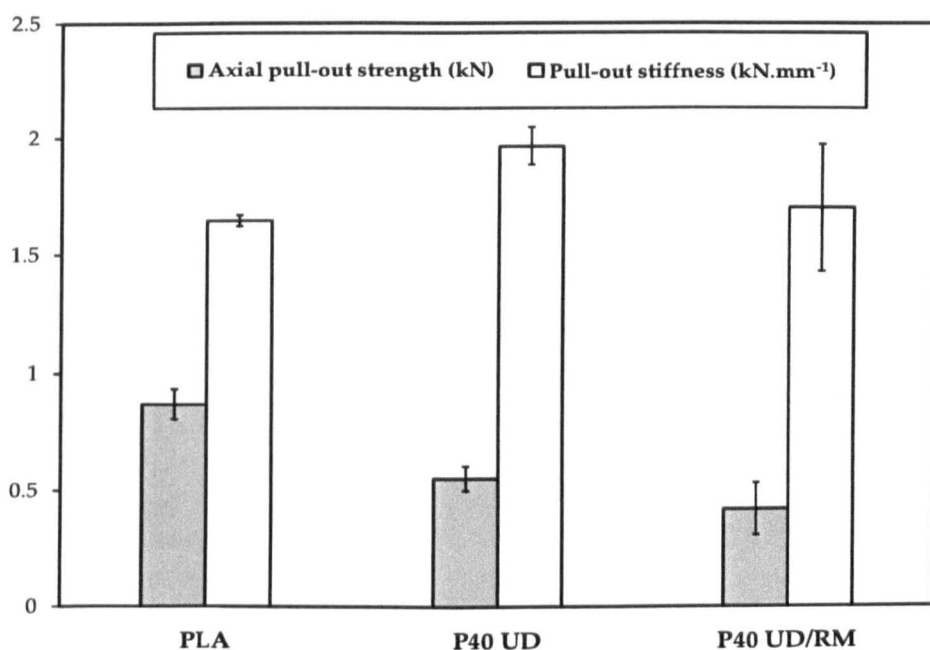


Figure 6-6: Axial pull-out strength and stiffness for PLA, P40 UD and P40 UD/RM screws.

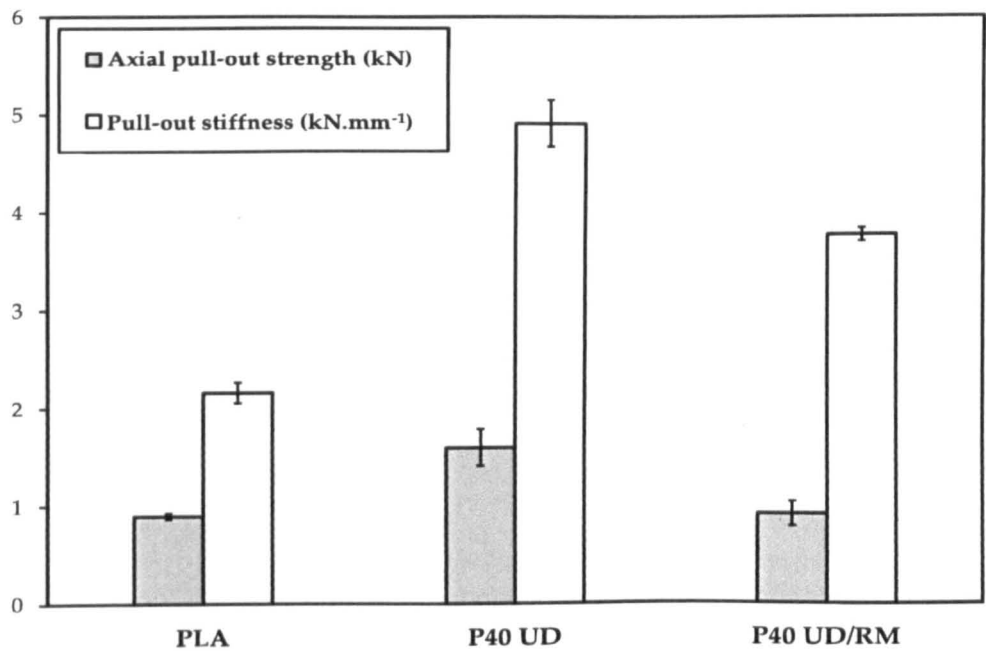


Figure 6-7: Axial pull-out strength and stiffness for PLA, P40 UD and P40 UD/RM headless screws.

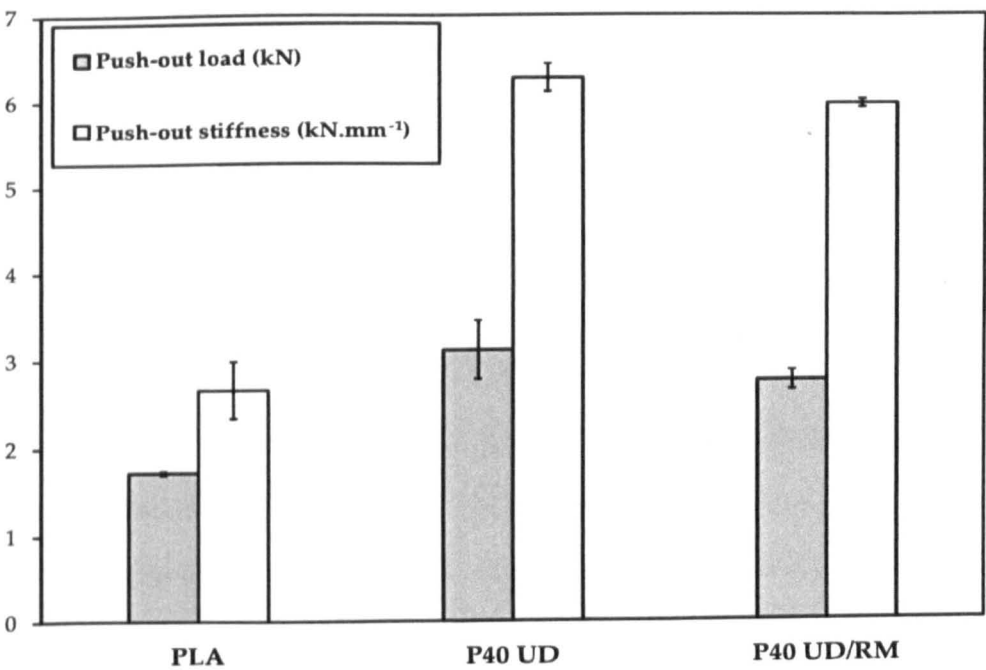


Figure 6-8: Push-out load to failure and stiffness for PLA, P40 UD and P40 UD/RM screws.

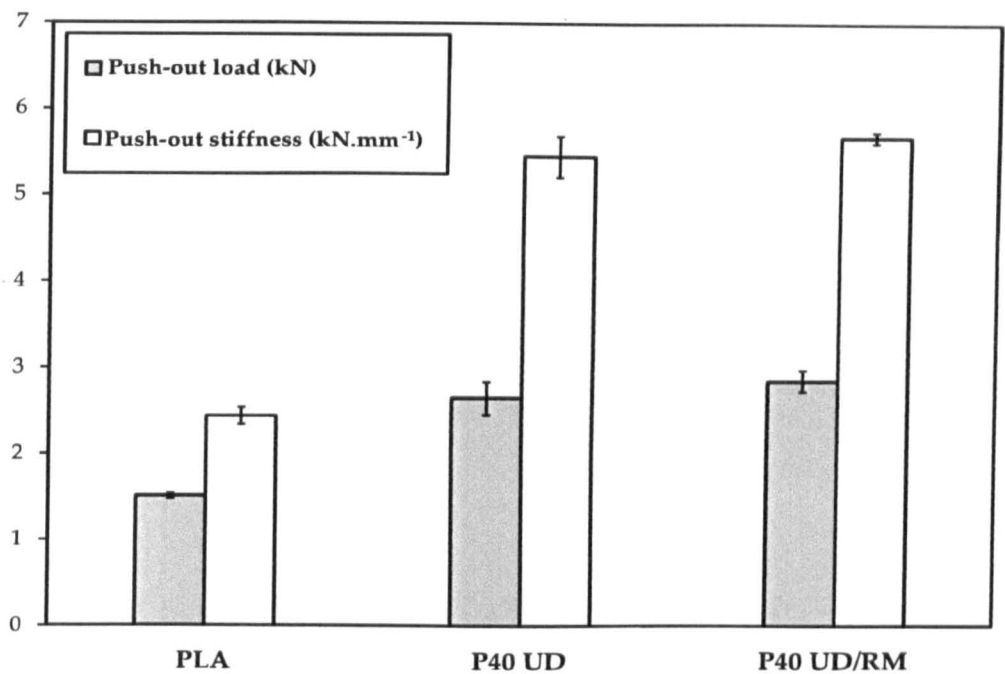


Figure 6-9: Push-out load to failure and stiffness for PLA, P40 UD and P40 UD/RM headless screws.

Double shear properties for the PLA, P40 UD and P40 UD/RM composite screws are shown in **Figure 6-10**. No significant difference ($P > 0.05$) between the maximum shear load and stiffness for P40 UD and P40 UD/RM screws was seen. The composite screws recorded an increase of ~ 40 % (significant, $P < 0.01$) in the shear stiffness in comparison with the pure PLA screws.

Figure 6-11 shows the torsional properties (maximum torque, breaking angle and torsional stiffness) for the PLA, P40 UD and P40 UD/RM composite screws investigated. The maximum torque values for the composite screws were slightly lower (not statistically significant, $P > 0.05$) than the PLA screws (~ 1000 mN.m). Breaking angles for the two composite screws were similar ($P > 0.05$) however half of the values obtained for PLA. Torsional stiffness for the P40 UD and P40 UD/RM screws were ~ 100 % ($P < 0.001$) and ~ 50 % ($P < 0.05$) higher than that for PLA (~ 100 mN.deg⁻¹) respectively. Failure modes for the PLA, P40 UD/RM and P40 UD screws associated with their respective mechanical tests are summarised in **Table 6-2**.

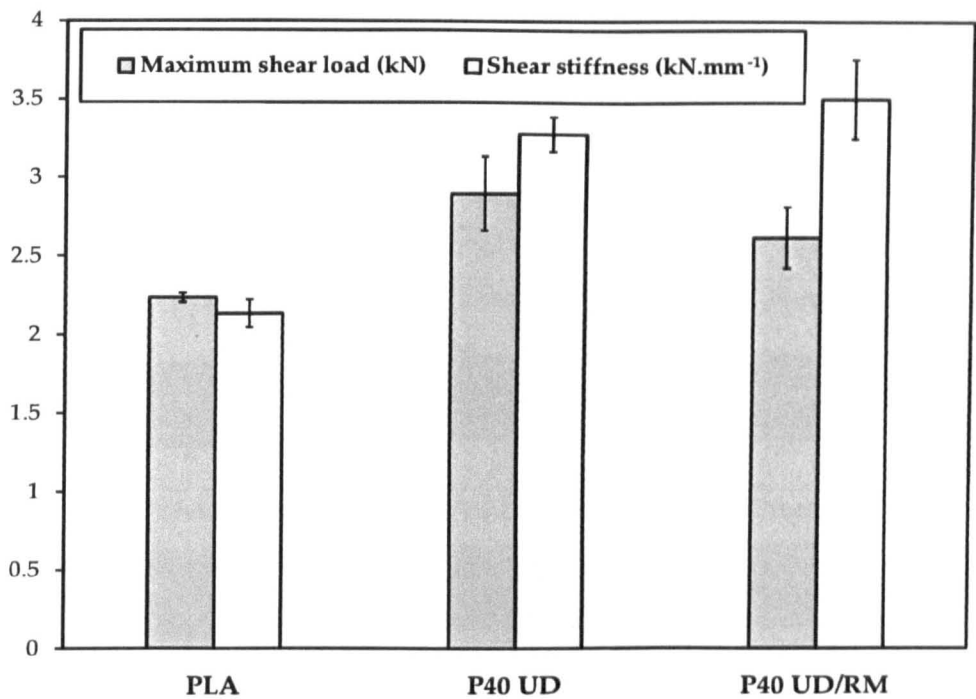


Figure 6-10: Shear load to failure and stiffness for PLA, P40 UD and P40 UD/RM screws.

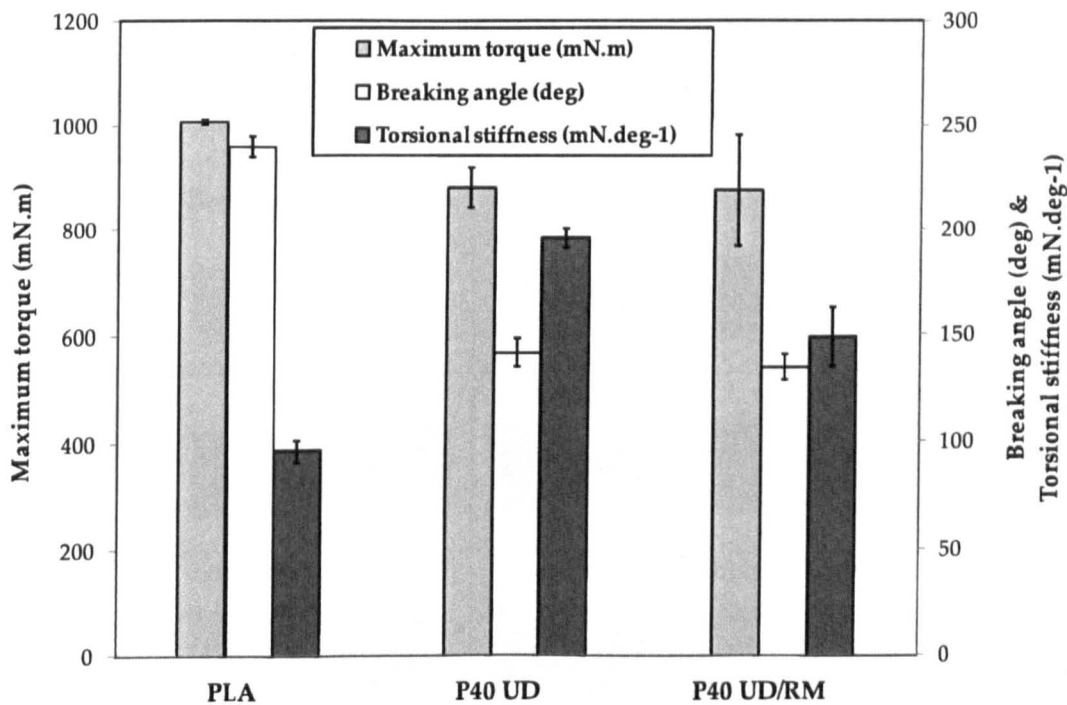










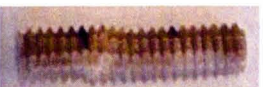



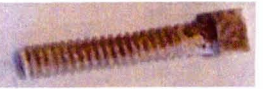








Figure 6-11: Maximum torque, breaking angle and torsional stiffness for PLA, P40 UD and P40 UD/RM screws.

Table 6-2: *Modes of failure for PLA, P40 UD/RM and P40 UD screws from the different mechanical tests conducted. Scale bars for all images represent 1 cm.*

Test	Mode of Failure		
	PLA screws	P40 UD/RM screws	P40 UD screws
Screw pull-out	Fracture at the core diameter 	Fracture below the head 	Fracture below the head 
Thread pull-out	Fractured at the core 	Fractured at the core 	Fractured at the core 
Screw push-out	Buckling 	Buckling 	Buckling 
Thread push-out	Buckling 	Buckling 	Buckling 
Torsion	Shear at gauge length 	Delamination at gauge length 	Delamination at gauge length 
Flexural testing (3 point bending)	Brittle failure 	Ductile failure 	Ductile failure 
Double Shear	Fractured at the core 	Fractured at the core 	Fractured at the core 

6.4.2 Degradation Properties

Wet mass change against time for PLA, P40 UD/RM and P40 UD screws during degradation in PBS at 37°C is seen in Figure 6-12. The wet mass change showed a rapid increase during the first week to ~ 0.9 % for PLA screws and ~ 0.7 % for composite screws. After 7 days, the wet mass profile for PLA screws remained constant ($P > 0.05$) whereas the composite screws decreased gradually to ~ 0.2 % towards the end of the study (42 days). No significant difference ($P > 0.05$) in the wet mass was observed between P40 UD/RM and P40 UD screws.

Figure 6-13 shows the change in pH profile of PBS with degradation time for PLA, P40 UD/RM and P40 UD screws. No significant difference ($P > 0.05$) in pH between the different samples was seen during the degradation period. The pH remained constant at ~ 7.5 for the duration of the study.

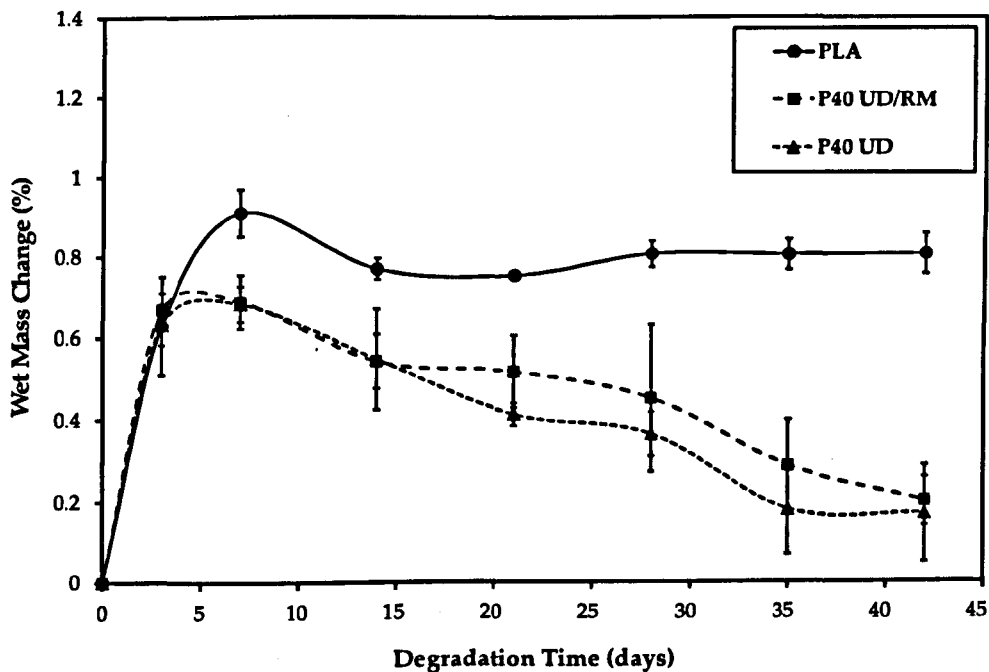


Figure 6-12: The percentage change in wet mass of PLA, P40 UD/RM and P40 UD composite screws immersed in PBS at 37°C.

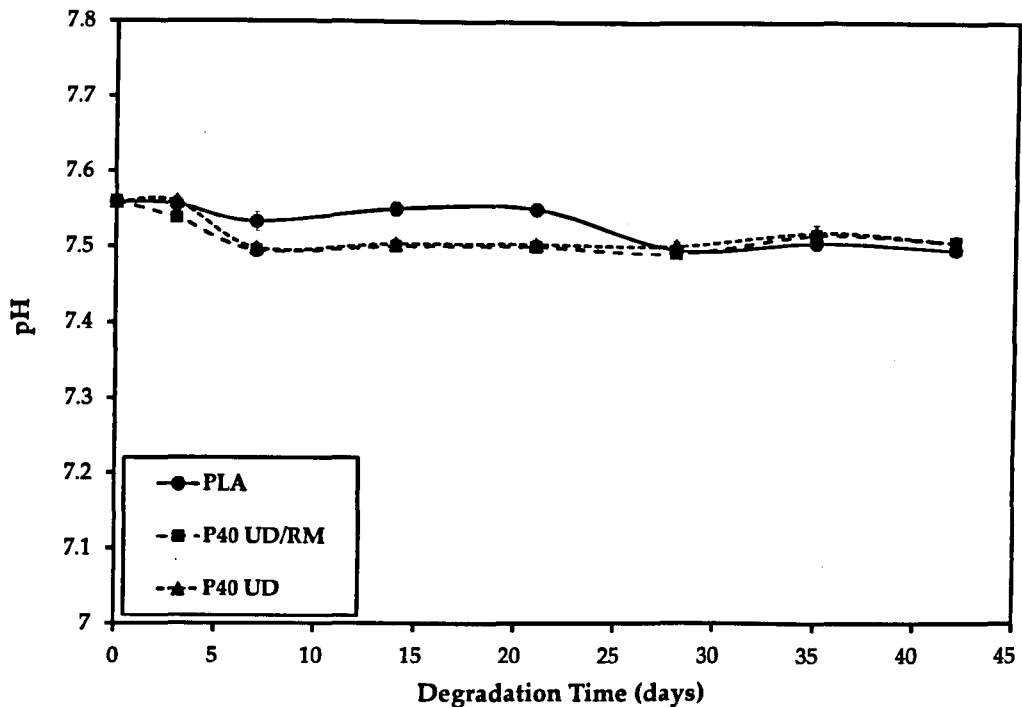


Figure 6-13: *pH change during immersion in PBS at 37°C for PLA alone, P40 UD/RM and P40 UD composite screws.*

The percentage of water uptake and mass loss against time for the samples investigated is seen in Figure 6-14 and Figure 6-15. Water uptake for PLA screws remained constant at ~ 0.8 % and no mass loss was observed until 42 days. No significant difference ($P > 0.05$) in water uptake and mass loss was observed between the composite screws (P40 UD/RM and P40 UD). The water uptake and mass loss for the composite screws increased gradually to ~ 1.25 % and - 1.1 % respectively.

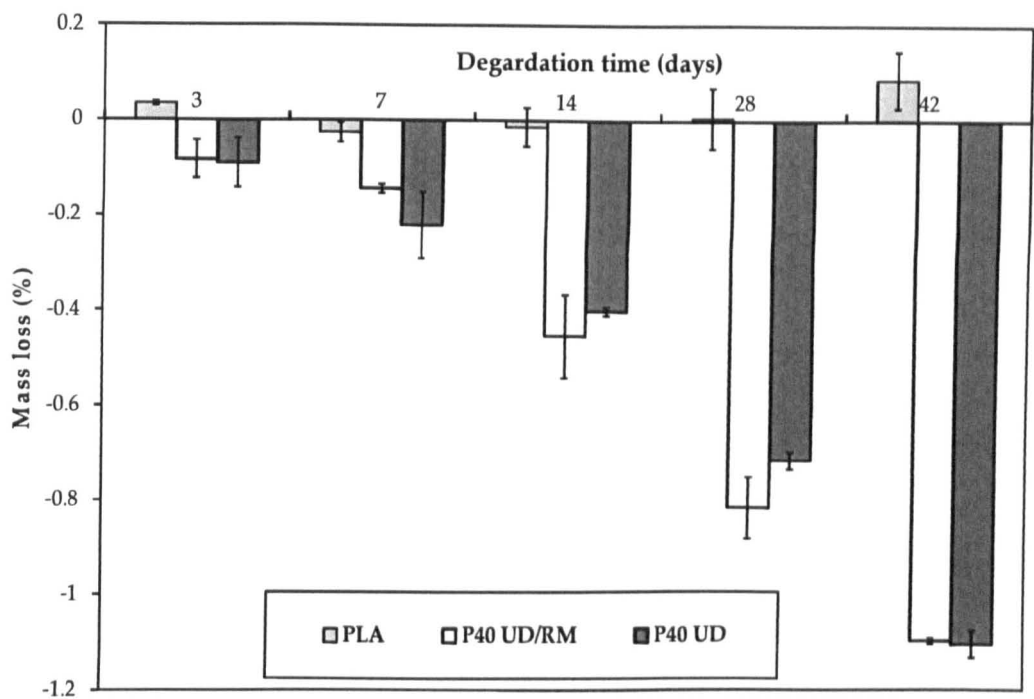


Figure 6-14: The percentage loss of mass with time for PLA alone, P40 UD/RM and P40 UD composite screws during degradation in PBS at 37°C.

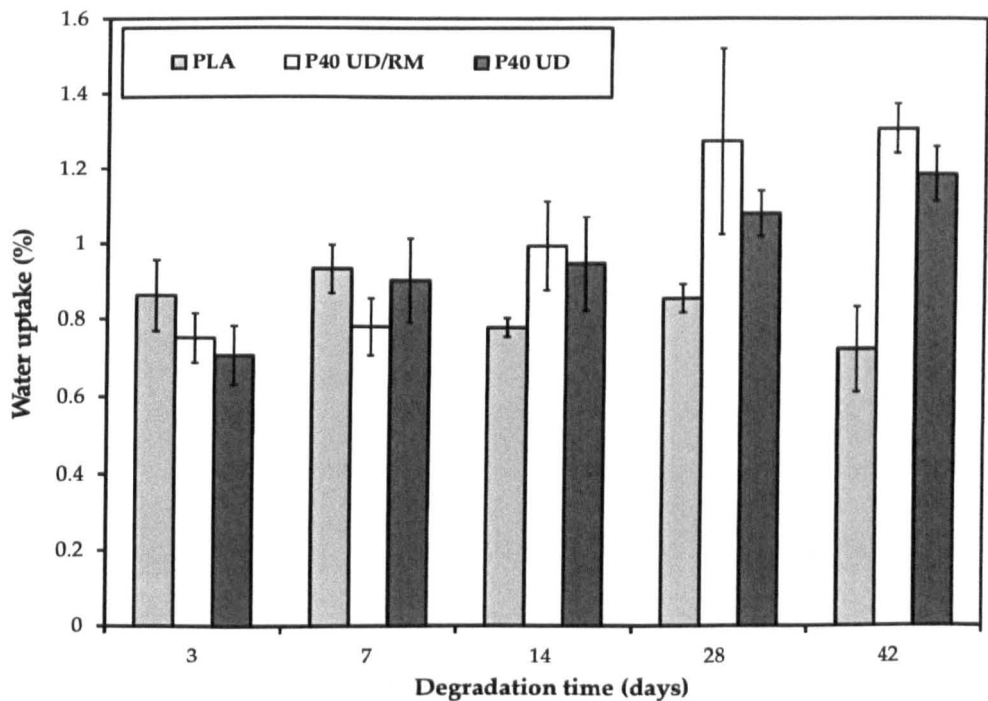


Figure 6-15: The percentage change in water uptake with time for PLA alone, P40 UD/RM and P40 UD composite screws during degradation in PBS at 37°C.

6.4.3 Mechanical Retention

Figure 6-16 and Figure 6-17 show the change in flexural properties for PLA, P40 UD/RM and P40 UD screws with degradation time. Flexural properties for P40 UD/RM and P40 UD screws decreased by ~ 50 % and ~ 30 % of the initial values (prior to degradation) respectively after 3 days of degradation in PBS, whereas no significant difference ($P > 0.05$) was seen for PLA screws. After 3 days immersion in PBS, P40 UD screws showed slightly higher flexural properties in comparison to P40 UD/RM and PLA screws. The maximum flexural load for PLA screws remained stable at ~ 170 N over 14 days in PBS at 37°C and then decreased slightly to ~ 130 N towards the end of the study. At 3 days, the maximum flexural load for P40 UD screws was ~ 260 N and afterwards decreased to ~ 130 N by the 42 day interval. The difference in flexural stiffness between the different screws investigated was not statistically significant ($P > 0.05$) over the degradation period (42 days). The flexural stiffness remained around 200 N. mm⁻¹ for the duration of the study.

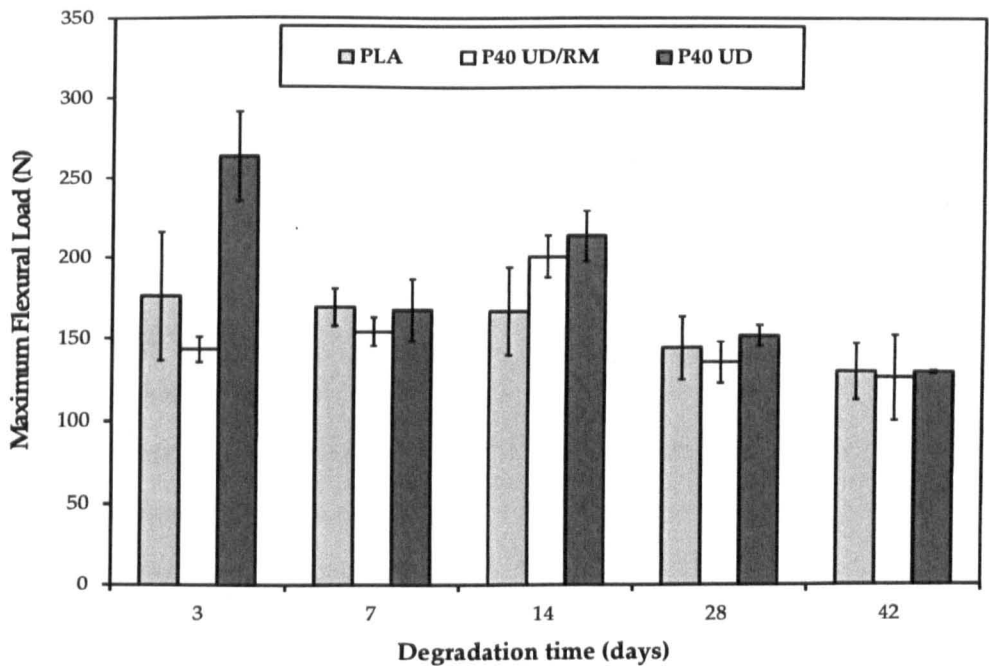


Figure 6-16: Flexural load to failure against time for PLA, P40 UD/RM and P40 UD screws. Samples measured wet, after immersion in PBS at 37°C.

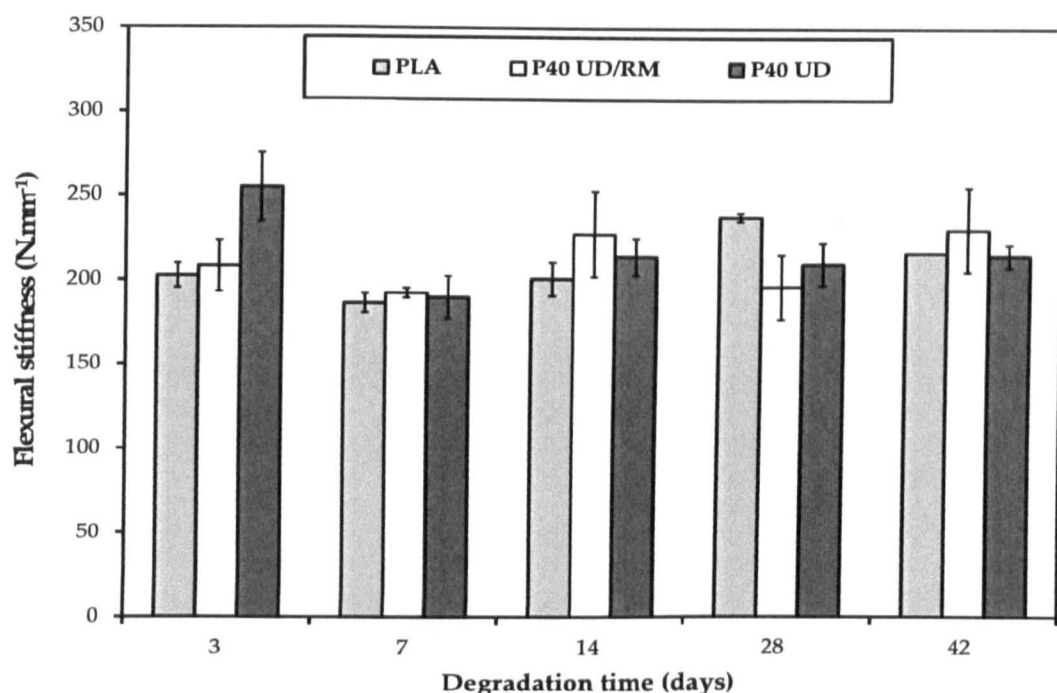


Figure 6-17: Change in flexural stiffness against time for PLA, P40 UD/RM and P40 UD screws. Samples measured wet, after immersion in PBS at 37°C.

The change in axial pull-out strength and stiffness for the screws against degradation time is shown in **Figure 6-18** and **Figure 6-19**. Composite screws (P40 UD/RM and P40 UD) lost approximately 50 % of their initial pull-out properties after degradation for 3 days in PBS at 37°C, while no change for PLA screws was seen. The axial pull-out strength for the PLA screws was significantly ($P < 0.01$) higher than that for the composite screws. It remained stable at ~ 0.85 kN for 28 days, after which it decreased to ~ 0.7 kN. No significant difference ($P > 0.05$) was observed between the pull-out strengths of the two sets of composite screws, which were approximately 0.55 kN for 14 days followed by ~ 15 % decrease by the end of the degradation study. The pull-out stiffness for PLA, P40 UD/RM and P40 UD screws was similar (no significant difference, $P > 0.05$) for 14 days, after which a decrease was seen for the composite screws; in particular the P40 UD/RM screws. The pull-out stiffness for PLA screws remained constant ($P > 0.05$) at ~ 2 kN. mm⁻¹ over the degradation study (42 days).

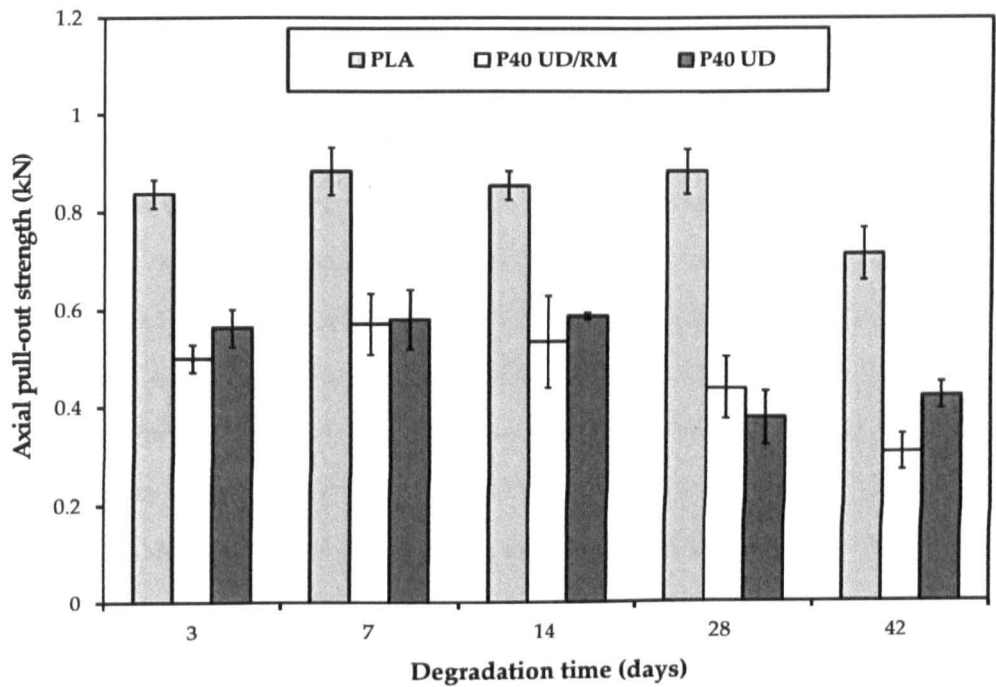


Figure 6-18: Axial pull-out strength over time for PLA, P40 UD/RM and P40 UD screws.
Samples measured wet, after immersion in PBS at 37°C.

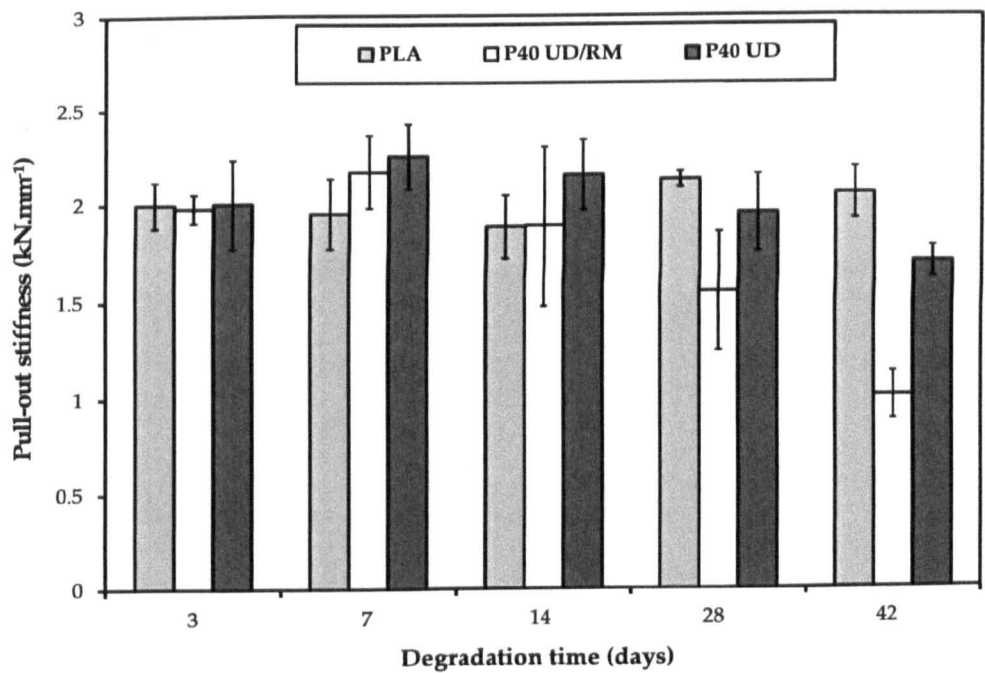


Figure 6-19: Pull-out stiffness over time for PLA, P40 UD/RM and P40 UD screws.
Samples measured wet, after immersion in PBS at 37°C.

From **Figure 6-20** and **Figure 6-21**, the change in the maximum shear load and stiffness over time can be seen for PLA, P40 UD/RM and P40 UD screws during degradation in PBS at 37°C. After 3 day immersion in PBS, maximum shear load for P40 UD/RM and P40 UD screws decreased by ~ 15 % of the initial values, whilst their stiffness decreased by ~ 50 % and ~ 40 %. Furthermore, PLA screws also showed ~ 20 % decrease in shear properties at day 3 time point. The maximum shear load for PLA screws was stable ($P > 0.05$) at approximately 1.8 kN during the study period of 42 days. For the composite screws, the shear loads were slightly higher than for the PLA screws. However, no significant differences ($P > 0.05$) in shear stiffness were seen between the PLA and composite screws up till 7 days, after which a slight decrease was seen for the composite screws at the 14 and 28 day interval. The composite screws exhibited a slightly higher stiffness (not statistically significant, $P > 0.05$) in comparison with the PLA screws at the end of the degradation study. Shear stiffness obtained for the screws varied between 1.8 and 2.2 kN. mm⁻¹ and the differences over time were seen to be not statistically significant ($P > 0.05$).

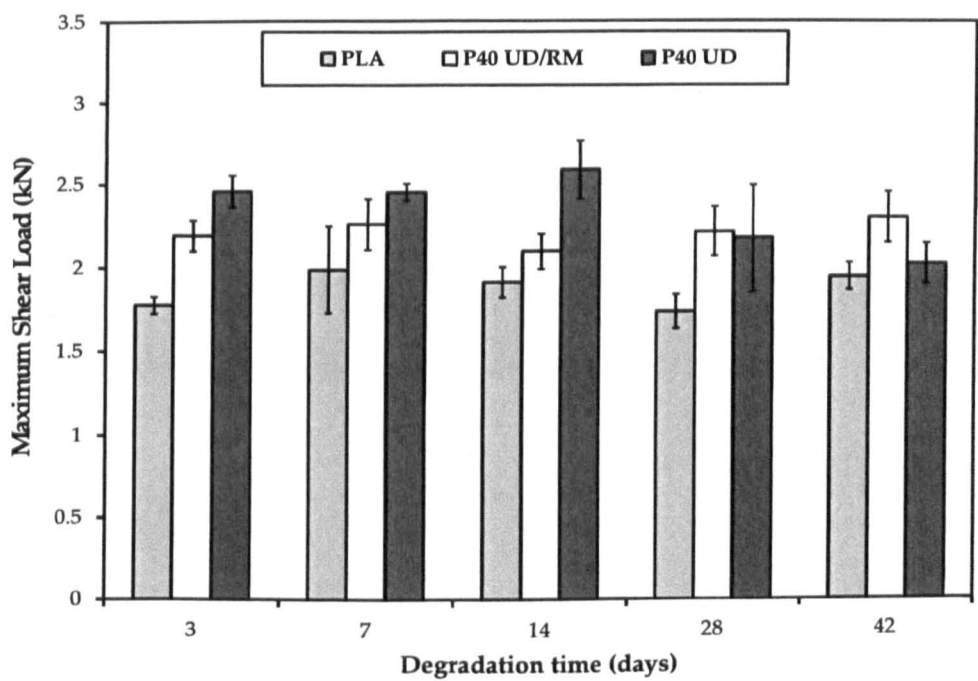


Figure 6-20: *Shear load to failure versus time for PLA, P40UD/RM and P40 UD screws. Samples measured wet, after immersion in PBS at 37°C.*

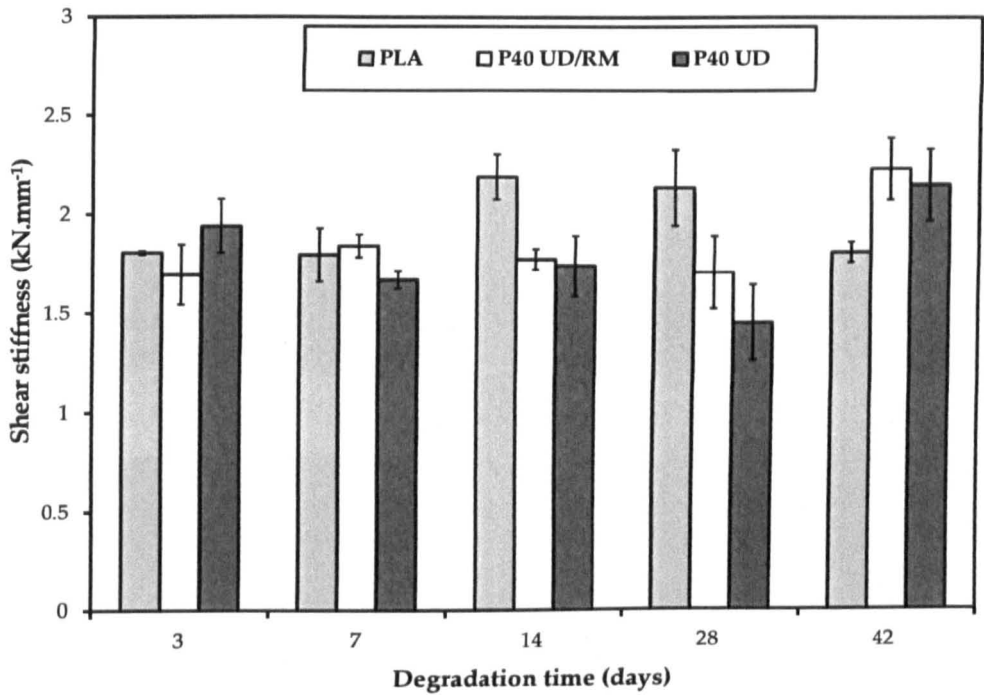


Figure 6-21: *Shear stiffness versus time for PLA, P40UD/RM and P40 UD screws. Samples measured wet, after immersion in PBS at 37°C.*

SEM micrographs of the fractured surfaces for P40 UD/RM and P40 UD composite screws before and after 42 days of degradation in PBS at 37°C can be seen in **Figure 6-22**. Before degradation, the fracture surfaces were flat and tiny gaps around the fibres were observed. After 42 days of degradation, fibre pull-out and clean fibre surfaces were observed. The fibres were also still present, which suggested that this glass formulation had not degraded over the course of the study.

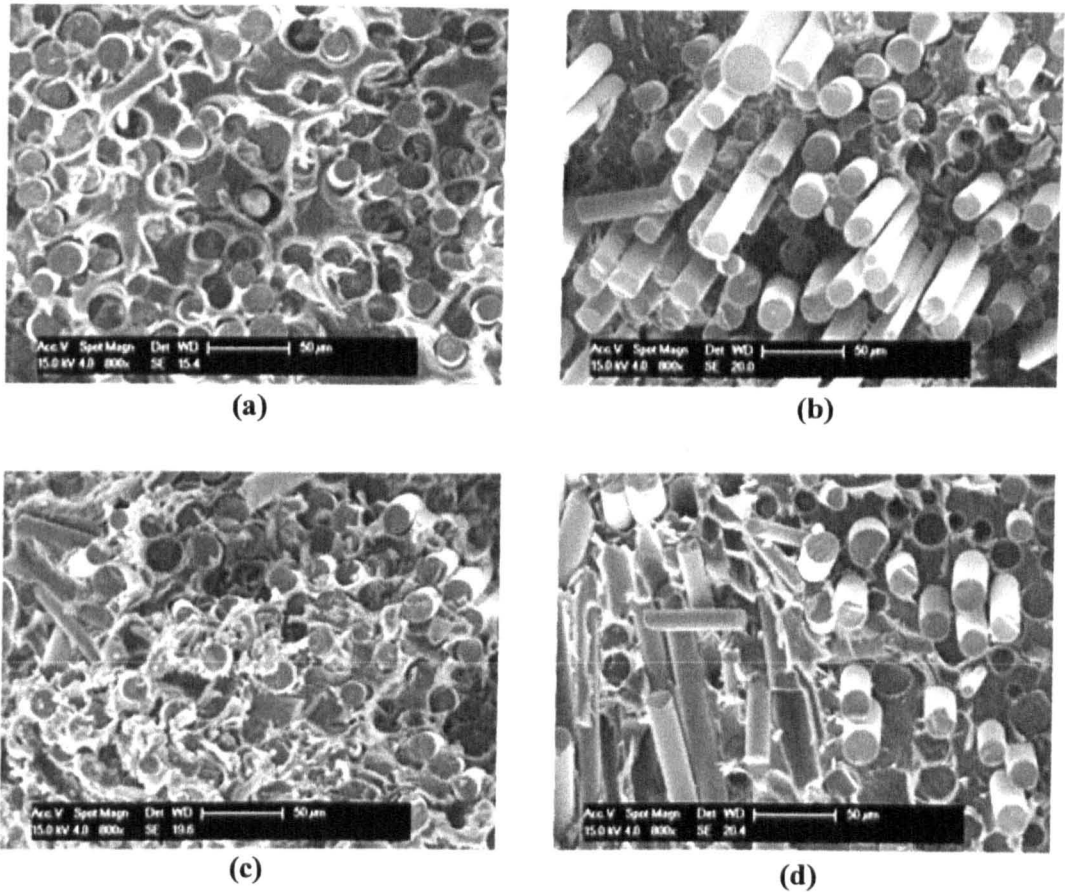


Figure 6-22: SEM micrographs of a fractured surface after flexural test for (a) P40 UD screw before degradation, (b) P40 UD screw after 6 weeks of degradation in PBS at 37°C, (c) P40 UD/RM screw before degradation and (d) P40 UD/RM screw after 6 weeks of degradation in PBS at 37°C. Scale bars for all micrographs represent 50 µm.

6.5 DISCUSSION

A plate and screw system is commonly utilised for treatment of internal bone fractures. The failure of this combination usually occurs in the bone (stripping the bone thread), screw (screw fracture) or plate, which can cause non-union and malunion of fractures. The mode of failure depends on the mechanical characteristics of the screws and plate and the screw thread design [21]. Thus, identification of mechanical properties and the effects of design parameters are required. Maximum load and stiffness were investigated to ascertain the mechanical properties of the screws instead of strength and modulus. This was due to the fact

that calculating the strength and modulus for the screws proved difficult due to screw geometry. Secondly, determining the maximum load and deformation rate that could be tolerated was deemed more significant for screw applications.

The holding power and pull-out strength represent the maximum tensile strength recorded for pulling the screws out of the bone or screw failure [22]. The performance of screws during bone fixation is controlled by different parameters such as thread depth, length, shape, surface finish and the mechanical properties of the screw materials. As the screw depth increases, the proportion of engaged bone with the thread and thus the holding power also increases. The screw length should have a similar effect to that of the thread depth. Sharp screw threads can cause cracks within the bone during insertion and consequently decrease the pull-out strength. However, a rough thread surface could increase interlocking with the bone and accordingly improve the holding power; however, a higher insertion torque would probably be required. Implants with mechanical properties closer to bone could prevent the stress concentration on the bone and thus increase the required load to failure [22, 23].

Initial pull-out strength acquired for the composite screws with heads was lower than for the PLA screws, which was related to their failure mode. The composite screws failed at just below the head (see Table 6-2) whereas the PLA screws failed at the inner diameter at insertion depth (i.e. at the edge of the test block). The head failure for the composite screws was ascribed to the manufacturing process. Axial pressure was applied to form the head, which caused buckling of the unidirectional fibres (parallel to the axis of the screw) and fractures at the edge of the head which resulted in stress concentration points. Bending and fracture of the fibres can be seen in Figure 6-2-b, both within the head and just below it. This point was proven further by testing the pull-out strength for headless screws; all these composite screws failed at their inner diameter at insertion depth, similar to the PLA screws. Initial strength for PLA screws with and without heads were similar as the failure

modes did not change, whilst pull-out strength for P40 UD and P40 UD/RM headless screws increased by ~ 200 % and 100 % in comparison to the screws with heads. During the push-out test, intact and headless screws failed via a buckling mode (see Table 6-2) and the strengths for the intact composite and headless screws were similar and higher than that for the PLA screws. Since the different screws failed during pull-out and push-out tests at the core diameter not by thread stripping, the strength of the screw threads must be greater than tensile and compressive properties of the screw materials. This could be confirmed through the following calculations.

6.5.1.1 Screw thread calculations

During the pull-out test or fixation of bone fracture, the screws can fail via two routes; screw failure or bone failure. Screw failure can occur via two modes; screw fracture (fracture at the cross-section) or thread failure due to shearing. Bone failure occurs through shearing of the bone. The maximum force that can be endured by the screw before failure (pull-out strength) depends on the mode of failure. It is possible to predict the maximum load accompanying each mode of failure (see Figure 6-23) by using the following equations [24-26]:

Screw fracture (Figure 6-23 a);

$$F_{max} = A_t \times \sigma_{st} \quad \text{Equation 6-1}$$

Thread failure (Figure 6-23 b);

$$F_{max} = A_s \times \sigma_{ss} \quad \text{Equation 6-2}$$

Bone failure (Figure 6-23 c);

$$F_{max} = A_b \times \sigma_{sb} \quad \text{Equation 6-3}$$

Where σ_{st} , σ_{ss} and σ_{sb} are the tensile strength and shear strength for the screw material and shear strength for the bone. A_t , A_s , and A_b are the tensile stress area of the screw and shear area for external thread (screw thread) and internal thread (tapped bone thread).

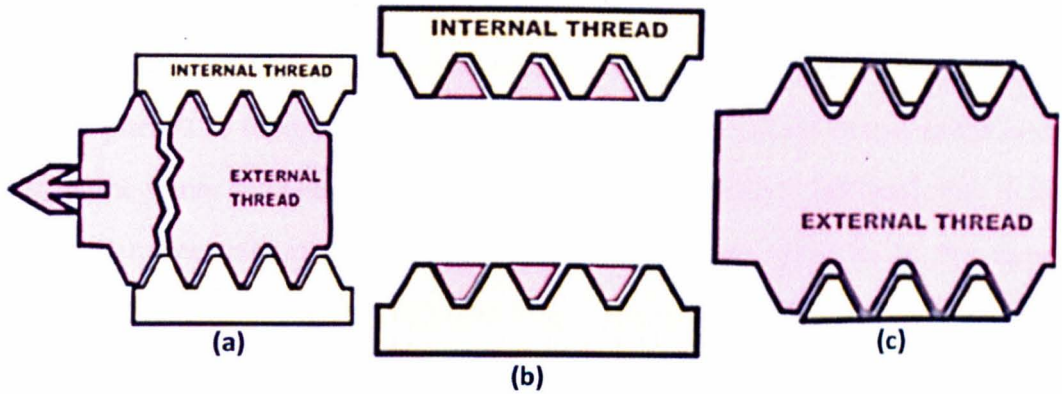


Figure 6-23: Failure modes associated with the pull-out test for the screws (a) tensile fracture at the core, (b) stripping of the external thread and (c) stripping of the internal thread [27].

Tensile stress area for the screw thread is given by the following equation:

$$A_t = 0.7854[D - 0.9382 P]^2 \quad \text{Equation 6-4}$$

$$A_t = 18.3 \text{ mm}^2$$

where D and P are major diameter (6 mm) and thread pitch (1.25 mm) for the screw.

$$A_s = \pi n L_e K_{n \max} \left[\frac{1}{2n} + 0.57735 (E_{s \min} - K_{n \max}) \right] \quad \text{Equation 6-5}$$

$$A_b = \pi n L_e D_{s \min} \left[\frac{1}{2n} + 0.57735 (D_{s \min} - E_{n \max}) \right] \quad \text{Equation 6-6}$$

where $K_{n \max}$ is the maximum minor diameter for internal thread, $E_{s \min}$ is the minimum pitch diameter for external thread, $D_{s \min}$ is the minimum major diameter for external thread, $E_{s \max}$ is the maximum pitch diameter for external thread, L_e is the screw thread engagement length (7 mm) and n is number of threads per mm (i.e. inverse of the thread pitch = 0.8).

According to standard BS 3643-1: 2007 [28],

$$K_{n \max} = (D - 1.0825 P) + EI + TD_1 \quad \text{Equation 6-7}$$

$$E_{n \max} = (D - 0.6495 P) + EI + TD_2 \quad \text{Equation 6-8}$$

$$E_{s \min} = (d - 0.6495 P) - es - Td_2 \quad \text{Equation 6-9}$$

$$D_{s\ min} = d - es - Td$$

Equation 6-10

where D and d are the major diameter for the internal and external thread (6 mm), P is the pitch (1.25 mm), EI is the lower deviation for the internal thread (0.028 mm), TD_1 is the minor diameter tolerance for the internal thread (0.265 mm), TD_2 is the pitch diameter tolerance for the internal thread (0.160 mm), es is the upper deviation for the external thread (-0.028 mm), Td_2 is the pitch diameter tolerance for the external thread (0.118 mm) and Td is the major diameter tolerance for the external thread (0.212 mm).

Thus, $K_{n\ max} = 4.9399$, $E_{n\ max} = 5.3761$, $E_{s\ min} = 5.0981$, and $D_{s\ min} = 5.8160$

Therefore, $A_s = 62.26\ mm^2$ and $A_b = 89.94\ mm^2$.

When the screw fails in pure tension mode, it typically fractures through the threaded portion (as this is smallest and weakest area). The tensile stress area is equivalent to the cross-sectional area of the core of the screw.

In the current study, the failure mode for all screws (PLA and composite) was screw fracture at the core diameter as expected. This was due to the tensile stress area of the screws being lower than shear area of the internal and external threads. Initially, it was hypothesised that the screws would fail at the thread (shear failure) and the screws were manufactured to try and ensure that reinforcement fibres had been incorporated into the thread, which can be seen in the X-ray photographs of the screws (see Figure 6-2-b). The threads of the composite screws were whitish, indicating high density components (i.e. glass fibres). Based on previous calculations, the failure mode could be controlled by thread design. For the screws used in this chapter, the failure load of the thread was high even if the thread was completely PLA (~ 3 kN pull-out load). Thus, reinforcement for the core alone should be of greater consideration in future manufacturing approaches.

Chapman *et al.* [22] predicted the shear failure force for internal threads (of polyurethane foam) by using the following simplified relation:

$$F_s = S A_b = (S L \pi D).TSF \quad \text{Equation 6-11}$$

$$TSF = 0.5 + 0.57735 \left(\frac{h}{P} \right) \quad \text{Equation 6-12}$$

where S is the material shear strength (MPa) (polyurethane foam), TSF is the thread shape factor, L is the length of thread engagement with the material and h is the thread depth.

According to this method, shear area by unit engagement length $\left(\frac{A_b}{mm} \right)$ equaled 14.866 mm² whereas the calculated shear area for the internal thread per unit length using Equation 6-6 would be 12.848 mm². This difference would effect on the accuracy of the predicted properties for the screws.

Screw failure during the insertion process happens when the applied torque is higher than the maximum torque for the screws. Removal of broken screws would accentuate the cost and increase the time associated with surgical procedures. The maximum torque depends on the material and design of the screws [1]. Thus, investigation of the torque profile for screws is essential to select the appropriate torque to be applied and prevent failure during surgical procedure. The screws sheared during the torsional test at the free section (i.e. between the head and the inserted length). The maximum torque for PLA screws was slightly higher than that for composite screws which was attributed to the presence of unidirectional fibres as mentioned previously.

Pull-out strength and maximum torque for some of the commercially available metallic and bioresorbable cortical and cancellous bone screws have been summarised in Table 6-3. The mechanical properties of the screws depend mainly on the dimensions and material of the screws. Table 6-3 also provides information on a variety of commercial screws with different pull-out strength and torque values. Generally, metallic screws are stronger than bioresorbable ones and also the failure associated with them commonly occurred in the screw for the bioresorbable,

whilst the bone failed before the metallic screws. This was suggested as due to the huge difference in the mechanical properties between metals and polymers.

Metallic and bioresorbable screws have similar pull-out failure loads [23, 29-35]. This was ascribed to the fact that the screw engaged predominantly with cancellous bone and partially with cortical and the mechanical properties of cancellous bone are much lower than either metal or the bioresorbable polymer. Moreover, some reports have demonstrated the superiority of bioresorbable screws over metallic ones [36, 37].

Wittenberg *et al.* [38] made a comparison of steel and PLA screws with respect to their pull-out strengths and failure modes (see Table 6-3). Metallic screws failed by splitting the bone around the thread (bone shearing). They attributed the lower pull-out strength for PLA to the failure at the screw head or inner diameter. It was also reported that there was no difference between the pull-out strength of self-tapped (steel screw) and pre-tapped screws (PLA) [39].

In this chapter, flexural and shear properties for the composite screws were superior to those of the PLA screws. The increase in the flexural and shear properties for composite screws was due to the reinforcement effect of phosphate glass fibres. Furthermore, composite screws demonstrated ductile behaviour which was desired for bone fixation devices in order to prevent sudden failure during bone healing period (see Table 6-2) [40].

Table 6-3: Mechanical properties (Pull-out and Torque) for some commercial metallic and bioresorbable screws.

Screw name & material	Screw dimensions (mm) Major /Minor diameter/Pitch/Length	Pull-out strength (kN)	Mode of failure	Maximum Torque (mN. m)	Reference
Metallic Screws					
Richards 316-L stainless steel	5/2.7/1/- ©	0.4 ± 0.02	Synthetic bone failure	1299 ± 260	[41]
	5/2.7/1.2/- ©	0.39 ± 0.01	Synthetic bone failure	1277 ± 129	[41]
	5/2.7/1.5/- ©	0.39 ± 0.01	Synthetic bone failure	3130 ± 610	[41]
	5/2.7/1.6/- ©	0.37 ± 0.01	Synthetic bone failure	2712 ± 362	[41]
	5/2.7/1.75/- ©	0.38 ± 0.01	Synthetic bone failure	3039 ± 633	[41]
	6/5/1/-	~1.36	Synthetic bone failure		[21]
	3/2.5/0.5/-	~ 0.47	Synthetic bone failure		[21]
	6/4/2.5/-	~1.24	Synthetic bone failure		[21]
	6/5/2.5/-	~1.1	Synthetic bone failure		[21]
	3.5/2/1.2/-	~1.23	Synthetic bone failure		[21]
	4.5/3.2/1.75/-	~1.2	Synthetic bone failure		[21]
Synthes stainless steel	4.5/3.2/-/-			1700 – 5700*	[42]
	4/1.9/1.75/40 ©	0.63 ± 0.01	Synthetic bone failure		[22]
	6.5/3/2.75/60 ©	1.13 ± 0.04	Synthetic bone failure		[22]
Bosworth titanium	6.35/-/-/39.7 ©	0.37 ± 0.1	Bone failure		[43]

(Cont.) Bioresorbable Screws					
Compression moulded SR-PLLA	4.5/-/-	0.96 ± 0.2	Screw failure	303 ± 40	[7]
Machined SR-PLLA	4.5/-/-	0.79 ± 0.07	Screw failure	521 ± 4	[7]
SR-PLLA	3.5/-/2.5/20	0.18	Screw failure	280	[6]
	3.5/-/2.5/40	0.12	Screw failure	360	[6]
PLLA	3.4/2.4/0.5/20	0.21 ± 0.03	Bone failure		[38]
		0.28 ± 0.01	Screw failure		[38]
	3.4/2.8/0.3/20	0.27 ± 0.06	Bone failure		[38]
		0.33 ± 0.06	Screw failure		[38]
	2.6/2/0.3/20	0.18 ± 0.002	Screw failure		[38]
Linvatec PLLA	5.7/-/-/36 ©	0.27 ± 0.06	Screw failure		[43]
High pressed extruded PLLA	4/2.5/-/- ©	0.45 ± 0.02	Screw failure	250± 10	[8]
	3.5/2.6/-/-	0.42 ± 0.02	Screw failure	260 ± 20	[8]
	4.5/3.3/-/-	0.72 ± 0.02	Screw failure	510 ± 20	[8]
	4.5/3.3/-/-	0.73 ± 0.02	Screw failure	490 ± 20	[8]
	6.5/4.1/-/- ©	1.2 ± 0.05	Screw failure	1130 ± 30	[8]
PLA	6/4.75/1.25/32	0.87 ± 0.1	Screw failure	1006 ± 8	Current study
	6/4.75/1.25/28 **	0.9 ± 0.05	Screw failure		
P40 UD	6/4.75/1.25/32	0.55 ± 0.1	Screw failure	881 ± 66	
	6/4.75/1.25/28 **	1.6 ± 0.3	Screw failure		
P40 UD/RM (70/30)	6/4.75/1.25/32	0.42 ± 0.2	Screw failure	876 ± 180	
	6/4.75/1.25/28 **	0.91 ± 0.2	Screw failure		

± Standard deviation (SD), * Torque values depend on the thickness of the synthetic cortical bone which varied from 3 mm to 11 mm, © represents the cancellous bone screws and ** refers to the headless screws.

Mechanical properties (bending, shear, pull-out and torque) for compression moulded self-reinforced poly lactic acid (SR-PLA) screws of 4.5 mm diameter were investigated by Pohjonen *et al.* [7]. The initial maximum bending and pull-out loads were 0.08 kN and 0.96 kN respectively, whilst the maximum shear load and torque were 3 kN and 303 mN.m respectively. They also reported that the shear, bending and pull-out values were acceptable for fixation of certain types of bone fractures (e.g. ankle fractures), whereas the torque values were lower than that for metallic screws which they attributed to a fibrillated (i.e. fully oriented) structure at high draw ratio. The fibrillated polymer structure behaved like unidirectional fibres within fibre-reinforced composites. This could also be the reason for the slight decrease in torque for P40 UD and P40 UD/RM screws in comparison to the PLA screws. It is well known that torsional testing is usually conducted in order to determine the shear properties for materials. Therefore, the maximum torque for isotropic materials (polymers) should be directly proportional to their shear strength. Nevertheless, maximum torque for anisotropic materials (fibre reinforced composites) should be governed by the minimum shear component (interlaminar shear strength) within the composite which should fail first under torsion. The interlaminar shear strength for composites is commonly lower than the shear strength for the matrix. Thus, it was expected that the maximum torque for the composites screws would be lower than that for PLA [44]. Breakage, entanglement of the long fibres (UD fibres) and the strength of fibre/matrix interface could also be responsible for the lower torsional properties observed for composite screws in comparison to the PLA alone [45].

Flexural, shear and torque for SR-PLA screws (4.5 mm diameter) were also examined by Suuronen *et al.* [5]. The maximum flexural and shear loads were 61.3 N and 1.77 kN whereas the maximum torque varied between 200 and 300 mN.m. The data obtained for PLA, P40 UD and P40 UD/RM screws (6 mm diameter) indicated

higher properties than those reported for resorbable screws in the literature (see Table 6-3). This was also suggested to be due to the reinforcement effect of the PBG fibres and the method of manufacture.

Initial pull-out strength for the composite headless screws in the current chapter were higher than most of the reported data for metallic and bioresorbable screws (see Table 6-3) when taking into account the different dimensions. Torque results were higher than the published values for bioresorbable screws and comparable with the metallic screws. However, further improvement is required in the manufacturing stage to avoid screw head failure during the insertion process.

Metallic screws are routinely used for internal fixation however removal of these screws after bone healing in some cases is required (and is routine in Europe), which causes further trauma to the patient. Even successful removal creates stress risers by leaving behind screw holes which could lead to re-fracture. Between 7 - 26 % of internal bone fractures have been reported to refracture after implant removal due to screw cavities [46, 47]. Thus, numerous approaches have been taken in order to accelerate bone remodelling, such as: bone grafting, injection of calcium phosphate cement and causing bleeding into the bone at the screw hole. Most of these trials were not completely successful [46]. The composite screws (in this chapter) could provide alternatives for metallic screws in order to eliminate the need for removal processes, as they are made from bioresorbable materials. These screws also contain phosphate glass fibres which have similar composition to natural bone [48]. Phosphate glasses break down in the body into calcium and phosphate ions and are bioactive and osteoconductive [49, 50].

Percentage of water uptake for glass fibre reinforced composites depends essentially on the void ratio [51]. Water uptake for the composite screws investigated was similar to pure PLA screws up to 7 days of degradation (see Figure 6-15) which was indicative of the integrity of the composite structure. After

14 days, the water uptake for the composite screws increased above that seen for the PLA screws. This was suggested to be due to the degradation of the fibre/matrix interface creating capillaries that could act as micro-voids.

Exposed surface area of degradable materials has a significant influence on the degradation rate, which increases with an increase in surface area to volume ratio [52, 53]. The increase in the degradation rate can be seen from the increase in mass loss for the specimens during the degradation study. The mass loss for P40 UD/RM and P40 UD composite screws (see Figure 6-14) was higher than that for the composite plates of the same composition (see Chapter 3). The surface area for the screws is higher than that for the rods and plates of comparable size. Thus, it was expected that the mass loss for screws would be higher than that for plates and rods. Fibre volume fraction also has a significant effect on the degradation rate and mass loss profiles for composites. As the fibre volume fraction increases, the amount of fibre/matrix interface also increases and the degradation rate and mechanical loss for composites will consequently increase [54]. After immersion in the degradation medium (PBS), the fibre/matrix interface started to degrade creating a capillary effect [55]. These capillaries allowed the degradation medium to reach further into the composites and would likely increase the rate of leaching out the degradation product into the surrounding medium which in effect accelerated the degradation process.

No significant change in the pH of the degradation medium (PBS) for the samples tested was seen (see Figure 6-13) which was ascribed to buffering effect of the PBS for little variations due to slight degradation of PGF and PLA.

Yao *et al.* [51] reported that flexural and tensile properties for FRC's are sensitive to the fibres properties, volume fraction and orientation, whilst shear properties are sensitive to the matrix properties [56]. The mechanical properties for PLA screws decreased slightly after 3 days of degradation in PBS at 37°C with respect to the initial values (before degradation), which was suggested to be due to the

plasticisation effect of water. The initial decrease in mechanical properties for composite screws at 3 days with respect to the 0 day results (before degradation) was suggested to be also due to the preliminary degradation of the fibre/matrix interface as no coupling agent was used [51, 54, 57-61]. All composite screws tested failed via a transverse splitting mode during the pull-out test due to interfacial shear failure and tensile failure of the fibres [62].

The percentage decrease in the mechanical properties depends on the direction of the applied load during the test with respect to the direction of the fibre/matrix interface. Therefore, the strength of the interface has a significant effect on the pull-out properties. During the axial pull-out test, the applied load was parallel to the unidirectional fibres (i.e. parallel to fibre/ matrix interface). Thus, the pull-out strength for the composite screws depended mainly on the strength of the bonding between the matrix and the fibres. Due to the presence of water during immersion time in PBS, the strength of the fibre/matrix interface diminished with degradation time. For the flexural and double shear tests, the load applied was perpendicular to fibre direction.

After 3 days of immersion in PBS, the mechanical properties for composite screws remained stable until the end of the study at 42 days. This suggested that the mechanical properties for the matrix (PLA) did not change significantly and the fibres used in this study (P40) were chemically durable. The fibres in the P40 UD/RM and P40 UD screws were still present after 42 days (see Figure 6-22). P40 UD and RM composites were investigated previously in Chapter 3 for up to 95 days in PBS and the fibres were still present without any obvious signs of degradation.

Lassila *et al.* [54] investigated the retention of flexural properties for unidirectional E-glass fibre reinforced composites in water at 37°C for 180 weeks. They reported that the flexural properties decreased initially and then remained constant until the end of the study. They ascribed the initial reduction to the saturation of the specimen with the water.

SEM was used to investigate degradation of the fibre/matrix interface for the specimens during the degradation process. Tiny gaps were seen around the fibres from the SEM micrographs of the cross-sections of composite screws. The gaps were suggested to be as a result of buckling of the unidirectional fibres during the head formation, particularly as the matrix was not molten and unable to flow sufficiently to maintain contact with the fibres. After 42 days of degradation in PBS, relatively clean fibre surfaces and fibre pull-out could be seen from the SEM micrographs which was indicative of degradation of the fibre/matrix interface (see **Figure 6-22-b** and **d**) [63, 64]. Length of pull-out fibres for P40 UD screws was longer than that for P40 UD composite plate and rods in **Chapters 4 and 5** which might be due to the existence of gaps around the fibres within the as prepared screws.

The initial mechanical properties for the composite screws were greater than those for pure PLA and potentially adequate for internal bone fixation. However, the screws did not maintain their initial mechanical properties for long periods during *in vitro* degradation. The reduction after 3 days was suggested to be mainly due to degradation of the fibre/matrix interface as a result of water absorption. This interface could be enhanced by surface treatment of the fibres using for e.g. coupling agents.

6.6 CONCLUSIONS

Totally bioresorbable screws for repairing internal bone fractures would obviate the need for second removal surgery and stress shielding. The mechanical properties associated with bioresorbable polymers are inadequate for load-bearing applications, thus fibre-reinforcement is one method used to improve their mechanical strength and stiffness. Initial mechanical properties for PLA, P40 UD and P40 UD/RM screws (6 mm diameter) were higher than reported previously for resorbable screws in the literature. This was suggested to be due to the reinforcement effect of PBG fibres and the method of manufacture. Head failure for the composite screws during pull-out was ascribed to buckling of the unidirectional

fibres during the manufacture process. Retention of mechanical properties for composite screws is mainly controlled by the fibre/matrix interface and water uptake. Water absorption can deteriorate the bond between the fibres and matrix causing reduction in the mechanical properties. It was seen that the mechanical properties (flexural, shear and pull-out) decreased initially at 3 days and maintained their properties afterwards until the end of the study at 42 days. This was due to the chemical durability of the fibres used (P40) and the stability of the matrix properties during the degradation. Improvement of the fibre/matrix interface is necessary to infer further control over the degradation of the composites and the initial reduction in the mechanical properties for the screws. All screws failed at the core diameter due to the fact that the tensile area was lower than the shear area of the thread. Thus, increased reinforcement of the core should provide greater improvement in properties and should be relatively easy to produce. Moreover, the manufacturing process of the screws could be improved to overcome issues such as buckling and the fracture of the fibres caused during formation of the screw head.

6.7 REFERENCES

1. Buijs, G.J., E.B. van der Houwen, B. Stegenga, R.R.M. Bos, and G.J. Verkerke, *Torsion Strength of Biodegradable and Titanium Screws: A Comparison. Journal of Oral and Maxillofacial Surgery*, 2007. 65(11): p. 2142-2147.
2. Ashammakhi, N., A.M. Gonzalez, P. Törmälä, and I.T. Jackson, *New resorbable bone fixation. Biomaterials in craniomaxillofacial surgery: present and future. European Journal of Plastic Surgery*, 2004. 26(8): p. 383-390.
3. Ell, V., M. Kellomäki, and P. Tormala, *In vitro properties of PLLA screws and novel bioabsorbable implant with elastic nucleus to replace intervertebral disc. Journal of Materials Science: Materials in Medicine*, 2005. 16: p. 655-662.
4. Waris, E., N. Ashammakhi, T. Raatikainen, P. Törmälä, S. Santavirta, and Y.T. Konttinen, *Self-reinforced bioabsorbable versus metallic fixation systems for metacarpal and phalangeal fractures: A biomechanical study. The Journal of Hand Surgery*, 2002. 27(5): p. 902-909.
5. Suuronen, R., T. Pohjonen, R. Taurio, P. Törmälä, L. Wessman, K. Rönkkö, and S. Vainionpää, *Strength retention of self-reinforced poly-L-lactide screws and plates: an in vivo and in vitro study. Journal of Materials Science: Materials in Medicine*, 1992. 3(6): p. 426-431.

6. Shetty, V., A.A. Caputo, and I. Kelso, *Torsion-axial force characteristics of SR-PLLA screws*. *Journal of Cranio-Maxillofacial Surgery*, 1997. 25(1): p. 19-23.
7. Pohjonen, T., P. Helevirta, P. Tormala, K. Koskikare, H. Patiala, and P. Rokkanen, *Strength retention of self-reinforced poly-L-lactide screws. A comparison of compression moulded and machine cut screws*. *Journal of Materials Science: Materials in Medicine*, 1997. 8(5): p. 311-320.
8. Takashi, M., N. Kozo, S. Ryoji, T. Hiroaki, T. Koichiro, and K. Takahide, *Initial strength of highpressed extrusion poly-L-lactide screw*. *Bio-Medical Materials and Engineering*, 2000. 10(3): p. 199-204.
9. Jukkala-Partio, K., E.K. Partio, P. Helevirta, T. Pohjonen, P. Tormala, and P. Rokkanen, *Treatment of subcapital femoral neck fractures with bioabsorbable or metallic screw fixation. A preliminary report*. *Ann Chir Gynaecol*, 2000. 89(1): p. 45-52.
10. Shikinami, Y. and M. Okuno, *Bioresorbable devices made of forged composites of hydroxyapatite (HA) particles and poly-lactide (PLLA). Part II: practical properties of miniscrews and miniplates*. *Biomaterials*, 2001. 22(23): p. 3197-3211.
11. Ruffieux, K., A. Dell'Agosti, B. Riesen, and E. Wintermantel, *Influence of Calcium Phosphates on the Degradation of Poly Lactic Acid for Medical Implants*. *Biomedizinische Technik/Biomedical Engineering*, 1996. 41(s1): p. 420-421.
12. Gantous, A. and J.H. Phillips, *The Effects of Varying Pilot Hole Size on the Holding Power of Miniscrews and Microscrews*. *Plastic and Reconstructive Surgery*, 1995. 95(7): p. 1165-1169.
13. Battula, S., A.J. Schoenfeld, V. Sahai, G.A. Vrabec, J. Tank, and G.O. Njus, *The effect of pilot hole size on the insertion torque and pullout strength of self-tapping cortical bone screws in osteoporotic bone*. *J Trauma*, 2008. 64(4): p. 990-5.
14. Larsen, M.W., W.S. Pietrzak, and J.C. DeLee, *Fixation of Osteochondritis Dissecans Lesions Using Poly(l-lactic Acid)/ Poly(glycolic Acid) Copolymer Bioabsorbable Screws*. *The American Journal of Sports Medicine*, 2005. 33(1): p. 68-76.
15. Zdero, R., S. Rose, E.H. Schemitsch, and M. Papini, *Cortical Screw Pullout Strength and Effective Shear Stress in Synthetic Third Generation Composite Femurs*. *Journal of Biomechanical Engineering*, 2007. 129(2): p. 289-293.
16. Zdero, R., M. Olsen, H. Bougherara, and E.H. Schemitsch, *Cancellous bone screw purchase: A comparison of synthetic femurs, human femurs, and finite element analysis*. *Proceedings of the Institution of Mechanical Engineers, Part H: Journal of Engineering in Medicine*, 2008. 222(8): p. 1175-1183.
17. ASTM D2584-94, *Standard Test Method for Ignition Loss of Cured Reinforced Resins* 1994.
18. ASTM F2502 - 05 *Standard Specification and Test Methods for Bioabsorbable Plates and Screws for Internal Fixation Implants*.

19. BS 2782-3:Methods 340A and 340B:1978, *Methods of testing plastics. Mechanical properties. Determination of shear strength of moulding material. Determination of shear strength of sheet material*
20. ASTM D7617 / D7617M - 11: *Standard Test Method for Transverse Shear Strength of Fiber-reinforced Polymer Matrix Composite Bars* 2011.
21. DeCoster, T.A., D.B. Heetderks, D.J. Downey, J.S. Ferries, and W. Jones, *Optimizing Bone Screw Pullout Force. Journal of orthopaedic trauma*, 1990. 4(2): p. 169-174.
22. Chapman, J.R., R.M. Harrington, K.M. Lee, P.A. Anderson, A.F. Tencer, and D. Kowalski, *Factors Affecting the Pullout Strength of Cancellous Bone Screws. Journal of Biomechanical Engineering*, 1996. 118(3): p. 391-398.
23. Beevers, D., *Metal vs bioabsorbable interference screws: initial fixation. Proceedings of the Institution of Mechanical Engineers, Part H: Journal of Engineering in Medicine*, 2003. 217(1): p. 59-75.
24. Walsh, R.A., *Electromechanical Design Handbook (3rd Edition)*, 2000, McGraw-Hill.
25. Jadon, V.K. and S. Verma, *Analysis and Design of Machine Elements* 2010: I K International Publishing House
26. Bickford, J.H. and S. Nassar, *Handbook of Bolts and Bolted Joints* 1998: M. Dekker.
27. <http://www.boltscience.com/pages/Thread%20Stripping%20Background.swf>. 2012.
28. BS 3643-1, *ISO metric screw threads. Principles and basic data* 2007.
29. Weiler, A., H.J. Windhagen, M.J. Raschke, A. Laumeyer, and R.F.G. Hoffmann, *Biodegradable Interference Screw Fixation Exhibits Pull-Out Force and Stiffness Similar to Titanium Screws. The American Journal of Sports Medicine*, 1998. 26(1): p. 119-128.
30. Seil, R., S. Rupp, P.W. Krauss, A. Benz, and D.M. Kohn, *Comparison of Initial Fixation Strength Between Biodegradable and Metallic Interference Screws and a Press-Fit Fixation Technique in a Porcine Model. The American Journal of Sports Medicine*, 1998. 26(6): p. 815-819.
31. Johnson, L.L. and G.E. vanDyk, *Metal and biodegradable interference screws: Comparison of failure strength. Arthroscopy: The Journal of Arthroscopic & Related Surgery*, 1996. 12(4): p. 452-456.
32. Abate, J.A., P.D. Fadale, M.J. Hulstyn, and W.R. Walsh, *Initial fixation strength of polylactic acid interference screws in anterior cruciate ligament reconstruction. Arthroscopy: The Journal of Arthroscopic & Related Surgery*, 1998. 14(3): p. 278-284.
33. Caborn, D.N.M., W.P. Urban, D.L. Johnson, J. Nyland, and D. Pienkowski, *Biomechanical comparison between BioScrew and titanium alloy interference screws for bone–patellar tendon–bone graft fixation in anterior cruciate ligament*

- reconstruction. *Arthroscopy: The Journal of Arthroscopic & Related Surgery*, 1997. 13(2): p. 229-232.
34. Kousa, P., T.L. Jarvinen, T. Pohjonen, P. Kannus, M. Kotikoski, and M. Jarvinen, Fixation strength of a biodegradable screw in anterior cruciate ligament reconstruction. *J Bone Joint Surg Br*, 1995. 77-B(6): p. 901-905.
 35. Hoffmann, R.F.G., R. Peine, H.J. Bail, N.P. Südkamp, and A. Weiler, Initial Fixation Strength of Modified Patellar Tendon Grafts for Anatomic Fixation in Anterior Cruciate Ligament Reconstruction. *Arthroscopy: The Journal of Arthroscopic & Related Surgery*, 1999. 15(4): p. 392-399.
 36. Weiler, A., R.F. Hoffmann, A.C. Stähelin, H.J. Bail, C.J. Siepe, and N.P. Südkamp, Hamstring tendon fixation using interference screws: a biomechanical study in calf tibial bone. *Arthroscopy : the journal of arthroscopic & related surgery : official publication of the Arthroscopy Association of North America and the International Arthroscopy Association*, 1998. 14(1): p. 29-37.
 37. Caborn, D.N.M., M. Coen, R. Neef, D. Hamilton, J. Nyland, and D.L. Johnson, Quadrupled semitendinosus-gracilis autograft fixation in the femoral tunnel: a comparison between a metal and a bioabsorbable interference screw. *Arthroscopy: The Journal of Arthroscopic & Related Surgery*, 1998. 14(3): p. 241-245.
 38. Wittenberg, J.M., R.H. Wittenberg, and J.A. Hipp, Biomechanical properties of resorbable poly-L-lactide plates and screws: A comparison with traditional systems. *Journal of Oral and Maxillofacial Surgery*, 1991. 49(5): p. 512-516.
 39. Foley, W.L., D.E. Frost, W.B. Paulin, and M.R. Tucker, Uniaxial pullout evaluation of internal screw fixation. *Journal of oral and maxillofacial surgery : official journal of the American Association of Oral and Maxillofacial Surgeons*, 1989. 47(3): p. 277-280.
 40. Brauer, D., C. Rüssel, S. Vogt, J. Weisser, and M. Schnabelrauch, Degradable phosphate glass fiber reinforced polymer matrices: mechanical properties and cell response. *Journal of Materials Science: Materials in Medicine*, 2008. 19(1): p. 121-127.
 41. Ricci, W.M., P. Tornetta, T. Petteys, D. Gerlach, J. Cartner, Z. Walker, and T.A. Russell, A comparison of screw insertion torque and pullout strength. *Journal of orthopaedic trauma*, 2010. 24(6): p. 374-8.
 42. Lawson, K.J. and J. Brems, Effect of insertion torque on bone screw pullout strength. *Orthopedics*, 2001. 24(5): p. 451-4.
 43. Ammon, J.T., M.J. Voor, and E.D. Tillett, A Biomechanical Comparison of Bosworth and Poly-L Lactic Acid Bioabsorbable Screws for Treatment of Acromioclavicular Separations. *Arthroscopy: The Journal of Arthroscopic & Related Surgery*, 2005. 21(12): p. 1443-1446.

44. Wan, Y.Z., Y.L. Wang, Q.Y. Li, and X.H. Dong, Influence of surface treatment of carbon fibers on interfacial adhesion strength and mechanical properties of PLA-based composites. *Journal of Applied Polymer Science*, 2001. 80(3): p. 367-376.
45. Mathew, L. and R. Joseph, Mechanical properties of short-isora-fiber-reinforced natural rubber composites: Effects of fiber length, orientation, and loading; alkali treatment; and bonding agent. *Journal of Applied Polymer Science*, 2007. 103(3): p. 1640-1650.
46. Alford, J.W., M.P. Bradley, P.D. Fadale, J.J. Crisco, D.C. Moore, and M.G. Ehrlich, Resorbable fillers reduce stress risers from empty screw holes. *J Trauma*, 2007. 63(3): p. 647-54.
47. Rosson, J., J. Egan, J. Shearer, and P. Monro, Bone weakness after the removal of plates and screws. Cortical atrophy or screw holes? *Journal of Bone & Joint Surgery, British Volume*, 1991. 73-B(2): p. 283-286.
48. Ahmed, I., M. Lewis, I. Olsen, and J.C. Knowles, Phosphate glasses for tissue engineering: Part 1. Processing and characterisation of a ternary-based P₂O₅-CaO-Na₂O glass system. *Biomaterials*, 2004. 25(3): p. 491-499.
49. Parsons, A.J., I. Ahmed, P. Haque, B. Fitzpatrick, M.I.K. Niazi, G.S. Walker, and C.D. Rudd, Phosphate Glass Fibre Composites for Bone Repair. *Journal of Bionic Engineering*, 2009. 6(4): p. 318-323.
50. Navarro, M. and J.A. Planell, Bioactive Composites based on Calcium Phosphates for Bone Regeneration. *Key Engineering Materials*, 2010. 441: p. 203-233.
51. Yao, J. and G. Ziegmann, Water Absorption Behavior and Its Influence on Properties of GRP Pipe. *Journal of Composite Materials*, 2007. 41(8): p. 993-1008.
52. Zong, X., S. Ran, K.-S. Kim, D. Fang, B.S. Hsiao, and B. Chu, Structure and Morphology Changes during in Vitro Degradation of Electrospun Poly(glycolide-co-lactide) Nanofiber Membrane. *Biomacromolecules*, 2003. 4(2): p. 416-423.
53. Chen, V.J. and P.X. Ma, The effect of surface area on the degradation rate of nanofibrous poly(l-lactic acid) foams. *Biomaterials*, 2006. 27(20): p. 3708-3715.
54. Lassila, L.V.J., T. Nohrström, and P.K. Vallittu, The influence of short-term water storage on the flexural properties of unidirectional glass fiber-reinforced composites. *Biomaterials*, 2002. 23(10): p. 2221-2229.
55. Michael, A.S. and C.C. Chu, Fiber-matrix interface studies on bioabsorbable composite materials for internal fixation of bone fractures. II. A new method using laser scanning confocal microscopy. *Journal of Biomedical Materials Research*, 1997. 37(3): p. 353-362.
56. Thomason, J.L., The interface region in glass fibre-reinforced epoxy resin composites: 2. Water absorption, voids and the interface. *Composites*, 1995. 26(7): p. 477-485.

57. Gautier, L., B. Mortaigne, and V. Bellenger, *Interface damage study of hydrothermally aged glass-fibre-reinforced polyester composites. Composites Science and Technology*, 1999. 59(16): p. 2329-2337.
58. Carol L, S., *Environmental durability of glass-fiber composites. Materials Science and Engineering: R: Reports*, 1994. 13(7): p. 265-323.
59. Foulc, M.P., A. Bergeret, L. Ferry, P. Ienny, and A. Crespy, *Study of hygrothermal ageing of glass fibre reinforced PET composites. Polymer Degradation and Stability*, 2005. 89(3): p. 461-470.
60. Camino, G., M.P. Luda, A.Y. Polishchuk, M. Revellino, R. Blancon, G. Merle, and J.J. Martinez-Vega, *Kinetic aspects of water sorption in polyester-resin/glass-fibre composites. Composites Science and Technology*, 1997. 57(11): p. 1469-1482.
61. Bian, X.S., L. Ambrosio, J.M. Kenny, L. Nicolais, and A.T. Dibenedetto, *Effect of water absorption on the behavior of E-glass fiber/nylon-6 composites. Polymer Composites*, 1991. 12(5): p. 333-337.
62. Behr, M., M. Rosentritt, R. Lang, and G. Handel, *Flexural properties of fiber reinforced composite using a vacuum/pressure or a manual adaptation manufacturing process. Journal of Dentistry*, 2000. 28(7): p. 509-514.
63. Mishra, S., A.K. Mohanty, L.T. Drzal, M. Misra, S. Parija, S.K. Nayak, and S.S. Tripathy, *Studies on mechanical performance of biofibre/glass reinforced polyester hybrid composites. Composites Science and Technology*, 2003. 63(10): p. 1377-1385.
64. Huang, G. and H. Sun, *Effect of water absorption on the mechanical properties of glass/polyester composites. Materials & Design*, 2007. 28(5): p. 1647-1650.

CHAPTER 7.

OVERALL THESIS SUMMARY AND FUTURE WORK

7.1 SUMMARY

The aim of this work was to manufacture fully bioresorbable bone fixation devices such as plates, rods and screws, with initial mechanical properties matching or slightly surpassing those of cortical bone (see Table 1-1). The healing process for a bone fracture involves formation of a callus at the fracture site, which can be very weak especially during the first six weeks [1]. Therefore, the implants manufactured were required to maintain their mechanical properties (within the range of cortical bone) for at least a 8 – 12 week period to provide adequate protection for the soft callus [2].

Fully resorbable fibre reinforced composites (FRC) were selected as a starting material to manufacture the implants proposed above to overcome limitations and complications of other commonly investigated bioresorbable materials. Mechanical properties and adverse reactions such as inflammation within the surrounding tissue have been reported as the main limitations for pure bioresorbable polymers (e.g. PLA, PGA and PCL) and particulate reinforced composites (e.g., PLA/HA and PLA/ CaP) [3-9]. PLA and phosphate glass fibres (PGF) were chosen as constituents for the bioresorbable FRC based on criteria of biocompatibility, biodegradability and mechanical properties. PLA was chosen as matrix to obtain a balance between mechanical properties and degradation time (see Table 2-2). Phosphate glass fibres were used to reinforce PLA due to their extremely promising characteristics;

- i. they are totally resorbable in aqueous medium,
- ii. control of their degradation rate is easily achieved,
- iii. they have good biocomptability and bioactivity,
- iv. some formulations are easy to manufacture into fibre,
- v. they have excellent mechanical properties [10-14].

Based on previous work within the group [11, 15-21], phosphate glass with composition of 40 P₂O₅-24 MgO-16 CaO-16 Na₂O-4 Fe₂O₃ in mol% (denoted as P40) was designated for this study due to its relatively low degradation rate, excellent biocompatibility and high Young's modulus in fibre form [11, 15, 21]. Although, lower durability fibres (50P₂O₅-40CaO-5Na₂O-5Fe₂O₃ (denoted as P50)) were also used in an attempt to standardise the preparation procedure for the composite rods due to the ease of fibre production as a result of dominance of their Q² structure (i.e. P50s are reported to have infinite chain lengths).

Continuous unidirectional (UD) and chopped strand random (RM) fibre mat composites were prepared with different fibre volume fractions by compression moulding at 210°C and 38 bar. Manufacture of FRC rods and screws was the main challenge for this project. Different methods were employed; i.e. compression moulding, compression moulding in a vacuum bag and machining. High void content was observed within the rods and screws produced via compression moulding of composite parts at 210°C. Accordingly, the mechanical properties for these devices were very low in comparison to published results. It is well known that the void ratio has a detrimental effect on service performance and mechanical properties of composites [22, 23]. Use of vacuum bag impregnation slightly reduced the void content and little improvement was consequently seen in their mechanical properties. The machining of thick composite bars (~ 4.5 mm) into rods and screws was attempted using a lathe machine to eliminate high void content. Deformation and softening (T_g for PLA is ~ 62°C) due to heat as a result of friction were the main complications of this machining method. Since the composite components were biodegradable, lathe cooling liquid (e.g. water) could not be used. Moreover, cutting the fibres in particular the unidirectional fibres within the screw thread creating a weak thread was also limited due to this machining method. Machining method using a lathe was successfully conducted for particulate composites (PLLA/HA) to produce bone plates, rods and screws by Shikinami *et al.* [24].

Finally, a novel method was introduced for manufacture of FRC rods as well as screws. This method was simply represented as compression moulding at temperature below the melting point of the composite matrix (otherwise known as thermomechanical deformation or forging). Shikinami *et al.* [3] used forging technique at 103°C for PLLA/HA composite plates in order to create polymer chain orientation causing enhancement for mechanical characteristics of the composites. Forging of PLA and composites was applied during their rubbery state (i.e. above T_g of PLA) and below the crystallisation temperature (T_c) in order to prevent an increase in matrix crystallinity which would lower the degradation rate of the implant [25-27]. The forging process window was selected between 70 – 90°C and this technique has numerous advantages; low processing temperatures, low cost, tiny void ratio, appropriate for different designs, shapes and materials, exclusion of aggressive thermal degradation and improvement of the matrix mechanical properties. The composite plates were forged at ~ 90°C into rods and screws (see *Figure 7-1*). Degradation and mechanical property retention were investigated for the devices manufactured.

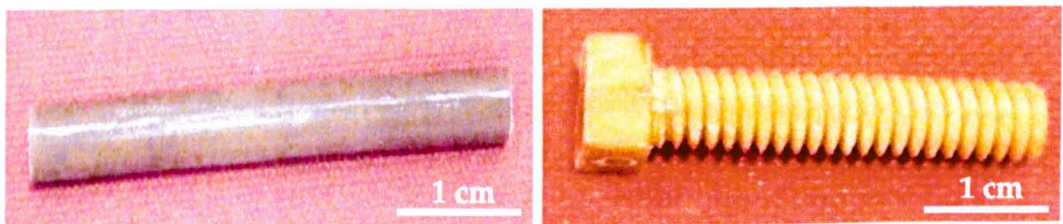


Figure 7-1: Photographs of the rod and screw prepared via forging process.

Water uptake for these composite devices was higher than for PLA alone which was attributed to the wicking effect of the media along the fibre/matrix interface [28]. Percentage mass loss for these composite devices, increased gradually over time in PBS at 37°C, whilst no mass loss was seen for PLA alone. Comparing the percentage mass loss for P40 composite plate, rods and screws after immersion in PBS at 37°C for 42 days, it was concluded that the screws and rods lost more mass than the plates. This was suggested to be due to an increase in fibre volume fraction for the

screws and rods in comparison to the composite plates. Ahmed *et al.* [29] also reported that the mass loss and water uptake for PLA/PGF increased when the fibre volume fraction increased which was attributed to an increase in water diffusion through the composites [30]. Random fibre mat composites absorbed lower amounts of water after 42 days than UD composites due to the inhibition of water diffusion by the arrangement of the chopped strand random fibre mats. P50 composite rods showed higher percentages of mass loss and water uptake than P40 composites due to degradation of the P50 fibres. Dissolution rate of P50 glass formulation is approximately ten times faster than the P40 composition (2.5×10^{-5} and $3 \times 10^{-6} \text{ g.cm}^{-2}.\text{h}^{-1}$ for P50 and P40 respectively) [31].

Ions released (i.e. cations and anions) showed good correlation with the mass loss profiles for the composite rods. Similar findings were also reported in the literature for bulk phosphate glass and composites (PCL/PGF and PLA/PGF) [32-35]. The linear relationship between mass loss and ion release and stability of pH of PBS for PLA (plate, rod and screws) at ~ 7.4 confirmed that mass loss for the composites was due to degradation of the fibre reinforcement. However, P40 composites only lost a very small fraction of their weight ($\sim 1\%$) during degradation in PBS. The pH for PBS remained neutral until the end of the degradation study which was said to be due to the ability of PBS to compensate for little variations in pH. Conversely, pH for the P50 composite rods decreased during the first week of immersion in PBS to approximately pH 5 due to release of high amounts of phosphate ions creating phosphoric acid (H_3PO_4) [36]. Phosphoric acid was produced by reaction of released PO_4^{3-} from the degradation of PGFs with water from the degradation medium.

Initial mechanical properties of the composite plates, rods and screws increase with increasing fibre volume fraction according to the rule of mixtures [23]. It was found that the percentage mechanical property loss for the composite rods and screws were greater in comparison with the composite plates. This was also attributed to the increase in fibre volume fraction [37]. As the fibre fraction increased, the amount of fibre/matrix interface would also increase which can have a significant effect on

the initial and retention of the mechanical properties. For example, if we assume that the gap created between the fibre and matrix during the degradation process [38, 39] has a thickness of half a micron, the resultant void would approximate to 10 % of the total fibre volume fraction. Mechanical properties for FRCs would decrease by increasing void content [40, 41].

The common problem associated with use of fibre reinforced composites in aqueous medium is that a poor fibre/matrix interface will result. Water attacks the fibre–matrix interface causing debonding and diffuses rapidly into the composites along the fibre–matrix interface via capillary action (i.e. wicking). Water diffusion at the interface can be ten times faster than through the bulk matrix [42]. Lassila *et al.* [43] showed that the mechanical properties for fibre-reinforced composites were dependent on water uptake. The decrease of mechanical properties after immersion in water was attributed to degradation of the fibre/matrix interface, plasticising effect of water and the amount of absorbed water. Water plasticising effect is temporary and can be recovered by dehydration of the composite specimens, whilst the fibre/matrix interface effect stated to be permanent.

Weak adhesion between the polymer matrix and glass fibres will inhibit transfer of applied stress from the polymer to the fibres. Thus, the mechanical strength of the composite would decrease significantly to be closer to the strength of the matrix alone [44]. Therefore, application of coupling agents is a potential route for improving and controlling the fibre/matrix interface whilst maintaining the initial mechanical properties for periods desirable for bone fixation. A coupling agent could also enhance the interface resistance to water attack. However, any coupling agent used here would have to be biocompatible and able to interact chemically with PLA and PGF. Studies on this are underway currently within the group, with preliminary work published [11, 15, 16].

Cytocompatibility for P40 composite plates and rods were investigated using Human osteosarcoma cell lines (HOS) and Human mesenchymal stem cells (MSCs). They exhibited good cytocompatibility due to the high chemical durability of the

P40 fibres. Moreover, P40 composites showed a higher CaP deposition in comparison with PLA alone which was ascribed to existence of PGF. Consequently, PGF would have potential capability to elicit new bone formation during *in vivo* experiments. The new bone formation was also previously seen by Scotchford *et al.* [45] for PCL/PGF composites during *in vivo* study in rats.

7.2 TO CONCLUDE

The following conclusions can be drawn from this thesis:

- A novel method was introduced in this project for reshaping fibre-reinforced composites plates into rods and screws (i.e. via forging). Besides the aforementioned advantages of the forging technique, it improved the mechanical properties for the matrix as well as the composites, which was attributed to both the orientation of polymer chains in the matrix and the short chopped strand random mat fibres rearranging along the principal axis of the rods.
- Totally bioresorbable devices (plates, rods and screws) can be manufactured with comparable initial mechanical properties to cortical bone based on PLA/PGF composite with fibre volume fraction ~ 30 % or higher. Their initial flexural, shear and compressive strengths varied within ranges of 100 - 250 MPa, 60 - 90 MPa, 130 - 420 MPa respectively and the flexural modulus ranged from 7 to 25 GPa depending on fibre volume fraction and architecture.
- Besides good cytocompatibility, P40 composites exhibited slow and gradual degradation and ion release rates which are desirable for bone fixation implant materials. Furthermore, P40 composite could potentially stimulate new bone formation during *in vivo* studies via CaP deposition.
- The end properties of the devices after or during degradation were mainly dependent on the stability of the fibre/matrix interface in an aqueous environment. The rapid initial decrease in mechanical properties after

immersion in PBS for the devices produced was attributed to the absence of a coupling agent.

7.3 FUTURE WORK

Based on the summary above and knowledge gained during this project, the following points are suggested to provide potential improvement in the mechanical and biological performance of the implants proposed.

7.3.1 Fibre-matrix interface

- Use of coupling agents to strengthen the fibre/matrix interface and resist water attack in order to maintain the initial mechanical properties for longer periods. Coupling agents should be biocompatible and able to chemically bond between the matrix (PLA) and the glass fibres.
- Using fibres with rougher surfaces potentially acting as mechanical interlocks and then improve the interface during the degradation process.
- Preparation of PLA/PGF composites via in situ polymerisation process would also enhance the fibre-matrix interface.

7.3.2 Characterisation methodology

- Applications of mechanical tests at physiological temperature (37°C) and under wet conditions (i.e. use of PBS buffer during the testing) in order to obtain comparable mechanical results to the actual properties under *in vivo* conditions.
- In this study, PBS was used as degradation medium to maintain pH value at ~ 7.4 and to examine effect of hydrolytic degradation on mechanical performance of the composite plates, rods and screws produced. Other degradation media such as cell culture medium could also be considered for future work in order to investigate the influence of enzymatic degradation to mimic the *in vivo* environment.

- Applications of *in vivo* testing using animal models (initially small animal models such as rabbit for example) for 6-12 months to assess the load-bearing capacity of the implants produced.
- It has been reported that inflammation within tissue near to the polymeric implant (e.g. PLA and PGA) was due to their acidic degradation products. For particulate composites, inflammation was attributed to the existence of filler particles after degradation of the implant. It is expected that PLA/PGF composites will not cause any adverse reactions for the surrounding tissue in particular using invert glass formulations such as P40 fibres, as the degradation products of the glass could potentially buffer the degradation products of the polymer. Brauer [46] reported that pH for degradation of invert glasses was close to neutral (pH ≈7.4). Moreover, Lehtonen *et al.* [47] found that acidic degradation products of PLA could be neutralised by release of cations (e.g. Na⁺, Ca²⁺, Mg²⁺). However, a long-term *in vitro* and *in vivo* study (1-2- years) is required to assess the degradation products and consequently the possibility of inflammation for the use of PLA/PGF composite implants.
- Finite element modelling for the resorbable screws using a metallic host material (stainless steel) and using natural bone (as host material) to examine the failure strength and modes to validate the FE model.
- Investigation of the effect of temperature and load on the degradation rate of the polymers and composites.
- Investigation of cyclic fatigue testing of the composites in wet conditions at 37°C.

7.3.3 Implant materials

- Preparation of phosphate glass multi-filament yarns and application of an online coating system using coupling agents or the bioresorbable matrix to produce a melt impregnated continuous glass fibre bundles [47].

- Preparation of composite rods via an extrusion/pultrusion system to scale-up rod manufacture.
- Continuous and more durable phosphate glass fibres can be prepared by adding trivalent cations such as Ti^{3+} and B^{3+} . It is expected that addition of these cations would decrease the glass solubility and consequently improve their cytocompatibility.
- Modify the composition of the phosphate glass fibres (lower P_2O_5 content) in which the degradation products will be basic to buffer the acidic degradation products of the matrix and maintain the neutral pH which would be a more favourable environment for living cells.

7.3.4 Implant design

- Modification of the screw-head design to be curved instead of with a stepped edge to avoid head slipping during the pull-out test.
- Based on calculations of the screw thread (see section 6.5.1.1), thread design has a significant influence on the screws performance such as holding power. Therefore, normalisation of screw thread will be essential to optimise the design for bone fixation applications.
- Manufacture of screws with only reinforced core (UD) and plain PLA thread using injection moulding machines.
- Manufacture of screws with different dimensions to be suitable for bone fixation at alternate locations of the body.

7.4 REFERENCES

1. Kalfas, I.H., *Principles of bone healing*. *Neurosurgical Focus*, 2001. 10(4): p. 1-4.
2. Furukawa, T., Y. Matsusue, T. Yasunaga, Y. Shikinami, M. Okuno, and T. Nakamura, *Biodegradation behavior of ultra-high-strength hydroxyapatite/poly (-lactide) composite rods for internal fixation of bone fractures*. *Biomaterials*, 2000. 21(9): p. 889-898.
3. Shikinami, Y. and M. Okuno, *Bioresorbable devices made of forged composites of hydroxyapatite (HA) particles and poly-L-lactide (PLLA): Part I. Basic characteristics*. *Biomaterials*, 1999. 20(9): p. 859-877.

4. Bergsma, J.E., W.C. de Bruijn, F.R. Rozema, R.R.M. Bos, and G. Boering, *Late degradation tissue response to poly(L-lactide) bone plates and screws*. *Biomaterials*, 1995. 16(1): p. 25-31.
5. Hoffmann, J., K. Friedrich, M. Evgstatiev, and U. Finkc, *A Totally Bioresorbable Fibrillar Reinforced Composite System: Structure and Properties*. *International Journal of Polymeric Materials*, 2001. 50(3): p. 469 - 482.
6. Bühler, M., P.-E. Bourban, and J.-A.E. Månson, *Cellular composites based on continuous fibres and bioresorbable polymers*. *Composites Part A: Applied Science and Manufacturing*, 2008. 39(12): p. 1779-1786.
7. Weiler, A., R.F.G. Hoffmann, A.C. Stahelin, H.-J. Helling, and N.P. Sudkamp, *Biodegradable implants in sports medicine: The biological base*. *Arthroscopy: The Journal of Arthroscopic & Related Surgery*, 2000. 16(3): p. 305-321.
8. Gunatillake, P.A. and R. Adhikari, *Biodegradable Synthetic Polymers for Tissue Engineering*. *European Cells and Materials*, 2003. 5: p. 1 -16.
9. Shikinami, Y., Y. Matsusue, and T. Nakamura, *The complete process of bioresorption and bone replacement using devices made of forged composites of raw hydroxyapatite particles/poly l-lactide (F-u-HA/PLLA)*. *Biomaterials*, 2005. 26(27): p. 5542-5551.
10. Ahmed, I., M. Lewis, I. Olsen, and J.C. Knowles, *Phosphate glasses for tissue engineering: Part 1. Processing and characterisation of a ternary-based P₂O₅-CaO-Na₂O glass system*. *Biomaterials*, 2004. 25(3): p. 491-499.
11. Haque, P., A.J. Parsons, I.A. Barker, I. Ahmed, D.J. Irvine, G.S. Walker, and C.D. Rudd, *Interfacial properties of phosphate glass fibres/PLA composites: Effect of the end functionalities of oligomeric PLA coupling agents*. *Composites Science and Technology*, 2010. 70(13): p. 1854-1860.
12. Bunker, B.C., G.W. Arnold, and J.A. Wilder, *Phosphate glass dissolution in aqueous solutions*. *Journal of Non-Crystalline Solids*, 1984. 64(3): p. 291-316.
13. Ropp, R.C., *Inorganic polymeric glasses*1992: Elsevier.
14. Vitale-Brovarone, C., G. Novajra, J. Lousteau, D. Milanese, S. Raimondo, and M. Fornaro, *Phosphate glass fibres and their role in neuronal polarization and axonal growth direction*. *Acta Biomaterialia*, 2012. 8(3): p. 1125-1136.
15. Parsons, A.J., I. Ahmed, P. Haque, B. Fitzpatrick, M.I.K. Niazi, G.S. Walker, and C.D. Rudd, *Phosphate Glass Fibre Composites for Bone Repair*. *Journal of Bionic Engineering*, 2009. 6(4): p. 318-323.
16. Haque, P., I.A. Barker, A. Parsons, K.J. Thurecht, I. Ahmed, G.S. Walker, C.D. Rudd, and D.J. Irvine, *Influence of compatibilizing agent molecular structure on the mechanical properties of phosphate glass fiber-reinforced PLA composites*. *Journal of Polymer Science Part A: Polymer Chemistry*, 2010. 48(14): p. 3082-3094.

17. Parsons, A.J., I. Ahmed, N. Han, R. Felfel, and C.D. Rudd, *Mimicking Bone Structure and Function with Structural Composite Materials*. *Journal of Bionic Engineering*, 2010. 7(Supplement 1): p. S1-S10.
18. Parsons, A., I. Ahmed, M.I.K. Niazi, R.R. Habeb, B. Fitzpatrick, G.S. Walker, I.A. Jones, and C.D. Rudd, *Mechanical and Degradation Properties of Phosphate Based Glass Fibre/PLA Composites with different Fibre Treatment Regimes*. *Science and Engineering of Composite Materials*, 2010. 17(4): p. 243 - 260.
19. Cozien-Cazuc, S., A. Parsons, G. Walker, I. Jones, and C. Rudd, *Effects of aqueous aging on the mechanical properties of $P_{40}Na_{20}Ca_{16}Mg_{24}$ phosphate glass fibres*. *Journal of Materials Science*, 2008. 43(14): p. 4834-4839.
20. Cozien-Cazuc, S., A.J. Parsons, G.S. Walker, I.A. Jones, and C.D. Rudd, *Real-time dissolution of $P_{40}Na_{20}Ca_{16}Mg_{24}$ phosphate glass fibers*. *Journal of Non-Crystalline Solids*, 2009. 355(50-51): p. 2514-2521.
21. Ahmed, I., A. Parsons, A. Jones, G. Walker, C. Scotchford, and C. Rudd, *Cytocompatibility and Effect of Increasing MgO Content in a Range of Quaternary Invert Phosphate-based Glasses*. *J Biomater Appl*, 2010. 24(6): p. 555-575.
22. Huang, H. and R. Talreja, *Effects of void geometry on elastic properties of unidirectional fiber reinforced composites*. *Composites Science and Technology*, 2005. 65(13): p. 1964-1981.
23. Lee, N.-J. and J. Jang, *The effect of fibre content on the mechanical properties of glass fibre mat/polypropylene composites*. *Composites Part A: Applied Science and Manufacturing*, 1999. 30(6): p. 815-822.
24. Shikinami, Y. and M. Okuno, *Bioresorbable devices made of forged composites of hydroxyapatite (HA) particles and poly-lactide (PLLA). Part II: practical properties of miniscrews and miniplates*. *Biomaterials*, 2001. 22(23): p. 3197-3211.
25. Cai, H., V. Dave, R.A. Gross, and S.P. McCarthy, *Effects of physical aging, crystallinity, and orientation on the enzymatic degradation of poly(lactic acid)*. *Journal of Polymer Science Part B: Polymer Physics*, 1996. 34(16): p. 2701-2708.
26. Tokiwa, Y., B. Calabia, C. Ugwu, and S. Aiba, *Biodegradability of Plastics*. *International Journal of Molecular Sciences*, 2009. 10(9): p. 3722-3742.
27. Zhou, Q. and M. Xanthos, *Nanoclay and crystallinity effects on the hydrolytic degradation of polylactides*. *Polymer Degradation and Stability*, 2008. 93(8): p. 1450-1459.
28. Wan, Y.Z., Y.L. Wang, X.H. Xu, and Q.Y. Li, *In vitro degradation behavior of carbon fiber-reinforced PLA composites and influence of interfacial adhesion strength*. *Journal of Applied Polymer Science*, 2001. 82(1): p. 150-158.
29. Ahmed, I., I. Jones, A. Parsons, J. Bernard, J. Farmer, C. Scotchford, G. Walker, and C. Rudd, *Composites for bone repair: phosphate glass fibre reinforced PLA with varying fibre architecture*. *Journal of Materials Science: Materials in Medicine*, 2011. 22: p. 1825 - 1834.

30. Onal, L., S. Cozien-Cazuc, I.A. Jones, and C.D. Rudd, Water absorption properties of phosphate glass fiber-reinforced poly- ϵ -caprolactone composites for craniofacial bone repair. *Journal of Applied Polymer Science*, 2008. 107(6): p. 3750-3755.
31. Ahmed, I., C.A. Collins, M.P. Lewis, I. Olsen, and J.C. Knowles, Processing, characterisation and biocompatibility of iron-phosphate glass fibres for tissue engineering. *Biomaterials*, 2004. 25(16): p. 3223-3232.
32. Georgiou, G., L. Mathieu, D.P. Pioletti, P.E. Bourban, J.A.E. Manson, J.C. Knowles, and S.N. Nazhat, Polylactic acid-phosphate glass composite foams as scaffolds for bone tissue engineering. *Journal of Biomedical Materials Research Part B: Applied Biomaterials*, 2007. 80B(2): p. 322-331.
33. Ahmed, I., A.J. Parsons, G. Palmer, J.C. Knowles, G.S. Walker, and C.D. Rudd, Weight loss, ion release and initial mechanical properties of a binary calcium phosphate glass fibre/PCL composite. *Acta Biomaterialia*, 2008. 4(5): p. 1307-1314.
34. Ahmed, I., M.P. Lewis, S.N. Nazhat, and J.C. Knowles, Quantification of anion and cation release from a range of ternary phosphate-based glasses with fixed 45 mol% P₂O₅. *J Biomater Appl*, 2005. 20(1): p. 65-80.
35. Mohammadi, S.M., I. Ahmed, N. Muja, C. Rudd, M. Bureau, and S. Nazhat, Effect of phosphate-based glass fibre surface properties on thermally produced poly(lactic acid) matrix composites. *Journal of Materials Science: Materials in Medicine*, 2011. 22(12): p. 2659-2672.
36. Ahmed, I., P.S. Cronin, E.A. Abou Neel, A.J. Parsons, J.C. Knowles, and C.D. Rudd, Retention of mechanical properties and cytocompatibility of a phosphate-based glass fiber/polylactic acid composite. *Journal of Biomedical Materials Research Part B: Applied Biomaterials*, 2009. 89B(1): p. 18-27.
37. Alvarez, V.A., A.N. Fraga, and A. Vázquez, Effects of the moisture and fiber content on the mechanical properties of biodegradable polymer-sisal fiber biocomposites. *Journal of Applied Polymer Science*, 2004. 91(6): p. 4007-4016.
38. Michael, A.S., C.C. Chu, and A.A. Ida, Fiber-matrix interface studies on bioabsorbable composite materials for internal fixation of bone fractures. I. Raw material evaluation and measurement of fiber - matrix interfacial adhesion. *Journal of Biomedical Materials Research*, 1997. 36(4): p. 469-477.
39. Michael, A.S. and C.C. Chu, Fiber-matrix interface studies on bioabsorbable composite materials for internal fixation of bone fractures. II. A new method using laser scanning confocal microscopy. *Journal of Biomedical Materials Research*, 1997. 37(3): p. 353-362.
40. Ghiorse, S.R., Effect of void content on the mechanical properties of carbon/epoxy laminates. *SAMPE Quarterly*, 1993. 24(2): p. 54 - 59.
41. Judd, N.C.W. and W.W. Wright, Voids and their effects on the mechanical properties of composites - An appraisal *SAMPE Journal*. , 1978. 14: p. 10 - 14.

42. Tsenoglou, C.J., S. Pavlidou, and C.D. Papaspyrides, *Evaluation of interfacial relaxation due to water absorption in fiber-polymer composites. Composites Science and Technology*, 2006. 66(15): p. 2855-2864.
43. Lassila, L.V.J., T. Nohrström, and P.K. Vallittu, *The influence of short-term water storage on the flexural properties of unidirectional glass fiber-reinforced composites. Biomaterials*, 2002. 23(10): p. 2221-2229.
44. Lehtonen, T. and J. Tuominen, *Biocompatible Composite and its Use, Patent US 2012/0040015 A1*, 2012.
45. Scotchford, C.A., M. Shataheri, P.S. Chen, M. Evans, A.J. Parsons, G.A. Aitchison, C. Efeoglu, J.L. Burke, A. Vikram, S.E. Fisher, and C.D. Rudd, *Repair of calvarial defects in rats by prefabricated, degradable, long fibre composite implants. J Biomed Mater Res A*, 2010. 96(1): p. 230-8.
46. Jones, J. and A. Clare, *Bio-Glasses: An Introduction* 2012: Wiley.
47. Lehtonen, T.J., J.U. Tuominen, and E. Hiekkänen, *Resorbable composites with bioresorbable glass fibers for load-bearing applications. In vitro degradation and degradation mechanism. Acta Biomaterialia*, 2013. 9(1): p. 4868-4877.